Supporting and stabilizing biomimetic membranes

Ibragimova, Sania

Publication date:
2011

Document Version
Early version, also known as pre-print

Supporting and stabilizing biomimetic membranes

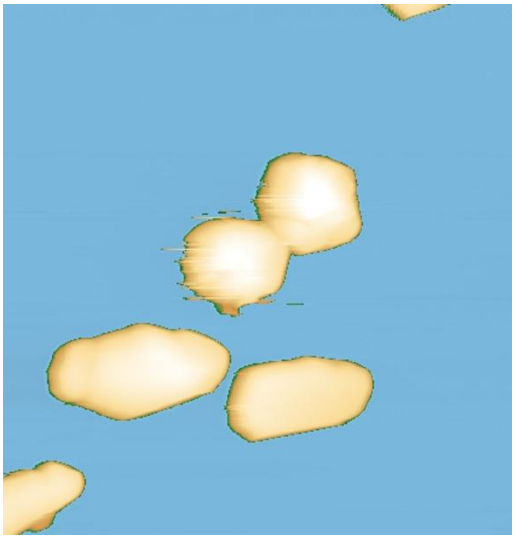
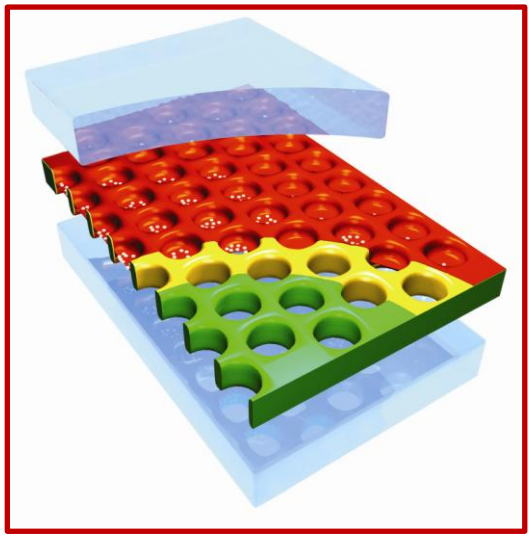
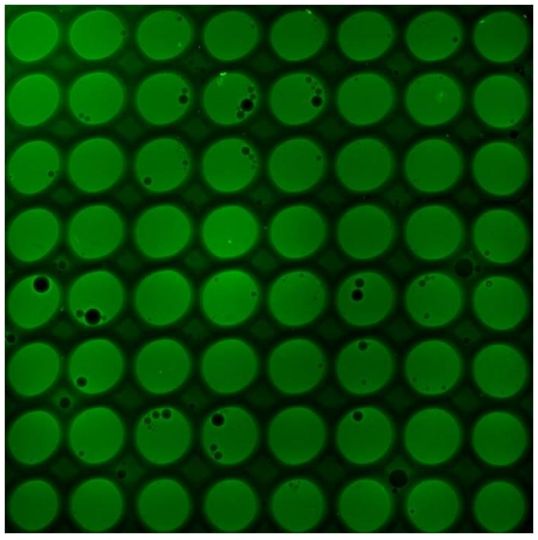

PhD dissertation

Sania Ibragimova

2011

DTU Physics
Department of Physics

Supporting and stabilizing biomimetic membranes

Sania Ibragimova

PhD dissertation

Supervisors
Henrik Bohr, DTU Physics
Claus Hélix-Nielsen, DTU Physics and Aquaporin A/S

Department of Physics
Technical University of Denmark
2800 Kgs. Lyngby
Denmark
May 9, 2011

Table of Contents

Abstract

Membranes that mimic biological cell membranes are known as biomimetic membranes (BMs). BMs with incorporated membrane proteins show exciting potential for biomedical and separation applications, such as in platforms for novel biosensors, in high-throughput screening of potential drug candidates and for hemodialysis systems. Another exciting application is to use BMs containing aquaporins (water-selective proteins) in a water purification system. Among the requirements for BMs used in separation applications are upscalability to square metres of membrane, compatibility with bulk transport across the membranes, and membrane stability. In order to realize a high-resistance membrane with an area of square meters, one method is to use a hydrophobic partition with an array of micrometer-sized apertures and span membranes across these apertures. However, challenges with poor membrane stability need to be met in order to create commercially viable BM-based technologies. Several strategies for stabilizing and supporting planar BMs are addressed in this thesis. First, lipid membrane array stability and longevity were improved by *in situ* encapsulation in a soft porous hydrogel, with leak-free membranes obtained for up to 9 days and functionality of inserted channel-forming peptides demonstrated 5 days after insertion into the membranes. Second, lipid membranes were prepared on a precast composite hydrogel support that was conjugated to the hydrophobic partition. Multi-aperture arrays of thin, robust lipid membranes in which proteins can be reconstituted could easily be formed on the support. By depositing a polyelectrolyte cushion support on the gel and tethering the lipid membranes to the support, we obtained BMs with lifetimes up to 17 hours. Third, lipid membranes were prepared on a versatile nanoporous diblock copolymer support, which can be tailored to alter its morphology, porosity, surface roughness and hydrophilicity. Lastly, biomimetic lipid bilayers were ”doped” with lipid bilayer-like triblock copolymers. Hybrid vesicles composed of both triblock polymer and lipids were deposited on solid supports. The mixed lipid-polymer vesicles showed promise for formation of robust membranes and could be designed either for tethering of vesicles or formation of planar, solid-supported membranes by varying the polymer content of the vesicles.

Resumé

Membraner som efterligner biologiske cellemembraner benævnes ofte biomimetiske membraner (BM). BM med indlejrede membranproteiner har stort potentiale for biomedicinske og separeringsanvendelser, som f.eks. platforme for biosensorer, i high-throughput screening af potentielle lægemidler og for hemodialysesystemer. En anden spændende anvendelse er at anvende BM som indeholder aquaporiner (vandselektive proteiner) i et vandfiltreringssystem. Blandt kravene til BM i separeringsanvendelser er at de kan opskaleres til kvadratmeter-arealer, at de er kompatible med massetransport over membranen samt at de har den fornødne stabilitet overfor transmembrane hydrostatiske/osmotiske trykforskelle. En måde hvorpå en tæt BM med et effektivt kvadratmeter-areal kan fremstilles er, at anvende en hydrofob skillevæg med en matrix af mikrometerstore aperturer hvorover membraner kan formes. Dog må udfordringen med stabilitet overvindes for at skabe kommercielt anvendelige BM-baserede teknologier. I denne afhandling studeres fire forskellige strategier for at stabilisere og understøtte plane BM. I én strategi øgedes stabiliteten og levetiden på en matrix af lipidmembraner gennem *in situ* indkapsling i en blød porøs hydrogel. Vi opnåede tætte membraner med levetider op til 9 dage, med funktionelle indlejrede ionkanaldannende peptider som var funktionelle i op til 5 dage efter membran-fremstilling. I en anden strategi formedes lipidmembraner på et færdigstøbt porøst komposit-hydrogel-underlag som fæstnedes til den hydrofobe skillevæg. Matricer af tynde, robuste lipidmembraner i hvilke proteiner kan indlejres kunne fremstilles på det porøse hydrogel-underlaget. Ved at deponere en polyelektrolyt-'pude' på hydrogelen hvorpå lipidmembranen kunne fæstnes, opnåede vi BM-levetider på optil 17 timer. I en tredje strategi dannedes lipidmembranen på et nanoporøst diblok-copolymer underlag som kunne tilpasses med hensyn til morfologi, porøsitet, styrke og hydrofobicitet. I en fjerde strategi formedes membraner udfra en blanding af lipider og amfifile triblok-copolymerer. Hybrid-vesikler som bestod af både triblok-copolymerer og lipider deponeredes på en fast overflade. Disse vesikler viste sig at være lovende i dannelsen af robuste membraner og kunne designes til enten at forblive i vesikelform på den faste overflade eller bringes til at danne plane membraner på den faste overflade ved at variere mængden af polymer i vesiklerne.

List of publications

Thesis papers

Paper I. *Hydrogels for in situ encapsulation of biomimetic membrane arrays*
S. Ibragimova, K. Stibius, P. Szewczykowski, M. Perry, H. Bohr, C. Hélix-Nielsen; Polymers for Advanced Technologies, doi 10.1002/pat.1850 (in press)

Paper II. *Tailoring properties of biocompatible PEG-DMA hydrogels with UV light*
S. Ibragimova, J. Benavente, R. Berg, K. Stibius, M. S. Larsen, H. Bohr, C. Hélix-Nielsen; European Polymer Journal; submitted

Paper III. *Biomimetic membrane arrays on cast hydrogel supports*
M. Roerdink Lander*, **S. Ibragimova***, C. Rein*, J. Vogel, K. Stibius, O. Geschke, M. Perry, C. Hélix-Nielsen; Langmuir; in press (* shared first authors)

Paper IV. *Supported hybrid lipid-polymer membranes*
S. Ibragimova, M. Marincel, M. Kumar, T. H. Nguyen, C. Hélix-Nielsen, J. L. Zilles; to be submitted to Biomacromolecules

Secondary papers

Appendix I. *Electrochemical characterisation of hydrogels for biomimetic applications*
L. Peláez, V. Romero, S. Escalera, V. Scileira, **S. Ibragimova**, K. Stibius, J. Benavente, C. Hélix-Nielsen; Polymers for Advanced Technologies; submitted

Appendix II. *Structure and stability of the spinach aquaporin SoPIP2;1 in detergent micelles and lipid membranes*
I. Plasencia, S. Survery, **S. Ibragimova**, J. S. Hansen, P. Kjellbom, C. Helix-Nielsen, U. Johanson, O. G. Mouritsen; PLoS ONE 2011:6(2):e14674.

Appendix III. *Supported lipid bilayers on engineered nanoporous polymers*
C. Rein*, **S. Ibragimova***, S. Kaufmann, P. Szewczykowski, E. Reimhult, T. Bjørnholm, C. Helix-Nielsen; in preparation (* shared first authors)

The story of the papers

The papers presented in this thesis reflect the work that was done during the three years of the PhD project. Their focus was on improving stability of biomimetic membranes. Although not mentioned specifically in the papers, biomimetic membrane stability was improved with the purpose to develop a novel water filtration device based on biomimetic membranes containing aquaporin proteins. Only papers I-IV are thesis papers. I contributed to the two papers in appendix I and II in a small way through collaboration with our project partners, but this work is outside the scope of my thesis. Appendix III is an early manuscript which deals with the work presented in chapter 6 and it is included for information about the methods used.

Paper I

The aim of paper I was to stabilize black lipid membranes (BLMs) formed across apertures in a hydrophobic ethylene tetrafluoroethylene support. These membranes were to be used as a matrix for aquaporin proteins in a reverse osmosis (RO)-type water filtration membrane. Paper I investigated hydrogels for *in situ* encapsulation of BLMs. To be compatible with a water filtration device, the gels had to be porous and have high water permeability, but at the same time be dense enough to provide stabilization and increase longevity of the BLMs. The encapsulation gels consisted of networks of poly(ethylene glycol)-dimethacrylate (PEG-DMA) or poly(ethylene glycol)-diacrylate (PEG-DA) that were polymerized using either a chemical initiator or a photoinitiator. All four gels were nanoporous and showed high water permeability. Lifetimes of free-standing BLM arrays in gel precursor solutions were short compared to arrays formed in buffer. However, polymerizing (crosslinking) the photoactivated PEG-DMA gel stabilized the membranes and resulted in BLM arrays that remained intact for up to nine days - a substantial improvement over lifetimes for free-standing BLM arrays. Incorporation of gramicidinA ion channels showed that the BLMs retained their integrity and functionality after encapsulation with hydrogel and channel activity after 5 days is demonstrated.

Paper II

Paper II continued characterization of the PEG-DMA photoactivated hydrogel. The polymerization reaction starts when the gel precursor solution is exposed to UV light. Fourier Transform Infrared Spectroscopy (FTIR) and Raman Spectroscopy (RS) showed that the optimal

crosslinking time for the gel was 6-10 minutes. Also, we found that the gel's properties can be tailored by varying the photocrosslinking time, namely that the water content of the gels can be varied between 50-90 wt%, which could be important for the gels' flux properties, for their interaction with lipid membranes and also later for shipping and handling of hydrogel-encapsulated membranes. The specific electrical resistance of the gel could be varied between 0.8-3.5 Ωm. For comparison, phosphate buffered saline has a resistivity of 8.4 Ωm (Ibragimova, unpublished results) and deionized water a resistivity of $1.8 \cdot 10^5$ Ωm^1. This showed that the gel had a low resistivity (and a high conductivity) and thus that ion channel-containing hydrogel-encapsulated membranes are compatible with biosensor applications. With FTIR and RS we identified spectral features of the hydrogel, which may be applicable as a diagnostic tool to study changes in the gel due to variation in parameters.

Paper III

Paper III describes the stabilization of BLMs with a composite ETFE/hydrogel sandwich. The sandwich consists of a perforated surface-treated ETFE film onto which a hydrogel composite support structure (based on 2-hydroxyethyl methacrylate, PEG-DMA and silica beads) is cast. The hydrogel structure is porous and water-permeable and was covalently tethered to the ETFE film to improve membrane stability. The hydrogel provides a backing in the apertures and promotes rapid self-thinning of the lipid bilayers. BLMs supported by the ETFE/hydrogel sandwich had lifetimes of at least 60 minutes, a significant improvement over free-standing BLMs which had minimum lifetimes of 15 minutes. A successful incorporation of α-hemolysin demonstrated that the BLMs were fully functional. The paper presents a simple method to prepare arrays of lipid bilayer membranes with low intrinsic electrical conductance on the highly permeable, self-supporting ETFE/hydrogel sandwiches.

Paper IV

Paper IV, which arises from my external research stay carried out at the University of Illinois, deals with stabilization of lipid vesicles by addition of synthetic triblock copolymers and formation of planar membranes from these mixed vesicles on solid supports. Biomimetic membranes constructed of self-assembling triblock copolymers with a hydrophilic-hydrophobic-hydrophilic pattern are typically more stable than lipid membranes and they can be easily

modified to control membrane properties. Lipids have the advantage of being better understood and of being similar to the native environment for membrane proteins. In this paper, $PMOXA_{15}$-$PDMS_{110}$-$PMOXA_{15}$ triblock copolymer was mixed with zwitterionic or positively charged lipids at several ratios to form hybrid vesicles. The rupture propensity of hybrid triblock copolymer-lipid vesicles could be tuned to create either vesicular or planar membranes on solid supports, depending on the lipid/polymer ratio and the lipid headgroup charge.

Appendix I

In this paper the electrochemical properties of the four hydrogels presented in paper I were investigated by electrochemical impedance spectroscopy. The chemically crosslinked hydrogels had lower effective electrical resistance and higher electrical capacitance than hydrogels with photoinitiated crosslinking. Electromotive force measurements demonstrated that at low salt concentrations both PEG-400-DA hydrogels presented an electropositive character, PEG-1000-DMA (photoinitiated) was approximately neutral and PEG-1000-DMA (chemically initiated) showed electronegative character. Sodium transport numbers approached the bulk NaCl electrolyte value at high salt concentrations for all hydrogels indicating screening of fixed charges in the hydrogels. Chemically initiated gels had higher average salt diffusional permeability $<Ps>$ and water permeability $<Pw>$ than photocrosslinked hydrogels. The paper shows that hydrogel electrochemical properties can be controlled by the choice of polymer and type of crosslinking used, and that their water and salt permeability properties are compatible with the use of hydrogels for biomimetic membrane encapsulation.

Appendix II

This paper addresses the structural stability of the spinach leaf plasma membrane aquaporin, SoPIP2:1 (the aquaporin used in the water filtration device) in various lipid and detergent environments. This is done in order to optimize reconstitution of the purified protein into biomimetic membranes. The paper characterizes the protein structural stability (secondary structure) after purification and after reconstitution into detergent micelles and liposomes using circular dichroism and fluorescence spectroscopy. Generally, SoPIP2;1 secondary structure was found to be predominantly α-helical in accordance with crystallographic data. The protein has a high thermal structural stability in detergent solutions, with an irreversible thermal unfolding

occurring at a melting temperature of 58°C. Incorporation of the protein into lipid membranes increased the structural stability as evidenced by an increased melting temperature of up to 70°C. The paper suggests suitable choices of detergent and lipid composition for reconstitution of SoPIP2;1 into biomimetic membranes.

Appendix III

This early manuscript draft addresses formation of supported lipid membranes on a nanoporous diblock copolymer support, based on 1,2-polybutadiene-b-polydimethylsiloxane with gyroid pore morphology. Four conformations of the support surface are analyzed by atomic force microscopy (AFM): hydrophobic and smooth, hydrophobic and corrugated, hydrophilic and smooth as well as hydrophilic and corrugated. The hydrophilic and smooth support was shown to be similar to a silicon dioxide surface in terms of roughness and hydrophilicity. Planar lipid membranes are formed on the silicon dioxide support, and the two hydrophilic block copolymer supports by vesicle deposition. The deposited vesicles contained a low molar fraction of PEG chain-conjugated lipids. The rationale for including the PEG chains was to provide a cushion layer for the lipid membrane. Supported lipid bliayer formation was confirmed by quartz crystal microbalance with dissipation monitoring (QCM-D) on silicon dioxide and by AFM on the diblock copolymer supports.

My contribution to the papers

Paper I. I was significantly involved in designing the experiments. I prepared the hydrogels for all measurements and performed volumetric stability and voltage clamp measurements. I evaluated the results and drafted the manuscript.

Paper II. I was significantly involved in designing the experiments. I prepared hydrogels and performed swelling and FTIR experiments. I evaluated most of the results and drafted the manuscript.

Paper III. I was significantly involved in designing, performing and analyzing voltage clamp and fluorescence microscopy experiments. I participated in writing the manuscript.

Paper IV. I was significantly involved in designing and performing all the experiments. I evaluated the results and drafted the manuscript.

Appendix I. I prepared hydrogels for all measurements and had a small part in writing the manuscript.

Appendix II. I prepared DPhPC vesicles, performed DLS measurements and had a small part in writing the manuscript.

Appendix III I was significantly involved in designing all experiments, prepared vesicles, performed DLS experiments, analyzed DLS and QCM-D experiments and had a significant role in writing the manuscript.

1. Introduction

There are many different types of biomimetic membranes - membranes that mimic biological cell membranes. These include free-standing planar membranes (made by painting or folding), spherical membranes known as vesicles and solid-supported planar membranes (made by Langmuir-Blodgett and Langmuir-Schaefer technique or by vesicle deposition). In this thesis, I have mostly focused on painted biomimetic membrane arrays (BMAs) and to a lesser degree addressed planar and vesicular membranes supported on porous and corrugated or solid and flat substrates.

BMAs with incorporated membrane proteins show exciting potential for biomedical and separation applications. Some examples of potential applications of BMAs in biomedicine are platforms for novel biosensors and high-throughput screening of potential drug candidates. BMAs present appealing alternatives to cell-based screening of drug candidates, because they allow information to be obtained using extremely low sample volumes and provide the ability to directly address specific drug-target interactions[2]. This is because cell membranes are complex and contain a large variety of lipids, proteins and other complexes[3], whereas the content of biomimetic membranes can be specified by the user[4].

BMAs also present interesting possibilities as platforms for addressable, multiplexed biosensor arrays. Advantages presented by using BMAs are that extremely low sample volumes can be used on which multiplexed measurements could be carried out to obtain a lot of information[5]. Potentially, a biomimetic membrane scaffold can be created that allows simultaneous monitoring of each individual membrane in the protein-containing membrane array electrically, optically and by monitoring transport of solutes and ions across the membrane. It is easy and straightforward to address each membrane in a BMA optically[5]. It is possible to detect interactions of G-protein coupled receptors with fluorescently labeled ligands[2], which shows that fluorescence microscopy could be used to screen receptor-ligand interactions in a BMA. Biomimetic membrane designs which support electrical measurements of membrane and ion channel electrical properties combined with fluorescence microscopy have been presented[6]. Electrical voltage-clamp measurements of a BMA are a very useful tool to quantify membrane thickness and ensure that

functional membranes are established[6]. It should in principle be possible to electrically address each individual membrane in a BMA by adding a material underneath the apertures to make wells which can be individually addressed. The principle has been demonstrated by Suzuki *et al* who electrically addressed each well in a 96-well plate membrane arrays with 3x3 membranes in each well[7]. A third way to address BMAs could be by forming individually well-defined wells underneath the arrays and detecting transport of small solutes, ions or water through transmembrane proteins across the membrane. This principle has been demonstrated by Hemmler *et al*[8], who visualized transport of the fluorescent dye calcein across individual membranes with incorporated α-hemolysin pores. There are many exciting possibilities for multiplexed measurements using addressable, protein-containing BMAs and new exotic possibilities for addressing BMAs may arise[9].

If BMAs with large incorporated protein arrays can be scaled to a sufficiently large effective area, they can be used for separation applications. An exciting application which is being pursued by a Danish company, Aquaporin A/S, is to use BMAs containing aquaporins (water-selective proteins[10]) in a water purification system. Such aquaporin-containing arrays show promise as a revolutionizing technology for production of ultrapure water and desalination of seawater. Aquaporins, nature's own water filters rapidly and selectively transport water molecules and have the potential to improve purity of ultrapure water 1000-fold[11, 12] compared to state-of-the-art reverse osmosis membranes. For more about this interesting field see the review by Nielsen[13]. Another envisaged application of aquaporin-containing large scale BMAs is for faster hemodialysis systems[9]. Requirements for BMAs used in separation applications are upscalability to square metres of membrane, compatibility with bulk transport across the membranes, impermeability of the membrane matrix, membrane stability, relatively low production complexity and cost-effectiveness.

The basic building block of a BMA is a biomimetic membrane, which can be constructed in several ways. One possibility is to support membranes on a flat, solid, hydrophilic support. Favoured supports include silica[14-16], freshly cleaved mica[17, 18], silicon[19], silicon nitride[20], alumina[21] and gold[22]. These systems in their basic form have severe drawbacks, such as denaturation of integral membrane proteins due to limited space between the lipid membrane and

the solid support[23]. Another drawback is that the limited aqueous compartment on the support side of the membrane limits bulk transport of water, ions and solutes across the membrane[13, 24]. Some of these substrates (such as silicon nitride[20], silicon[25, 26] and alumina[21, 27-29]) have been made porous and free-standing lipid membranes created across the pores by vesicle fusion[26-28], Langmuir-Blodgett technique[25] or by painting[20, 21, 29]. Issues that were encountered with creation of membranes on nanoporous substrates by vesicle fusion were related to low membrane coverage and leak currents/decrease in membrane resistance[24] and membranes formed by Langmuir-Blodgett technique are not compatible with incorporation of most transmembrane proteins[30]. A drawback of painting membranes in submicron apertures is that the functional membrane area in such small apertures is significantly decreased, due to the presence of a solvent annulus[9]. Although materials such as mica, silica and gold provide good stabilization for biomimetic membranes, the materials and fabrication techniques for producing aperture arrays in these materials would not be cost-effective for square meter areas and could therefore not be used for commercial separation applications.

Another BMA conformation is to span solvent-containing membranes across apertures in a hydrophobic scaffold between two aqueous compartments, where the organic solvent forms an annulus around the edge of the aperture and the lipid monolayer leaflets meet in the middle of the aperture to form a lipid bilayer resembling the lipid bilayer of a cell membrane[31, 32]. Functional transmembrane proteins are inserted into this region. These membranes can be free-standing or supported on a porous substrate. In this thesis, porous substrates which are nanoporous and compatible with bulk transport across the membrane as well as relatively easy and cheap to produce were introduced as membrane supports. These are more corrugated than the typical flat silica, mica and gold substrates and therefore presented an interesting challenge in creating stable membranes.

Free-standing solvent-containing membranes have an inherent instability, which is best explained by examining the dimensions of the system. The lipid bilayer has a thickness of 4-10 nm[33, 34], whereas the walls of an aperture in a partition scaffold have a height between 20-200 µm, which means that the lipid membrane has to compensate for more than a 1000-fold difference in thickness to span the aperture. The role of the solvent is to help the membrane to

match the height of the aperture by forming an annulus around the perimeter of the aperture[35]. The solvent slowly diffuses from the annulus, which is believed to cause membrane destabilization over time and eventually lead to membrane collapse[36, 37]. To make a free-standing 4 nm-thick biomimetic membrane that spans over a single aperture with an area of square meters is not feasible due to lack of stability. In order to realize a high-resistance membrane with an area of square meters, one method is to use an aperture array with micrometer-sized holes and span supported membranes across these apertures.

Although creation of a single solvent-containing lipid membrane across an aperture in Teflon is a well-established technique, dating back to the 1960's[31], solvent-containing BMAs across aperture arrays have emerged fairly recently. Some reasons for this are the difficulty of creating reproducible membrane arrays[9] and that planar membranes suspended over apertures have generally low stability. Advances have been made in this field in recent years, where fast and reproducible methods for creating aperture arrays in Teflon[38] and automated painting of lipid membranes across such aperture arrays[6, 39] have been demonstrated, allowing reproducible membrane arrays to be created. However, challenges with poor membrane stability still need to be met in order to create commercially viable biomimetic membrane-based technologies. A benchmark for BMA stability is that it should have a lifetime exceeding 1 day[24]. This has been achieved in some formats for single-aperture solvent-containing lipid membranes[36, 40-44] as well as for submicron-aperture BMAs[20, 25]. However, in apertures of this size, the solvent torus would take up a large percent of the aperture area and the functional membrane area would be small[9]. To increase the functional membrane area, the aperture diameter should be increased, but this leads to a decrease in membrane stability[9, 20, 25, 45].

An intriguing way to improve the stability of biomimetic membranes is to replace lipids with lipid-bilayer-like amphiphilic block copolymers. These are chemically and mechanically stable[46, 47] and provide an amphiphilic structure that allows incorporation of membrane proteins[48]. Their stability is accredited to that they have a higher thickness than lipids[49, 50]. However, this may be a drawback in terms of lower functional transmembrane protein incorporation compared to a lipid bilayer due to a hydrophobic mismatch between the hydrophobic block of the polymer and the hydrophobic band of the membrane protein[51]. A promising compromise could be to mix lipids

and polymers to obtain their favourable qualities – high stability gained from the polymer and a protein-favourable environment provided by the lipids. In this thesis, I present a method for making mixed lipid-polymer vesicular membranes and producing planar membranes from these on solid substrates.

2. Aim

This PhD-project was scientifically and financially a part of the project *"Industrial biomimetic water membranes"* funded by the Danish National Advanced Technology Foundation (Højteknologifonden, J.nr 023-2007-1). The latter project is devoted to the development of a new membrane filter technology for the production of ultra pure water. The technology copies nature´s own way of water filtration where specific water channels – aquaporins – in living cells filter and transport water. The central aim of my PhD project was to stabilize the biomimetic membrane arrays used in the water filtration devices, but these stabilization strategies are applicable for a broader audience, essentially for anyone who is interested in obtaining more stable biomimetic membranes. Some applications of these membranes can be as model systems for study of transmembrane proteins or with incorporated proteins in biosensor or separation devices.

I started by addressing free-standing biomimetic membranes made from lipid bilayers suspended in a suitable solvent incorporated into multi-aperture hydrophobic ethylene tetrafluoroethylene (ETFE) partitions. Perforated ETFE partitions for the project were available through DTU-Nanotech and the fabrication procedure is described by Vogel *et al*[38]. Lipids were deposited into the multi-aperture partition by a painting technique described by Hansen *et al*, who was also a part of the "*Industrial biomimetic water membranes*" project[6]. Membrane stability was quantified by voltage clamp electrophysiology (VCE), which allowed temporal measurement of the capacitance and conductance of the membrane, providing a measure of the thickness of the membranes, how well they seal the apertures and the membrane array's longevity. Also, it was possible to assess membrane functionality by incorporating transmembrane ion channels and demonstrating current flow across a single channel. I also used fluorescence microscopy to characterize the lipid membranes, the supports used for lipid membranes, vesicles, fluorescently-dyed proteins and other components of the system.

Several strategies for stabilizing and supporting planar biomimetic membranes are addressed in this thesis. One important criterion when selecting a stabilization strategy was that it should be possible to make the system porous, allowing for bulk transport of water and small molecules

across the membrane when the relevant transporter proteins were incorporated. These strategies are summarized in Figure 1 and will be discussed in detail in the following chapters.

2.1. Encapsulation of membranes with hydrogel

The first strategy used to improve lipid membrane array stability and longevity was to encapsulate it in a soft porous hydrogel (Fig. 1A). Hydrogels are hydrophilic polymer networks that can absorb up to thousands of times their dry weight in water[52]. In this strategy, the lipid membrane array is created in a hydrogel precursor solution, which is subsequently crosslinked in order to place a hydrogel cushion on each side of the lipid bilayer. An advantage of encapsulating lipid membrane arrays with a hydrogel, is that the hydrogel could lie close to the membrane and interact strongly with the polar groups of the lipids, improving membrane stability. Hydrogel encapsulation is also claimed to slow down solvent diffusion out of the annulus[36], which addresses a problem which is typical for solvent-containing lipid membranes. The problem is leakage of the solvent from the torus of the membrane to the aqueous phase, leading to effective thinning of the membrane and a decrease in membrane stability over time[53]. There were several requirements placed on the gel. Firstly, it should be liquid and crosslinkable *in situ* at room temperature, in order to maintain the lipid membranes in the liquid crystalline state[54] and to be compatible with the method of making the membrane arrays[6]. Secondly, the crosslinking process should not result in large gel volume changes as this would destabilize the biomimetic membrane. Thirdly, the porosity of the encapsulating gel should be able to provide sufficient stability while preserving good water and solute permeabilities. Poly(ethylene glycol)-di(meth)acrylate (PEG-D(M)A) based hydrogels fulfill these requirements. I characterized these hydrogels and showed successful hydrogel encapsulation of multiple black lipid membranes (BLMs) formed across an aperture array. Methods that I worked with for analyzing the hydrogels are Fourier Transform Infrared spectroscopy, Raman spectroscopy, size exclusion chromatography and water flux measurements (the latter two mainly done by P. Szewczykowski). Electrical impedance spectroscopy on the hydrogels to determine their resistivity and ionic permeability were carried out by a project partner at the University of Malaga, the group of J. Benavente. Lipid membranes in hydrogel precursor solution and encapsulated in hydrogel were studied using VCE and bright-field microscopy. This work is covered in papers I and II and appendix paper I and will be discussed in chapter 4.

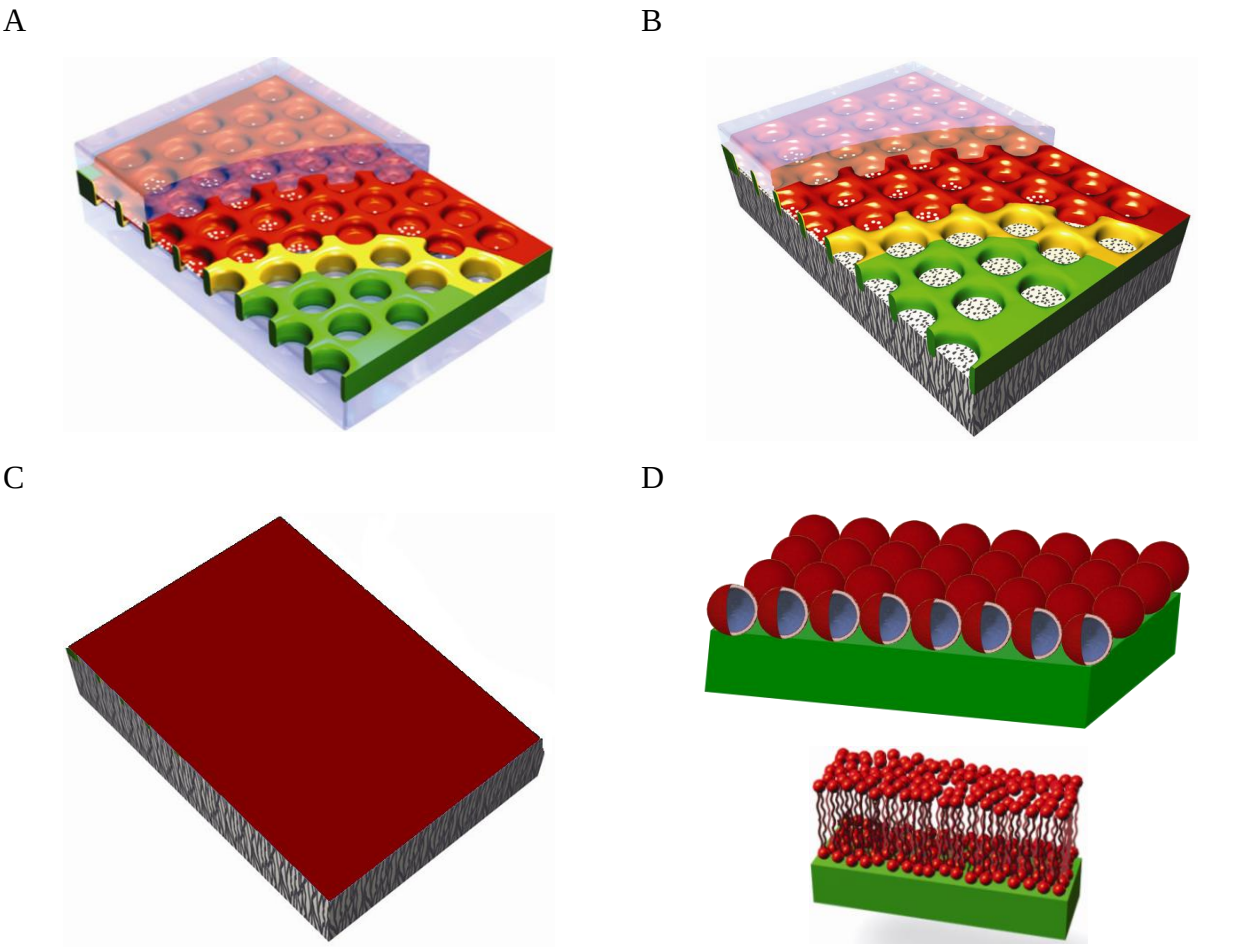

Figure 1. Strategies used in this thesis for stabilizing biomimetic membranes. (A) Black lipid membranes (BLMs) (red) spanning an aperture array in plasma-treated (yellow) ethylene tetrafluoroethylene (ETFE) (green) with incorporated transmembrane proteins (white dots) encapsulated in hydrogel (transparent layer). This strategy is addressed in papers I, II, appendix I and chapter 4. (B) BLMs (red) spanning an aperture array in plasma-treated (yellow) ETFE (green) with incorporated transmembrane proteins (white dots) supported on a precast nanoporous hydrogel slab (white layer). This strategy is addressed in paper III and chapter 5. (C) Supported lipid membranes (red) prepared by vesicle deposition on a nanoporous polymer support (white layer). This strategy is described in chapter 6 and appendix III. (D) Vesicular or planar supported mixed lipid-polymer membranes (red) on a solid support (green). This strategy is addressed in paper IV and chapter 7.

2.2. Membranes on a nanoporous hydrogel support

The second strategy involved using a hard, flat, hydrophilic porous substrate on which a lipid bilayer is created (Fig. 1B). The support had to be hydrophilic in order to be able to support a hydrated lipid bilayer on it and it had to be porous to allow small solute transport across the lipid membranes. Flat substrates are preferred due to ease of forming and studying the formed membrane and hard substrates, because these should provide a good mechanical stability to the

membranes. I worked with an ETFE/hydrogel sandwich support on which the lipid membrane array was painted.

The hydrogel support was formed by polymerization of an aqueous solution of 2-hydroxyethyl methacrylate (HEMA) and PEG-DMA in the presence of silicon dioxide beads. The hydrogel was cast using a mold such that the polymerized hydrogel would form a supportive layer under the apertures. The rationale behind this design was to optimize the lipid-partition interactions at the aperture rim, while providing maximal support for the membranes across the aperture arrays. In order to ensure good contact between the composite hydrogel and the ETFE partition, the ETFE surface was surface-modified with HEMA using surface plasma polymerization on the partition side facing the hydrogel. The polyHEMA support was further modified by layer-by-layer deposition of polyelectrolyte layers. Polyelectrolytes mimic the cell cytoskeleton[55], which has a supporting and stabilizing function in cells. An avidin-biotin linkage is used to tether the biomimetic cytoskeleton to the biomimetic membrane. The rationale is that adding a "cytoskeleton" and tethering the membrane to it will improve membrane stability. The thickness of the polyelectrolyte cushion can be controlled by the number of deposited layers. I used a single layer of poly(sodium styrene sulfonate) (PSS) or nine alternating layers of PSS and poly(ethyleneimine). Methods that I used here are VCE and fluorescence microscopy. This work is covered in paper III and will be discussed in chapter 5.

2.3. Membranes on a nanoporous polymer support

The third strategy involved formation of lipid bilayers by vesicle deposition on a porous diblock copolymer substrate (Fig. 1C). The rationale for choosing this substrate was the same as for polyHEMA, that it had to be hydrophilic, porous, flat and hard. The diblock copolymer used was a 1,2-polybutadiene-b-polydimethylsiloxane (PB-PDMS) with a gyroid morphology, with the PDMS etched away to create a nanoporous substrate[56]. The support surface was photooxidized to make it hydrophilic[57]. Lipid membranes were deposited on the nanoporous, hydrophilic PB support by vesicle deposition instead of painting of solvent-containing membrane arrays for two reasons. Firstly, an ETFE-PB sandwich support with half-way filling of the PB through the apertures was not available. Secondly, vesicle deposition is a favoured method for formation of lipid bilayers, because it presents the fewest obstacles to transmembrane protein insertion into

the planar lipid bilayer[13]. Methods that I worked with in this strategy are dynamic light scattering (DLS) to characterize vesicle size, quartz crystal microbalance with dissipation monitoring (QCM-D) to characterize vesicle deposition on a reference silica substrate (practical work done by S. Kaufmann, analysis of data by me) and atomic force microscopy (AFM) to characterize vesicle deposition on PB (mostly done by C. Rein). This work will be discussed in chapter 6 and is the basis for appendix III.

2.4. Hybrid lipid-polymer membranes on a solid support

The fourth strategy, which was carried out during my external research stay at the University of Illinois explored using hydrophilic-hydrophobic-hydrophilic triblock copolymers as a replacement for lipids to create biomimetic membranes. While lipids have the advantage of being better understood and of being similar to the native environment for membrane proteins, copolymer membranes also have some advantages, particularly in the area of stability. There are also many possibilities for engineering block copolymer membranes to achieve the desired combination of properties, by adjusting parameters such as the block length, molecular weight, chemical composition, hydrophilic/hydrophobic balance and molecular architecture[58]. Lipid-polymer membranes were deposited on a solid substrate (quartz or mica) by vesicle deposition (Fig. 1D) instead of painting of solvent-containing membrane arrays for the same reasons as for the PB support. I synthesized vesicles with different ratios of poly-(2-methyloxazoline)-polydimethylsiloxane-poly-(2-methyloxazoline) triblock copolymer to zwitterionic or positively charged lipids and investigated the deposition and rupture of these vesicles on quartz and mica. These mixed lipid-polymer vesicles show promise for formation of robust membranes and can be designed either for tethering of vesicles or formation of planar, solid-supported membranes. I used DLS, electrophoretic light scattering and stopped-flow osmotic measurements to characterize the vesicles in terms of size, charge and water permeability and used transmission electron microscopy to inspect the vesicles visually. Vesicle deposition on two solid supports, quartz and mica, was characterized by QCM-D and AFM respectively. This work is addressed in paper IV and will be discussed in chapter 7.

The last section of this thesis provides a summary of the achieved goals and addresses possible future directions.

3. Background

3.1. Biomimetic membranes

Transmembrane proteins have many functions in biological systems, and act for example as channels, receptors or transporters. There is considerable interest in studying the function of these proteins. To study functional transmembrane proteins, the protein must be embedded in a matrix compatible with protein structure and function[59], such as a cell membrane (Fig. 2). However, cellular membranes have a complex composition, which makes it difficult to address and study specific proteins in them. A typical cell membrane is made up of a lipid bilayer with a complex lipid composition and contains a variety of proteins, carbohydrates, glycolipids and cholesterols and other membrane-bound components and is supported by a cytoskeleton[3].

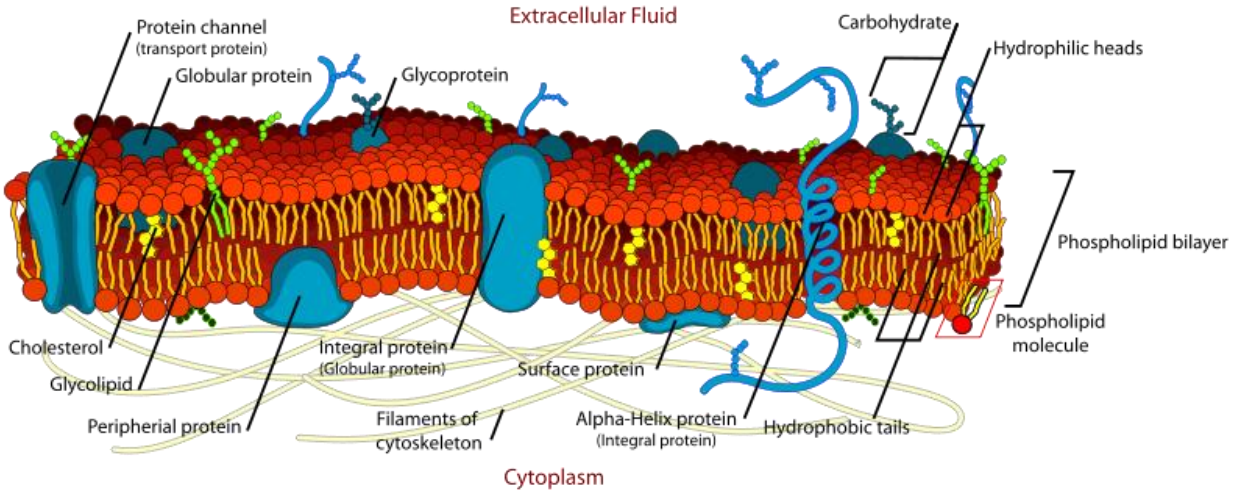

Figure 2. Sketch of a cell membrane showing membrane-associated and transmembrane proteins, cytoskeleton, cholesterols, glycoproteins, glycolipids and carbohydrates. This sketch does not capture the full complexity of a cell membrane. For example, it does not reflect that the lipid bilayer is made up of a variety of lipids, which can assemble to form patches, which vary in fluidity and can also change layer by flip-flop motions. Also, it does not give a correct representation of the complexity of signaling pathways and membrane fusion and budding events that take place at the membrane. Figure from [60].

To make it easier to study membrane-associated and transmembrane proteins, artificial cell membranes which mimic the cell membrane are used. These are known as **biomimetic membranes**. The fundamental component of a biomimetic membrane is a lipid bilayer.

Recently, artificial cell membranes consisting of diblock and triblock copolymers have also been presented[46, 61, 62].

Lipids are amphiphilic molecules with a polar head group and hydrophobic acyl chains. When in aqueous solution, lipids self-assemble into ordered structures. The hydrophilic head groups interact readily with water, because of they can form hydrogen bonds with the water molecules. The hydrophobic acyl chains are insoluble in water, because they are non-polar and cannot form hydrogen bonds with water molecules. In an aqueous environment the hydrophobic acyl chains force the adjacent water molecules to arrange themselves in well-ordered structures[63]. To minimize this effect, the hydrophobic acyl chains cluster together, exposing as few hydrophobic groups as possible to the aqueous environment. Other forces acting on the lipids that affect their conformation are ionic and dipole-dipole interactions between the head groups as well as steric interactions and van der Waals forces. In biological membranes, phospholipids spontaneously arrange themselves in a spherical bilayer, because it is the conformation with the lowest total energy for the forces acting on the lipids. In artificial cell membranes, three conformations are prevalent. These are free-standing membranes (Fig. 3A), vesicles (Fig. 3B) or planar supported membranes (Fig. 3C).

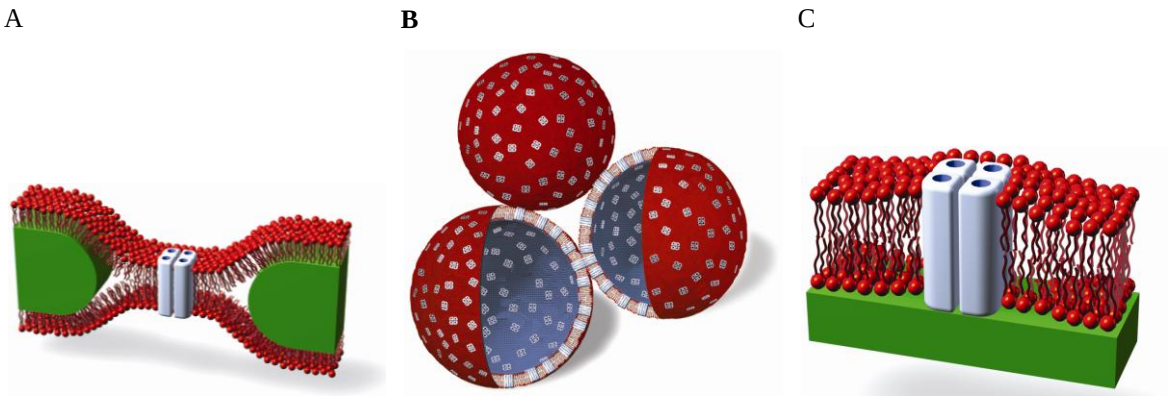

Figure 3. Biomimetic membrane formats. (A) Free-standing membrane. Black lipid or polymer membranes (red) spanning an aperture in a hydrophobic scaffold (green) with an incorporated transmembrane protein (white rods). The membrane separates two aqueous compartments. The white triangular sections between the membrane monolayers and the scaffold contain an organic solvent. (B) Vesicular membranes. Vesicles with lipid or polymer membranes (red) separating two aqueous compartments. The intravesicular aqueous compartment is coloured blue. Incorporated transmembrane proteins are shown as white squares. (C) Planar supported membranes. Lipid or polymer membranes (red) supported on a solid support (green) with an incorporated transmembrane protein (white rods).

Depending on whether the free-standing membranes are made up of lipids or polymers they are known as black lipid membranes (BLMs) or black polymer membranes (BPMs). They are termed “black”, because they are dark in reflected light. This phenomenon arises, because the membranes have a thickness of only a few nanometers, so that light reflecting from the front of the membrane destructively interferes with light reflecting from the back of the membrane. These membranes span an aperture in a hydrophobic scaffold and contain a solvent annulus. Vesicles composed of lipids are called liposomes, and vesicles made up of polymers are called polymersomes. If these vesicles also contain reconstituted protein, they are often referred to as proteoliposomes and proteopolymersomes respectively. Vesicle size and lamellarity (number of lipid bilayers in the vesicle) can be decided by the method of preparation. Vesicles can be divided into multilamellar (containing multiple lipid bilayers) and unilamellar (containing a single lipid bilayer) vesicles. Unilamellar vesicles can be further subdivided by size into small unilamellar vesicles (SUVs), large unilamellar vesicles (LUVs) and giant unilamellar vesicles (GUVs). The third conformation of biomimetic membrane is as solid-supported membranes, which can consist of lipids or polymers. Issues with denaturation of transmembrane proteins due to the proximity of the bottom membrane leaflet to the solid support in this format[23], led to approaches to increase the spacing to the support while maintaining the mechanical stabilization.

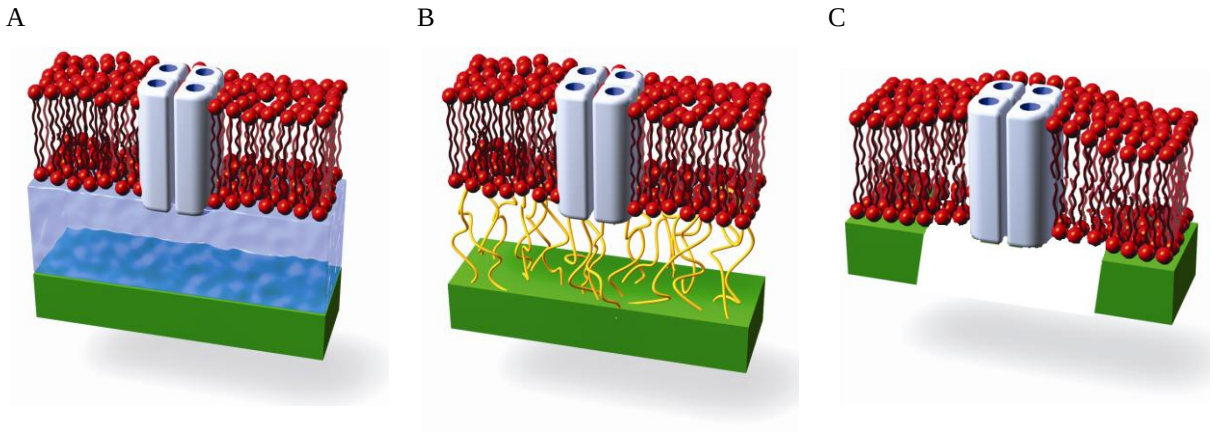

Figure 4. Biomimetic supported membrane formats (A) Cushion-supported biomimetic membrane. A polymer cushion (blue) is introduced between the solid support (green) and the biomimetic membrane (red) and interacts with both non-covalently. (B) Hydrophilic cushion spacers (yellow) which are covalently linked to the solid support (green) and non-covalently interacting with the biomimetic membrane (red) or covalently attached to lipids or proteins (white) in the biomimetic membrane. (C) Porous solid-supported membrane. Lipid or polymer membranes (red) supported on a porous solid support (green) with an incorporated transmembrane protein (white rods).

These approaches are shown in Figure 4 and include introducing a non-covalently bound cushion layer[64] (Fig. 4A) or a covalently linked cushion[65] (Fig. 4B) or making the support porous[25] (Fig. 4C). In the next section I will present some typical and some more "exotic" biomimetic membrane components.

3.2. Biomimetic membrane components

The lipid composition in biomimetic membranes is selected based on requirements for stability, as well as requirements placed on the membrane by the proteins to be reconstituted[13]. Some typical biomimetic membrane components are shown in Figure 5. Free-standing membranes (Fig. 3A) are typically made from phospholipids (such as 1,2-diphytanoyl-*sn*-glycero-3-phosphocholine (DPhPC); Fig. 5A) in an organic solvent (such as decane; Fig. 5E)[6]. Vesicular (Fig. 3B) or supported (Fig. 3C) lipid membranes are typically made from phospholipids (such as 1,2-dioleoyl-*sn*-glycero-3-phosphocholine (DOPC); Fig. 5B) without an organic solvent[66]. A desire to increase the stability of the biomimetic membranes together with advances in lipid polymerization chemistry led to the use of polymerizable lipids with reactive moieties in the headgroup[67] (1,2-diphytanoyl-*sn*-glycero-3-phosphoethanolamine-N-acrylate (DPhPE-A); Fig. 5C) or acyl chain region[68] (1,2-di-10,12-tricosadiynoyl-*sn*-glycero-3-phosphocholine (DTPC); Fig. 5D). These are used to crosslink the lipids to create stable biomimetic structures. Also, crosslinkable organic solvents (such as n-butylmethacrylate; Fig. 5F) have been used to obtain more stable biomimetic membranes[69]. Another interesting approach to improve membrane stability is to use lipids from organisms from Archaea, because they live in extreme environments such as high temperatures and low pH[70]. Many Archaean membranes are formed from bipolar lipids, bolalipids,[71], which span the membrane and in this way increase structural stability[72]. Synthetic bolalipids (such as 2,2-di-*O*-(3,7,11,15-tetramethylhexadecyl)-3,3-di-*O*-(1″,32″-ditriacontanyl)-bis-(rac-glycerol)-1,1-diphosphocholine (C_{22}PhytBAS); Fig. 5G) can be produced in milligram quantities[73], making it possible to use them in large-scale biomimetic membrane designs.

Recent developments in block-copolymer research have led to the use of diblock (such as polyethyleneoxide-polyethylethylene (PEO-PEE); Fig. 5H)[46] and triblock (such as poly(2-methyloxazoline)-block-poly(dimethylsiloxane)-block-poly(2-methyloxazoline) (PMOXA-

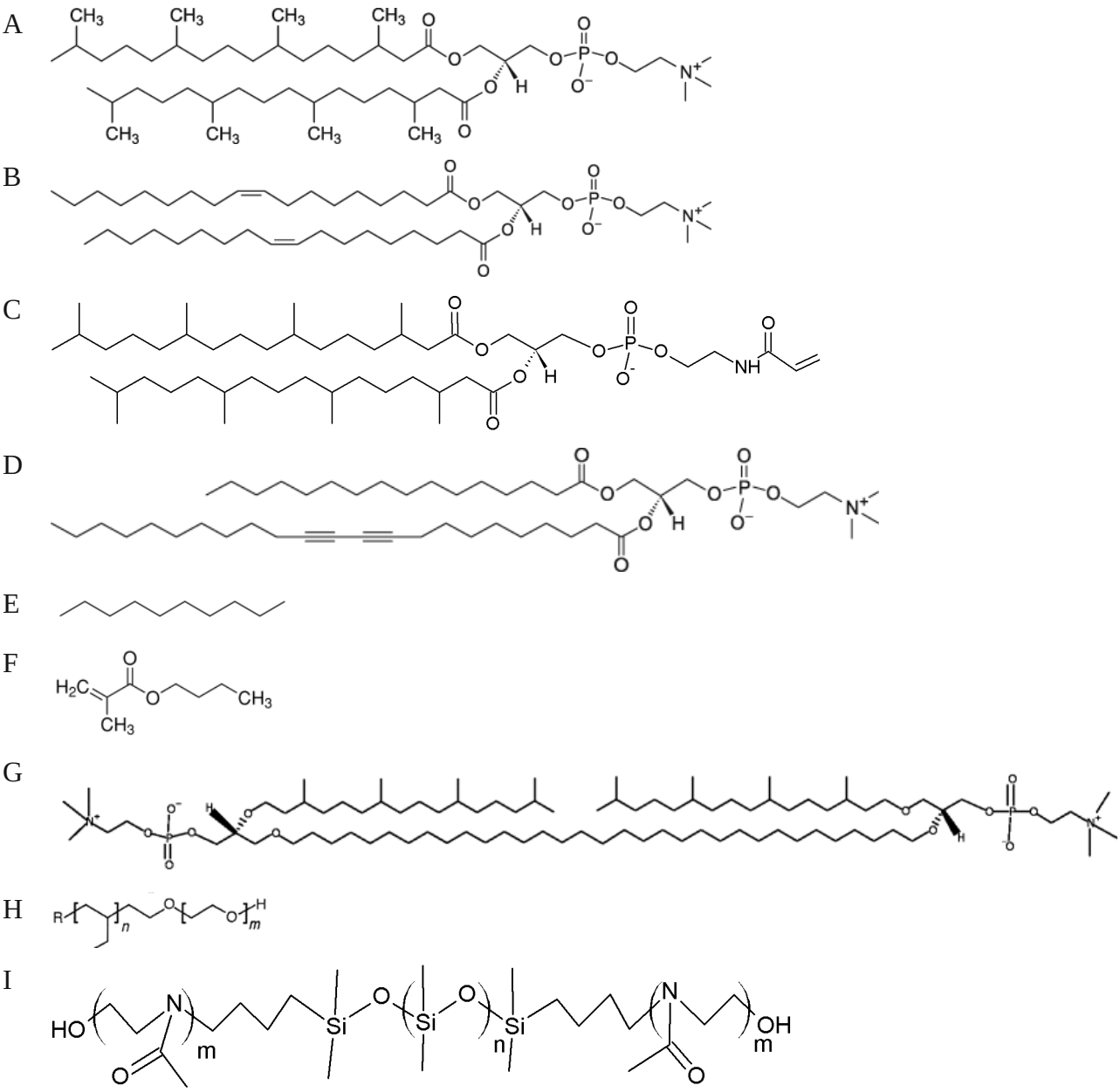

Figure 5. Biomimetic membrane components. (A) Phospholipid used for BLMs 1,2-diphytanoyl-*sn*-glycero-3-phosphocholine (DPhPC). (B) Phospholipid used for vesicles and supported membranes 1,2-dioleoyl-*sn*-glycero-3-phosphocholine (DOPC). (C) Head-group crosslinkable phospholipid 1,2-diphytanoyl-*sn*-glycero-3-phosphoethanolamine-N-acrylate (DPhPE-A). (D) Acyl chain crosslinkable phospholipid 1,2-di-10,12-tricosadiynoyl-*sn*-glycero-3-phosphocholine (DTPC). (E) Organic solvent used for BLMs and BPMs decane. (F) Crosslinkable solvent n-butylmethacrylate. (G) Bolalipid 2,2-di-*O*-(3,7,11,15-tetramethylhexadecyl)-3,3-di-*O*-(1″,32″-ditriacontanyl)-bis-(rac-glycerol)-1,1-diphosphocholine (C_{22}PhytBAS). (H) Diblock copolymer polyethyleneoxide-polyethylethylene (PEO-PEE). (I) Triblock copolymer poly(2-methyloxazoline)-blockpoly(dimethylsiloxane)-block- poly(2-methyloxazoline) (PMOXA-PDMS-PMOXA). Figure adapted from [13].

PDMS-PMOXA); Fig. 5I)[62] copolymers as replacements for lipids in biomimetic membranes. Diblock copolymers consist of a hydrophilic block covalently linked to a hydrophobic block, thus resembling the amphiphilic nature of lipids. Triblock copolymers have a hydrophilic-hydrophobic-hydrophilic composition reminiscent of bolalipids or of a phospholipid bilayer. Block copolymers are chemically and mechanically stable[46, 47] and provide an amphiphilic structure that allows incorporation of membrane proteins[48]. Their stability is accredited to that they have a higher thickness than lipids[49, 50]. There are also many possibilities for engineering block copolymer membranes to achieve the desired combination of properties, by adjusting parameters such as the block length, molecular weight, chemical composition, hydrophilic/hydrophobic balance and molecular architecture[58]. In the following sections I will discuss strategies that are used for forming lipid and polymer membranes and how they are functionalized with proteins.

3.3. Biomimetic membrane formation

Free-standing membranes (Fig. 3A) are formed across an aperture in a hydrophobic scaffold, where the scaffold separates two aqueous compartments. First, a small aperture is created in a hydrophobic material such as Teflon. Typically the diameter of such an aperture is tens of micrometers[30]. Formation of free-standing membranes has traditionally been carried out by either the ”painting” method[31] or the ”folding” method[74]. In the ”painting” method (Fig. 6), the hydrophobic scaffold is placed in a chamber, separating two aqueous compartments. The lipid[31] or polymer[75, 76] components are dissolved in a hydrocarbon solvent (typically decane or squalene) and the solution is applied with a brush or pipette and spread across the aperture in the hydrophobic material. A lipid monolayer spontaneously forms at the interface between the organic and aqueous phases on either side of the lipid/solvent droplet. Thinning occurs in the center of the droplet, because the lipid/solvent solution primarily wets the hydrophobic aperture walls. Once the two sides of the droplet come close enough together, the lipid monolayers fuse and form a lipid bilayer. The solvent is squeezed out to the perimeter of the aperture and forms a solvent annulus, which is important for stabilizing the membrane[35].

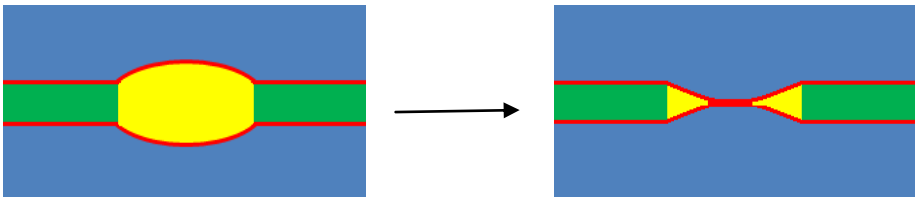

Figure 6. Sketch of BLM and BPM formation by the ”painting” method. A droplet of lipids or polymers (red) dissolved in an organic solvent (yellow) is deposited in an aperture in a hydrophobic scaffold (green) separating two aqueous compartments (blue). The solvent is squeezed out to the perimeter of the aperture and a lipid bilayer (or diblock polymer bilayer or triblock polymer monolayer) is formed in the center of the aperture.

In the ”folding” method, a vertical set-up with two aqueous compartments separated by an aperture is used and the height of the solutions in each compartment is independently controlled (Fig. 7). Both compartments are filled with aqueous buffer and a monolayer of lipids[74] or polymers[61] in a low molecular weight hydrocarbon solvent (e.g. pentane[13]) is spread at the air-water interface. One way of folding the membrane is to lower the solution level in one compartment below the aperture and then raise the level again, depositing a lipid monolayer on each pass to form a completed lipid bilayer across the aperture.

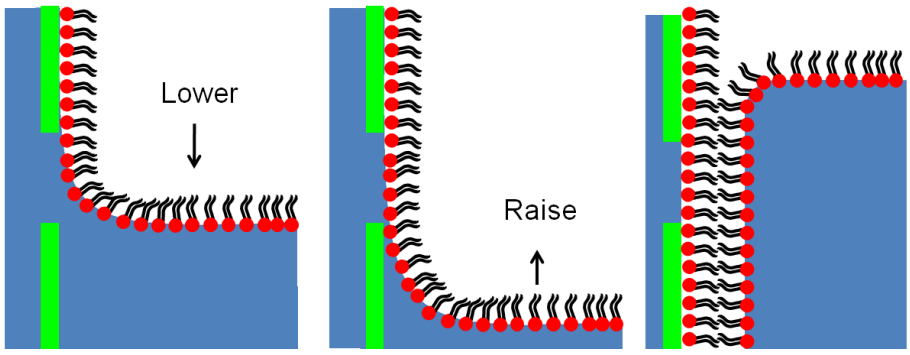

Figure 7. Sketch of BLM and BPM formation by the ”folding” method. Two aqueous compartments (blue) are separated by a hydrophobic scaffold (green) with an aperture. Lipids or polymers (red and black) are spread as a monolayer on top of one of the aqueous compartments. Lowering and raising the water level of this compartment forms a lipid bilayer/diblock copolymer bilayer/triblock copolymer monolayer across the aperture.

A commonly used method for forming liposomes is the film-hydration technique[77]. The film hydration technique can also be used for diblock[47] and triblock copolymers[50]. In the film hydration technique the lipid components are first dissolved in an organic solvent to ensure homogeneous mixing of the lipids or polymers. Then, the solvent is evaporated using nitrogen gas or argon gas and residual solvent is removed using a vacuum pump. The dry lipid film is hydrated by adding an aqueuos solution and agitating. When thin lipid films are hydrated, stacks

of liquid crystalline bilayers become fluid and swell (Fig. 8A). The hydrated lipid sheets detach during agitation and self-close to form large, multilamellar vesicles (MLVs) to prevent interaction of water with the hydrocarbon core of the bilayer at the edges. Another method to make vesicles with polymers is the co-solvent method where the polymer is dissolved in a solvent such as ethanol and added drop wise to an aqueous solution[50, 78]. Many other methods for forming vesicles are available, such as detergent dialysis[79, 80] and others[77]. Reducing the size of the multilamellar vesicles requires energy input in the form of sonic energy (sonication[81], Fig. 8C) or mechanical energy (extrusion[82], Fig. 8B).

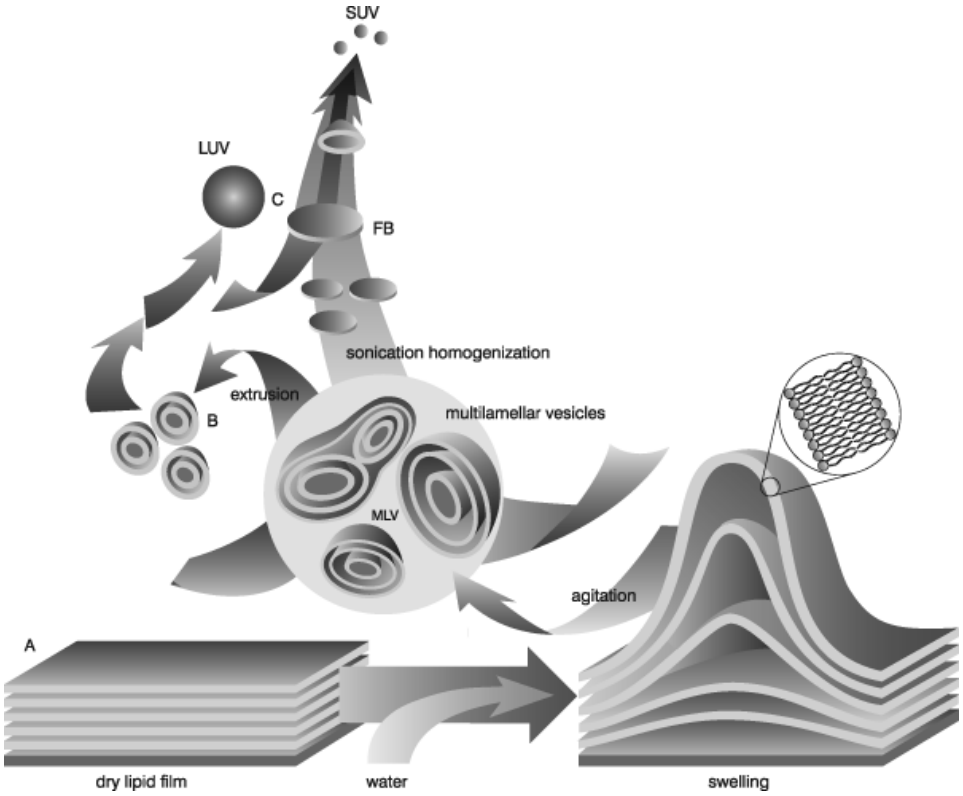

Figure 8. Preparation of vesicles. (A) Preparation of multilamellar vesicles. First, a dry lipid or polyemer film is prepared. Addition of water causes the lamella of lipid bilayers/diblock copolymer bilayers/triblock copolymer monolayers to swell. Agitation helps them to detach and form closed MLV structures. (B) Extrusion of MLVs through a polycarbonate membrane with a defined pore diameter is used to form smaller MLVs (for pore diameter > 0.2 μm) or large unilamellar vesicles (LUVs, for pore diameter < 0.2 μm). (C) LUVs and MLVs form small unilamellar vesicles (SUVs) upon sonication. Figure from [83].

Sonication typically produces small, unilamellar vesicles (SUVs) with diameters of 15-50 nm. The most common instrumentation for preparation of sonicated vesicles is a bath sonicator. A test tube of the MLV solution is placed in a bath sonicator and sonicated for 5-10 minutes above

the gel-crystalline phase transition temperature of the lipid. Mean size and size distribution of vesicles produced by sonication vary between batches. Sonication has been used to obtain polymersomes from diblock[47] and triblock copolymers[84].

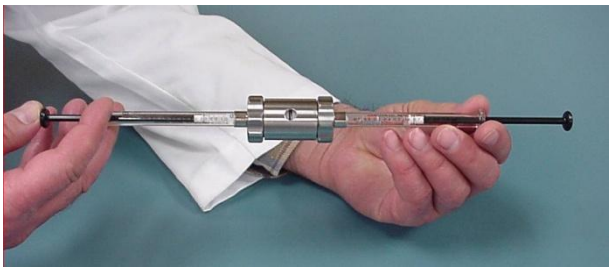

Figure 9. Extruder used for the production of large unilamellar vesicles. Figure from [85].

Extrusion typically produces large unilamellar vesicles. The most common instrumentation for preparation of extruded vesicles is an extruder (Fig. 9). The MLV solution is placed in the extruder and forced through a polycarbonate membrane with a defined pore size. This yields LUVs with a diameter similar to the pore diameter used and the size is quite reproducible from batch to batch. Prior to extrusion, MLV solutions are prefiltered though a larger pore size (typically 0.2 µm-1 µm) or submitted to several freeze-thaw cycles to make a homogeneous solution and reduce fouling of the polycarbonate membrane[82]. Extrusion has been used to obtain polymersomes from diblock[47] and triblock copolymers[50].

Giant unilamellar vesicles can be formed by the electroformation method. In this method the lipids[86], diblock copolymers[46, 87] or triblock copolymers[50, 88] are dissolved in an organic solvent such as chloroform and sprayed onto electrodes. The organic solvent is removed under nitrogen gas. The electrodes are immersed in aqueous buffer and GUVs are formed by applying an ac voltage, typically around 3V (1-10 Hz) for lipids[47] and around 10V (5-10 Hz) for block copolymers[89].

The third format of biomimetic membranes is planar supported membranes (Fig. 3C). Planar supported lipid membranes on a solid support can be made by Langmuir-Blodgett (vertical) transfer followed by Langmuir-Schaefer (horizontal) transfer from a water-air interface (Fig. 10A)[90] or through vesicle collapse (Fig. 10B)[66]. The first deposition method generally results in

fault-free micron-sized bilayers whereas the vesicle deposition method requires tuning of conditions to obtain micro-sized fault-free bilayer areas[13]. A combination of the Langmuir-Blodgett technique followed by vesicle fusion has also been used[91]. For vesicle collapse, the solid supports must be hydrophilic, and common support materials include silica[14-16, 19, 92], borosilicate glass[19, 93] and freshly cleaved mica[17, 18].

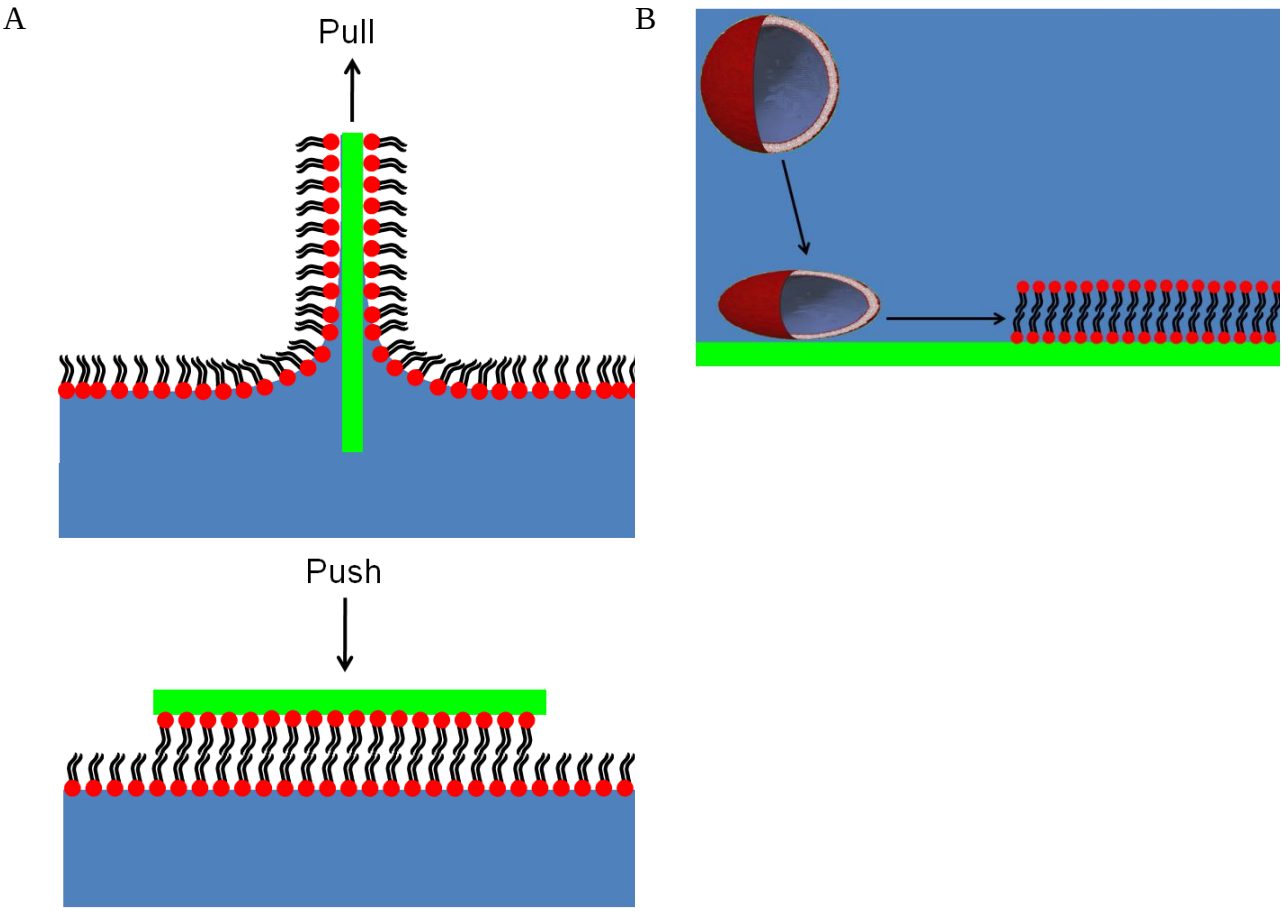

Figure 10. Techniques for forming supported lipid bilayers. (A) A hydrophilic substrate is pulled vertically through a lipid monolayer spread at an air-water interface (Langmuir-Blodgett technique), followed by horizontally pushing it through another lipid monolayer (Langmuir-Schaefer technique). (B) Vesicles in solution adsorb and spontaneously fuse to the hydrophilic surface to form a solid-supported lipid bilayer.

Solid-supported planar diblock copolymer bilayers have been made by Langmuir-Blodgett transfer followed by Langmuir-Schaefer transfer[58] or by vesicle deposition[94]. Supported planar triblock copolymer monolayers have been made by Langmuir-Blodgett transfer[95, 96] or by vesicle deposition, where a charged polymer was used to induce vesicle rupture[97]. However, the high rupture strength of triblock copolymer vesicles presents difficulty with using this method for

uncharged polymers. Solid-supported, planar triblock copolymer membranes have also been made by a ”grafting from” synthesis on a gold surface[98]. The “grafting from” approach is a method used to tether polymers on a solid substrate surface. The initiators are immobilized onto the surface followed by *in situ* surface-initiated polymerization to generate tethered polymers[99]. However, the ”grafting from” approach gives rise to highly packed polymer chains with a low membrane fluidity, which could reduce protein incorporation[100].

In general, protein incorporation into biomimetic membranes is difficult. At this point I will overview state-of-the-art in protein incorporation into biomimetic membranes.

3.4. Protein incorporation into biomimetic membranes

Protein incorporation during membrane formation

Some of the above-mentioned techniques for creating biomimetic membranes are compatible with incorporation of protein during membrane creation, whereas for others protein reconstitution is carried out after the membrane is formed. Also, at which stage the protein is added depends on the experimental requirements. Often, proteins are incorporated after membrane formation in order to be able to confirm, quantify or characterize their insertion. For a long time, lipid membranes have enjoyed the spotlight in the biomimetic membrane field, but recently protein incorporation into polymeric membranes has started to emerge. Interestingly, this was often despite a mismatch between the hydrophobic block of the polymer and the hydrophobic band of the membrane protein[51]. An explanation put forward for why these proteins are still functional within the polymeric membrane is that the flexibility of the hydrophobic block as well as its polydispersity give rise to regions with a matching hydrophobic thickness in the vicinity of the protein[101]. These systems are expected to have better stability than lipid-based systems, but may experience lower protein incorporation due to the thickness mismatch. I will first discuss protein incorporation that can be carried out in lipid and polymer membranes (free-standing, vesicular or planar supported) during membrane creation.

Free-standing lipid and polymer membranes (Fig. 3A) require the addition of solvent to create the membrane. Some robust peptides (e.g. gramicidin[67]) and proteins (e.g. pig surfactant protein type 1[102]) can withstand this and be added directly to the membrane forming solution (lipid or

polymer dissolved in solvent). Most transmembrane proteins, however, would be denatured by this treatment and can not be added during bilayer formation. These are added by other methods to the formed free-standing membranes.

To incorporate transmembrane peptides and proteins into vesicles (Fig. 3B), the proteins are first purified and then solubilized with detergent[103]. The purification and stabilization procedure involves several steps that must be optimized for each protein to be incorporated[13].

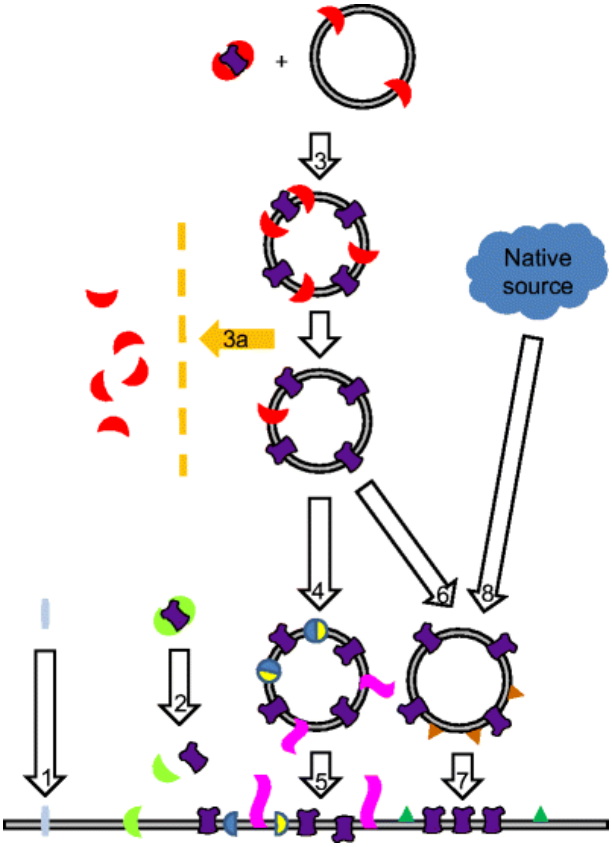

Figure 11. Strategies for incorporating transmembrane proteins into planar lipid and polymeric membranes. Small peptides (light blue) may be inserted directly from solution (arrow 1) to the membrane (grey). Some proteins (purple) can be inserted with the aid of a suitable detergent (green). When the detergent concentration is brought below the critical micelle concentration the protein is free and inserts (arrow 2), leaving small amounts of detergent in the membrane. Many proteins are prepared in detergent (red) and mixed with liposomes (grey circles) containing detergent (arrow 3). Detergents are then removed by dialysis (arrow 3a). The resulting proteoliposomes can be modified with fusion promoters (arrow 4) and fused with the membrane (arrow 5). Fusion can be confirmed via various assays, e.g. the nystatin/ergosterol (yellow/blue semicircles) assay. Fusion (arrow 7) may be promoted by having charged amphiphiles (brown and green triangles), e.g. anionic PS lipids and cationic DOTAP in the interfaces (arrow 6) or with the aid of fusion peptides (pink). Proteoliposomes may also be obtained directly from native sources (dark blue shape) (arrow 8). Figure from [13].

The solubilized proteins are then mixed with liposomes containing a small percentage of detergent (Fig. 11 arrow 3). Thereafter, detergents are removed by dialysis (Fig. 11 arrow 3a)[103] or with the aid of macroporous polymeric spheres (biobeads)[104], resulting in proteoliposomes. Although incorporation of proteins into proteoliposomes has been dominant in the biomimetic membrane field, recently successful reconstitution of proteins into polymersomes made from triblock copolymers has been achieved[62, 89, 105-109]. Incorporation of protein into polymersomes in these cases was carried out by using drop-wise addition of polymer-protein-ethanol solutions to the aqueous phase. However the use of solvent can be detrimental to protein stability[13]. Solvent-free protein reconstitution into triblock polymersomes has also recently been achieved[49, 110, 111]. Interaction of the peptide alamethicin (but not transmembrane penetration) with diblock copolymer vesicle membranes has been reported[112]. Suprisingly, protein incorporation into diblock copolymer membranes has not been shown (or at least published yet), but in principle it should work, because these membranes are structurally similar to lipid bilayers with a hydrophilic-hydrophobic-hydrophilic environment and the possibility to obtain a similar membrane thickness.

Planar supported membranes (Fig. 3C) are made, as mentioned above, by the Langmuir-Blodgett (LB) and Langmuir-Schaefer (LS) technique or by vesicle deposition. Proteins can be incorporated into the vesicles which are used for vesicle deposition as described above. The proteoliposomes are subsequently collapsed on a solid support surface. This is the most common method for forming solid-supported lipid membranes. A drawback of solid-supported lipid membranes is that the distance between the lipid membrane and the support is less than 2 nm[23] and the inserted protein which can typically extend up to tens of nm from the membrane[23] hits the surface and becomes denatured or immobilized. This problem has been addressed by increasing the distance to the surface by adding a non-covalently bound spacer layer[64] (Fig. 4A), a tethered spacer layer[65, 113-115] (Fig. 4B) or by using a nanoporous support[20, 25] (Fig. 4C). The spacer layer is typically a cushioning polymer layer[64], such as poly(ethylene glycol)[116] or polyelectrolytes[55, 117-120]. For reviews of polymer-supported planar lipid membranes, see [30, 64, 121, 122]. Another approach, which is less common, is to tether the proteins on to a surface and then subsequently construct a lipid environment around them[123, 124]. However, this approach requires that the protein is stable during immobilization before lipid is added.

The second common technqiue for creating planar supported lipid bilayers is the LB/LS technique. It is difficult to incorporate transmembrane proteins into the lipid bilayer with this technique, because prior to transfer portions of the proteins within the monolayer are exposed to air and can become irreversibly denatured[30]. This should also apply to membranes created from diblock copolymers by LB and LS techniques, since these would (similarly to lipids) form a monolayer at the air-water interface and could irreversibly denature incorporated transmembrane proteins. However, recent work has shown that by using triblock copolymers, it is possible to obtain Langmuir films composed of ABA monolayers at the air-water interface with the hydrophilic A-block uppermost and that this orientation is preserved upon transfer to a gold substrate[96]. This construct resembles a lipid bilayer and the authors demonstrate incorporation of functional transmembrane proteins (bacteriorhodopsin and cytochrome oxidase)[96]. This work is at odds with an article by Haefele *et al*[125] which shows that ABA monolayers at the air-water interface consist of ”U-turn” ABA monomers, which have both of their hydrophilic chains in the aqueous phase (Fig. 12).

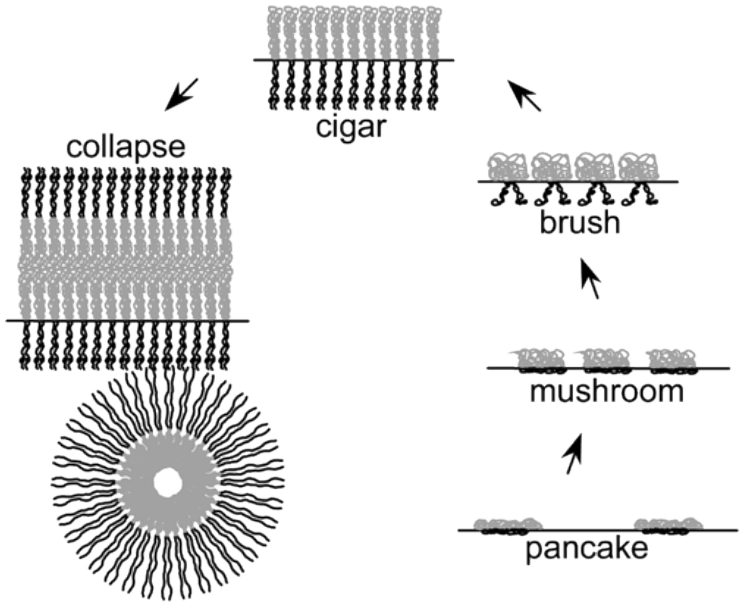

Figure 12. A schematic representation of ABA Langmuir film organization during polymer monolayer compression at the air-water interface. The lowest surface pressure is for the pancake conformation and increases counterclockwise. The bottom phase is an aqueous solution and the top phase is air. Hydrophobic and hydrophilic blocks are depicted in grey and black, respectively. Figure from [125].

With increased pressure, the hydrophobic and hydrophilic chains become more and more stretched out, until at high surface pressures, the monolayer collapses and flips so that the hydrophilic A-block is uppermost, but then directly curls up to form micelles. Another limitation of the LB/LS techniques for transmembrane protein incorporation is that even if it is possible to obtain the correct ABA conformation at the air-water interface, high surface pressure is required to do so. At high pressure Langmuir-Blodgett copolymer films become densely packed[125], which may reduce transmembrane protein incorporation and/or lead to denaturation of transmembrane proteins. Also, relatively large quantities of proteins would be required for incorporation by this method[91].

Protein incorporation after membrane formation

Various strategies are used for incorporation of membrane proteins into preformed lipid or polymer biomimetic membranes. These are explained thoroughly in a review by Nielsen[13]. Small hydrophobic molecules and peptides (e.g. gramicidin and alamethicin) can directly insert into free-standing or supported lipid[126] and polymer[61, 127] membranes from solution (Fig.11 arrow 1). Some proteins can be solubilized in a detergent (such as Triton X-100) above the detergent's critical micelle concentration (CMC) and be inserted by dilution below the CMC leading to release of free protein and incorporation of the protein into planar (free-standing or supported) lipid membranes[128] (Fig.11 arrow 2). Insertion of proteins by this method has been demonstrated for black triblock copolymer membranes[48, 127] and planar supported triblock copolymer membranes[96].

However, most large transmembrane proteins can only be added by inserting them into proteoliposomes (Fig.11 arrow 3) or obtaining proteoliposomes from native sources (Fig. 11 arrow 8), and subsequently fusing these proteoliposomes with the planar lipid membrane (Fig. 11 arrows 5 and 7)[13, 129]. Insertion of transmembrane proteins into liposomes and polymersomes was addressed in the above section.

Fusion of protein-containing vesicles with the planar membrane can be confirmed via various assays, such as the nystatin/ergosterol assay[130]. In this assay, vesicles containing nystatin,

ergosterol and the transmembrane protein to be delivered are fused to a planar ergosterol-free lipid membrane. Nystatin monomers assemble to form ion channels, which are stabilized at the edges of ergosterol-rich domains[131]. Upon fusion, ergosterol diffuses away into the excess lipid matrix and the nystatin channels dissociate. Voltage clamp electrophysiology is used to monitor fusion events, which can be observed as characteristic conductance spikes followed by a slow decrease in conductance as the nystatin channels gradually dissociate (Fig. 13). Vesicle fusion can be enhanced by using charged lipids, e.g. by using anionic lipids (e.g. lipids with phosphatidylserine headgroups) in the vesicles and cationic lipids (e.g. 1,2-dioleoyl-3-trimethylammoniumpropane (DOTAP)) in the planar membrane[132]. Fusion can also be promoted by applying an osmotic gradient[131, 133], by polymer-induced crowding[133, 134] or by fusion-inducing proteins (e.g. Soluble *N*-ethylmaleimide-sensitive-factor attachment protein receptor (SNARE) complexes)[135].

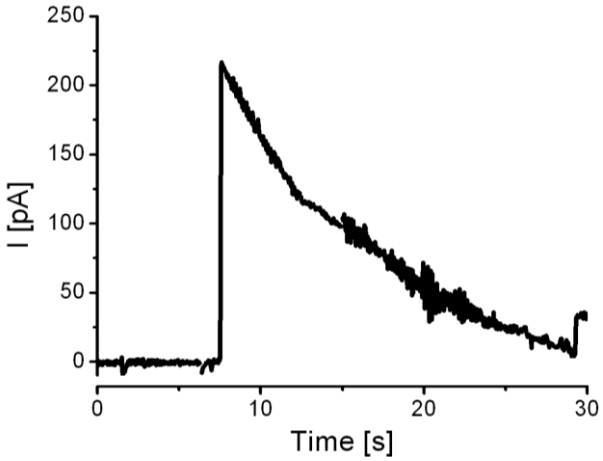

Figure 13. Bilayer current versus time observed for a nystatin/ergosterol vesicle fusion with a planar lipid bilayer showing the characteristic "current spike", followed by a slow decrease in conductance as the nystatin monomers dissociate, causing collapse of the ion channels. Vesicle composition was 8 mg/ml POPE:POPS:POPC:Ergosterol (45:25:20:10 mol:mol) with 50 µg/ml incorporated nystatin in 1.2 osmolar buffer. Vesicles were extruded through 200 nm filters. The receiving membrane composition was 25 mg/ml DPhPC:DOTAP (80:20 mol:mol) in decane. Membranes were painted on 8x8 aperture arrays in ETFE (aperture diameter 300 µm). Osmolarity of the buffer in the cis chamber to which vesicles were added was raised to 3 Osm after vesicle addition. Osmolarity of buffer in the trans chamber was 436 mOsm. A 60mV DC potential was applied across the membrane and the signal filtered at 20 Hz. Figure from Ibragimova and Rein, unpublished results.

3.5. Stabilization of biomimetic membranes

Challenges with poor membrane stability still need to be met in order to create commercially viable biomimetic membrane-based technologies. In this section, I will provide an overview of the strengths and weaknesses of the various formats of biomimetic membrane and how they can be stabilized.

Solid-supported membranes

Solid-supported membranes are *per se* favoured due to their stability and robustness[30]. Another advantage of solid-supported membranes is that they can are accessible for study by a plethora of powerful analytical techniques that are surface-specific (such as quartz crystal microbalance with dissipation, fluorescence recovery after photobleaching, atomic force microscopy, electrochemical impedance spectroscopy, surface plasmon resonance, etc[13, 30, 122]). However, the choice of substrate used for supporting biomimetic membranes is somewhat limited. In order to support a high quality membrane with few membrane defects and high lipid mobility the surface should be hydrophilic, smooth, and clean[30]. Commonly used solid supports for biomimetic membranes include silica[14-16], freshly cleaved mica[17, 18], silicon nitride[20] and gold[22, 136, 137]. Other supports which have been used include titanium oxide[138, 139], indium-tin oxide[140], silver[141], alumina[21, 142] and platinum[143]. These systems in their basic form also have a severe drawback, namely denaturation of most integral membrane proteins due to limited space between the lipid membrane and the solid support[23]. Also, solid-supported membranes provide access to only one side of the membrane[144]. Another drawback, which effectively eliminated the use of these substrates in the "*Industrial biomimetic water membranes"* project, is that the limited aqueous compartment on the support side of the membrane limits bulk transport of water, ions and solutes across the membrane[13, 24], making it incompatible with separation applications[13].

Polymer-supported membranes

A solution used to address denaturation of proteins on a solid support is to decouple the biomimetic membrane from the support by a polymeric cushion layer (see Fig. 4A, Fig. 4B). This system still provides a good support for the membrane and can be studied by surface-senstive techniques, while reducing the risk of integral protein denaturation[30, 64]. An important criterion when choosing an appropriate polymer is that the supported membrane must be

thermodynamically and mechanically stable. This requires careful adjustment of the wetting behaviour at the surface-polymer interface, the surface-membrane interface and the membrane-polymer interface[64]. The surface-polymer-membrane system is only stable if there is complete wetting between the surface and the hydrated polymer, and between the membrane and the hydrated polymer and the membrane-surface interaction is repulsive. In this way, polymer cushions mimic the extracellular matrix and the cell-surface glycocalyx, which maintain distinct distances between neighbouring cells. An alternative for stabilizing the system is to covalently attach the polymer layer to the substrate and/or to covalently attach the lipid membrane to the polymer layer. Desirable properties for the polymer support are that it should be soft, hydrophilic, not too highly charged, and not extensively cross-linked[145]. Polymer supports that have been explored include dextran[146, 147], cellulose[148], chitosan[149-151], polyacrylamide[65], polyelectrolytes[117, 151-154] and lipopolymers[113, 115, 155-159]. Polyelectrolytes and lipopolymes are popular choices for the cushion material. Polyelectrolytes can be adsorbed from solution onto a variety of substrates (such as mica[160] and quartz[153, 161] or on gold via mercaptoundecanoic acid[152, 154]) by layer-by-layer deposition, and allow control over the resulting film thickness by choosing the number of layers deposited. A disadvantage of polyelectrolytes is that the strength of the attractive forces to the support is based on electrostatic interactions and is thus influenced by the ionic strength and pH of the solution, placing limitations on the experimental conditions that can be used. Also, too much charge can adversely affect the function and mobility of membrane constituents and incorporated proteins[30]. Lipopolymers consist of a soft hydrophilic polymer layer with lipid-like molecules at their surface which can insert into a phospholipid membrane and tether it to the polymer spacer. They are less affected by solution conditions than polyelectrolytes, but can interfere with lipid and protein mobility in the membrane depending on the degree of tethering[113]. However, for the *"Industrial biomimetic water membranes"* project, polymer-supported membranes were not usable as they do not solve the issue of limited transmembrane transport.

Membranes on a nanoporous support

The use of biomimetic membranes in separation applications requires a massive flux across the biomimetic membrane. Problems with bulk transport and transmembrane protein denaturation can be addressed by making porous substrates. For planar bilayers, this implies that the support

must be sufficiently porous in order to allow substantial flow while being dense enough to support the membrane. Some of the substrates used for solid-supported membranes (such as silicon nitride[20], silicon[25, 26], silica[162] and alumina[21, 27-29, 163]) have been made porous and free-standing lipid membranes have been created across the pores (Figs. 14A and 4C). However, problems with membrane coverage, leak currents across the membrane[24] or membrane functionality[9, 30] remained to be resolved. Most importantly for the "*Industrial biomimetic water membranes"* project, using materials such as mica, silica and gold for stabilization of biomimetic membranes and the fabrication techniques for producing the aperture arrays in them would not be cost-effective for square meter areas and could therefore not be used for commercial separation applications.

In general flat, hydrophilic supports such as silica, mica and gold have been favoured for lipid bilayer formation and stabilization, because stable membranes could be formed on these substrates and because these substrates are compatible with a number of analytical techniques (as discussed earlier). Novel applications of biomimetic lipid bilayers, such as commercial separation applications, have created a demand for novel substrates which are cheap, porous and not necessarily atomically flat. Novel porous substrates that are capable of supporting lipid bilayers are emerging and some examples include nanofiltration membranes[164], microfiltration membranes[165-168], agar[169], agarose[43, 44, 169-173] and silica xerogel[174, 175]. In this thesis, two nanoporous polymeric substrates that are compatible with bulk transport across the membrane as well as relatively easy and cheap to produce were introduced as membrane supports. These substrates were polybutadiene-polydimethylsiloxane (PB-PDMS) and poly(2-hydroxyethyl methacrylate) (polyHEMA). These substrates are more corrugated than the typical flat silica, mica and gold substrates and therefore presented an interesting challenge in creating stable membranes.

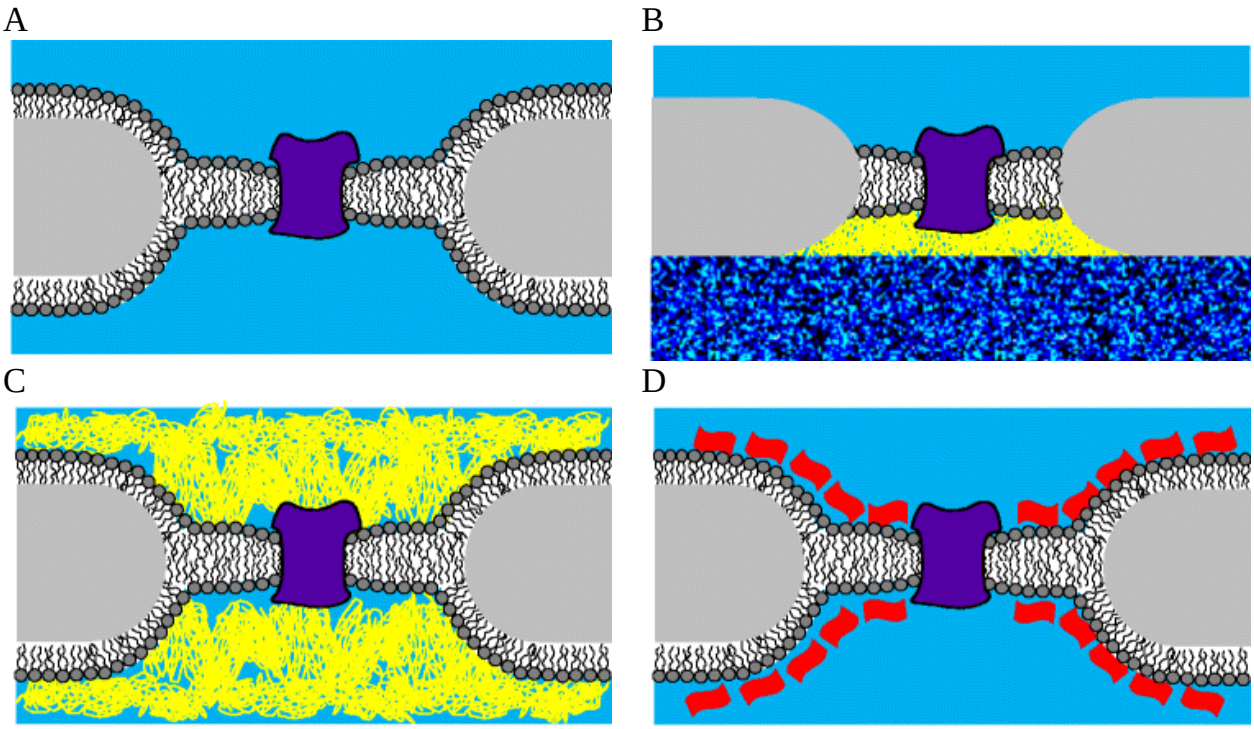

Figure 14. Cross-sectional representations of porous-supported biomimetic membranes with an incorporated transmembrane protein (purple). (A) Free-standing biomimetic membrane formed across a porous support (such as ETFE[67] or silica[162]). The membrane (solvent-free or solvent-containing) is formed in an aperture (light grey). (B) A biomimetic membrane formed across a porous support and supported by a porous cushion (dark blue). (C) Hydrogel-encapsulated biomimetic membrane. The hydrogel polymer meshwork (yellow) is formed *in situ* around the biomimetic membrane. (D) A surface layer-encapsulated biomimetic membrane. The monomolecular layer of protein (red) self-assembles into a two-dimensional lattice creating identical pores 2–8 nm in diameter[179]. Figure from [13].

PB-PDMS is a versatile material, because many of its properties (such as porosity, geometry, hydrophobicity and roughness) can be modified. PB-PDMS can self-organize into a variety of nanoscale morphologies[176] (such as a gyroid morphology[177]), which is maintained after cross-linking. Subsequently, the PDMS block can be etched away with hydrogen fluoride[177] or tetrabutylammonium fluoride[178] to obtain a porous structure which makes the material compatible with separation applications[177]. The hydrophobic, nanoporous PB substrate can be made hydrophilic (both on the surface and/or within the pores) by photooxidation[57], making it suitable as a biomimetic membrane support. In this thesis, I will present planar lipid bilayer formation by the vesicle deposition method on the hydrophilic polybutadiene support (Fig. 1C).

A nanoporous substrate comprising polyHEMA, PEG-DMA and silica beads is also presented in this thesis. The presence of silica particles in the polymer hydrogel greatly enhances both the

mechanical stability of the gel and the flux of water through the hydrogel[120] and the substrate permeability can be modulated by the amount of silica present in the hydrogel composite[120]. These properties make the composite polymer material suitable for separation applications. The substrate was used as a support for an ETFE-suspended lipid membrane array created by the painting method (Figs. 1B and 14B). Surface-functionalization of the ETFE enabled covalent coupling of the composite polyHEMA substrate and the ETFE support, which we showed to give a drastic improvement of lipid membrane longevity and effective functional area.

Free-standing membrane (on a microporous support)

Black lipid membranes are suspended across an aperture in solution and have no unwanted interactions with an underlying support (Fig. 14A). This means that transmembrane proteins embedded within the lipid bilayer remain fully mobile and functional[30]. Other advantages of free-standing membranes are also that both membrane leaflets are accessible and that bulk transport across the membrane is feasible. Fewer analytical methods are currently used for studying black lipid membranes than those available for supported membranes, and these typically include electrical measurements and fluorescence microscopy[9]. Also, since the membrane lacks a support, it suffers from poor stability which limits the lifetime of the lipid bilayer[30]. A free-standing lipid bilayer with incorporated proteins formed across an aperture is not sufficiently stable to be used in a technological separation device[13].

The inherent instability of free-standing lipid membranes is best explained by examining the dimensions of the system. The lipid bilayer has a thickness of 4-10 nm[33, 34], whereas an aperture in the partition scaffold has a thickness of circa 20-200 μm, which means that the lipid membrane has to compensate for more than a 1000-fold difference in thickness to span the aperture. The role of the solvent is to help the membrane to match the height of the aperture by forming an annulus around the perimeter of the aperture[35]. The solvent slowly diffuses from the annulus, which is believe to cause membrane destabilization over time and eventually lead to membrane collapse[36, 37]. Membrane stability can be increased by decreasing the aperture diameter[9, 20, 25, 45]. However, in smaller apertures, the solvent torus takes up a larger percent of the aperture area and the functional membrane area is reduced[9].

Advances in lipid polymerization chemistry have given rise to new biomimetic membrane components[180] which can improve the stability of free-standing membranes. These include polymerizable lipids with reactive moieties in the headgoup[36, 67] or acyl chain region[68, 144, 181-184]. These are used to crosslink the lipids to create stable biomimetic structures. Shenoy *et al* found some limitations regarding which polymerizable lipids easily form BLMs and atrributed this to the propensity of the lipids to phase-separate into domains and to the surface elasticity of the films (estimated from LB monolayer pressure-area isotherms)[144]. Heitz *et al* found that membrane fluidity was reduced by the use of acyl chain-polymerizable lipids, and showed that it can be increased by using a mixture of polymerizable and nonpolymerizable lipids[183]. They also found that lipid cross-linking near the headgroup provides the best combination of BLM electrical integrity, stability, and maintenance of α-hemolysin (α-HL) activity[181]. The use of acyl chain-crosslinkable lipids increased BLM lifetime more than twenty-fold[183]. A drawback of these lipids is that they need to be handled in yellow light (placing special requirements on the laboratory conditions) before polymerization to avoid autopolymerization[181].

Another approach for stabilization of free-standing membranes could be to use crosslinkable organic solvents. Although this approach was demonstrated for proteoliposomes[69], it may work for free-standing membranes as well. This stabilization approach was shown by Graff *et al*, who formed proteoliposomes and allowed them to swell with solvent, which inserted between the lipid monolayers. They showed that the lipid membranes maintained their lateral mobility, while their stability was improved. Some issues remain to be addressed. Proof is needed that this stabilization method is generally compatible with the presence of active embedded transmembrane proteins. The authors demonstrated that OmpF channel activity was preserved after polymerization of the solvent. However, OmpF is a robust protein, because it is a β-barrel protein[59, 185], so the approach needs to be addressed with a more ”fragile” protein as well. Additionally, the authors show that polymerization of the solvent reduces OmpF activity and speculate that this is due to expulsion or closure of some of the reconstituted proteins due to the internal stress in the membrane caused by crosslinking[69]. This suggests that activity of other incorporated proteins should be reduced as well. Also, the presence of solvent in the membrane should increase membrane thickness and result in a hydrophobic mismatch between the

hydrophobic part of the membrane and the hydrophobic domain of the embedded transmembrane protein, which should influence protein incorporation and functionality.

Another interesting approach to improve membrane stability is to use lipids from organisms from Archaea, because they live in extreme environments such as high temperatures and low pH[70]. Many Archaean membranes are formed from bolalipids[71], which span the membrane and in this way increase structural stability[72]. An intriguing way to improve the stability of biomimetic membranes is to replace lipids with lipid-bilayer-like amphiphilic block copolymers, namely diblock[46] or triblock[62] copolymers. Block copolymers have been used to create black polymer membranes[61], polymersomes[46, 62] and supported polymer membranes[58, 97, 98]. Block copolymers are chemically and mechanically stable[46, 47] and provide an amphiphilic structure that allows incorporation of membrane proteins[48]. There are also many possibilities for engineering block copolymer membranes to achieve the desired combination of properties by adjusting parameters such as the block length, molecular weight, chemical composition, hydrophilic/hydrophobic balance and molecular architecture[58]. The stability of block copolymer membranes is accredited to that they have a higher thickness than lipid membranes[49, 50]. However, this may be a drawback in terms of lower functional transmembrane protein incorporation compared to a lipid bilayer due to a hydrophobic mismatch between the hydrophobic block of the polymer and the hydrophobic band of the membrane protein[51]. A promising compromise could be to mix lipids and polymers to obtain their favourable qualities – high stability gained from the polymer and a protein-favourable environment provided by the lipids. In this thesis, I present a method for making planar mixed lipid-polymer vesicular membranes and producing planar membranes from these on solid substrates.

Encapsulation of free-standing membranes

Potential for stabilization of free-standing biomimetic membranes has also been demonstrated by encapsulation strategies using hydrogels[36, 40-42, 67, 186] (Figs. 1A and 14C) and bacterial surface layers (S-layers, Fig. 14D)[147, 167, 187-191]. The encapsulated free-standing membranes gain stability and are compatible with bulk transmembrane flux. Hydrogels are based on an aqueous gelling solution which contains monomers and polymerization initators. They polymerize to form gels that are highly absorbent with a flexibility determined by the polymer and the degree of

crosslinking. The hydrogel-encapsulation strategy involves bilayer formation in a hydrogel precursor solution, followed by crosslinking (driven by chemical initiation, photoinitiation or thermal initiation) which results in a lipid bilayer that is tightly sandwiched within the hydrogel. This approach has been shown to be compatible with incorporation of α-hemolysin, a polypeptide which forms heptameric pores in lipid membranes, in the membrane and channel currents could be measured up to three weeks after membrane formation[42]. In this thesis, I have investigated the hydrogel-encapsulation approach for stabilizing biomimetic membrane arrays.

The S-layer approach (Fig. 14D) uses surface-layer proteins found on the exterior of walled bacteria[187]. S-layers typically consist of a single type of protein or glycoprotein and form lattice structures. They are added after lipid bilayer formation and assemble at lipid-water interfaces, and form a scaffold similar to that at the bacterial membrane. They can be added to one or both sides of the membrane[191]. The assembly is driven by electrostatic interaction between exposed carboxy groups on the inner face of the S-layer lattice and the zwitterionic lipid head groups. S-layer proteins can form very tight structures, with sieving properties[187]. Ionophores (such as valinomycin[189], alamethicin[167] and α-hemolysin[188]) have been shown to retain their functionality when incorporated in S-layer-supported lipid membranes. However, α-hemolysin could not be incorporated when added on the S-layer side due to the sieving properties of the S-layer lattice. S-layers were shown to increase the longevity[167] and mechanical stability of lipid membranes, but surprisingly they decreased the membranes' electrical stability (i.e. the applied transmembrane voltage that could be maintained before membrane rupture)[187].

Stabilization of arrays

To make a free-standing 4 nm thick biomimetic membrane that spans over a single aperture with an area of square meters is not feasible due to lack of stability. In order to realize a high-resistance membrane with a large area (square meters), one method is to use an aperture array with micron- or submicron-sized holes and span membranes across these apertures. For membrane arrays, as for single-aperture free-standing membranes, the membrane stability and longevity increase with a decrease in aperture size[45]. Membrane arrays with lifetimes exceeding 1 day have been created across submicron-aperture arrays in silicon nitride and silicon[20, 25].

Unfortunately, using square meters of these materials as well as fabrication of apertures for such large areas in them is not compatible with separation applications due to low cost-efficiency.

In principle, the same stabilization strategies as are used for single-aperture membranes should be applicable for stabilizing membrane arrays. Besides aperture diameter, parameters that affect the stability of a membrane array are the aperture-to-aperture distance[9], aperture rim shape and smoothness[38], the number of apertures[6] and their geometrical arrangement[9]. It has been suggested that membrane stability would be improved by placing apertures sufficiently close together, so that the membrane array can form a continuous, self-repairing membrane[9]. A smooth, round and uniform rim is believed to improve ease of membrane formation and membrane stability by stabilizing the contact between the lipid bilayer and the aperture rim[35, 38]. Control of the rim geometry and topography is also important for obtaining reproducible membrane characteristics. Intuitively, membrane stability should decrease as the number of apertures in the array is increased. Interestingly, Hansen *et al*[6] found that an increase in the number of apertures in a membrane array increased membrane longevity, which is ascribed to the fact that lipid transfer between neighbouring membranes gives a self-healing property to the membrane and that the membranes spanning the edge of the array have fewest neighbouring membranes and are more likely to rupture. By increasing the number of apertures in the array the percentage of "edge apertures" is decreased, which leads to membrane stabilization. Stabilizing membrane arrays is challenging, because the membrane area is much larger than the area of a single-aperture membrane and for separation applications, rupture of even a single membrane in the array is unacceptable. In the following chapters I will present advances in membrane array stabilization that were achieved in this thesis.

4. Encapsulation of membranes with hydrogel

In the ”*Industrial biomimetic water membranes*” project, we designed novel water filtration membranes which were based on free-standing lipid membranes painted across an aperture array as a biomimetic matrix for the aquaporin water channels. As outlined in the background, free-standing lipid membrane are accessible on both sides and are compatible with bulk transmembrane flux, but lack the stability necessary for separation applications. Several strategies for increasing the stability of free-standing biomimetic membranes were outlined in the background section.

4.1. Motivation for the encapsulation strategy

In the hydrogel encapsulation strategy, the lipid membrane array is created in a hydrogel precursor solution, which is subsequently crosslinked in order to place a hydrogel cushion on each side of the lipid bilayer (Figs. 1A and 14C, described in papers I and II and appendix II). We used this strategy for several reasons. Firstly, gels are appealing materials for membrane supports, because they can provide mechanical stability while giving the membrane access to a bulk aqueous environment, allowing transport of water, ions and analytes to incorporated transmembrane proteins.

The second advantage is conferred by using *in situ* polymerized gels instead of a precast gel slab. In this way, a defect-free high resistance biomimetic membrane array can be formed in the hydrogel precursor solution. The hydrogel monomers are hydrophilic and can interact with the polar groups of the lipids and lie close to them. Polymerization would thus make a gel which followed the contours of the preformed defect-free membrane instead of trying to create a defect-free membrane on a precast gel slab. The close interaction between the membrane and the gel achieved using the hydrogel-encapsulation method should provide a good support for the membrane and improve membrane longevity. Further modification of the lipid headgroup with an acrylate moiety was carried out to obtain covalent attachment of the gel to the membrane (similar to the strategy of tethering lipid membranes on polymer layers on a solid support).

The third advantage was that hydrogel encapsulation of the membrane confines the solvent in the annulus and slows down solvent diffusion out of the annulus[36]. Leakage of the solvent from the torus of the membrane to the aqueous phase leads to effective thinning of the membrane and a decrease in membrane stability over time[53]. Thus, containing the solvent should improve membrane stability as well. Furthermore, *in situ* hydrogel encapsulation of free-standing single aperture membranes has been shown to improve membrane stability and longevity[36, 40-42, 186].

4.2. Requirements for the gel

There were several requirements placed on the gel to make it compatible for a water filtration device. Firstly, the gel should be liquid at room temperature in order to be compatible with the method of making the membrane arrays[6]. Free-standing membranes are made by folding or painting and both methods require the presence of an aqueous compartment on each side of the lipid bilayer (Figs. 6 and 7). Secondly, the gel should be crosslinkable *in situ* at room temperature, in order to maintain the lipid membranes in the liquid crystalline state[54]. Crosslinking of gels can be initiated thermally[41, 42], chemically[36] or using photoinitiation[40]. The requirement of crosslinking at room temperature eliminated thermal initiation, leaving chemical initiation and photoinitiation as available options. Thirdly, the crosslinking process should not result in large gel volume changes as this would destabilize the biomimetic membrane. Fourth, the porosity of the encapsulating gel should be such that the gel can provide sufficient stability while preserving good water and solute permeabilities. Lastly, the hydrogel-encapsulation method should be compatible with incorporation of transmembrane proteins.

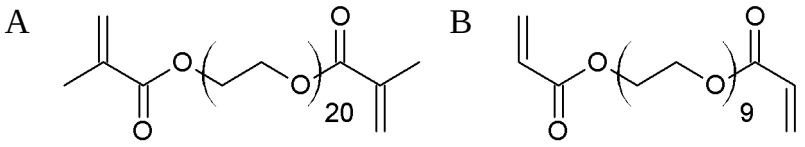

Figure 15. Chemical structures of polymers used for hydrogel encapsulation.. (A) Poly(ethylene glycol)-1000-dimethacrylate (PEG-1000-DMA), (B) Poly(ethylene glycol)-400-diacrylate (PEG-400-DA).

Hydrogels based on poly(ethylene glycol)-dimethacrylate (PEG-DMA) or poly(ethylene glycol)-diacrylate (PEG-DA) fulfill the first two requirements. I crosslinked these monomers (Fig. 15) either with the help of a chemical initiator or a photoinitiator (table 1). The chemical initiator used was ammonium persulfate (APS) and the catalyst N,N,N',N'-tetramethylethylenediamine

Table 1. The four hydrogel precursor solutions (HPSs) investigated. An X in front of the sample name signifies that the gel is crosslinked. Table from [67].

Sample	Polymer	Initiator
400 P	PEG-400-DA 100 mM	Darocur 5 mM
400C		TEMED 15 mM, APS 15 mM
1000P	PEG-1000-DMA 65 mM	Darocur 5 mM
1000C		TEMED 10 mM, APS 10 mM

(TEMED) was added. The photoinitiator used was 2-Hydroxy-2-methyl-1-phenylpropan-1-one (Darocur). For all hydrogels, concentrations of PEG and initiator were selected so that the hydrogels crosslinked within 10 minutes of initiation. I characterized the hydrogels shown in table 1 and showed successful hydrogel encapsulation of multiple BLMs formed across an aperture array in photoinitiated PEG-1000-DMA. The monomer forms a crosslinked polymer meshwork after gelation (Fig. 16).

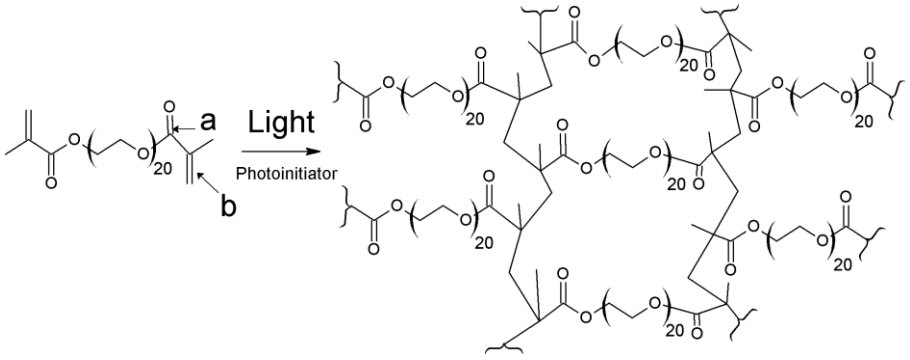

Figure 16. Chemical structure of PEG-1000-DMA and of a crosslinked PEG-1000-DMA meshwork found in the gel. Gelation occurs through radical polymerization in which the methacrylate groups participate in an addition reaction to form a branched polymeric network. The C=O (a) and C=C (b) bonds to which FTIR spectral peaks are assigned are indicated. Figure from [192].

4.3. Characterization of the hydrogels

In paper I the volumetric stability, water permeability and porosity of the gels were characterized. The crosslinking process should not cause large gel volume changes as this would destabilize the biomimetic membrane. We found that the gels shrink slightly upon crosslinking and that the change in volume does not exceed 1.2 vol%. They shrink further upon refrigeration (4 °C) from room temperature, but the final reduction in volume is less than 2.4 vol%. We

concluded that the hydrogels had volumetric stability, and were not likely to break membranes due to crosslinking.

Lipids are often kept as a stock solution in chloroform, but the chloroform is removed by nitrogen gas and further drying in a vacuum chamber and the lipid dissolved in another solvent, such as decane to make the bilayer forming solution. The gels were tested for compatibility with organic solvents which could be used in the bilayer forming solution (hexane, heptanes, octane, decane, dodecane, tetradecane, hexadecane or ethanol) or in the lipid stock solution (chloroform) to ensure that the hydrogel did not degrade due to interaction with solvent present in the lipid membrane. The gels did not show any visible disruption upon addition of organic solvents which could be used within the bilayer forming solution (Fig. 17A), but were broken down by chloroform (Fig. 17B). We concluded that the hydrogels were compatible out of a solvent point-of-view with membrane formation, as long as all traces of chloroform were removed.

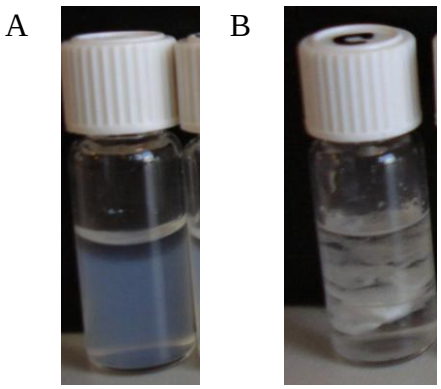

Figure 17. Solvent resistance of hydrogels. (A) A representative "good" gel sample, which did not show any visible break down of the gel upon addition of solvent. (B) A gel sample broken down by chloroform. Figure from Ibragimova, unpublished results.

Next, the transport properties of the different gels were analyzed to quantify transport of water, ions and small solutes through the gel. The gels had water permeabilities ranging between 30–150 $\cdot 10^{-12}$ $m.s^{-1}.Pa^{-1}$. Photoinitiated gels were less water permeable than chemically initiated gels with no correlation between the hydrogel PEG chain length and flux reduction. For comparison, the water permeability of a typical reverse osmosis (RO) membrane (the membranes that are used on the market for obtaining ultra pure water) is $5.6 \cdot 10^{-12}$ $m.s^{-1}.Pa^{-1}$ [12]. The water permeability still exceeded the permeability of a typical RO membrane at least five-fold. We

concluded that the hydrogels are not the permeability limiting factor in biomimetic separation devices, allowing the overall device permeability properties to be determined by the biomimetic membrane.

Transport of small solutes to the membrane is limited by gel pore size. The cut-off pore size of the gels was determined using PEG beads to be circa 10 kDa, corresponding to 7 nm pore diameter (determined by DLS) and circa 8 kDa for X1000P, corresponding to 6 nm pore diameter. Transport of ions through the gels was characterized using electrochemical impedance spectroscopy by our project partner in Malaga, and is the subject matter of the paper in Appendix II. They find that chemically initiated gels had higher average salt diffusional permeability $<Ps>$ ($1 \cdot 10^{-7}$ m/s) than photocrosslinked ($3 \cdot 10^{-8}$ m/s) hydrogels. The $<Ps>$ of the chemically initiated gels is only 3-7 fold less than what has been reported for microfiltration polysulfone membranes with a nominal pore size of 200 nm[193], which is much larger than the nm size pores for the gels and reflects the high water content of the gels. The paper in Appendix II shows that hydrogel electrochemical properties can be controlled by the choice of polymer and type of crosslinking used, and that their salt permeability properties are compatible with the use of hydrogels for biomimetic membrane encapsulation.

Furthermore, variation of photocrosslinking time was an additional parameter that could be used to tailor gel properties of photoinitiated gels, as is described in paper II. We showed in paper II that the water content of the gel can be varied from 50-90 wt%, which could be relevant for the gel's flux properties, the gel's interactions with lipid membranes, as well as for long-term use, handling and shipping of a hydrogel-encapsulated membrane. Also, the specific resistance of the photoinitiated gels depended on the photocrosslinking time and could be varied between 0.8-3.5 Ωm. For comparison, phosphate buffered saline has a resistivity of 8.4 Ωm (Ibragimova, unpublished results) and deionized water has a resistivity of $1.8 \cdot 10^{5}$ Ωm[1]. This showed that the gel had a low resistivity (and a high conductivity) and thus that ion channel containing hydrogel-encapsulated membranes are compatible with biosensor applications. Using Fourier Transform Infrared Spectroscopy to analyze dried gels (C=C and C=O peaks for the gel coincided with peaks for water), we observed a characteristic peak shift in the C=O groups from the methacrylate moieties (Fig. 16 arrow a) due to crosslinking. We found that a crosslinking time of

at least 6 minutes was necessary to obtain a fully crosslinked gel, as evidenced by the position of the C=O peak and the reduction in the number of C=C bonds in the methacrylate moieties (Fig. 16 arrow b). Using Raman spectroscopy, we obtained a spectral signature of the hydrated gel, observed a decrease in peaks assigned to C=C bonds with an increase in crosslinking time (up to 10 minutes) and identified rest products from the photoinitiator for the gel crosslinked for 15 minutes. From this we concluded that an optimal crosslinking time for the gel was 6-10 minutes, and by varying the crosslinking time we could vary the gel's water content and resistivity. With FTIR and RS we identified spectral features of the hydrogel, which may be applicable as a diagnostic tool to study changes in the gel due to variation in parameters.

4.4. Membrane formation and encapsulation with hydrogel

Having established that the PEG-DMA- and PEG-DA-based hydrogels have mesh size, water flux, ion flux, solvent resistance and volumetric stability parameters compatible with their use as encapsulation material, I investigated *in situ* encapsulation of biomimetic lipid membranes. The membranes were created in an 8x8 aperture array in ETFE by the painting method, with the aqueous compartments filled with hydrogel precursor solution (Fig. 18). After membrane formation, the hydrogel precursor solution was polymerized *in situ*, to form a gel around the lipid membrane array. I selected to use photoinitiated hydrogels for membrane encapsulation for several reasons. Firstly, the initiator can be added directly to the HPS yielding a homogeneous distribution of initiator without spontaneous onset of polymerization, whereas the chemical initiator had to be added after membrane formation to avoid polymerization of the gel before the membrane was formed. This meant that proper mixing was not possible and the initiator could not be homogeneously distributed. If the chemical initiator was added to the HPS before membrane formation, the timeframe within which a membrane could be formed was short (under 5 minutes) and the level of control over membrane formation was low since crosslinking started directly. Secondly, UV irradiation yielded precise control of the time point at which the polymerization reaction began, which increased controllability of membrane formation and improved the chance of a "good membrane" being formed. Thirdly, variation of photocrosslinking time was an additional parameter that could be used to tailor gel properties, as is described in paper II.

I characterized lipid membrane lifetimes in hydrogel precursor solutions. Two lipids, DPhPC (Fig. 5A) and DPhPE-acrylate (Fig. 5C) were used for membrane formation. DPhPC is a commonly used lipid for BLM formation[13] and DPhPE-acrylate had a crosslinkable headgroup, which should allow the gel to become covalently tethered to the lipid membrane upon crosslinking. We found that the stability of painted BLMs was drastically reduced in hydrogel precursor solutions compared to BLMs in buffer, with the majority of membranes rupturing within 5 minutes. We found that the destabilization is caused by the initiator, the presence of which affects BLM lifetime, but does not compromise BLM formation per se. The pre-encapsulation step, where both polymer and initiator are present, generally tends to destabilize the BLMs.

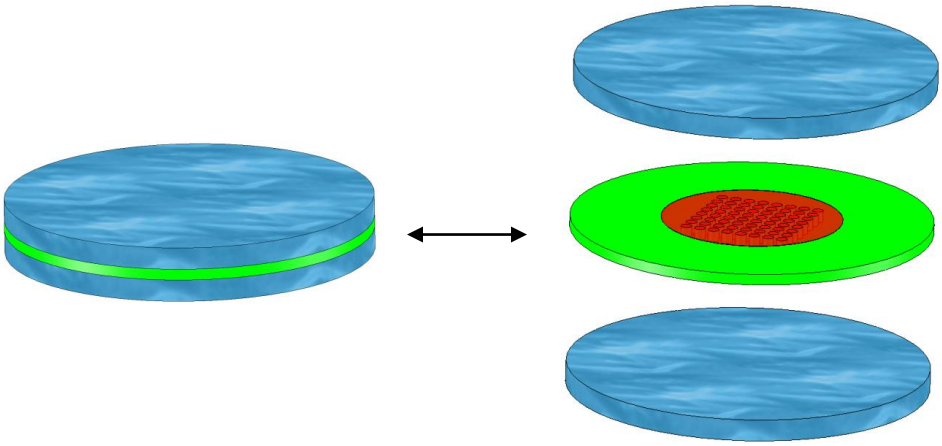

Figure 18. Schematic representation of the hydrogel-encapsulated lipid membrane (closed and exploded views). For BLM encapsulation BLMs (semi-transparent red circular area) are painted across the 8x8 aperture array in the ETFE partition (green disk) and encapsulated by hydrogel on both sides (blue disks). Figure from [67].

We selected PEG-1000-DMA instead of PEG-400-DA for encapsulation as it showed slightly better minimum lifetimes (although still very small) and concluded that due to the low stability of BLMs in HPS it is necessary to start the crosslinking immediately upon membrane formation. Several membranes ruptured during crosslinking. If they did not, the DPhPC BLMs survived for up to 1.5 days once they were encapsulated. DPhPE-acrylate membranes performed significantly better than DPhPC membranes with lifetimes ranging from 2 days (minimum) to 9 days. We performed a control experiment where the PEG-1000-DMA was omitted to deduce whether the stabilization effect was due to crosslinking of the lipid headgroups to each other or due to

covalent bonds forming between the lipid headgroups and the gel, and the results indicated that the stabilization effects were due to the presence of the gel. By tethering the membrane to the hydrogel, we obtain a support that is similar to a polymer-supported membrane on a solid surface, also making a biomimetic system that resembles a cytoskeleton-supported plasma membrane[36].

This is a novel stabilization strategy for supporting biomimetic membrane arrays, so it is difficult to directly compare to state-of-the-art. Stabilization of membrane arrays formed on aperture arrays in silicon (aperture diameter 300 nm) gave lifetimes of up to 24 hours[25] and lifetimes of up to 4 days were achieved in aperture arrays in silicon nitride (aperture diameter 200 nm)[20]. Although our apertures have a thousand-fold larger diameter, we still obtain higher membrane lifetimes. Some groups have used the hydrogel encapsulation strategy for stabilization of single-aperture membranes and shown that it improves membrane longevity. When comparing to these results, one should keep in mind that using single-aperture membranes, per se increases membrane stability compared to using a membrane array. Shim *et al* obtained up to 66 hour lifetime (2.8 days) for single-aperture (100 µm diameter) DPhPC membranes in an *in situ* polymerized agarose gel[41]. Jeon *et al* obtained lifetimes of up to 5 days for single-aperture (200 µm) PEG-DMA-encapsulated DPhPC membranes[40]. Malmstadt *et al* increased the lifetime of PEG-DMA-encapsulated single-aperture (200 µm) membranes to 11 days by using a mixture of DPhPC and headgroup crosslinkable acrylate-modified DPhPE lipids (20:1)[36]. Kang *et al* showed up to 3 week lifetime of agarose-encapsulated single aperture (100 µm) DPhPC membranes[42]. We obtained lifetimes of up to 9 days when we used headgroup crosslinkable lipids which could tether to the hydrogel, a system similar to that used by Malmstadt *et al*. The reason that we are able to obtain similar membrane lifetime (up to 9 days) as Malmstadt *et al* despite an almost 150-fold increase in membrane area (8x8 membrane aperture arrays, 300 µm diameter), could be because our lipid membranes consist entirely of headgroup-crosslinkable lipids that can tether the membrane more strongly to the hydrogel than if only one in twenty lipids is tetherable. Another factor that could improve the lifetime of our membranes is the presence of a rather large stabilizing solvent annulus (Fig. 19).

The electrical characteristics, namely the capacitance and conductance, of the hydrogel-encapsulated membranes were monitored using voltage-clamp measurements. The hydrogel-encapsulated membranes were electrically tight (conductance of circa 200 nS), and had similar conductance values to free-standing membranes. The capacitance values corresponded to an overall specific membrane capacitance of 0.035–0.088 μF.cm^{-2}, which is much lower than the specific capacitance for fully thinned solvent-containing membranes (0.4–0.6 μF.cm^{-2}) reported in the literature[53]. The low specific capacitance value measured does not preclude the existence of bilayer patches, but if they exist they only constitute 9–22% of the total aperture area and the rest of the aperture array area has solvent-containing lipid patches. This is consistent with the bright field image of the membrane arrays where large solvent annuli are clearly visible (Fig.19).

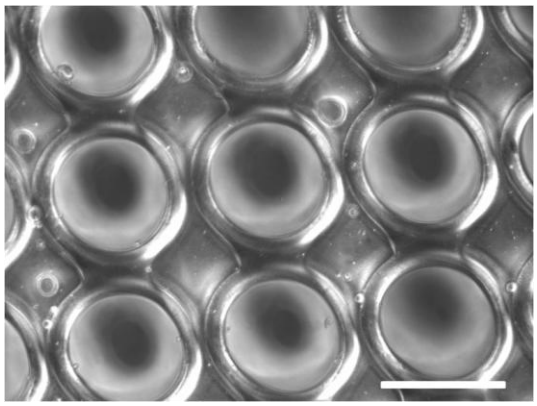

Figure 19. Optical microscope image of a hydrogel-encapsulated lipid membrane. showing lipid membranes with annular regions which reflect the existence of Plateau-Gibbs borders. Scale bar 300 μm. Figure from [67].

Of course, an optimized thinning of the BLMs would increase the effective bilayer area. It was not possible to thin the membranes after the crosslinking was completed. No spontaneous thinning (quantified by membrane capacitance) during UV exposure or after encapsulation in the gel was observed. The presence of X1000P seemed to ‘‘freeze’’ the membrane array, by stabilizing the solvent at the membrane boundary and protecting the membrane from rupture. Thus, membranes would need to be thinned before encapsulation. On the other hand this would also tend to make membranes even more unstable before crosslinking. Thus we are faced with a compromise between larger bilayer areas and reasonable BLM formation success rates and lifetimes.

4.5. Protein incorporation

We proved that we have areas where the lipid bilayer thickness is compatible with the hydrophobic spanning segments of transmembrane proteins by incorporating the channel-forming peptide gramicidin A into the BLMs followed by X1000P encapsulation (Fig. 20). We demonstrated single gramicidin channel currents in a 5-day old membrane. This also shows that the tethered membrane is sufficiently fluid to accommodate insertion of gramicidin.

Figure 20. Single channel gramicidin current trace from an X1000P-encapsulated 5 day old DPhPE-A membrane in buffer adjusted to 1M KCl. A 60mV DC potential was applied across the membrane and the signal filtered at 10 Hz. Figure from [67].

The hydrogel-encapsulation method is compatible with incorporation of small ionophores before crosslinking. Due to the short lifetimes of the BLMs in hydrogel precursor solution (<1 minute), methods of protein incorporation such as incorporation of detergent-stabilized protein from solution or delivery of protein by vesicle fusion cannot be efficiently used for delivery of transmembrane proteins to BLMs suspended in the hydrogel precursor solution. This entails that the peptide or protein that is incorporated should preferably to be added to the bilayer forming solution, which limits the choice of proteins that can be incorporated.

The gel's cut-off pore size was found to be 6 nm, which means that peptides can be added on top of the gel after crosslinking and should be able to diffuse to the membrane, as was shown for the PEG-1000-DMA gel with the 33.2 kDa[194] polypeptide α-hemolysin by other groups[36, 40]. Also the available bilayer area restricts incorporation of a large amount of protein. Bulky, sensitive proteins (such as aquaporins) need to be inserted into vesicles to be incorporated into BLMs and cannot be inserted by the hydrogel-encapsulation method as described here. For proteoliposome fusion with the BLMs to take place, it is necessary to improve stability of BLMs in the hydrogel precursor solution.

5. Membranes on a nanoporous hydrogel support

5.1. Motivation for the nanoporous hydrogel support strategy

The second strategy involved using a hard, flat, hydrophilic nanoporous substrate deposited under the ETFE partition as a support for BLMs (Figs. 1B and 14B). Lipid membranes were created across the apertures by the painting method and stabilized by the nanoporous support. This strategy has shown promise for supporting single-aperture-suspended BLMs with support materials made of precast agarose gels[43, 44, 171, 173, 195]. The nanoporous support presented here was a composite hydrogel formed by polymerization of an aqueous solution of 2-hydroxyethyl methacrylate (HEMA, Fig. 21A) and poly(ethylene glycol) dimethacrylate (PEG-DMA) in the presence of silicon dioxide beads.

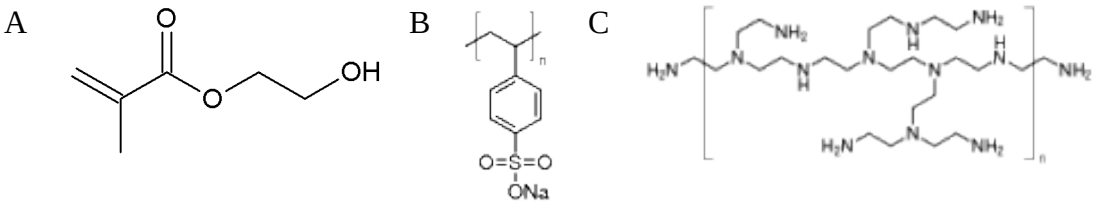

Figure 21. Chemical structures of (A) 2-hydroxyethyl methacrylate (HEMA), (B) poly(sodium 4-styrene sulfonate) (PSS), (C) poly(ethyleneimine) (PEI). Figure from [197].

This material was attractive as a BLM support for several reasons. Firstly, the hydrogel can provide mechanical stability while giving the membrane access to a bulk aqueous environment, allowing transport of water, ions and analytes to incorporated transmembrane proteins and not hampering flux. Secondly, the presence of silica beads increases the porosity (and hence water permeability) and the mechanical stability of the support[196]. Thirdly, the polyHEMA-based hydrogel was harder than PEG-DMA hydrogel, which we believed would better protect the membrane against high hydraulic pressure. Lastly, the entire system was readily upscalable as it was easy and cheap to prepare. Using a precast support for the biomimetic membranes would, albeit making defect-free membrane formation dependent on the topography of the support surface, in principle be compatible with delivery of transmembrane proteins to the biomimetic membrane on the unsupported side of the membrane by vesicle fusion. The hydrogel was cast using a mold such that the polymerized hydrogel would form a supportive layer under the

apertures. The rationale behind this design was to optimize the lipid-partition interactions at the aperture rim, while providing maximal support for the membranes across the aperture arrays.

To further improve BLM stability we coupled the hydrogel support to the ETFE partition, a strategy which has shown success in membrane stabilization by providing the membrane with mechanical stability and slowing leakage of the solvent annulus[186]. In order to ensure good contact between the composite hydrogel and the ETFE partition the ETFE surface was surface-modified with HEMA using surface plasma polymerization on the partition side facing the hydrogel.

The polyHEMA support was further modified by layer-by-layer deposition of polyelectrolyte layers. Polyelectrolytes have previously been used as a cushion layer on solid supports for stabilizing lipid membranes[117, 152-154, 160, 161]. Polyelectrolytes mimic the cell cytoskeleton[55], which has a supporting and stabilizing function in cells. An avidin-biotin linkage was used to tether the biomimetic cytoskeleton to the biomimetic membrane. The rationale for this design was that adding a "cytoskeleton" and tethering the membrane to it would improve membrane stability. The thickness of the polyelectrolyte cushion can be controlled by selecting the number of deposited layers. As the polyelectrolyte cushion, I used a single layer of the polyanion poly(sodium 4-styrene sulfonate) (PSS, Fig. 21B) or nine alternating layers of PSS and the polycation poly(ethyleneimine) (PEI, Fig. 21C).

5.2. Characterization of the support

The composite hydrogel precursor solution was an aqueous solution containing HEMA, PEG-DMA and silica particles (0.5-10 µm diameters). The HPS polymerized upon addition of a chemical initiator, ammonium persulfate. Characterization of the polyHEMA support was carried out by the other co-authors of paper III. The presence of silica particles in the polymer hydrogel was shown by Roerdink Lander *et al* (who were also a part of the *"Industrial biomimetic water membranes"* project) to greatly enhance both the mechanical stability of the gel and the flux of water through the hydrogel[196]. The permeability increased with the amount of silica present in the hydrogel composite, with permeabilities up to 24 $g.m^{-2}.min^{-1}$ obtained at 1 bar for a 1 mm thick slab of composite hydrogel, which contained 44 wt % silica. This corresponds to $4 \cdot 10^{-12}$

$m.s^{-1}.Pa^{-1}$. In comparison, the water permeability of a 1 mm thick slab of photoinitiated PEG-1000-DMA hydrogel presented in the previous chapter was $39 \cdot 10^{-12}$ $m.s^{-1}.Pa^{-1}$. A pore size distribution analysis of the composite hydrogel showed that the majority of the pore diameters was 2-5 μm, with a minority of pore diameters below 500 nm. The smaller pores indicate that an interfacial skin layer forms to some extent on the polyHEMA surface, which explains why lower water flux is observed for this composite gel than for the PEG-DMA gel. The water flux obtained for the polyHEMA gel was sufficiently high for a water filtration device.

Jörg Vogel (also involved in the *"Industrial biomimetic water membranes"* project) investigated three different methods for integrating the composite hydrogel support into the ETFE apertures: physical clamping of the gel with the ETFE partition (in this case the gel was not conjugated to the partition), mold casting with direct integration of polyHEMA with the ETFE partition (with conjugation) and a "negative plug" method in which the apertures are first plugged with a sacrificial material, filled with polyHEMA (with conjugation to the ETFE) and subsequently the plug is removed[198]. The "negative plug" method was shown to be incompatible with conjugation of the hydrogel to the support due to creeping of the plug material onto the HEMA-treated side of the ETFE partition[198]. In the mold-casting method, a Teflon mold was filled with the hydrogel precursor solution (Fig. 22A) and an ETFE partition with two polymethylmethacrylate (PMMA) rings was placed on top, with the HEMA-treated side down towards the HPS. The hydrogel polymerized to form a support below each aperture over the entire aperture array. I investigated formation of membranes on clamped and mold-cast polyHEMA supports.

The surface topography of the hydrogel areas in the apertures was analyzed by focus-variation optical scanning, showing the desired backing of the ETFE partition apertures with the composite hydrogel, with marginal penetration of the hydrogel into the apertures (Fig. 22B). The hydrogel had a surface roughness of circa 1 μm, increasing the surface area in the apertures (compared to an ideally flat surface) by around 11%. The surface roughness is higher than the surface roughness of flat solid supports typically used for supported lipid membranes, such as mica, gold and silicon, which presents a challenge in formation of defect-free long-lived membranes. Despite this, we obtain thin lipid membranes which are electrically tight with relatively good stability.

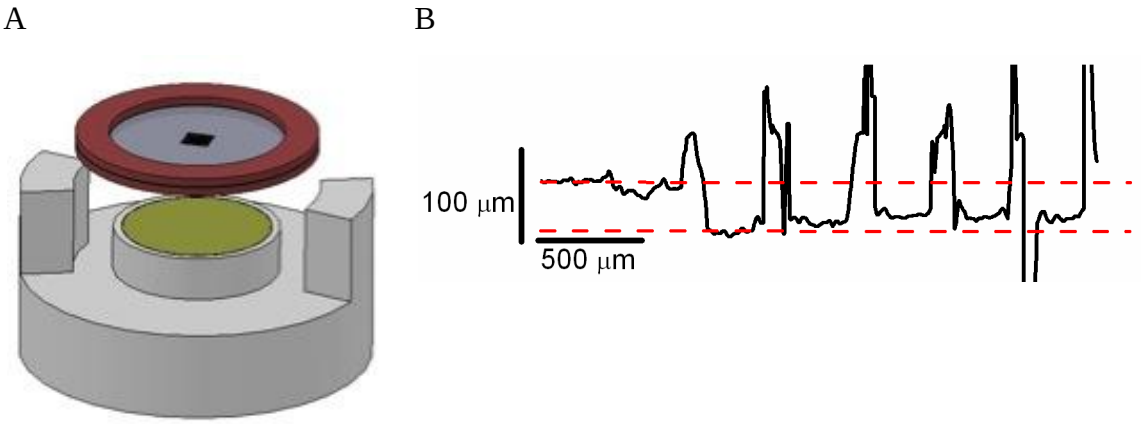

Figure 22. (A) Schematic of the ETFE scaffold (grey) with PMMA rings (red) and the Teflon mold used for casting of the hydrogel support. The hydrogel-forming solution (green) is contained in a reservoir with a depth of 500 μm. (B) Profile scan across five apertures. The dashed red lines indicate the surface of the ETFE sheet. Figure from [120].

We found dependence between the evenness factor of the polyHEMA support and the success of forming tight, long-lived membranes (table 2). The evenness factor, E_f, is defined as $\sum_{i=1}^{4} \frac{r_i}{4d_i}$, where r_i is the distance from the top of the ETFE partition to the highest polyHEMA surface in an aperture and d_i is the distance from the top of the ETFE partition to the lowest polyHEMA surface in an aperture. The evenness factor is calculated for four neighbouring apertures in a row and the value is averaged to obtain an evenness factor for the sample. The closer the calculated value is to 1 the more even the filling is. The distribution of the polyHEMA should be even and no large height differences of the polyHEMA between apertures should exist in order to obtain leak-free long-lived membranes. The depth of filling of the polyHEMA support (below or partly inside the apertures) was not critical for membrane formation and quality (Vogel, Ibragimova and Rein, unpublished results).

Table 2. Relationship between polyHEMA evenness and membrane quality (n=21). The number of samples with a specific polyHEMA evenness factor and membrane quality is indicated. Table from [199].

Evenness factor	**Membrane**		
	good	**bad**	**none**
0.77±0.09	4	0	1
0.53±0.18	0	2	3
<0.4	2	1	8

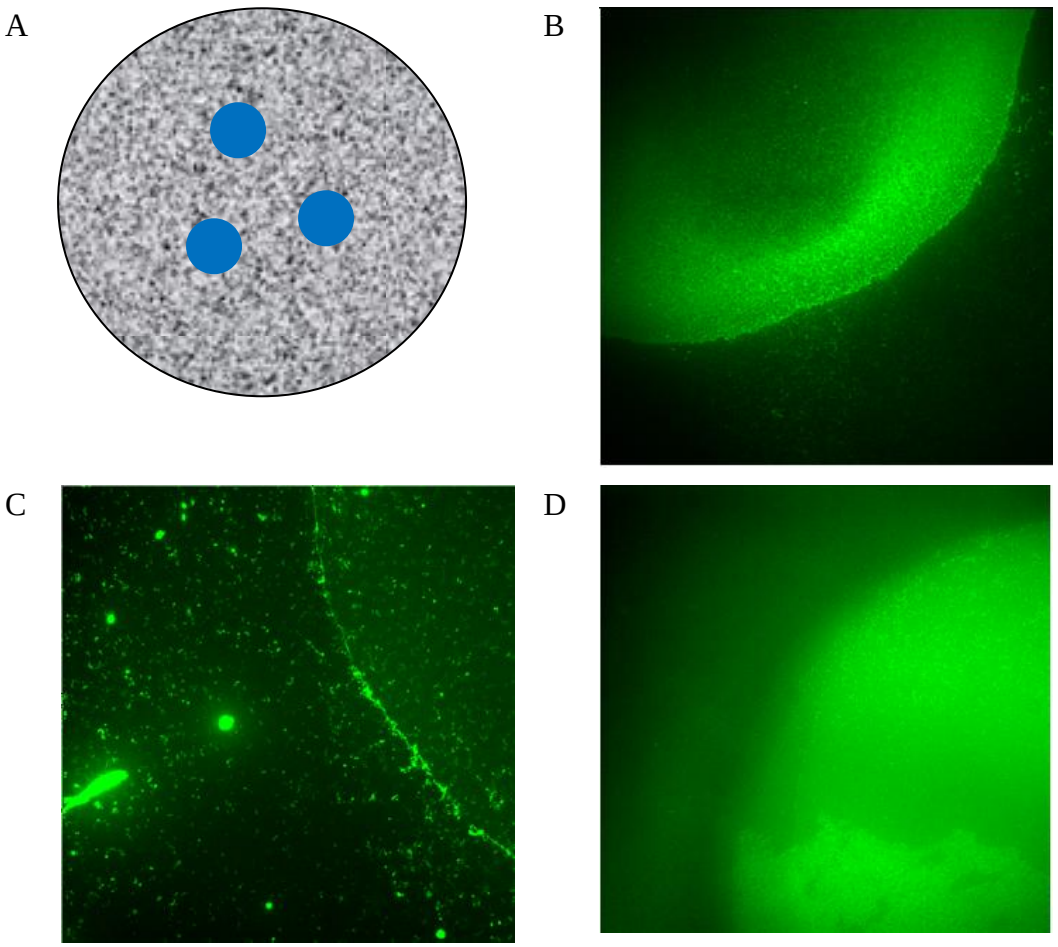

Figure 23. (A) The polyelectrolyte binding assay**.** The idea is to deposit the first polyelectrolyte in droplets (blue circles) on the polyHEMA surface (grey circle), rinse thoroughly, deposit the second polyelectrolyte layer over the entire surface, rinse thoroughly, deposit avidin-FITC over the entire surface and rinse thoroughly. The presence of polyelectrolyte layers is visualized through the binding of fluorescently labelled avidin to said layers. (B) PSS droplets deposited on polyHEMA, followed by avidin-FITC (C) PEI droplets deposited on polyHEMA, followed by avidin-FITC. (D) PEI droplets deposited on polyHEMA, followed by PSS over the entire surface and subsequently avidin-FITC. Figure from [199].

Adsorption of the polyelectrolytes PEI and PSS and subsequent adsorption of avidin labelled with fluorescein isothiocyanate (avidin-FITC) onto polyHEMA was confirmed with a fluorescence assay (Fig. 23) carried out by Mark Perry (also involved in the *"Industrial biomimetic water membranes"* project). The assay was based on depositing droplets of the first polyelectrolyte on the polyHEMA substrate, rinsing thoroughly, depositing the second component (second polyelectrolyte or avidin-FITC) over the entire surface, rinsing thoroughly and using avidin-FITC as the last layer and rinsing thoroughly and finally visually inspecting the samples under a fluorescence microscope to view the distribution of avidin-FITC. The presence

of polyelectrolyte layers is visualized through the binding of fluorescently labelled avidin to said layers (Fig. 23A).

Both PSS (Fig. 23B) and PEI (Figs. 23C and 23D) were found to bind to the polyHEMA, as observed by the presence of the droplet rim. PSS was found to bind more strongly to PEI than to polyHEMA (Fig. 23D), which is as expected since the polyanionic PSS and the polycationic PEI should experience strong electrostatic attractive forces to each other. Avidin-FITC was found to bind more strongly to PSS than to PEI (compare Fig. 23B and 23C). Avidin was also found to bind to the silica particles (small green dots on the bulk substrate seen in Figs. 23B and 23C). In other studies, avidin has been shown to have a net positive charge at neutral pH and bind to negatively charged surfaces[200]. This is in agreement with the results observed here, since SiO_2 particles and PSS are negatively charged.

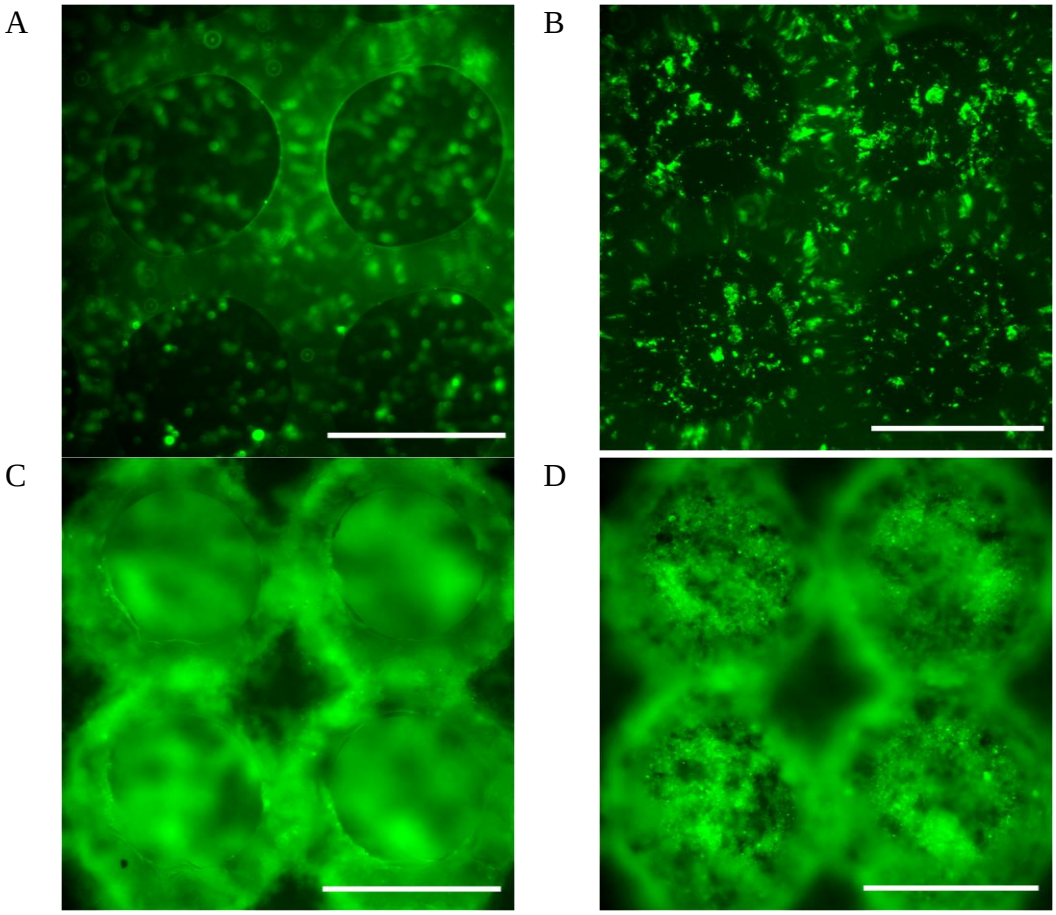

Figure 24. Fluorescent image of PEI-PSS-Avidin-FITC deposition on polyHEMA/ETFE sandwiches. Scale bar 300 µm. (A) clamped polyHEMA ETFE imaged in ETFE plane (B) and in the polyHEMA plane. (C) well-bonded polyHEMA/ETFE imaged in ETFE plane (D) and in the polyHEMA plane. Figure from [199].

Conjugation of the composite hydrogel to the ETFE partition was confirmed by depositing PEI onto the polyHEMA/ETFE sandwich, followed by PSS and fluorescently labelled avidin. Avidin was located over the entire polyHEMA support for clamped polyHEMA and ETFE (Figs. 24A, B), but localized only inside the apertures for the mold-cast polyHEMA-ETFE (Figs. 24C, D). No avidin-FITC was found underneath the diamond structures of the ETFE in the mold-cast samples, indicating that a tight bonding has been obtained here.

5.3. Membrane formation

Lipid membranes were established across the 8x8 aperture arrays in polyHEMA/ETFE sandwiches. Free-standing lipid membranes suspended across aperture arrays in an unsupported ETFE partition were prepared for comparison. Membranes were formed in the apertures by the painting method. The bilayer forming solution consisted of a mixture of lipids (36 mol DPhPC: 9 mol DOTAP: 5 mol DSPE-PEG2000-biotin) in decane. The cationic lipid DOTAP was included for two reasons. Firstly, because the membrane was intended as a receiving membrane for vesicle fusion and we wanted to have positive charges in the receiving membranes and negative charges in the vesicles to enhance vesicle-bilayer fusion (a strategy described in the background section). Secondly, DOTAP has been shown to electrostatically "stitch" gel-state bilayers together to form defect-free membranes of several square micrometers; therefore, DOTAP can be seen as a bilayer-stabilizing agent[201]. PEG-conjugated lipids were included to provide a soft cushion for the bilayers resting on top of the hydrogel surface. The biotin moiety at the end of the PEG chain was included for tethering the lipid membrane to the underlying support via biotin-avidin linkages.

Membranes were characterized by voltage clamp and fluorescence microscopy measurements. The membrane conductance indicated that electrically tight membranes that covered all 64 apertures were formed in all cases (Fig. 28B). The array electric specific capacitance, C_m, for the free-standing and the hydrogel-supported membranes are shown in Figure 25. A high C_m value indicates the presence of thin BLMs, with values of 0.3-0.4 μF/cm^2 expected for thin decane-containing free-standing bilayers[53].

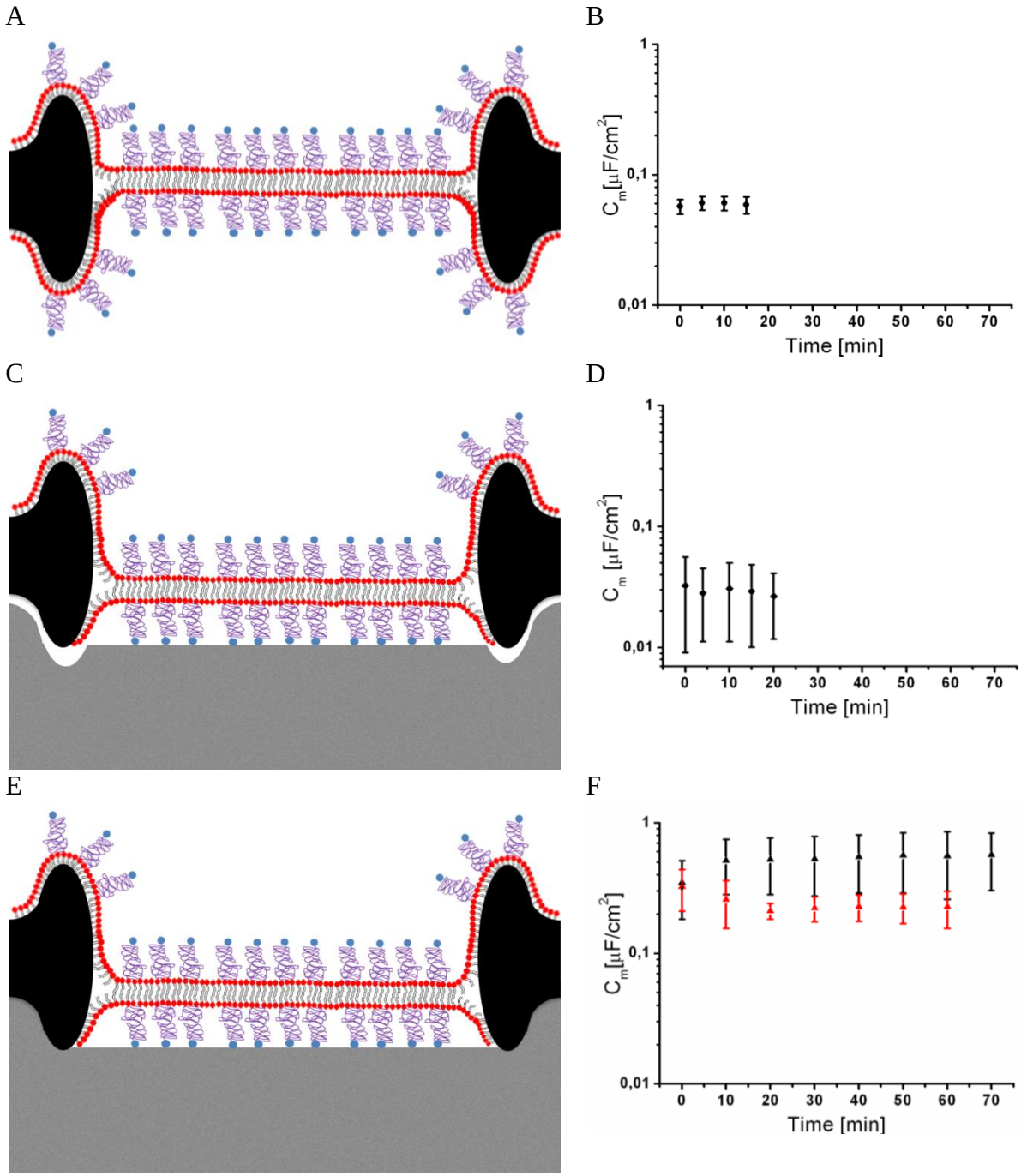

Figure 25. Schematic representation of free-standing and supported BLMs made from DPhPC:DOTAP:DSPE-PEG2000-biotin (36 mol:9 mol:5 mol) in decane painted across 8x8 aperture arrays in ETFE. (A) Free-standing membranes (lipid headgroups are represented by red circles and lipid acyl chains by black lines) spanning an aperture in an ETFE (black) scaffold showing PEG-biotin tethers (PEG is represented by wavy purple lines, biotin is represented by blue circles) extending from the membrane. (B) Mean C_m vs time (n=9) for the membranes in (A). (C) BLMs supported on a clamped polyHEMA/ETFE sandwich. PolyHEMA is represented by a grey block. (D) Mean C_m vs time (n=10) for the membranes in (C). (E) BLMs supported on mold-cast conjugated polyHEMA/ETFE sandwich. (F) Mean C_m vs time for the membranes in (E). Two trends were observed: (1) development of C_m to a mean value of 0.3 µF/cm^2 (red triangles, n=4); (2) development of C_m to a mean value of 0.6 µF/cm^2 (black triangles, n=4). Ímages in the left column were made by Erik Bäckström. Figure from [199].

Free-standing BLMs (Fig. 25A) appeared thick and did not thin automatically, as evidenced by a stable, low membrane array specific capacitance not exceeding 0.06 μF/cm^2 (Fig. 25B) and by the apertures being evenly filled with fluorescently labeled lipids (Fig. 26A). This is similar to C_m values (up to 0.09 μF.cm^{-2}) obtained for PEG-DMA hydrogel-encapsulated BLMs. Membranes supported on clamped polyHEMA/ETFE supports (Fig. 25C), did not decrease in thickness as can be seen by the decrease in the specific capacitance (Fig. 25D) and decreased in the mean membrane lifetime (Fig. 28A). We concluded that clamped polyHEMA supports do not improve membrane characteristics, which may be due to mechanical stress on the membranes induced by clamping.

In contrast, C_m values for membranes formed on mold-cast polyHEMA/ETFE (Fig. 25E) indicated formation of thin, decane-containing lipid bilayer membranes directly upon formation. Thereafter, the membranes either stabilized at a specific capacitance of 0.30 μF/cm^2 or thinned further to obtain average specific capacitance values of 0.6 μF/cm^2 were observed and occasionally up to 0.9 μF/cm^2 (Fig. 25F). In comparison, a specific capacitance of 0.78 μF/cm^2 was reported for "solvent-free" membranes formed from squalene[202]. The high C_m values obtained suggested that the membranes that were formed contained very little or no solvent. Fluorescence images of the formed membranes (membrane formation was confirmed by concomitant electrical voltage clamp measurements) showed negligible Plateau-Gibbs tori (Fig. 26B) and a reduced amount of lipid in the diamond-shaped areas between apertures, indicating that excess decane solvent had been "squeezed out" during membrane self-assembly and thinning. We found that the hydrogel facilitated self-thinning of the BLMs, without the need for manual thinning, which may be due in part to the presence of silica particles. Silica is a commonly used solid support for lipid membranes and the material is known to have sufficiently strong interactions with lipid vesicles to facilitate spreading and rupture of the vesicles and self-assembly into a lipid bilayer on the surface. Thus, it may be due to interactions with the silica particles in the composite hydrogel that the lipid membranes thin to bilayers.

The minimum lifetime of the membranes until the first out of 64 membranes ruptures, is shown in Figure 25. After 15 min, membrane rupture occurred in the free-standing, non-thinned membranes and after 20 min for non-thinned membranes supported on clamped

polyHEMA/ETFE. By comparison, the first membrane ruptured after 60 min in the mold-cast hydrogel-supported membrane arrays. Thus, addition of the composite hydrogel support significantly increased the time until first rupture.

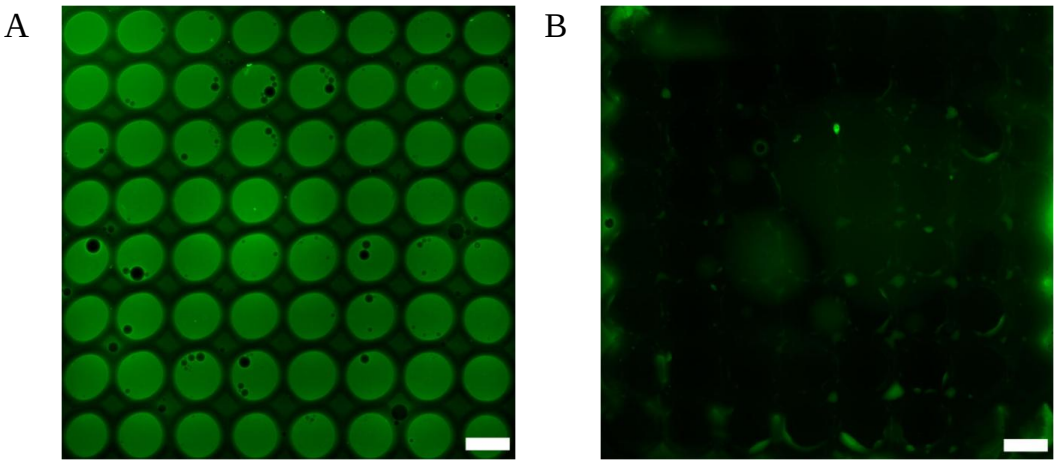

Figure 26. (A) Fluorescent images of established unsupported free-standing membranes immediately after formation. (B) Same for mold-cast polyHEMA/ETFEl-supported membrane arrays directly after formation. Scale bars are 300 μm. Figure from [120].

To further stabilize the lipid membranes, we deposited a single layer of PSS on the polyHEMA and tethered the lipid membrane to this support using avidin-biotin linkages (Fig. 27A). Average C_m values of 0.26 μF/cm^2 (Fig. 27B) were observed for membranes formed on these supports directly after membrane formation, indicating that thin, decane-containing lipid bilayer membranes were formed. These membranes also thinned automatically, albeit they were slightly thicker than the membranes supported on mold-cast polyHEMA/ETFE. The mean lifetime of the membranes was increased from 1.7 h for polyHEMA/ETFE supported membranes to 4.5 h for polyHEMA-PSS-avidin supported membranes and the maximum lifetime from 2.8 h to 8.4 h (Fig. 28A). We concluded that deposition of the membrane on PSS and tethering of the membrane to the underlying support successfully improved membrane stability.

Increasing the thickness of the cushion by using nine polyelectrolyte layers (Fig. 27C) increased membrane longevity further, to a mean membrane lifetime of 5.1 h and lifetimes up to 17 h (Fig. 28A). The variability in lifetime also increased, showing that it is important to have control over the polyelectrolyte deposition.

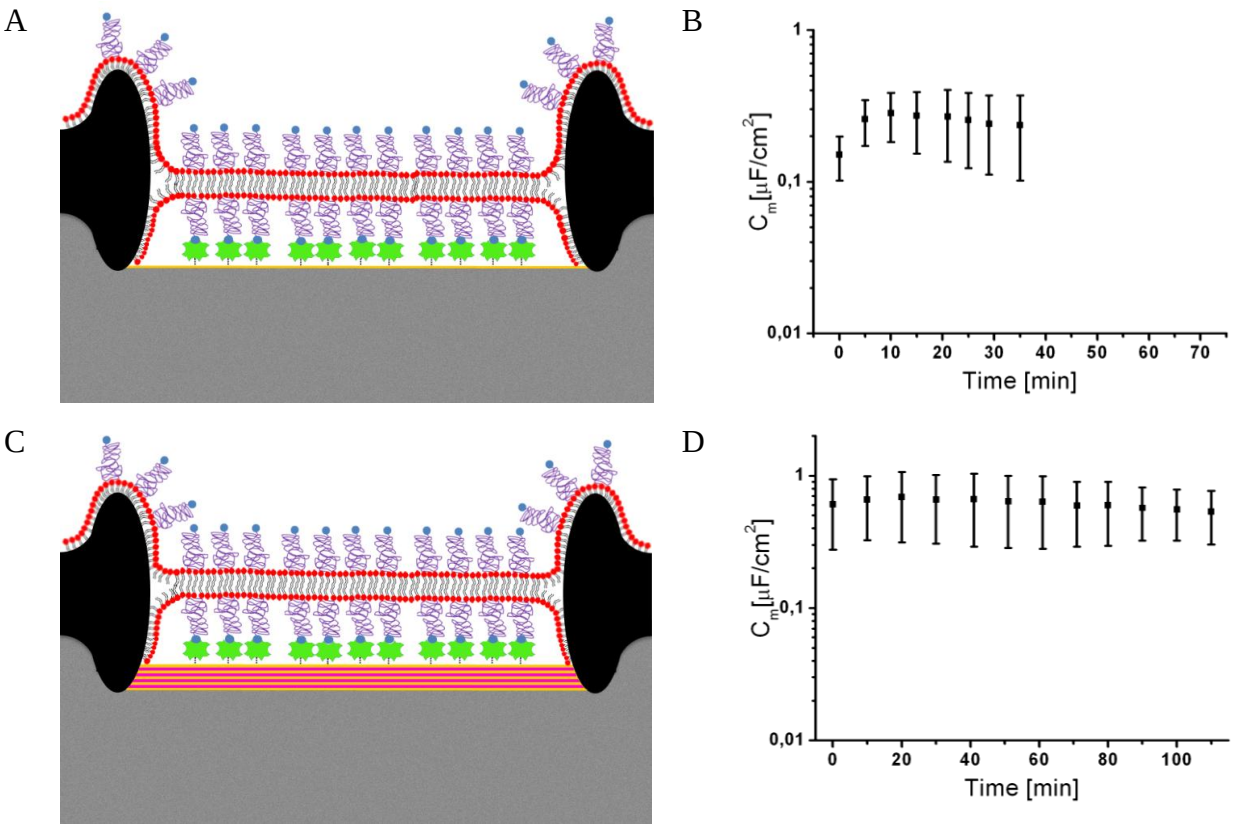

Figure 27. Schematic representation of supported BLMs with the same composition as in Figure 25 painted across 8x8 aperture arrays in ETFE. (A) PolyHEMA-PSS-Avidin-supported membranes. The negatively-charged polyelectrolyte PSS (yellow rectangle) lies on top of the polyHEMA (grey block). Avidin (green shape) lies on top of the PSS. The biotin moieties on the PEG chains should tether the membrane to the avidin on the support. (B) Mean C_m vs time (n=7) for the membranes in (A). (C) PolyHEMA-9xPE-avidin-supported membranes. Negatively-charged PSS and positively charged PEI (purple rectangle) are deposited alternating layer-by-layer. (D) Mean C_m vs time (n=5) for the membranes in (C). Ímages in the left column were made by Erik Bäckström. Figure from [199].

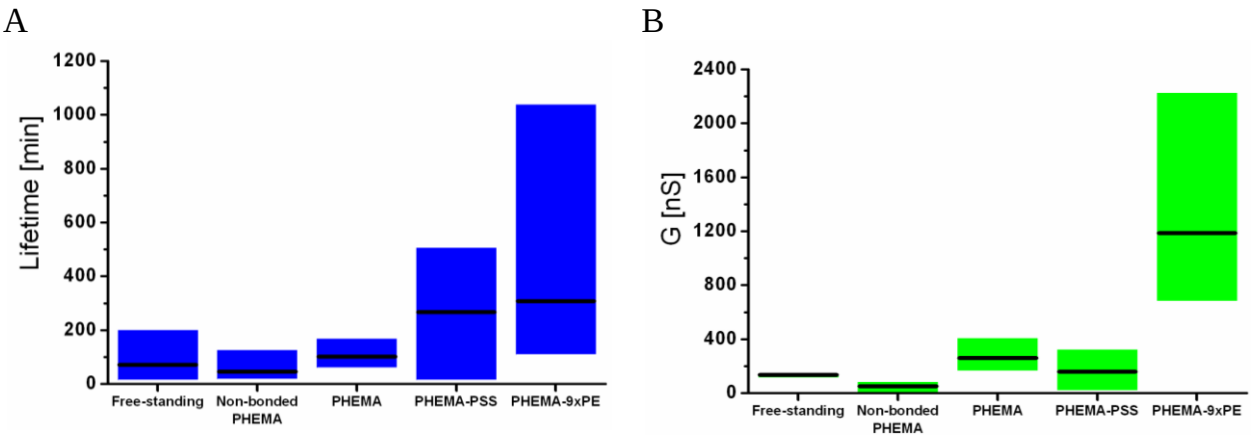

Figure 28. Electrical characteristics of free-standing and supported BLM arrays consisting of 8x8 individual membranes. (A) Lifetime and (B) average conductance (measured 10 min after membrane formation) of free-standing BLMs (n = 9) and BLMs supported on clamped polyHEMA/ETFE (n=10), mold-cast polyHEMA/ETFE (n=8), polyHEMA-PSS (n=7) and polyHEMA-9xPE (n=5). Figure from [199].

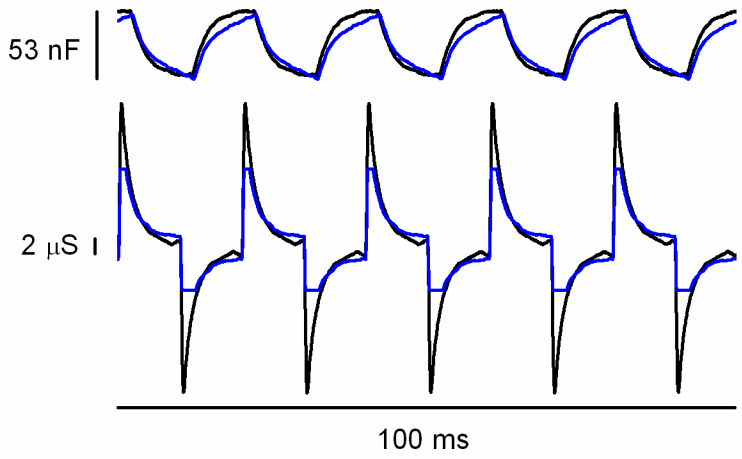

Figure 29. Membrane signals for high conductance membranes supported on polyHEMA-9xPE (black) obtained when triangular and square input signals are applied. Membrane signals for membranes supported on polyHEMA (blue) is shown for comparison. The lack of transient spikes in the lower blue signal is an artefact. The upper signals are used to calculate membrane capacitance and the lower signals to calculate membrane conductance. Figure from [199].

The mean specific capacitance of membranes formed on the polyelectrolyte multilayer support was 0.62 µF/cm^2 (Fig. 27D), which indicates that thin membranes are formed on this support. However, the membrane conductance was also increased, which could indicate the presence of defects in the membrane and give rise to the high capacitance values observed. The shape of the transmembrane signal (which is used to calculate the capacitance, see [203]) obtained when a triangular waveform is applied can give an indication of the membrane quality, with square-like signals corresponding to defect-free membranes and more triangular-like signals corresponding to leaky membranes (a completely triangular signal would correspond to an ohmic resistor-like membrane). The membrane capacitance signals for membranes supported on polyHEMA with nine polyelectrolyte layers (polyHEMA-9xPE, Fig. 29 black) had a square-like shape, typical of leak-free membranes. For comparison, I show the membrane capacitance signals for a polyHEMA-supported membrane with a similar conductance which was observed directly before membrane rupture. The membrane capacitance signal was more triangular (Fig. 29 blue) and could be observed for less than 2 minutes. On the other hand, the signals shown for the polyHEMA-9xPE were observed during the entire membrane lifetime. This suggests that the increase in membrane conductance is due to a contribution from the polyelectrolyte multilayers, and not due to the presence of defects in the formed BLMs.

Some groups have used the nanoporous hydrogel support strategy for stabilization of single-aperture membranes and shown that it improves membrane longevity. The support that was used in these cases consisted of agarose slabs placed on one or both sides of the lipid membrane. When comparing to these results, one should keep in mind that using single-aperture membranes, per se increases membrane stability compared to using a membrane array. Beddow *et al* obtained membrane lifetimes up to 24 hours in a 100-200 µm aperture in poly(tetrafluoroethylene) (PTFE)[44]. Maurer *et al* show lifetimes up to 48 hours in a 100-200 µm aperture in silicon nitride[173]. Costello *et al* used 1-palmitoyl-2-stearoyl-*sn*-glycero-3-phosphocholine **(**PSPC) lipids and obtained membranes with lifetimes of up to 20 days in single apertures (250-500 µm diameter) in PTFE[43]. Here, we present a novel composite hydrogel support which facilitated formation of thin BLMs in the ETFE aperture arrays. The membranes formed rapidly, thinned automatically and were stable with lifetimes up to 3 hours. The lifetime could be increased to up to 17 hours by building up a cytoskeleton-like support consisting of polyelectrolytes and tethering the membrane to the underlying support using avidin-biotin linkages. In comparison, encapsulating membranes *in situ* in PEG-DMA hydrogels gave lifetimes up to 219 hours, a 13-fold improvement in lifetime. However, the PEG-DMA encapsulated membranes also had a specific capacitance that was tenfold lower than the specific capacitance of membranes supported on polyHEMA. Since the specific capacitance is inversely proportional to the membrane thickness[36], this means that the membranes encapsulated by PEG-DMA hydrogel were also approximately ten times thicker. Thinner membranes provide a larger area of lipid bilayer, without solvent, which also favours higher transmembrane protein incorporation. These results demonstrate the delicate balance when choosing membrane thickness, as thicker membranes should be more stable, but thinner membranes should be able to incorporate more protein.

5.4. Protein incorporation

We demonstrated the functionality of BLMs formed on mold-cast polyHEMA/ETFE supports by showing functional incorporation of the polypeptide α-hemolysin (α-HL). α-HL was added to the unsupported side of the BLMs. In less than 1 min, α -HL heptamer channel formation in the membrane was observed (Fig. 30).

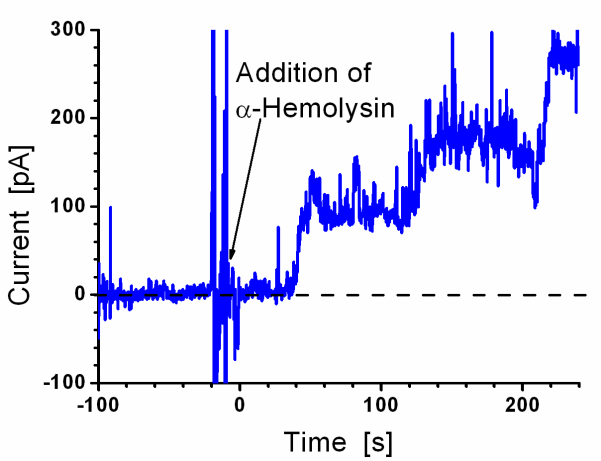

Figure 30. Current trace of a hydrogel-supported BLM indicating the formation of α -HL heptameric pores. A stepwise increase in the current with a mean single channel current amplitude of 57 pA was obtained. Figure from [120].

The specific capacitance values for the polyHEMA-supported membranes together with the fluorescence microscope images of the membranes show that thin, almost "solventless" membranes were obtained, and these should be favourable for protein incorporation. Delivery of proteins by vesicle fusion should in principle be possible on the unsupported side of the BLMs, because the membranes are accessible for vesicle fusion and stable sufficiently long (at least an hour) for vesicle fusion to be carried out. This still needs to be investigated.

6. Membranes on a nanoporous polymer support

6.1. Motivation for the nanoporous polymer support strategy

Membrane supports for separation applications such as water filtration need to be upscalable (to square meter areas) and porous to be compatible with transmembrane flux. The commonly favoured solid supports for lipid membranes (such as mica, silicon and gold) are not porous, and making them porous would be laborous and costly and using square meter areas of these substrates would not be cost-efficient. One of the reasons that mica, silicon and gold have for so long dominated as supports for membranes is that they are very flat, which makes it easier to form defect-free membranes. The need for large areas of supported biomimetic membrane has led to the emergence of novel nanoporous supports. These are, however, often more corrugated (than mica etc.), which creates a challenge with creating defect-free membranes. This field is still very new and only few supports have been reported in the literature. These include agarose[149, 170, 172], agar[169], chitosan[149], nanofiltration membranes[164], microfiltration membranes[165-168] and silica xerogel[174, 175].

In this chapter, I present a nanoporous substrate (developed by project partners at DTU Nanotech and DTU Chemical Engineering) based on a diblock copolymer. We show that lipid membranes can be created on this support (Fig. 1C) by the vesicle deposition method. The diblock copolymer used was a 1,2-polybutadiene-b-polydimethylsiloxane (PB-PDMS, Fig. 31).

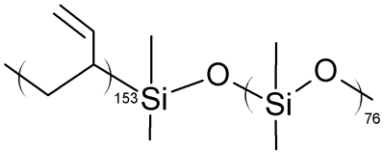

Figure 31. Chemical structure of 1,2-polybutadiene-b-polydimethylsiloxane (PB-PDMS).

PB-PDMS is a versatile material, because many of its properties (such as porosity, geometry, hydrophobicity and roughness) can be modified. PB-PDMS can self-organize into a variety of nanoscale morphologies[176] (Fig. 32). By selecting the appropriate volume fraction of the PB block (in this case 0.57[56]) and heating the sample to an appropriate temperature (in this case 140 °C[56]), a gyroid morphology[177] can be obtained, which is maintained after cross-linking. Cross-

linking is initiated using the thermal initiator dicumyl peroxide[56]. The mechanical stability of the substrate can be modulated by the degree of cross-linking (which can be tuned by controlling the amount of cross-linker and the reaction time). There are also many possibilities for engineering diblock copolymer substrates to achieve the desired combination of properties, by adjusting parameters such as the block length, molecular weight, chemical composition, hydrophilic/hydrophobic balance and molecular architecture[58].

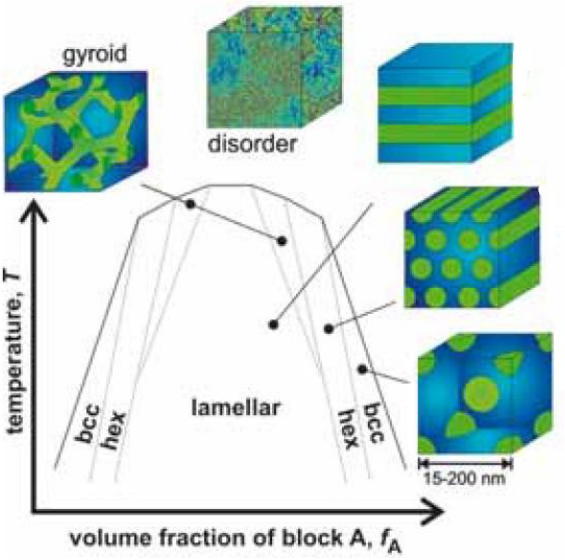

Figure 32. Phase diagram showing the different morphologies obtainable by diblock copolymers depending on the volume fraction of one block and temperature. Figure from [56].

Subsequently, the PDMS block can be etched away with hydrogen fluoride[177] or tetrabutylammonium fluoride[178] to obtain a porous structure which makes the material compatible with separation applications[177]. The permeability of the porous gyroid PB substrate is determined by the pore size and the number of pores. The pore size can be controlled by the length of the PDMS chain and the number of pores by the length of the PB chain[56, 177]. The hydrophobic, nanoporous PB substrate can be made hydrophilic (both on the surface and/or within the pores) by photooxidation[57], making it suitable as a biomimetic membrane support. The entire preparation procedure is shown schematically in Figure 33.

Advantages of PB-PDMS nanoporous substrates are their versatility, mechanical stability as well as porosity which makes them compatible with flux applications. The substrate could in prinicple be upscaled to square meters since it conforms into a gyroid morphology by self-assembly,

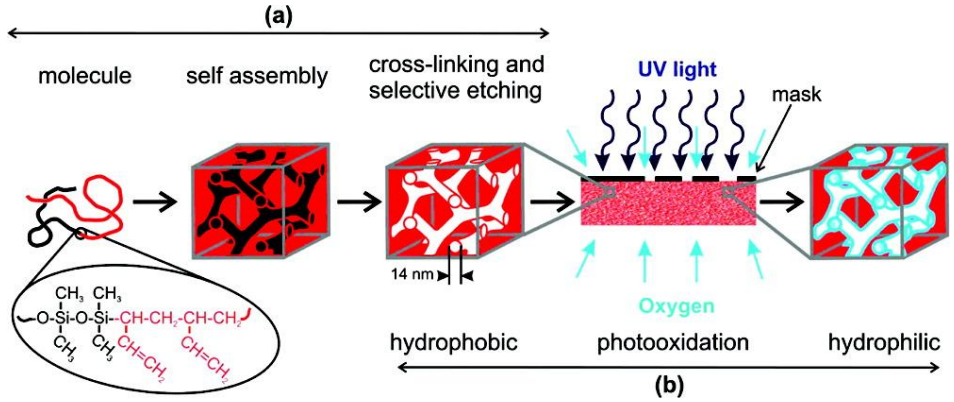

Figure 33. Conceptual scheme showing processing of the PB-PDMS diblock copolymer to create a support suitable for biomimetic membranes. (a) The diblock copolymer self-assembles and assumes a gyroid morphology and is crosslinked to fixate the structure. The PDMS block is selectively etched away. A hydrophobic nanoporous substrate is formed. (b) Controlled photofixation of oxygen onto the pore walls creates hydrophilic pores. Hydrophilic patterns can be created by application of UV masks. Figure from [57].

making it easy to obtain a porous structure. Using a precast support for the biomimetic membranes would, albeit making defect-free membrane formation dependent on the topography of the support surface, in principle be compatible with delivery of transmembrane proteins to the biomimetic membrane on the unsupported side of the membrane by vesicle fusion.

6.2. Characterization of the support

The support had average pore diameters of 14 nm[57] with a surface porosity of 0.54 (meaning that 54% of the surface area is pore area)[56]. Water fluxes up to $1 \cdot 10^{-9}$ $m.s^{-1}.Pa^{-1}$ could be obtained for a 50 µm thick polished slab of PB (Bolinger *et al*, unpublished data), which was sufficient for a water filtration application. In comparison , the polyHEMA composite gel had fluxes up to $4 \cdot 10^{-12}$ $m.s^{-1}.Pa^{-1}$ for a 1 mm thick gel slab and the PEG-1000-DMA hydrogel had fluxes up to $39 \cdot 10^{-12}$ $m.s^{-1}.Pa^{-1}$ for a 1 mm thick gel slab.

The PB substrate was cured in a glass petri dish with one surface cured against air and one surface cured against glass (Fig. 34A). Study of the air-cured surface with atomic force microscopy showed that this surface was often covered with a "skin-layer", which reduced the porosity of the surface (Fig. 34B). The skin layer could be removed by gentle polishing, exposing the gyroid pore morphology of the substrate (Fig. 34C), characterized by a "knitting-

needle" pattern, similar to what has previously been observed with scanning electron microscopy (Fig. 35)[56].

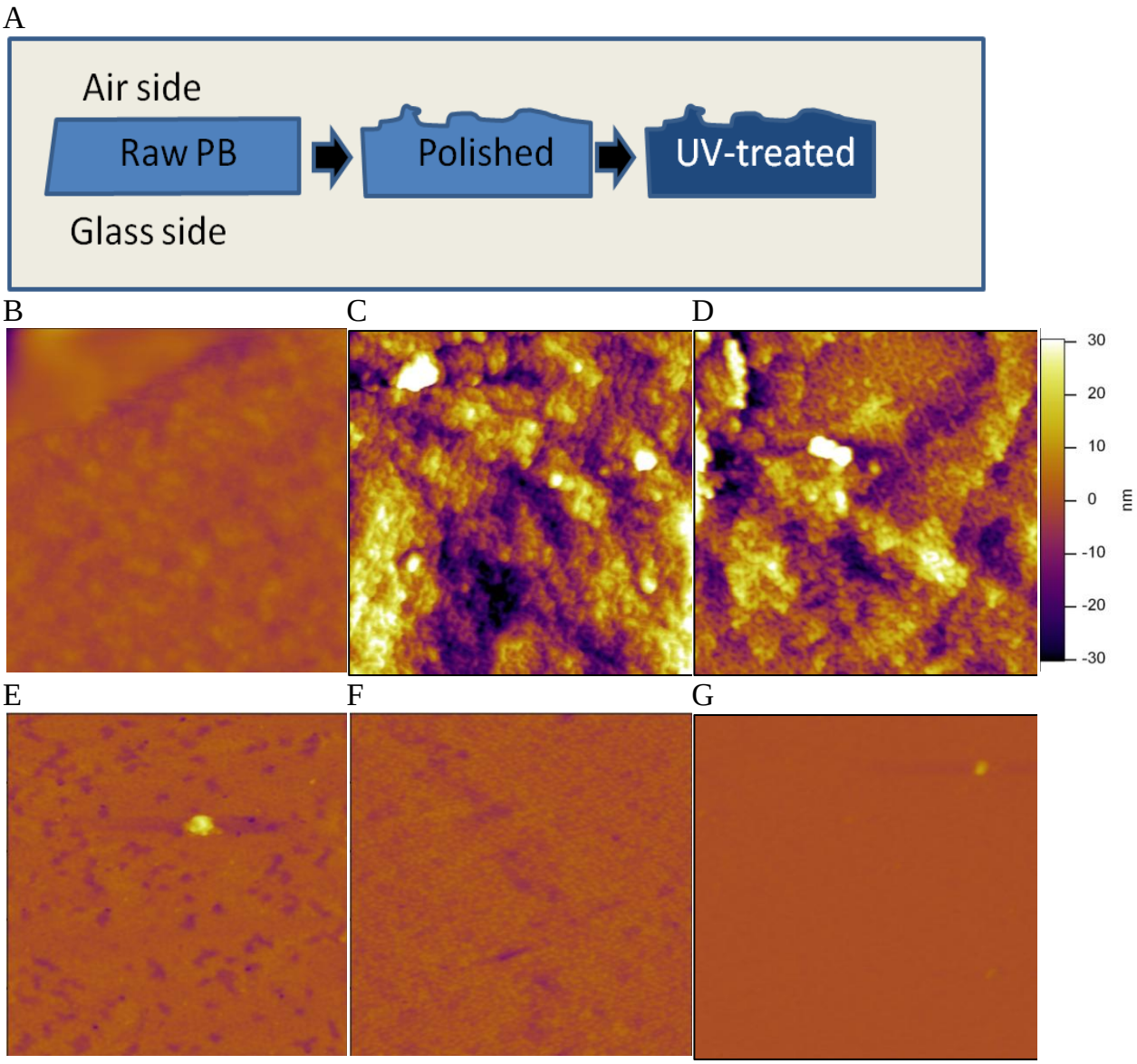

Figure 34. AFM images of the PB substrate. (A) Schematic representation of the processing of the crosslinked, nanoporous PB substrate. The PB substrate is cured in a glass petri dish with one surface cured against air and one surface cured against glass. The surface cured against air is polished as described in [56]. Both the air-cured and the glass-cured surfaces are subsequently photo-oxidized to make them hydrophilic. AFM topographic images are obtained in tapping mode. AFM images are 1 µm x 1 µm. Height scales are the same in all images, colouring as indicated by the scale bar. Samples shown are (B) PB air side, (C) PB air side polished, (D) PB air side polished and UV-treated, (E) PB glass side, (F) PB glass side UV-treated, (G) Silicon dioxide surface used as a reference. Figure from [204].

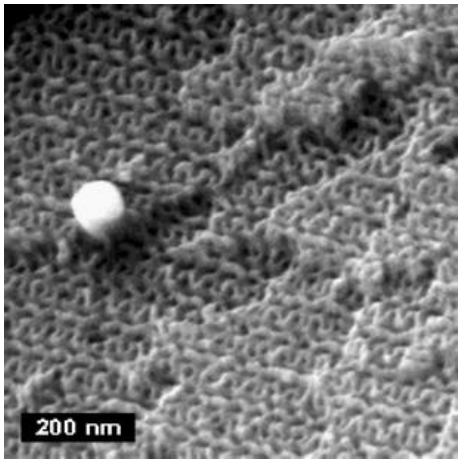

Figure 35. Scanning electron microscopy (SEM) image of ”knitting needle” pattern observed for gyroid morphology of an etched PB-PDMS sample The bright phase corresponds to PB and the dark phase corresponds to the pores (where PDMS was etched away). Figure from [56].

The glass-cured PB surface was less corrugated than the air-cured surface (Fig. 34E). The topographic image of this surface shows that it is porous, but does not have the same clear gyroidal pore morphology as the air-cured surface. Also, the “skin layer” is absent on the glass-cured side. Photo-oxidation of the surfaces changed the surface chemistry without changing the surface topology (Figs. 34D and F). A silicon dioxide wafer surface was used as a reference surface. It had a surface roughness (Fig. 34G) similar to that of the glass-cured PB surface.

Force-distance measurements of the polybutadiene and silicon dioxide surfaces were carried out with an AFM tip coated with hexanedecanethiols, which rendered the tip hydrophobic. The adhesion energy of the probe to the substrate in MilliQ water was used to quantify substrate hydrophilicity relative to another substrate (table 3). A low adhesion energy indicates a more hydrophilic support surface compared to one with a high adhesion energy. We found that the silica surface had a similar hydrophilicity to the photo-oxidized glass-cured PB surface. Both surfaces are expected to be negatively charged at physiological pH (as photo-oxidation of PB adds hydroxyl groups to the substrate surface), but a comparison of the surface chemistry has not yet been carried out. We regarded the two surfaces as similar in this study. Photo-oxidation drastically reduced the adhesion energy of both the glass-cured and air-cured sides of the PB, showing that the substrate has been made hydrophilic. The adhesion energy of the UV-treated air-cured side was approximately 10 times higher than that of the UV-treated glass-cured side,

indicating that the air-cured side was more hydrophobic. This could be due to reduced access of UV-light to the substrate during photo-oxidation, because of the increased surface roughness.

Table 3. Adhesion strength of the PB and silica surfaces obtained from force-distance measurements using a biolever coated with a monolayer of hexadecanethiols. n indicates number of force-distance curves used for the statistics. For the unpolished PB air surface, the skin layer interferes with the probing, causing problems with adhesion calculations. Table from [204].

Surface		**n**	**Adhesion energy (aJ)**
PB air side	As is	400	N/A
	Polished	400	770±1100
	UV –treated	400	49±190
PB glass side	As is	100	38± 27
	UV-treated	2500	3.7± 17
Si	As is	100	4.7± 10

6.3. Membrane formation

Membranes were created by vesicle deposition on the silicon dioxide surface and the air-cured and glass-cured hydrophilic polybutadiene surfaces (Fig. 36). The vesicles consisted of mainly DOPC lipids, with a small molar fraction of DOPE lipids conjugated with poly(ethylene glycol) (M_w= 2000 g/mol) chains. The PEG chains were included in order to provide a cushioning polymer layer on the substrate for the lipid membranes.

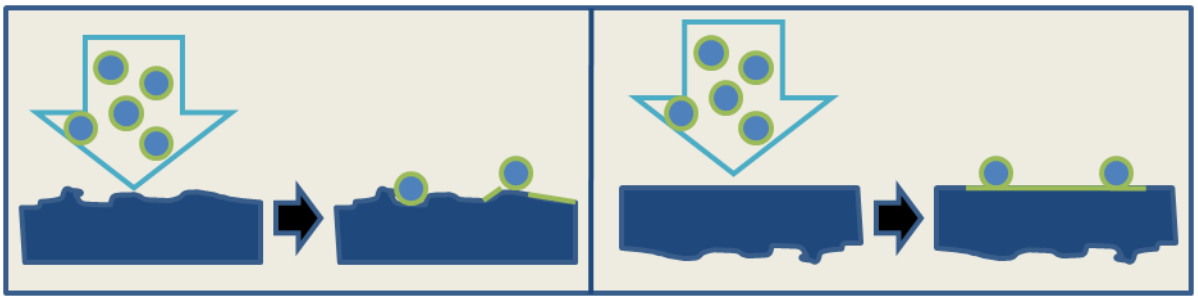

Figure 36. Lipid membranes were formed by vesicle (green circles filled with blue) deposition on the silicon dioxide surface and the UV-treated PB surfaces (both air-cured and glass-cured sides). Vesicle deposition was monitored by QCM-D on silicon dioxide surfaces and by AFM on PB surfaces.

The compositions of the vesicles used for deposition on the surfaces were chosen such that the fractions of PEG2000 represented two different conformation-regimes. Vesicles containing only 2 mol% PEG2000 would have the PEG-chains in the more collapsed “mushroom-regime”, while

vesicles containing 5 mol% PEG2000 would be in the transition region between having the PEG chains in the "mushroom-regime" or in a more elongated "brush-regime"[205]. Large unilamellar vesicles were prepared by film rehydration followed by extrusion through a 200 nm polycarbonate filter. Vesicles with a hydrodynamic diameter of 130-140 nm (table 4) were obtained.

Table 4. Vesicle hydrodynamic diameter obtained by DLS. All vesicle solutions are extruded 21 times through a 200 nm polycarbonate filter (n=3). Table from [204].

Vesicle composition (mol%)		d_H (nm)	PDI
DOPC	DOPE-PEG2000		
95	5	133±1	0.125
98	2	142±2	0.095

The two types of PEG-containing vesicles were deposited on silica and the deposition monitored by quartz crystal microbalance with dissipation monitoring (QCM-D) in order to verify the vesicles' ability to form self-assembled lipid bilayers. The rationale was that if the vesicles could not rupture on silica, then they would not be likely to do so on polybutadiene either. The QCM-D experiments were also used to identify what vesicle concentration and deposition time were necessary for lipid bilayer formation on silicon dioxide and to thus identify a starting point for the experimental conditions necessary for deposition of vesicles on polybutadiene.

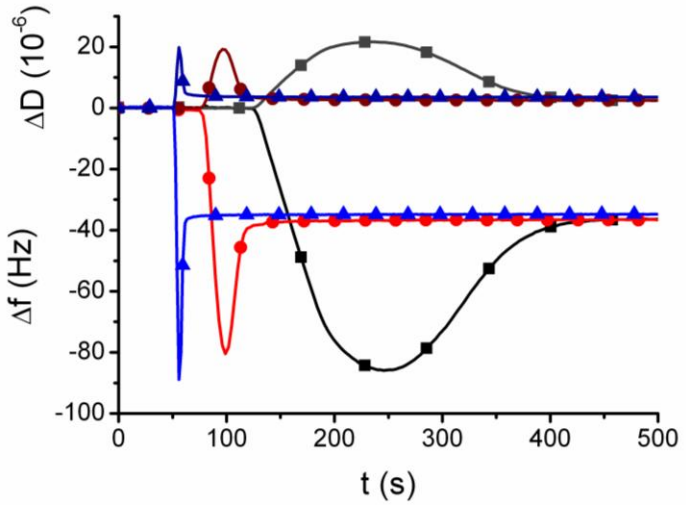

Figure 37. Vesicle deposition kinetics on silica obtained by QCM-D. Kinetics of DOPC:DOPE-PEG2000 (98 mol: 2mol) vesicles with concentrations of 0.1 mg/ml (black/grey), 0.5 mg/ml (red/mauve) and 5 mg/ml (blue/royal blue). Figure from [204].

We found that the vesicle deposition kinetics increase with vesicle concentration (Fig. 37), but reach a similar equilibrium, which is what we expected. We observed lipid bilayer formation on silicon dioxide within 5 minutes of vesicle addition for 0.1 mg/ml DOPC:DOPE-PEG2000 (98:2) vesicles and within 10 seconds for 5 mg/ml. From this, we assumed that when using 8 mg/ml of vesicles, a 5 minute adsorption time on polybutadiene would be sufficient for the system to reach equilibrium. To be on the safe side, we allowed the vesicles to adsorb for up to 1 hour. Similar kinetics as for DOPC:DOPE-PEG2000 (98:2) on silica were also observed for vesicles containing 5 mol% PEG2000, but these had a pronounced crystal dependency with 2 out of 6 experiments showing no vesicle rupture.

The changes in frequency and dissipation (from vesicle injection to stabilization of the deposition kinetics, table 5) obtained for 2 mol% PEG2000 vesicles and 5 mol% PEG2000 vesicles are similar to values reported for PEG-conjugated supported POPC lipid bilayers[205]. Also, the deposition kinetics (with first a decrease in *f* and an increase in *D* upon vesicle injection, followed by an increase in *f* and a complementary decrease in *D*) indicate that vesicles adsorb until a critical surface coverage is reached, whereupon the vesicles start to rupture on the surface, releasing water and self-assembling into a lipid bilayer. This is typical adsorption behaviour on silicon dioxide for vesicles made of lipids with PC headgroups[66]. The QCM-D data also shows that a high bilayer area can be obtained on silicon dioxide using these vesicles. The modelled layer thickness obtained is close to theoretical values predicted by deGennes theory for PEG2000-supported lipid bilayers as reported by [205]. From the QCM-D results, we concluded that both vesicle systems could form lipid bilayers on silicon dioxide.

Table 5. Change in dissipation and change in frequency obtained for adsorbed vesicles on silicon dioxide obtained with QCM-D (n=6 for 2 mol% PEG2000, n=4 for 5 mol% PEG2000). The frequency and dissipation data were used to model the thickness of the adsorbed layer (with the inbuilt Voigt model in the Q-tools software and modelling a single adsorbed layer) and to calculate the bilayer area. The bilayer area was calculated as described in [14]. How the thickness and bilayer area are obtained is described in Appendix III. Table from [204].

Vesicle composition (mol%)		Δf (Hz)	ΔD (10^{-6})	t (nm)	Bilayer area (%)
DOPC	DOPE-PEG2000				
98	2	-35.60±2.39	1.06±0.06	7.7±0.3	94.4±0.3
95	5	-42.48±2.49	0.72±0.29	8.6±0.3	96.4±1.5

The lipid vesicles were then deposited on hydrophilic, nanoporous glass-cured and air-cured polybutadiene substrates and membrane formation was monitored by force-distance measurements with an AFM. Force curves on both glass-cured and air-cured PB surfaces showed characteristic features of SLB formation, so-called "jump-in" events[205, 206]. The "jump-in" events are visible as abrupt changes in the distance of the AFM tip at constant force (Fig. 38) and occur when the AFM tip penetrates through the lipid bilayer. This makes it easy to identify where the lipid bilayer begins and ends. The force-distance curves could also be used to obtain the thickness of the PEG chains attached to the lower and upper lipid bilayer leaflet. The breakthrough force (Fig. 38) was used to assess the stability of the outer PEG-layer, where a higher breakthrough force corresponds to a more stable and less compressible layer. The breakthrough force was found to be higher for supported lipid membranes formed from 5 mol% PEG2000 vesicles than those with 2 mol% PEG2000. This could indicate that an increase in the concentration of PEGylated lipids in the vesicles improves the mechanical stability of the lipid bilayers, as has been found in previous studies[205]. For more on the calculation of the PEG thickness and the breakthrough force, see appendix III. I will not go into detail on this, as the thickness calculations were carried out by Christian Rein.

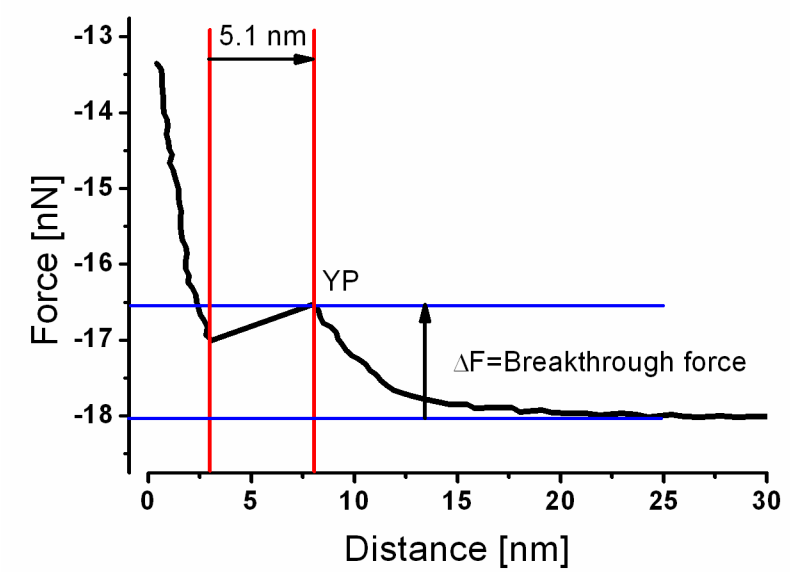

Figure 38. Force-distance curve for a deposited layer of DOPC:DOPE-PEG2000 (98 mol:2 mol) vesicles on the glass-cured side of PB, showing the distinctive "jump-in" event corresponding to the presence of a lipid bilayer. Figure from [204].

Thus, from the presence of characteristic "jump-in" events in the force-distance curves, we found that lipid bilayers could be formed on both the air-cured and the glass-cured hydrophilic PB surfaces. Next we addressed whether large areas of defect-free membranes were formed on these surfaces. As the glass-cured surface was found to be smoother than the air-cured surface, it should be easier to form defect-free membranes on it. For this reason, we investigated the surface coverage of lipid membranes on the glass-cured hydrophilic PB surface, calculated as the number of "jump-in" events over the total number of pixels. We found that the surface coverage of both DOPC:DOPE-PEG2000 (98 mol:2 mol) and DOPC:DOPE-PEG2000 (95 mol:5 mol) lipid bilayers on the glass-cured hydrophilic polybutadiene surface was below 50% of the substrate area (table 6), which is much lower than the coverage shown on silicon dioxide by QCM-D (table 5).

Table 6: SLB coverage on the glass-cured hydrophilic Pb surfaces measured by AFM. Table from [204].

Surface	Coverage (%)
2 mol% Pb (n=1)	28
5 mol% Pb (n=1)	46

The lower surface coverage could be due to a difference in surface chemistry between the silicon dioxide and polybutadiene, as it has been previously shown that the support surface chemistry can play a large role in supported lipid bilayer (SLB) formation[138]. The difference in coverage may also arise due to differences between the two measuring techniques: whereas QCM-D provides information on global characterization of vesicle deposition, AFM allows characterization of the local organization of the SLB. It has been shown in the literature that preparation of the surface and the vesicle solutions could have a large influence on the process of vesicle deposition, affecting both the tendency to form SLBs and the quality of the formed bilayers[66]. In future work, the protocol for vesicle deposition on PB needs to be rigorously examined in order to improve the SLB coverage.

7. Hybrid lipid-polymer membranes on a solid support

7.1. Motivation for using a mixture of lipids and triblock copolymers for biomimetic membranes

Recent developments in block-copolymer research have led to use of triblock copolymers as replacements for lipids in biomimetic membranes. While lipids have the advantage of being better understood and of being similar to the native environment for membrane proteins, copolymer membranes also have some advantages. The versatility of polymer chemistry allows modification to block length, molecular weight, chemical composition, hydrophilic/hydrophobic balance and molecular architecture[58]. Changing these parameters allows control of membrane morphology, molecular packing, membrane stability, fluidity, thickness and permeability.

Also, some block copolymers have been shown to have greater temporal and mechanical stability than lipids[46, 47]. Their stability is accredited to that they have a higher thickness than lipids[49, 50]. The higher thickness of block copolymers may present issues with lower protein incorporation, due to a mismatch between the hydrophobic block of the polymer and the hydrophobic band of the membrane protein[51]. A promising biomimetic membrane consists of a triblock hydrophilic-hydrophobic-hydrophilic copolymer PMOXA-PDMS-PMOXA (Fig. 5I). Functional incorporation of a variety of transmembrane proteins in PMOXA-PDMS-PMOXA triblock copolymers has been demonstrated[48, 49, 62, 89, 96, 105, 106, 108-111, 127] despite the hydrophobic mismatch. An explanation put forward for why these proteins are still functional within the polymeric membrane is that the flexibility of the hydrophobic block as well as its polydispersity give rise to regions with a matching hydrophobic thickness in the vicinity of the protein[101]. By making biomimetic membranes containing both lipids and triblock copolymers, we believe that the membrane can gain improved stability from the block copolymers and provide a better environment for protein incorporation due to the presence of lipids.

We wanted to make planar membranes from the PMOXA-PDMS-PMOXA triblock copolymers, similar to the systems presented in the previous chapters. We decided to form by membranes by vesicle deposition because it presents the fewest obstacles for incorporation of membrane proteins. Painted polymer membranes have been formed across aperture arrays using a similar

polymer with shorter PMOXA and PDMS blocks[61]. Very recently, mica-supported membranes have also been formed using tubular polymersomes[207]. However, these membranes are reported to have a low thickness (1.6 nm), much lower than the thickness expected for lipid bilayers (3-5 nm)[34], which should make these systems incompatible with incorporation of most transmembrane proteins. The triblock copolymers used by us had two times longer block lengths ($PMOXA_{15}$-$PDMS_{110}$-$PMOXA_{15}$ vs $PMOXA_7$-$PDMS_{60}$-$PMOXA_7$), and vesicles formed from this polymer had a high rupture strength, which presented some difficulty for forming membranes by the vesicle deposition method. Using mixed lipid-copolymer vesicles facilitated formation of a planar membrane.

Mixed lipid-polymer membranes were formed on quartz and mica supports (Fig. 1D). I synthesized vesicles with different ratios of $PMOXA_{15}$-$PDMS_{110}$-$PMOXA_{15}$ triblock copolymer (Fig. 5I) to zwitterionic (POPC, Fig. 39A) or cationic (DOTAP, Fig. 39B) lipids and investigated the deposition and rupture of these vesicles on the solid supports.

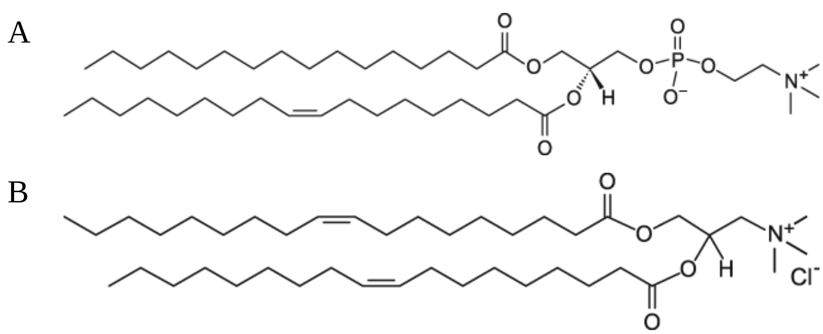

Figure 39. Chemical structures of (A) 1-palmitoyl-2-oleoyl-*sn*-glycero-3-phosphocholine (POPC) and (B) 1,2-dioleoyl-3-trimethylammonium-propane (DOTAP). Figure from [208].

7.2. Characterization of mixed vesicles

Vesicles formed from mixtures of lipid and triblock copolymer were visually inspected by transmission electron microscopy (TEM), and their size, charge and water permeability were characterized. I will hereafter refer to the PMOXA-PDMS-PMOXA triblock copolymer studied as ABA. Vesicles with the following compositions were prepared by the film hydration method: POPC, 89 mol% POPC: 11 mol% ABA, 67 mol% POPC:33 mol% ABA, 33 mol% POPC:67 mol% ABA, DOTAP, 89 mol% DOTAP:11 mol% ABA, 67 mol% DOTAP:33 mol% ABA, 33

mol% DOTAP:67 mol% ABA and ABA. Large unilamellar vesicles with hydrodynamic diameters ranging from 105 to 217 nm were obtained by extrusion as observed by dynamic light scattering (DLS). Electrophoretic light scattering (ELS) measurements showed that the zetapotential of DOTAP was screened in the presence of ABA, which means that the ABA and DOTAP molecules must reside within the same vesicle, indicating that hybrid lipid-polymer vesicles were formed.

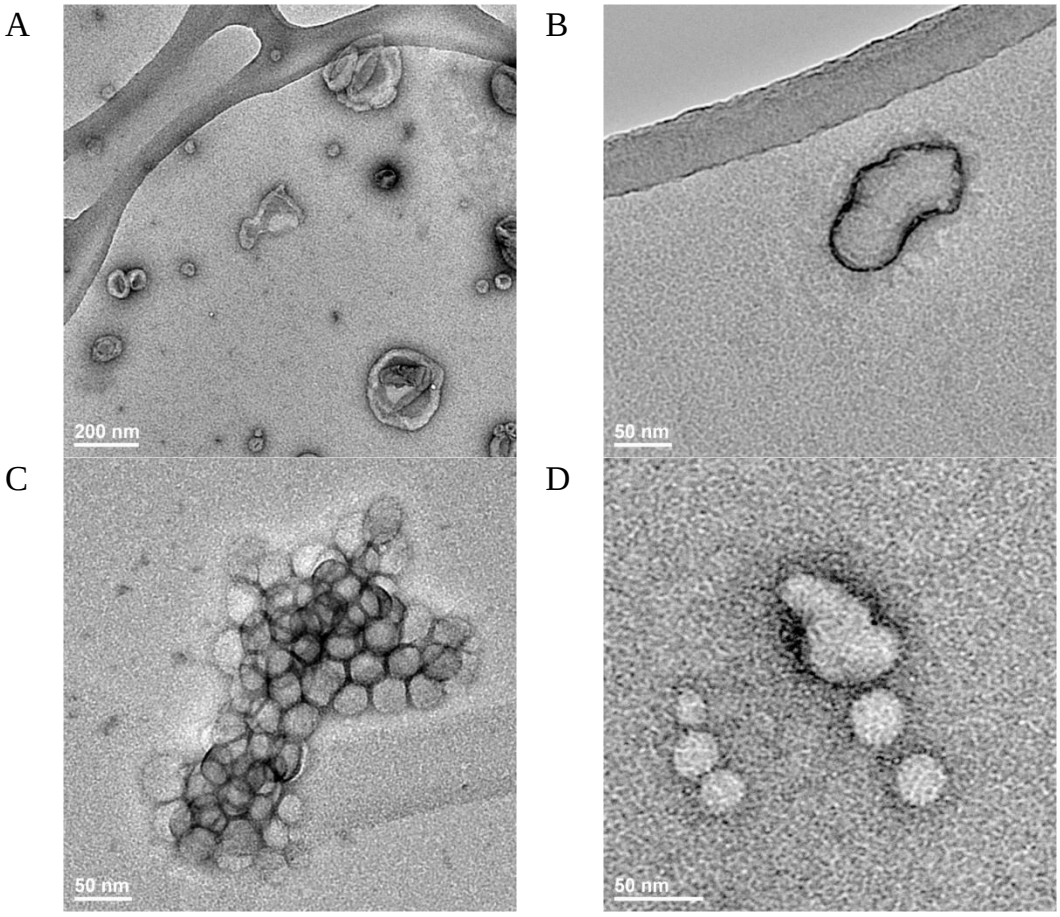

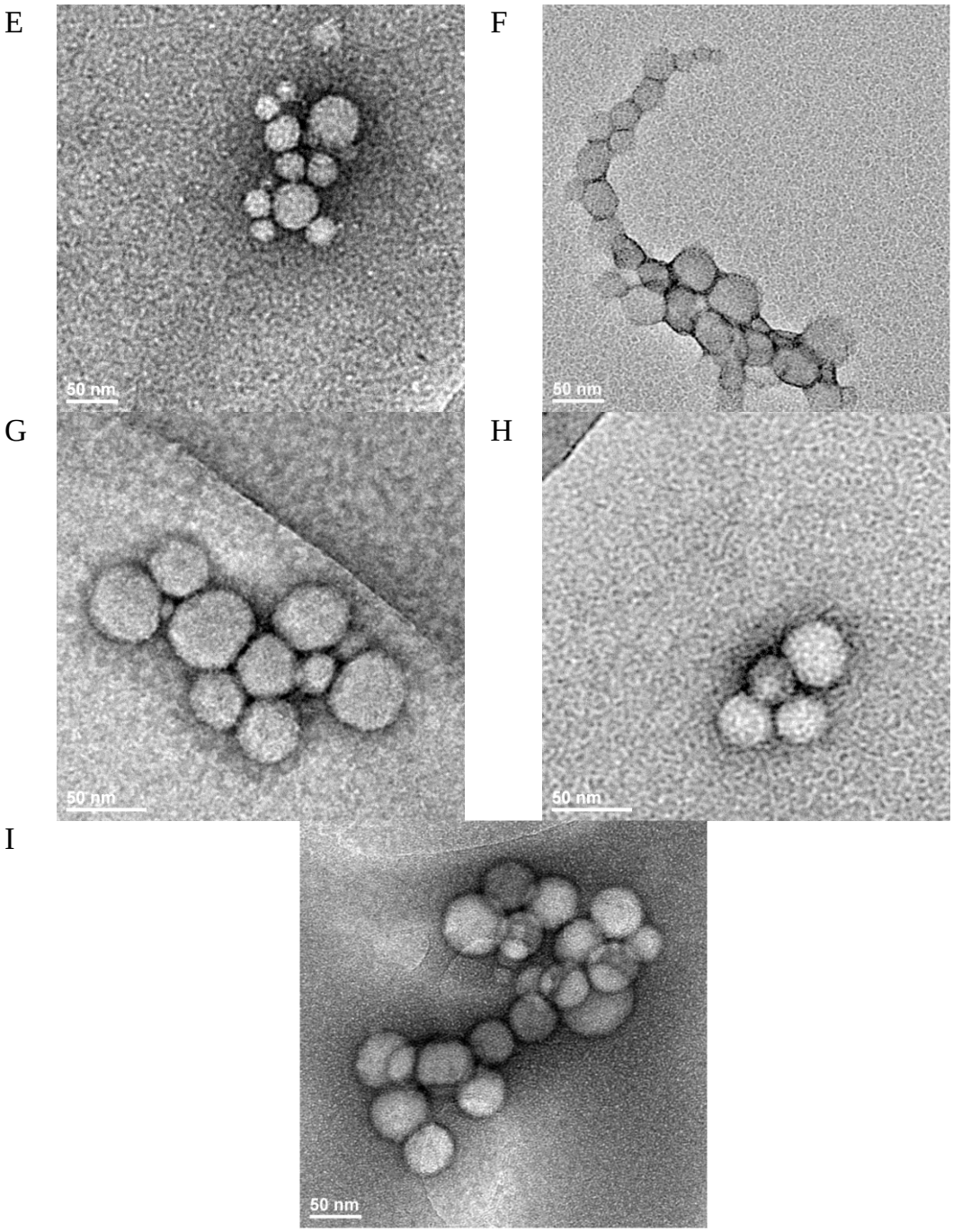

Figure 40. TEM images of lipid vesicles, polymer vesicles and mixed lipid/ABA vesicles stained with 1% uranyl acetate. (A) POPC, (B) DOTAP, (C) 89 mol% POPC:11 mol% ABA, (D) 89 mol% DOTAP:11mol% ABA, (E) 67 mol% POPC:33 mol% ABA, (F) 67 mol% DOTAP:33 mol% ABA, (G) 33 mol% POPC:67 mol% ABA, (H) 33 mol% DOTAP:67 mol% ABA and (I) ABA. Figure from [209].

The vesicles were deposited on holey hydrophilic carbon grids, dyed with uranyl acetate and viewed by TEM. POPC (Fig. 40A) liposomes did not resist dehydration in TEM, leading to collapsed structures in vacuum. DOTAP (Fig. 40B) liposomes were difficult to find on the grid

and the ones that we found appeared to have fused. ABA vesicles (Fig. 40I) formed spherical particles which did not shrivel. 89 mol% DOTAP:11 mol% ABA (Fig. 40D), had some fused structures and some spherical particles. All other ABA/lipid mixtures looked like spheres that were similar to the spheres observed for ABA and did not give rise to two distinct populations of vesicles (Figs. 40C, 40E-H). TEM, DLS and ELS results consistently showed that hybrid vesicles were formed when using a mixture of ABA and lipids.

The TEM images also show that the ABA-containing vesicles (which maintain their spherical shape) are more robust than lipid vesicles, which shrivel in vacuum. Suprisingly, as little as 11% ABA was sufficient to prevent POPC-containing vesicles from shriveling.

Since the ABA block copolymer has a larger hydrophobic thickness than a lipid bilayer, we wanted to see how the presence of a hydrophobically thicker ABA affected the water permeability of the vesicular membrane and whether the mixed vesicles could withstand osmotic pressure (we applied 23 bars) better than lipid vesicles. We investigated the vesicles' water permeability, P_f, with stopped flow measurements and found that mixed vesicles are more impermeable to water than pure lipid vesicles (table 7). The decrease in water permeability with an increased ABA content suggests that the vesicular membrane becomes thicker, which may be due to a progressive change from partial ABA insertion into the membrane to ABA fully spanning the membrane. Increasing polymer content provides the mixed vesicles with an impassive barrier and the ability to withstand higher osmotic pressure, which is an attractive property for a selective separation device, such as a water filtration membrane.

Table 7. Water permeability of mixed lipid/polymer vesicles. Table from [209].

Lipid polymer ratio (mol%)			P_f (μm/s)
POPC	DOTAP	ABA	
100	-	-	22.6±1.3
89	-	11	7.5±0.6
-	100	-	13.2±0.1
-	89	11	9.5±0.5
-	-	100	0.8 [49]

7.3. Vesicle deposition on silicon dioxide

The deposition and rupture of the mixed vesicles on a silicon dioxide support was studied by QCM-D. We found that we could obtain three scenarios depending on the type and amount of lipid added (Fig. 41). In scenario I, vesicles adsorbed to the quartz substrate and ruptured to form a planar biomimetic membrane. In scenario II vesicles adsorbed until the quartz surface was saturated, but did not rupture even upon addition of the fusogen calcium and finally in scenario III, vesicles adsorbed until the quartz surface was saturated with vesicles and could be made to rupture by adding calcium.

Vesicle compositions that were found to follow scenario I were pure lipid vesicles (POPC and DOTAP) and mixed DOTAP:ABA vesicles consisting of predominantly DOTAP (89 mol% DOTAP:11 mol% ABA and 67 mol% DOTAP:33 mol% ABA). Scenario II was observed for pure polymer vesicles and mixed lipid:ABA vesicles consisting of predominantly ABA (33 mol% DOTAP:67 mol% ABA and 33 mol% POPC:67 mol% ABA). Vesicle compositions that were found to follow scenario III were mixed POPC:ABA vesicles consisting of predominantly POPC (89 mol% POPC:11 mol% ABA and 67 mol% POPC:33 mol% ABA).

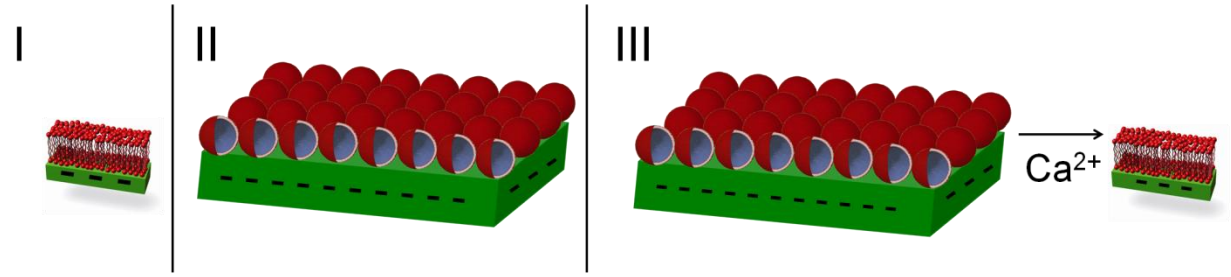

Figure 41. The type of supported membrane formed can be decided by varying the type and concentration of lipid in the membrane. (I) Planar membrane, (II) vesicular membrane and (III) vesicular membrane which can be triggered to form a planar membrane by addition of calcium. Figure from [209].

A progressive change in adsorption properties observed by QCM-D as the molar ratio of lipid in the vesicles is decreased indicates that mixing of lipid and polymer takes place and that different ratios of lipid to polymer can be obtained in the vesicles. Our results show that adding as little as 33 mol% lipid helps vesicles to adsorb onto the silica surface. We found that increasing the lipid content leads to progressively increased flattening of the mixed vesicles on the silica surface until the vesicles reach a transition from scenario II rupture behavior to scenario I where they

spontaneously rupture (for DOTAP-containing vesicles) or scenario III where they can be induced to rupture by adding calcium (for POPC-containing vesicles). Another way to say this is that a decrease in polymer content leads to increased vesicle flattening on the silica surface, which shows that the polymer makes the vesicles more stable from rupture. The lipid headgroup charge affected the stability and deposition behavior of the mixed vesicles. Both zwitterionic and cationic lipids were able to make mixed vesicles with ABA and both experienced stabilization by ABA. However, TEM and QCM-D results showed that ABA stabilizes POPC-containing vesicles better than it stabilizes DOTAP-containing vesicles. Another difference between using DOTAP or POPC was that calcium had no effect on DOTAP-containing vesicles, but helped to rupture POPC-containing vesicles, which is consistent with results reported by Richter *et al* for DOTAP and POPC vesicles[18, 66].

7.4. Vesicle deposition on mica

We also looked at deposition of some of the vesicles on a molecularly flat mica support using AFM. We found that ABA vesicles adsorb as vesicles on mica (Fig. 42A), just as on silica. POPC vesicles ruptured on mica to make bilayer patches (Fig. 42B) with a thickness of around 4 nm. 89 mol% POPC:11 mol% ABA vesicles ruptured (Fig. 42C) to make bilayer patches with thicknesses of 5-10 nm. 67 mol% POPC:33 mol% ABA vesicles do not rupture on mica (Fig. 42D), as vesicles are observed with a thicknesses of 40 nm and higher. As on quartz, we found that an increased lipid content in the mixed vesicles resulted in decreased mechanical stability of the vesicles. We found that 89 mol% POPC:11 mol% ABA vesicles ruptured on mica, but not on quartz, which we attribute to stronger interactions of the mica support (than of the silicon dioxide support) with the vesicles. Both mica and silica are hydrophilic, but supported bilayer formation on the two surfaces has been reported to differ[18], which could be due to a difference in surface charge[97].

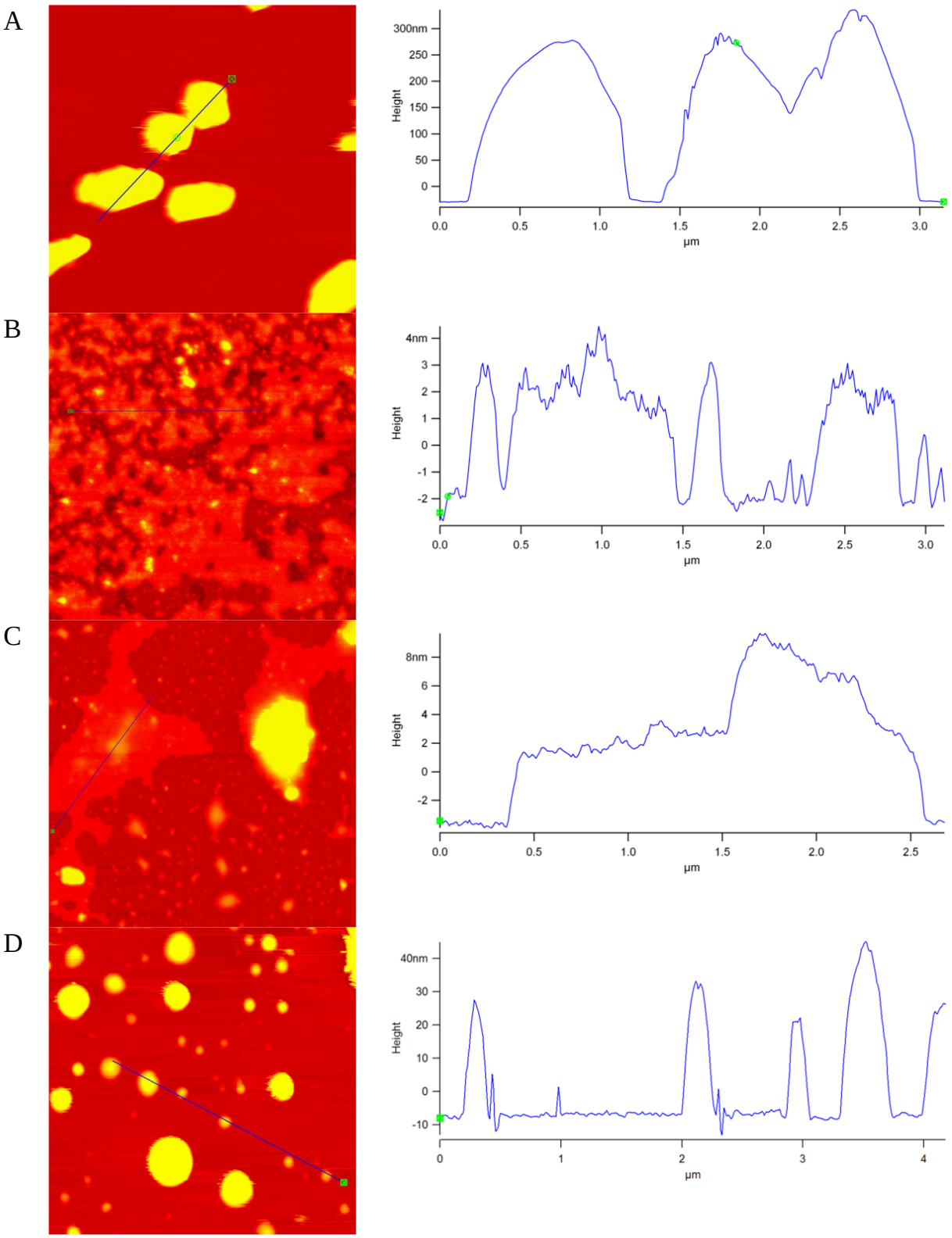

Figure 42. AFM images of ABA vesicles and POPC-containing vesicles on mica obtained in tapping mode in air. Each image shows an area of 5 µm x 5 µm. A height profile corresponding to the blue line is shown for each topographic image. (A) ABA, (B) POPC, (C) 89 mol% POPC:11 mol% ABA and (D) 67 mol% POPC:33 mol% ABA. Figure from [209].

7.5. Mechanism of increased stability

The polymer may increase stability through several possible mechanisms. First, the polymer may physically shield the POPC lipids due to the large headgroup size of the PMOXA. This would result in steric repulsion between vesicles. Second, in mixed DOTAP/ABA vesicles, the polymer screens the positive charge of the DOTAP. This reduces the electrostatic attraction of DOTAP to the quartz and mica surfaces, reducing vesicle-surface interactions and thereby increasing vesicle stability. Third, addition of the polymer increases the hydrophobic thickness of the membrane. ABA has a hydrophobic thickness of 10 nm[50], whereas a lipid membrane has a hydrophobic thickness of 3 nm[34]. The increased membrane thickness should also increase vesicle stability. Fourth, the ABA polymer consists of one piece which may span the entire membrane, whereas two lipids make up a bilayer and they are not covalently joined. This should make the membrane more rigid and provide it with stability from mechanical stress as has been shown for bolalipids [72, 210]. Lastly, block copolymers can be stretched[47], whereas lipid membranes cannot be stretched beyond 5% of their original area without rupture under osmotic or other stresses[211]. The deposition and rupture properties demonstrated likely reflect contributions from multiple mechanisms.

8. Conclusions and perspectives

This PhD-project was a part of the project *"Industrial biomimetic water membranes"* devoted to the development of a new membrane filter technology for the production of ultrapure water. The technology copies nature´s own way of water filtration where specific water channels – aquaporins – in living cells filter and transport water. The central aim of my PhD project was to stabilize the biomimetic membrane arrays used in the water filtration devices. Several strategies for stabilizing and supporting planar biomimetic membranes are addressed in this thesis and the main findings are summarized below.

8.1. Encapsulation of membranes with hydrogel

Hydrogels show promise as materials for encapsulating biomimetic membranes, because they have volumetric stability and compatibility with solvents used for bilayer formation. Their nano-scale pore sizes, ion flux and water flux properties make them promising in biomimetic devices, where they can support the biomimetic membranes, while allowing vectorial flux of matter to and through the biomimetic membrane. We have demonstrated that multi-aperture arrays of lipid membranes can be successfully encapsulated with hydrogel *in situ*. Encapsulation of lipid membranes spanning an 8x8 aperture array with an area of 4.5 mm^2 gave rise to leak-free membranes for up to 1.5 days. Further improvement in longevity (leak-free membranes observed for up to 9 days) was achieved by covalently attaching the lipid membranes to the encapsulating gels. It is possible to create a robust biomimetic membrane in which proteins can be reconstituted. We showed that the protein was still functional in the membrane 5 days after protein insertion.

However, the main challenge still remains: how to improve the stability of the membranes in the hydrogel precursor solution before crosslinking and to ensure that protein function is not compromised by maneuvers used to crosslink the hydrogels. Preliminary experiments show that both thinner and more stable BLMs could be obtained in PEG-1000-DMA hydrogel precursor solution using vertically oriented membranes. Tight BLMs were observed by voltage clamp measurements for 20 hours (Fig. 43). Another path to pursue to improve longevity of BLMs in hydrogel precursor solutions could be to combine the hydrogel-encapsulation strategy with

another stabilization strategy. For example, BLMs could be created on a nanoporous support in the presence of hydrogel precursor solution. Another envisioned approach is that black triblock copolymer membranes (which show improved stability over lipid membranes) could be used instead of lipid membranes and encapsulated with hydrogel.

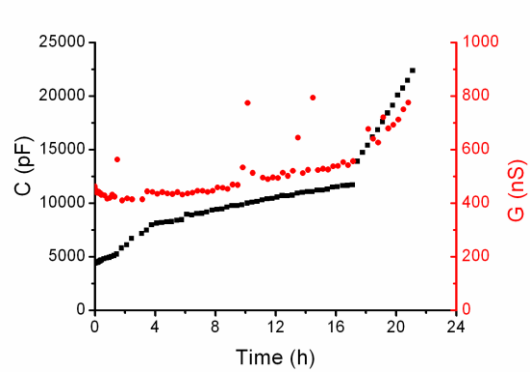

Figure 43. Temporal electrical characteristics of DPhPC made across 8x8 (300 µm diameter) apertures in ETFE by a modified folding method, the auto-painting method[39], where the BLMs span the apertures vertically. The aqueous buffer consists of UV-crosslinkable PEG-1000-DMA hydrogel precursor solution. No crosslinking was carried out. Capacitance is shown by black squares and conductance by red circles. Figure from Ibragimova, unpublished results.

8.2. Membranes on a nanoporous hydrogel support

The second stabilization strategy was to prepare lipid membranes on a precast hydrogel support. We present a water-permeable, nanoporous, hydrophilic and relatively smooth composite hydrogel support consisting of polyHEMA, PEG-DMA, and silica beads. This composite hydrogel can be conjugated to an ETFE partition and used as a support for lipid membranes formed across an array of apertures in the partition. We have demonstrated that multi-aperture arrays of thin lipid membranes can easily be formed on the support and that it is possible to create a robust biomimetic membrane (with lifetimes up to almost 3 hours) in which proteins can be reconstituted. Furthermore, the hydrogel support significantly facilitates the formation of thin BLMs in the aperture arrays without the need for manual thinning that is typically necessary to form thin membranes. By depositing a polyelectrolyte cushion support on the polyHEMA gel and tethering the lipid membranes to the support via avidin-polymer linkages, we were able to improve the membrane longevity further, attaining lifetimes up to 17 hours. With this approach,

rapid fabrication of large arrays of BLMs that allow large flux across the supported membranes should be feasible.

Future work should look into the fluidity of the formed membranes on the polyHEMA support as well as the membranes on polyelectrolyte-polyHEMA supports using fluorescence recovery after photobleaching measurements. BLMs on the polyelectrolyte support should also be visualized by fluorescence microscopy to investigate whether the solvent is similarly expelled as on the polyHEMA support. Transmembrane protein delivery and incorporation by the vesicle fusion should be demonstrated for the polyHEMA system and demonstrated by any protein delivery method on the polyelectrolyte system. Furthermore, a systematic study is required to investigate what number of polyelectrolyte layers is optimal for use in this system for supporting membranes.

The longevity of lipid membranes obtained on the nanoporous support could perhaps be improved by *in situ* encapsulation of the BLMs with PEG-DMA hydrogel after formation on the support. I carried out a preliminary voltage-clamp experiment on the same lipid membrane composition as used on the polyHEMA support. I formed the BLM array on a mold-cast polyHEMA/ETFE-PSS-Avidin support and encapsulated the membrane in PEG-DMA gel after formation (Fig. 44). The result was promising, with electrically tight, thin membranes with a lifetime of 6.7 hours obtained on the first attempt.

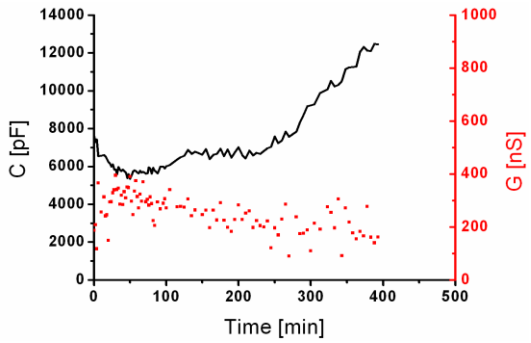

Figure 44. Electrical characteristics of polyHEMA-PSS-Avidin supported BLMs formed across an 8x8 aperture array in ETFE and encapsulated with X1000P hydrogel on the other side. Capacitance is shown in black and conductance in red. Figure from Ibragimova, unpublished results.

8.3. Membranes on a nanoporous polymer support

The third stabilization strategy was to prepare lipid membranes on a precast polymeric support. Novel supports for lipid membranes are emerging due to a need for cheap, porous materials for applications that require large areas of lipid membranes. Here, we present lipid membrane formation on a versatile diblock copolymer material developed at DTU Nanotech[56, 57, 177]. The support is prepared from PB-PDMS and can be made nanoporous and water-permeable by etching away the PDMS block, making it compatible with a water filtration device due to the large water flux that can be achieved. There are many possibilies for tailoring the substrate, for example to alter its morphology, porosity, surface roughness and hydrophilicity. The support can be made hydrophilic and relatively smooth, which should make it compatible with formation of biomimetic lipid membranes. We demonstrated that it is possible to create lipid membranes on the PB support and to detect the presence of a lipid bilayer by "jump-in" events in force-distance AFM measurements. However, we also found that the membrane coverage on PB was low, as indicated by AFM measurements.

Future work should further address membrane coverage and optimize the vesicle deposition protocol to obtain leak-free lipid membranes that completely cover the surface. AFM may not be the optimal method for characterizing membrane coverage. I suggest a voltage-clamp set-up where the polybutadiene is glued underneath an aperture or aperture array in an ETFE partition and membranes are formed on the PB support by vesicle deposition (Fig. 45) or by the painting method. Monitoring of the membrane conductance will indicate whether tight, leak-free membranes are formed.

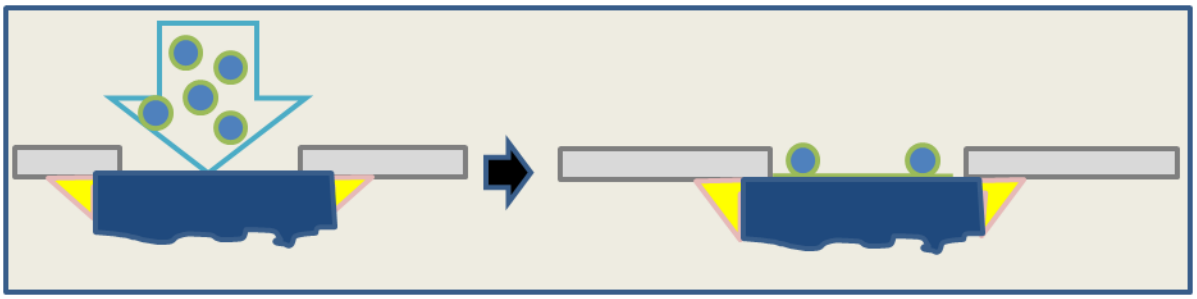

Figure 45. The hydrophilic PB substrate (blue) could be glued (yellow) under an ETFE partition aperture (grey) and lipid membranes formed on the substrate by vesicle deposition (green circles filled with blue) or painting. Leak-free membrane formation can be confirmed by voltage clamp measurements.

Furthermore, the PB support could be integrated with an ETFE partition (with an aperture array), similarly to the work shown with polyHEMA. The polybutadiene support could be placed close to the ETFE already during the crosslinking in the oven, allowing it to attain close proximity to the ETFE, by using it as a ”mold” against which the PB is cured. Also, polybutadiene contains double bonds, which could be used to conjugate the PB support to an ETFE partition surface-modified with an appropriate chemical moiety. I believe that delimiting a large surface area by dividing it up using an aperture array could be advantageous for membrane stability and formation of leak-free membranes. The ETFE partitions with aperture arrays used in this thesis, had diamond-shaped hollows between the apetures, which could act as solvent-lipid reservoirs (as can be seen in Fig. 26A). By painting the lipid membranes instead of forming membranes by vesicle deposition, one can obtain stabilizing solvent reservoirs between the apertures, which are believed to improve self-healing of the membrane. Longevity of membranes on polybutadiene supports remains to be addressed. Furthermore, transmembrane protein incorporation and functionality on the PB support need to be demonstrated. If membranes are formed by the vesicle deposition method, proteins could be inserted directly into the vesicles. If the painting strategy is pursued, proteins could be incorporated using the methods described in Figure 11.

8.4. Hybrid lipid-polymer membranes on a solid support

The fourth stabilization strategy entailed ”doping” biomimetic lipid bilayer membranes with lipid bilayer-like triblock copolymers. Block copolymers have shown improvements in terms of mechanical and temporal stability compared to lipids[46, 47, 61]. Triblock copolymers have emerged fairly recently as biomimetic membrane components and only a handful of articles shows successful formation of solid-supported triblock copolymer membranes. For a review, see Belegrinou *et al*[100]. This work demonstrates preparation of a solid-supported membrane composed of a mixture of lipids and triblock copolymers. Biomimetic membranes on solid negatively-charged silicon dioxide and mica supports were prepared by vesicle deposition. We produced hybrid vesicles composed of both triblock polymer and zwitterionic or cationic lipids. These vesicles could tether well to negatively charged silicon dioxide and mica surfaces. The vesicles gained stability properties from the polymer and adhesion properties from the lipid. The mixed lipid-polymer vesicles show promise for formation of robust membranes and can be

designed either for tethering of vesicles or formation of planar, solid-supported membranes by varying the lipid content of the vesicles.

In future work, it would to be interesting to address whether PMOXA-PDMS-PMOXA and POPC and DOTAP lipids mix homogeneously or separate to make patches (Fig. 46), whether ABA spans the membrane fully or only inserts partially (Fig. 46) and what effect the polymer to lipid ratio has on this. Polymer:lipid mixing could be addressed by differential scanning calorimetry, as shown by Ruysschaert *et al*[50].

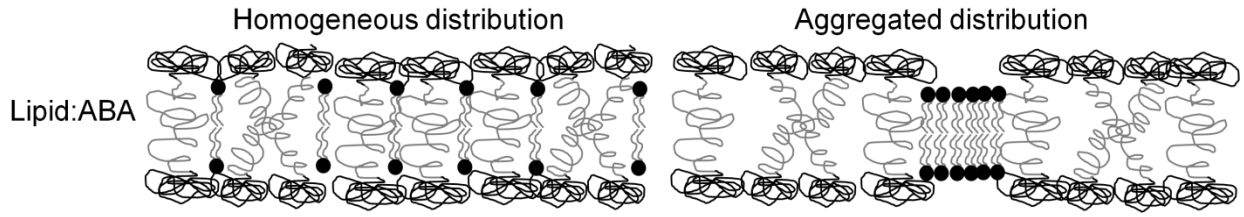

Figure 46. Hypothetic structures of hybrid membranes composed of ABA triblock copolymers and POPC or DOTAP lipids. Lipids might either disperse evenly into the ABA membrane in a homogenous distribution or segregate into domains leading to an aggregated distribution. ABA triblock copolymers might fully span the lipid bilayer or partially insert the PDMS unit into the acyl chain portion of the lipid bilayer and form a "U"-shape. Figure from [209].

To make these membranes compatible with a water purification device, the next step would be to demonstrate their deposition on a porous support and address whether defect-free membranes are formed on this support. The subsequent step would be to demonstrate incorporation of functional tansmembrane proteins. In principle, these systems should be well-suited for incorporation of functional transmembrane proteins as lipids provide the thickness of biological membranes and the triblock copolymers provide a spacer that prevents the protein from colliding with the support surface and being immobilized or denatured. It would also be interesting to quantify and compare how much transmembrane protein can be incorporated into pure ABA membranes and hybrid ABA/lipid membranes.

8.5. What is meant by membrane stability?

Challenges with poor membrane stability still need to be met in order to create commercially viable biomimetic membrane-based technologies. Surprisingly, there is no consensus on a standard way to characterize and quantify biomimetic membrane stability in order to compare the different comformations of membrane.

Among stability parameters that are mentioned for solid-supported membranes are delamination of the membrane[113, 212] or the ability to withstand drying (such as being transferred from water to air and back again or harsher treatments such as thorough drying with nitrogen gas[212]). Vesicular membrane stability, on the other hand, addresses chemical stability (such as hydrolysis and oxidation of phospholipids[213]) and physical stability (such as breakage into small lipid aggregates[210], aggregation and fusion of vesicles[213] or membrane permeability[46], leakage[210, 213] and rupture[46] of vesicles). Vesicles are said to be physically stable if they can tolerate a broad range of pH[213], temperature[210] or applied mechanical stress[46]. Vesicular stability is also claimed if the vesicles remain unchanged over a certain period of time (i.e. tolerate aging) [213] or upon interaction with different support surfaces[209].

Free-standing membranes are characterized by their ability to withstand rupture, which can be monitored mechanically[25, 45], optically[25, 45] or electrically[6, 21, 32, 36, 45, 67]. Quantification of stability can include mechanical stability (e.g. what pressure can be applied to the membrane before it ruptures[25, 26, 36, 45, 187] or what mechanical vibration can be withstood[41, 42, 172]), electrical stability (e.g. what voltage can be applied to the membrane before it ruptures[169, 170, 172, 187]) or aging stability (i.e. what length of time the membrane can withstand rupture[6, 21, 25, 36, 67]). A benchmark for biomimetic membrane longevity is a lifetime exceeding 1 day[24].

However, these criteria only address structural stability, but another very important factor of biomimetic membranes that needs to be addressed is the functional stability of the proteins associated with the membrane. Many applications of biomimetic membranes involve incorporation of transmembrane proteins, where protein function is vital for the application. Therefore it is equally (or perhaps more) important, to benchmark biomimetic membrane stability by exposing the membrane with the incorporated proteins to various conditions (such as

time, mechanical stress, temperature variation etc) and showing that the protein maintains its function. This has been done in some work[40-42].

In light of this discussion, it is strange that solid-supported planar membranes are claimed to be more stable than free-standing membranes[30], because stability is defined differently for these two membrane formats and the definition is influenced by which application the membrane has and what analytical techniques can be used to study it. A common use of free-standing membranes is to study ion channels and in order to be able to measure single-channel conductance it is necessary to have a leak-free high resistance membrane. Study of solid-supported membranes on the other hand do not always require a large defect-free membrane area and therefore membrane "rupture" is not as important. In fact the statement "solid-supported planar membranes are claimed to be more stable than free-standing membranes" can be interpreted as "it is possible to study membranes supported on a solid surface for a longer amount of time than free-standing membranes due to the requirements placed upon them by the techniques which are used to study them".

In this thesis, I have touched on various aspects of stability that are named here. In the hydrogel encapsulation and nanoporous hydrogel support approaches, I have defined stability of membranes as the length of time that the membranes do not rupture, which was monitored electrically by the ability of the membranes to maintain a low membrane conductance. For membranes supported on the nanoporous substrate polybutadiene, membrane stability was addressed in terms of compressibility due to an applied mechanical force (with an AFM cantilever, see appendix III). Lastly, the triblock copolymer-containing biomimetic membranes were in the format of vesicles or in the format of planar solid-supported membranes. Stability of the vesicles was compared in terms of the ability to withstand osmotic pressure and in terms of rupture propensity due to interaction with a support surface. Although not described in paper IV, vesicle diameter was also monitored over time, in this way checking that the vesicles were stable, i.e. did not fuse with each other or reform into smaller vesicular structures. In QCM-D measurements, stability of the formed solid-supported membranes could be observed in terms of lack of delamination from the surface.

In this work, I have shown some promising strategies for support of biomimetic membranes, which improved their stability. To make biomimetic membranes suitable for technological applications, they still need to be made so stable that they can easily be handled and transported without losing functionality. In the future, the approaches mentioned here could also be combined to obtain tough and robust biomimetic membranes.

9. Acknowledgements

This thesis marks the end of my three-year PhD period. The PhD time has been filled with lots of new experiences, experiments and people. Looking back to the start of the road, I would like to extend my sincere thanks to all the people who have helped me along the way.

First, I would like to very much thank my supervisors Claus and Henrik, who have supported and encouraged me all the way. Claus, thank you for teaching me about black lipid membranes and voltage clamp electrophysiology, for sharing your expertise on wine production, and for your guidance in how to write and phrase a scientific paper and present results. Thank you for showing me the ropes at the Biophysical conference and for all the good scientific discussions and also for the laughs. For taking the time to train me for presentations and for all our skype meetings while I was in the US for my external research stay. I feel that I have grown as a scientist under your guidance. Thank you also to my colleagues at Aquaporin and DTU Physics who have contributed in various ways during these three years to my everyday. Thank you to Peter for giving me the opportunity to experience carrying out my PhD as part of the research work of a company. Thanks to my project managers Mark, Karin and Jesper for your guidance and feedback and for your training in the lab with voltage clamp, FTIR and fluorescence microscopy. My fellow PhD students, especially Kamila and Christian, thank you for being around, for swapping stories and helping each other out, thanks for the Tuesday beers and table football. Christian, you and I have really been working side by side, and I wanted to say thank you and that I have really enjoyed working with you. Marianne, thank you for teaching me about patents, for the interesting discussion we had about this thesis and in general for our always intresting discussions. Thomas, thank you for the many times you have lent a hand in the lab, for being so amusing and for the many lifts to the train. Dorthe and Jesper G, thank you for your help in the last stage of my PhD and the first stage of my pregnancy, with taking care of the lab work involving chemicals dangerous for the baby. Thank you also to Hans, the project coordinator of the MEMBAQ project of which I was a part, for our adventures as ”the dynamic duo” at press conferences in Prague and London. Thank you to Dorte Glass and Henning Nicolajsen for helping me with all the formal matters and paperwork, and especially for the warm welcome I always received. Thank you to Tomas Bohr, Jørn Bindslev Hansen and Thomas

Bligaard for teaching me all about making an oral presentation and Ib Chorkendorff for teaching me how to write grant applications.

Thank you also to my second lab at the University of Illinois, where I spent a wonderful summer in the group of Julie Zilles. I would like to take this opportunity to thank Julie for opening up her lab to me and making me feel so welcome. I really enjoyed our scientific discussions and appeciate your thorough feedback on the manuscript which resulted from my stay there. A special thank you to Michelle for all your help, from finding me a place to live to training me in the lab to opening your home to me or taking me strawberry picking in the Illinois countryside. I am very happy about all the work we did, I have really enjoyed working together with you! Thank you of course also to Manish (and Claus) who are the reasons for me going to Illinois. Thanks Manish for all the clever feedback both during my stay there and now afterwards. Thank you to Helen Nguyen for providing me with access to the QCM-D and for valuable discussions about the obtained data. Thanks to my roomies Sabine, Encarna and Kelly for all the good times together, for our sangrias on the balcony and for making my stay so memorable. Thank you of course also to all the other people in the lab who invited me out for all the wonderful barbeques, game nights and other social events (like the maize maze), I will never forget the great times I had in Urbana-Champaign!

I would also like to thank the people who provided formal training sessions – Scott McLaren who taught me the AFM, Wacek Swiech who taught me the TEM and Michael Kaszuba at Malvern who trained me in DLS and ELS. I would also like to thank Liplasome A/S and Anders Falk Vikbjerg for providing me with access to the Zetasizer in Kongens Lyngby.

Furthermore, thank you to my co-authors and collaborators. Erik Reimhult, for our work together on polybutadiene and for always being a source of knowledge and help. Stefan Kaufmann, for the good work you have done and for the helpful advice about AFM and QCM-D. Rolf Berg, thank you for training me in using Raman Spectroscopy and our collaboration on the hydrogel paper. Juana Benavente, you have been there right from the beginning and now we have three papers together, I am very happy about our collaboration and I was really glad to finally meet

you in person in Montpellier. Ines Plasencia, for inviting me to be a co-author on your paper, for your interesting presentations about circular dichroism and for your warmth.

Thank you for funding for my work from MEMBAQ, a Specific Targeted Research Project (STREP), by the European Commission under the Sixth Framework Programme (NMP4-CT-2006-033234), funding from the Danish National Advanced Technology Foundation (023-2007-1) and from the Danish National Research Foundation.

Thank you also to Ulf Berg who put me on the nanotechnology path and Maria Sörensson and Knut Deppert who have believed in and encouraged me through my master's and PhD educations. Thank you to my family for their support all these years.

Finally, all my gratitude to Erik, without whom this thesis would not have been possible. Thank you for your patience and help through my PhD time, for help in the last days with creating pictures for the thesis, proof-reading and pepping, for your encouragement and endless belief in me. You are my rock and my blessing and I am grateful for you every day.

Whoever I have failed to mention, forgive me and thank you from the bottom of my heart.

10. Abbreviations

400C	100 mM PEG-400-DA, 5 mM Darocur in buffer
400P	100 mM PEG-400-DA, 15 mM TEMED, 15 mM APS in buffer
1000C	65 mM PEG-1000-DMA, 5 mM Darocur in buffer
1000C	65 mM PEG-1000-DA, 10 mM TEMED, 10 mM APS in buffer
AFM	Atomic Force Microscopy
α-HL	α-hemolysin
APS	Ammonium persulfate
BFS	Bilayer forming solution
BLM	Black lipid membrane
BM	Biomimetic membrane
BMA	Biomimetic membrane array
BPM	Black polymer membrane
C_{22}PhytBas	2,2-di-*O*-(3,7,11,15-tetramethylhexadecyl)-3,3-di-*O*-(1″,32″-ditriacontanyl)-bis-(rac-glycerol)-1,1-diphosphocholine
C_m	Specific membrane capacitance
CMC	Critical micelle concentration
Darocur1173	2-hydroxy-2-methyl-1-phenyl-propan-1-one
DLS	Dynamic light scattering
DOPC	1,2-dioleoyl-*sn*-glycero-3-phosphocholine
DOPE-PEG2000	1,2-dioleoyl-*sn*-glycero-3-phosphoethanolamine-N-[methoxy(polyethylene glycol)-2000]
DOTAP	1,2-dioleoyl-3-trimethylammoniumpropane
DPhPC	1,2-diphytanoyl-sn-Glycero-3-Phosphocholine
DPhPE-A	1,2-diphytanoyl-*sn*-glycero-3-phosphoethanolamine-N-acrylate
DPPC	1,2-dipalmitoyl-sn-glycero-3-phosphocholine
DSPE	1,2-distearoyl-*sn*-glycero-3-phosphoethanolamine
DTPC	1,2-di-10,12-tricosadiynoyl-*sn*-glycero-3-phosphocholine
E_f	Evenness factor
ETFE	Ethylene tetrafluoroethylene
FITC	Fluorescein isothiocyanate
FTIR	Fourier Transform Infrared Spectroscopy
GUV	Giant unilamellar vesicle
HEMA	2-hydroxyethyl methacrylate
HPS	Hydrogel precursor solution
LB	Langmuir-Blodgett
LS	Langmuir-Schaefer
LUV	Large unilamellar vesicle
MLV	Multilamellar vesicle
PB-PDMS	1,2-polybutadiene-b-polydimethylsiloxane
PDMS	Polydimethylsiloxane
PEG-DA	Poly(ethylene glycol)-diacrylate
PEG-DMA	Poly(ethylene glycol)-dimethacrylate
PEI	Poly(ethyleneimine)

PEO-PEE	Polyethyleneoxide-polyethylethylene
P_f	Water permeability
PMMA	Polymethylmethacrylate
PMOXA-PDMS-PMOXA	Poly-(2-methyloxazoline)-polydimethylsiloxane-poly-(2-methyloxazoline)
POPC	1-palmitoyl-2-Oleoyl-sn-Glycero-3-Phosphocholine
POPE	1-palmitoyl-2-oleoyl-*sn*-glycero-3-phosphoethanolamine
POPS	1-palmitoyl-2-oleoyl-*sn*-glycero-3-phospho-L-serine (sodium salt)
PSPC	1-palmitoyl-2-stearoyl-*sn*-glycero-3-phosphocholine
PSS	Poly(sodium 4-styrene sulfonate)
PTFE	Poly(tetrafluoroethylene)
PTPC	1-palmitoyl-2-10,12 Tricosadiynoyl-sn-Glycero-3-Phosphocholine
QCM-D	Quartz Crystal Microbalance with Dissipation monitoring
RO	Reverse osmosis
SEM	Scanning Electron Microscopy
SiO_2	Silicon dioxide
S-layer	Surface layer
SLB	Supported lipid bilayer
SNARE	Soluble *N*-ethylmaleimide-sensitive-factor attachment protein receptor
SUV	Small unilamellar vesicle
TEM	Transmission electron microscopy
TEMED	N,N,N',N'-tetramethyl-ethane-1,2-diamine
VCE	Voltage clamp electrophysiology
X400C	Crosslinked gel. 100 mM PEG-400-DA, 5 mM Darocur.
X400P	Crosslinked gel. 100 mM PEG-400-DA, 15 mM TEMED, 15 mM APS.
X1000C	Crosslinked gel. 65 mM PEG-1000-DMA, 5 mM Darocur.
X1000C	Crosslinked gel. 65 mM PEG-1000-DA, 10 mM TEMED, 10 mM APS.
XP	5 mM Darocur in buffer with 15 min UV irradiation
YP	Yielding point

11. References

1. Pashley, R. M.; Rzechowicz, M.; Pashley, L. R.; Francis, M. J., De-Gassed Water Is a Better Cleaning Agent. *The journal of physical chemistry. B* **2005,** 109, (3), 1231-1238.
2. Fang, Y.; Hong, Y. L.; Webb, B.; Lahiri, J., Applications of biomembranes in drug discovery. *Mrs Bulletin* **2006,** 31, (7), 541-545.
3. Tien, H. T.; Ottova, A.; Tien, H. T.; Ottova-Leitmannova, A., The lipid bilayer concept: Experimental realization and current applications. In *Membrane Science and Technology*, Elsevier: 2003; Vol. 7, pp 1-73.
4. Ottova-Leitmannova, A.; Ti Tien, H., Bilayer lipid membranes: An experimental system for biomolecular electronic devices development. *Progress in Surface Science* **1992,** 41, (4), 337-445.
5. Suzuki, H.; Takeuchi, S., Microtechnologies for membrane protein studies. *Analytical and Bioanalytical Chemistry* **2008,** 391, (8), 2695-2702.
6. Hansen, J. S.; Perry, M.; Vogel, J.; Groth, J. S.; Vissing, T.; Larsen, M. S.; Geschke, O.; Emneus, J.; Bohr, H.; Nielsen, C. H., Large scale biomimetic membrane arrays. *Analytical and Bioanalytical Chemistry* **2009,** 395, (3), 719-727.
7. Suzuki, H.; Le Pioufle, B.; Takeuhci, S., Ninety-six-well planar lipid bilayer chip for ion channel recording Fabricated by hybrid stereolithography. *Biomedical Microdevices* **2009,** 11, (1), 17-22.
8. Hemmler, R.; Bose, G.; Wagner, R.; Peters, R., Nanopore unitary permeability measured by electrochemical and optical single transporter recording. *Biophysical journal* **2005,** 88, (6), 4000-4007.
9. Hansen, J. S.; Hélix-Nielsen, C., Creating Scalable and Addressable Biomimetic Membrane Arrays in Biomedicine. In *Advances in Biomimetics / Book 1*, George, A., Ed. 2011.
10. Agre, P.; Bonhivers, M. l.; Borgnia, M. J., The Aquaporins, Blueprints for Cellular Plumbing Systems. *Journal of Biological Chemistry* **1998,** 273, (24), 14659-14662.
11. Nielsen, C. H., Osmotic Water Purification: Insights from Nanoscale Biomimetics. *Environmental Nano Technologies* **2010,** 1, (1), 58-65.
12. Greenlee, L. F.; Lawler, D. F.; Freeman, B. D.; Marrot, B.; Moulin, P., Reverse osmosis desalination: water sources, technology, and today's challenges. *Water Research* **2009,** 43, (9), 2317-2348.
13. Nielsen, C. H., Biomimetic membranes for sensor and separation applications. *Analytical and Bioanalytical Chemistry* **2009,** 395, (3), 697-718.
14. Graneli, A.; Rydstrom, J.; Kasemo, B.; Hook, F., Formation of supported lipid bilayer membranes on SiO2 from proteoliposomes containing transmembrane proteins. *Langmuir* **2003,** 19, (3), 842-850.
15. Reimhult, E.; Hook, F.; Kasemo, B., Temperature dependence of formation of a supported phospholipid bilayer from vesicles on SiO2. *Physical Review. E, Statistical, Nonlinear, and Soft Matter Physics* **2002,** 66, (5 Pt 1), 051905.
16. Reimhult, E.; Hook, F.; Kasemo, B., Vesicle adsorption on SiO2 and TiO2: Dependence on vesicle size. *Journal of Chemical Physics* **2002,** 117, (16), 7401-7404.
17. Richter, R. P.; Brisson, A., QCM-D on mica for parallel QCM-D-AFM studies. *Langmuir* **2004,** 20, (11), 4609-4613.

18. Richter, R. P.; Brisson, A. R., Following the formation of supported lipid bilayers on mica: a study combining AFM, QCM-D, and ellipsometry. *Biophys J* **2005,** 88, (5), 3422-3433.
19. Tamm, L. K.; McConnell, H. M., Supported phospholipid bilayers. *Biophysical journal.* **1985,** 47, (1), 105-113.
20. Han, X. J.; Studer, A.; Sehr, H.; Geissbuhler, I.; Di Berardino, M.; Winkler, F. K.; Tiefenauer, L. X., Nanopore arrays for stable and functional free-standing lipid bilayers. *Advanced Materials* **2007,** 19, (24), 4466-4470.
21. Romer, W.; Lam, Y. H.; Fischer, D.; Watts, A.; Fischer, W. B.; Goring, P.; Wehrspohn, R. B.; Gosele, U.; Steinem, C., Channel Activity of a Viral Transmembrane Peptide in Micro-BLMs: Vpu1-32 from HIV-1. *Journal of the American Chemical Society* **2004,** 126, (49), 16267-16274.
22. Terrettaz, S.; Ulrich, W.-P.; Guerrini, R.; Verdini, A.; Vogel, H., Immunosensing by a Synthetic Ligand-Gated Ion Channel *Angewandte Chemie International Edition* **2001,** 40, (9), 1740-1743.
23. Tanaka, M.; Sackmann, E., Supported membranes as biofunctional interfaces and smart biosensor platforms. *Physica Status Solidi a-Applications and Materials Science* **2006,** 203, (14), 3452-3462.
24. Reimhult, E.; Kumar, K., Membrane biosensor platforms using nano- and microporous supports. *Trends in Biotechnology* **2008,** 26, (2), 82-89.
25. Simon, A.; Girard-Egrot, A.; Sauter, F.; Pudda, C.; D'Hahan, N. P.; Blum, L.; Chatelain, F.; Fuchs, A., Formation and stability of a suspended biomimetic lipid bilayer on silicon submicrometer-sized pores. *Journal of Colloid and Interface Science* **2007,** 308, (2), 337-343.
26. Mey, I.; Stephan, M.; Schmitt, E. K.; Müller, M. M.; Amar, M. B.; Steinem, C.; Janshoff, A., Local Membrane Mechanics of Pore-Spanning Bilayers. *Journal of the American Chemical Society* **2009,** 131, (20), 7031-7039.
27. Drexler, J.; Steinem, C., Pore-Suspending Lipid Bilayers on Porous Alumina Investigated by Electrical Impedance Spectroscopy. *The journal of physical chemistry. B* **2003,** 107, (40), 11245-11254.
28. Hennesthal, C.; Drexler, J.; Steinem, C., Membrane-Suspended Nanocompartments Based on Ordered Pores in Alumina. *Chemphyschem* **2002,** 3, (10), 885-889.
29. Horn, C.; Steinem, C., Photocurrents Generated by Bacteriorhodopsin Adsorbed on Nano-Black Lipid Membranes. *Biophysical journal* **2005,** 89, (2), 1046-1054.
30. Castellana, E. T.; Cremer, P. S., Solid supported lipid bilayers: From biophysical studies to sensor design. *Surface Science Reports* **2006,** 61, (10), 429-444.
31. Mueller, P.; Rudin, D. O.; Ti Tien, H.; Wescott, W. C., Reconstitution of Cell Membrane Structure in vitro and its Transformation into an Excitable System. *Nature* **1962,** 194, (4832), 979-980.
32. White, S. H., A study of lipid bilayer membrane stability using precise measurements of specific capacitance. *Biophysical journal* **1970,** 10, 1127-1148.
33. White, S. H.; Thompson, T. E., Capacitance, area and thickness variations in thin lipid films. *Biochimica et Biophysica Acta* **1973,** 323, (1), 7-22.
34. Lewis, B. A.; Engelman, D. M., Lipid Bilayer Thickness Varies Linearly with Acyl Chain-Length in Fluid Phosphatidylcholine Vesicles. *Journal of Molecular Biology* **1983,** 166, (2), 211-217.
35. White, S. H., Analysis of torus surrounding planar lipid bilayer membranes. *Biophysical journal* **1972,** 12, (4), 432-445.

36. Malmstadt, N.; Jeon, L. J.; Schmidt, J. J., Long-Lived Planar Lipid Bilayer Membranes Anchored to an in situ Polymerized Hydrogel. *Advanced Materials* **2008,** 20, (1), 84-89.
37. Coster, H. G. L.; Tien, H. T.; Ottova-Leitmannova, A., Dielectric and electrical properties of lipid bilayers in relation to their structure. In *Membrane Science and Technology*, Elsevier: 2003; Vol. 7, pp 75-108.
38. Vogel, J.; Perry, M.; Hansen, J. S.; Bolinger, P. Y.; Nielsen, C. H.; Geschke, O., A support structure for biomimetic applications. *Journal of micromechanics and microengineering* **2009,** 19, (2), 025026.
39. Hansen, J. S.; Perry, M.; Vogel, J.; Vissing, T.; Hansen, C. R.; Geschke, O.; Emneus, J.; Nielsen, C. H., Development of an automation technique for the establishment of functional lipid bilayer arrays. *Journal of micromechanics and microengineering* **2009,** 19, (2), 025014.
40. Jeon, T. J.; Malmstadt, N.; Schmidt, J. J., Hydrogel-encapsulated lipid membranes. *Journal of the American Chemical Society* **2006,** 128, (1), 42-43.
41. Shim, J. W.; Gu, L. Q., Stochastic sensing on a modular chip containing a single-ion channel. *Analytical Chemistry* **2007,** 79, (6), 2207-2213.
42. Kang, X. F.; Cheley, S.; Rice-Ficht, A. C.; Bayley, H., A storable encapsulated bilayer chip containing a single protein nanopore. *Journal of the American Chemical Society* **2007,** 129, (15), 4701-4705.
43. Costello, R. F.; Peterson, I. R.; Heptinstall, J.; Walton, D. J., Improved Gel-Protected Bilayers. *Biosensors and Bioelectronics* **1999,** 14, 265-271.
44. Beddow, J. A.; Peterson, I. R.; Heptinstall, J.; Walton, D. J., Reconstitution of Nicotinic Acetylcholine Receptors into Gel-Protected Lipid Membranes. *Analytical Chemistry* **2004,** 76, (8), 2261-2265.
45. Hopkinson, D. P. Measurements and Modeling of the Failure Pressure of Bilayer Lipid Membranes. PhD thesis, Virginia Polytechnic Institute, Blacksburg, 2007.
46. Discher, B. M.; Won, Y. Y.; Ege, D. S.; Lee, J. C. M.; Bates, F. S.; Discher, D. E.; Hammer, D. A., Polymersomes: Tough vesicles made from diblock copolymers. *Science* **1999,** 284, (5417), 1143-1146.
47. Lee, J. C. M.; Bermudez, H.; Discher, B. M.; Sheehan, M. A.; Won, Y. Y.; Bates, F. S.; Discher, D. E., Preparation, stability, and in vitro performance of vesicles made with diblock copolymers. *Biotechnology and Bioengineering* **2001,** 73, (2), 135-145.
48. Meier, W.; Nardin, C.; Winterhalter, M., Reconstitution of channel proteins in (polymerized) ABA triblock copolymer membranes. *Angewandte Chemie-International Edition* **2000,** 39, (24), 4599-4602.
49. Kumar, M.; Grzelakowski, M.; Zilles, J.; Clark, M.; Meier, W., Highly permeable polymeric membranes based on the incorporation of the functional water channel protein Aquaporin Z. *Proceedings of the National Academy of Sciences of the United States of America* **2007,** 104, (52), 20719-20724.
50. Ruysschaert, T.; Sonnen, A. F.; Haefele, T.; Meier, W.; Winterhalter, M.; Fournier, D., Hybrid nanocapsules: interactions of ABA block copolymers with liposomes. *Journal of the American Chemical Society* **2005,** 127, (17), 6242-6247.
51. Kumar, M.; Payne, M. M.; Poust, S. K.; Zilles, J. L., Polymer-based Biomimetic Membranes for Desalination. In *Biomimetic membranes for sensor and separation applications*, Hélix-Nielsen, C., Ed. Springer Verlag: in preparation.
52. Hoffman, A. S., Hydrogels for biomedical applications. *Advanced Drug Delivery Reviews* **2002,** 54, (1), 3-12.

53. Benz, R.; Frohlich, O.; Lauger, P.; Montal, M., Electrical Capacity of Black Lipid Films and of Lipid Bilayers Made from Monolayers. *Biochimica et Biophysica Acta* **1975,** 394, (3), 323-334.
54. Hazel, J. R., In *Physiological Regulation of Membrane Fluidity* 1988; pp 149-188.
55. Kohler, G.; Moya, S. E.; Leporatti, S.; Bitterlich, C.; Donath, E., Stability and fusion of lipid layers on polyelectrolyte multilayer supports studied by colloidal force spectroscopy. *European Biophysics Journal: with biophysics letters* **2007,** 36, (4-5), 337-347.
56. Szewczykowski, P. P. Nano-porous Materials from Diblock Copolymers and its Membrane Application. PhD thesis, Technical University of Denmark, Kgs Lyngby, 2009.
57. Ndoni, S.; Li, L.; Schulte, L.; Szewezykowski, P. P.; Hansen, T. W.; Guo, F. X.; Berg, R. H.; Vigild, M. E., Controlled Photooxidation of Nanoporous Polymers. *Macromolecules* **2009,** 42, (12), 3877-3880.
58. Belegrinou, S.; Dorn, J.; Kreiter, M.; Kita-Tokarczyk, K.; Sinner, E. K.; Meier, W., Biomimetic supported membranes from amphiphilic block copolymers. *Soft Matter* **2010,** 6, (1), 179-186.
59. Nielsen, C. H., Protein–Lipid Interactions in Biological Membranes. In *Handbook of Molecular Biophysics*, Bohr, H., Ed. Wiley Verlag: Weinheim, 2009.
60. http://cellbiology.med.unsw.edu.au/units/science/lecture0803.htm
61. Gonzalez-Perez, A.; Stibius, K. B.; Vissing, T.; Nielsen, C. H.; Mouritsen, O. G., Biomimetic triblock copolymer membrane arrays: a stable template for functional membrane proteins. *Langmuir* **2009,** 25, (18), 10447-10450.
62. Nardin, C.; Thoeni, S.; Widmer, J.; Winterhalter, M.; Meier, W., Nanoreactors based on (polymerized) ABA-triblock copolymer vesicles. *Chemical Communications* **2000**, (15), 1433-1434.
63. Israelachvili, J. N., *Intermolecular and surface forces / Jacob N. Israelachvili*. Academic Press: London ; San Diego :, 1991.
64. Tanaka, M.; Sackmann, E., Polymer-supported membranes as models of the cell surface. *Nature (London)* **2005,** 437, (7059), 656-663.
65. Kuhner, M.; Tampe, R.; Sackmann, E., Lipid mono- and bilayer supported on polymer films: composite polymer-lipid films on solid substrates. *Biophysical journal.* **1994,** 67, (1), 217-226.
66. Richter, R.; Mukhopadhyay, A.; Brisson, A., Pathways of lipid vesicle deposition on solid surfaces: a combined QCM-D and AFM study. *Biophysical journal* **2003,** 85, (5), 3035-3047.
67. Ibragimova, S.; Stibius, K.; Szewczykowski, P.; Perry, M.; Bohr, H.; Hélix-Nielsen, C., Hydrogels for in situ Encapsulation of Biomimetic Membrane Arrays. *Polymers for Advanced Technologies*, doi 10.1002/pat.1850 (in press).
68. Daly, S. M.; Heffernan, L. A.; Barger, W. R.; Shenoy, D. K., Photopolymerization of mixed monolayers and black lipid membranes containing gramicidin A and diacetylenic phospholipids. *Langmuir* **2006,** 22, (3), 1215-1222.
69. Graff, A.; Winterhalter, M.; Meier, W., Nanoreactors from Polymer-Stabilized Liposomes. *Langmuir : the ACS journal of surfaces and colloids* **2001,** 17, (3), 919-923.
70. Schleper, C.; Puehler, G.; Holz, I.; Gambacorta, A.; Janekovic, D.; Santarius, U.; Klenk, H. P.; Zillig, W., Picrophilus gen. nov., fam. nov.: a novel aerobic, heterotrophic, thermoacidophilic genus and family comprising archaea capable of growth around pH 0. *J. Bacteriol.* **1995,** 177, (24), 7050-7059.

71. De Rosa, M.; Gambacorta, A., The Lipids of Archaebacteria. *Progress in Lipid Research* **1988,** 27, (3), 153-176.
72. Dannenmuller, O.; Arakawa, K.; Eguchi, T.; Kakinuma, K.; Blanc, S.; Albrecht, A. M.; Schmutz, M.; Nakatani, Y.; Ourisson, G., Membrane properties of archaeal macrocyclic diether phospholipids. *Chemistry-a European Journal* **2000,** 6, (4), 645-654.
73. Febo-Ayala, W.; Morera-Felix, S. L.; Hrycyna, C. A.; Thompson, D. H., Functional Reconstitution of the Integral Membrane Enzyme, Isoprenylcysteine Carboxyl Methyltransferase, in Synthetic Bolalipid Membrane Vesicles. *Biochemistry : a weekly publication of the American Chemical Society* **2006,** 45, (49), 14683-14694.
74. Montal, M.; Mueller, P., Formation of Bimolecular Membranes from Lipid Monolayers and a Study of their Electrical Properties. *Proceedings of the National Academy of Sciences of the United States of America* **1972,** 69, (12), 3561-3566.
75. Nardin, C.; Winterhalter, M.; Meier, W., Giant Free-Standing ABA Triblock Copolymer Membranes. *Langmuir : the ACS journal of surfaces and colloids* **2000,** 16, (20), 7708-7712.
76. Rein, C.; Pszon-Bartosz, K.; Stibius, K. B.; Björnholm, T.; Hélix-Nielsen, C., Free-Standing Biomimetic Polymer Membrane Imaged with Atomic Force Microscopy. *Langmuir* **2011,** 27, (2), 499-503.
77. Woodle, M. C.; Papahadjopoulos, D., Liposome preparation and size characterization. *Methods in Enzymology* **1989,** 171, 193-217.
78. Nardin, C.; Hirt, T.; Leukel, J.; Meier, W., Polymerized ABA Triblock Copolymer Vesicles. *Langmuir : the ACS journal of surfaces and colloids* **2000,** 16, (3), 1035-1041.
79. Claassen, D. E.; Spooner, B. S., Liposome formation in microgravity. *Advances in Space Research* **1996,** 17, (6-7), 151-160.
80. Ollivon, M.; Lesieur, S.; Grabielle-Madelmont, C.; Paternostre, M., Vesicle reconstitution from lipid-detergent mixed micelles. *Biochimica et Biophysica Acta (BBA) - Biomembranes* **2000,** 1508, (1-2), 34-50.
81. Pereira-Lachataignerais, J.; Pons, R.; Panizza, P.; Courbin, L.; Rouch, J.; Lopez, O., Study and formation of vesicle systems with low polydispersity index by ultrasound method. *Chemistry and Physics of Lipids* **2006,** 140, (1-2), 88-97.
82. Kolchens, S.; Ramaswami, V.; Birgenheier, J.; Nett, L.; O'Brien, D. F., Quasi-elastic light scattering determination of the size distribution of extruded vesicles. *Chemistry and Physics of Lipids* **1993,** 65, (1), 1-10.
83. Lasic, D. D., *Liposomes in gene delivery*. CRC Press: 1997.
84. Liang, X.; Mao, G.; Ng, K. Y. S., Effect of chain lengths of PEO-PPO-PEO on small unilamellar liposome morphology and stability: an AFM investigation. *Journal of Colloid and Interface Science* **2005,** 285, (1), 360-372.
85. http://avestin.com/English/lf.html
86. Angelova, M. I.; Dimitrov, D. S., Liposome electroformation. *Faraday Discussions of the Chemical Society* **1986,** 81, 303-311.
87. Dimova, R.; Seifert, U.; Pouligny, B.; Forster, S.; Dobereiner, H. G., Hyperviscous diblock copolymer vesicles. *European Physical Journal E* **2002,** 7, (3), 241-250.
88. Wang, J. Y.; Chin, J. M.; Marks, J. D.; Lee, K. Y. C., Effects of PEO-PPO-PEO Triblock Copolymers on Phospholipid Membrane Integrity under Osmotic Stress. *Langmuir* **2010,** 26, (15), 12953-12961.

89. Sauer, M.; Haefele, T.; Graff, A.; Nardin, C.; Meier, W., Ion-carrier controlled precipitation of calcium phosphate in giant ABA triblock copolymer vesicles. *Chemical Communications* **2001**, (23), 2452-2453.
90. Cruz, A.; Perez-Gil, J., Langmuir films to determine lateral surface pressure on lipid segregation. *Methods in Molecular Biology* **2007,** 400, 439-457.
91. Kalb, E.; Frey, S.; Tamm, L. K., Formation of supported planar bilayers by fusion of vesicles to supported phospholipid monolayers. *Biochimica et Biophysica Acta (BBA) - Biomembranes* **1992,** 1103, (2), 307-316.
92. Klosgen, B.; Spangenberg, T.; Niehus, H.; Gutberlet, T.; Steitz, R.; Fragneto, G., Membranes at interfaces: Structure studies by AFM and time-resolved neutron reflectivity. *Cellular & Molecular Biology Letters* **2002,** 7, (2), 240.
93. Cremer, P. S.; Boxer, S. G., Formation and Spreading of Lipid Bilayers on Planar Glass Supports. *The journal of physical chemistry. B* **1999,** 103, (13), 2554-2559.
94. Dorn, J.; Belegrinou, S.; Kreiter, M.; Sinner, E. K.; Meier, W., Planar Block Copolymer Membranes by Vesicle Spreading. *Macromolecular Bioscience* **2011,** 11, (4), 514-525.
95. Kita-Tokarczyk, K.; Itel, F.; Grzelakowski, M.; Egli, S.; Rossbach, P.; Meier, W., Monolayer interactions between lipids and amphiphilic block copolymers. *Langmuir* **2009,** 25, (17), 9847-9856.
96. Ho, D.; Chu, B.; Lee, H.; Montemagno, C. D., Protein-driven energy transduction across polymeric biomembranes. *Nanotechnology* **2004,** 15, (8), 1084-1094.
97. Rakhmatullina, E.; Meier, W., Solid-supported block copolymer membranes through interfacial adsorption of charged block copolymer vesicles. *Langmuir* **2008,** 24, (12), 6254-6261.
98. Rakhmatullina, E.; Mantion, A.; Burgi, T.; Malinova, V.; Meier, W., Solid-Supported Amphiphilic Triblock Copolymer Membranes Grafted from Gold Surface. *Journal of Polymer Science Part a-Polymer Chemistry* **2009,** 47, (1), 1-13.
99. Zhao, B.; Brittain, W. J., Polymer brushes: surface-immobilized macromolecules. *Progress in Polymer Science* **2000,** 25, (5), 677-710.
100. Belegrinou, S.; Menon, S.; Dobrunz, D.; Meier, W., Solid-supported polymeric membranes. *Soft Matter* **2011,** 7, (6), 2202-2210.
101. Pata, V.; Dan, N., The Effect of Chain Length on Protein Solubilization in Polymer-Based Vesicles (Polymersomes). *Biophysical journal* **2003,** 85, (4), 2111-2118.
102. Curstedt, T.; Johansson, J.; Barros-Söderling, J.; Robertson, B.; Nilsson, G.; Westberg, M.; Jörnvall, H., Low-molecular-mass surfactant protein type 1. *European Journal of Biochemistry* **1988,** 172, (3), 521-525.
103. Plasencia, I.; Survery, S.; Ibragimova, S.; Hansen, J. S.; Kjellbom, P.; Helix-Nielsen, C.; Johanson, U.; Mouritsen, O. G., Structure and Stability of the Spinach Aquaporin SoPIP2;1 in Detergent Micelles and Lipid Membranes. *PLoS ONE* **2011,** 6, (2), e14674.
104. Deniaud, A.; Rossi, C.; Berquand, A.; Homand, J.; Campagna, S.; Knoll, W.; Brenner, C.; Chopineau, J., Voltage-Dependent Anion Channel Transports Calcium Ions through Biomimetic Membranes. *Langmuir : the ACS journal of surfaces and colloids* **2007,** 23, (7), 3898-3905.
105. Nardin, C.; Widmer, J.; Winterhalter, M.; Meier, W., Amphiphilic block copolymer nanocontainers as bioreactors. *European Physical Journal E* **2001,** 4, (4), 403-410.
106. Graff, A.; Sauer, M.; Van Gelder, P.; Meier, W., Virus-assisted loading of polymer nanocontainer. *Proceedings of the National Academy of Sciences of the United States of America* **2002,** 99, (8), 5064-5068.

107. Choi, H. J.; Montemagno, C. D., Artificial organelle: ATP synthesis from cellular mimetic polymersomes. *Nano Letters* **2005,** 5, (12), 2538-2542.
108. Onaca, O.; Sarkar, P.; Roccatano, D.; Friedrich, T.; Hauer, B.; Grzelakowski, M.; Güven, A.; Fioroni, M.; Schwaneberg, U., Functionalized Nanocompartments (Synthosomes) with a Reduction-Triggered Release System. *Angewandte Chemie - hrsg. von der Gesellschaft deutscher Chemiker* **2008,** 120, (37), 7137-7139.
109. Grzelakowski, M.; Onaca, O.; Rigler, P.; Kumar, M.; Meier, W., Immobilized Protein-Polymer Nanoreactors. *Small* **2009,** 5, (22), 2545-2548.
110. Choi, H. J.; Germain, J.; Montemagno, C. D., Effects of different reconstitution procedures on membrane protein activities in proteopolymersomes. *Nanotechnology* **2006,** 17, (8), 1825-1830.
111. Graff, A.; Fraysse-Ailhas, C.; Palivan, C. G.; Grzelakowski, M.; Friedrich, T.; Vebert, C.; Gescheidt, G.; Meier, W., Amphiphilic Copolymer Membranes Promote NADH:Ubiquinone Oxidoreductase Activity: Towards an Electron-Transfer Nanodevice. *Macromolecular Chemistry and Physics* **2010,** 211, (2), 229-238.
112. Vijayan, K.; Discher, D. E.; Lal, J.; Janmey, P.; Goulian, M., Interactions of Membrane-Active Peptides with Thick, Neutral, Nonzwitterionic Bilayers. *The journal of physical chemistry. B* **2005,** 109, (30), 14356-14364.
113. Naumann, C. A.; Prucker, O.; Lehmann, T.; Ruhe, J.; Knoll, W.; Frank, C. W., The polymer-supported phospholipid bilayer: tethering as a new approach to substrate-membrane stabilization. *Biomacromolecules* **2002,** 3, (1), 27-35.
114. Purrucker, O.; Fortig, A.; Jordan, R.; Tanaka, M., Supported membranes with well-defined polymer tethers--incorporation of cell receptors. *Chemphyschem* **2004,** 5, (3), 327-335.
115. Wagner, M. L.; Tamm, L. K., Tethered polymer-supported planar lipid bilayers for reconstitution of integral membrane proteins: silane-polyethyleneglycol-lipid as a cushion and covalent linker. *Biophysical journal* **2000,** 79, (3), 1400-1414.
116. Munro, J. C.; Frank, C. W., In situ formation and characterization of poly(ethylene glycol)-supported lipid bilayers on gold surfaces. *Langmuir* **2004,** 20, (24), 10567-10575.
117. Kugler, R.; Knoll, W., Polyelectrolyte-supported lipid membranes. *Bioelectrochemistry* **2002,** 56, (1-2), 175-178.
118. Delajon, C.; Gutberlet, T.; Steitz, R.; Mohwald, H.; Krastev, R., Formation of polyelectrolyte multilayer architectures with embedded DMPC studied in situ by neutron reflectometry. *Langmuir* **2005,** 21, (18), 8509-8514.
119. Reich, C.; Neff, P. A.; Bausch, A. R.; Radler, J. O.; Nickel, B., Supported membranes on polyelectrolyte layers studied by X-ray reflectometry. *Physica Status Solidi a-Applications and Materials Science* **2006,** 203, (14), 3463-3467.
120. Roerdink Lander, M.; Ibragimova, S.; Rein, C.; Vogel, J.; Stibius, K.; Geschke, O.; Perry, M.; Hélix-Nielsen, C., Biomimetic membrane arrays on cast hydrogel supports. *Langmuir*, in press.
121. Sackmann, E. E.; Tanaka, M. M., Supported membranes on soft polymer cushions: fabrication, characterization and applications. *Trends in Biotechnology* **2000,** 18, (2), 58-64.
122. Rossi, C.; Chopineau, J., Biomimetic tethered lipid membranes designed for membrane-protein interaction studies. *European biophysics journal* **2007,** 36, (8), 955-965.
123. Karlsson, O. P.; Lofas, S., Flow-Mediated On-Surface Reconstitution of G-Protein Coupled Receptors for Applications in Surface Plasmon Resonance Biosensors. *Analytical Biochemistry* **2002,** 300, (2), 132-138.

124. Stenlund, P.; Babcock, G. J.; Sodroski, J.; Myszka, D. G., Capture and reconstitution of G protein-coupled receptors on a biosensor surface. *Analytical Biochemistry* **2003,** 316, (2), 243-250.
125. Haefele, T.; Kita-Tokarczyk, K.; Meier, W., Phase Behavior of Mixed Langmuir Monolayers from Amphiphilic Block Copolymers and an Antimicrobial Peptide. *Langmuir : the ACS journal of surfaces and colloids* **2006,** 22, (3), 1164-1172.
126. Woolley, A. G.; Wallace, B., Model ion channels: Gramicidin and alamethicin. *Journal of Membrane Biology* **1992,** 129, (2), 109-136.
127. Wong, D.; Jeon, T. J.; Schmidt, J., Single molecule measurements of channel proteins incorporated into biomimetic polymer membranes. *Nanotechnology* **2006,** 17, (15), 3710-3717.
128. Becucci, L.; Carbone, M. V.; Biagiotti, T.; D'Amico, M.; Olivotto, M.; Guidelli, R., Incorporation of the HERG Potassium Channel in a Mercury Supported Lipid Bilayer. *Journal of Physical Chemistry B* **2008,** 112, (4), 1315-1319.
129. Racker, E., Reconstitution of cytochrome oxidase vesicles and conferral of sensitivity to energy transfer inhibitors. *Journal of Membrane Biology* **1972,** 10, (1), 221-235.
130. Woodbury, D. J.; Miller, C., Nystatin-induced liposome fusion. A versatile approach to ion channel reconstitution into planar bilayers. *Biophysical journal.* **1990,** 58, (4), 833-839.
131. Helrich, C. S.; Schmucker, J. A.; Woodbury, D. J., Evidence that nystatin channels form at the boundaries, not the interiors of lipid domains. *Biophysical journal* **2006,** 91, (3), 1116-1127.
132. Simberg, D.; Weisman, S.; Talmon, Y.; Barenholz, Y., DOTAP (and other Cationic lipids): Chemistry, biophysics, and transfection. *Critical reviews in therapeutic drug carrier systems* **2004,** 21, (4), 257-317.
133. Malinin, V. S.; Frederik, P.; Lentz, B. R., Osmotic and Curvature Stress Affect PEG-Induced Fusion of Lipid Vesicles but Not Mixing of Their Lipids. *Biophysical journal* **2002,** 82, (4), 2090-2100.
134. Lentz, B. R., Polymer-induced membrane fusion: potential mechanism and relation to cell fusion events. *Chemistry and Physics of Lipids* **1994,** 73, (1-2), 91-106.
135. Wang, T.; Smith, E. A.; Chapman, E. R.; Weisshaar, J. C., Lipid Mixing and Content Release in Single-Vesicle, SNARE-Driven Fusion Assay with 1-5 ms Resolution. *Biophysical journal* **2009,** 96, (10), 4122-4131.
136. Bunjes, N.; Schmidt, E. K.; Jonczyk, A.; Rippmann, F.; Beyer, D.; Ringsdorf, H.; Graber, P.; Knoll, W.; Naumann, R., Thiopeptide-Supported Lipid Layers on Solid Substrates. *Langmuir : the ACS journal of surfaces and colloids* **1997,** 13, (23), 6188-6194.
137. Lahiri, J.; Kalal, P.; Frutos, A. G.; Jonas, S. J.; Schaeffler, R., Method for Fabricating Supported Bilayer Lipid Membranes on Gold. *Langmuir : the ACS journal of surfaces and colloids* **2000,** 16, (20), 7805-7810.
138. Reimhult, E.; Hook, F.; Kasemo, B., Intact Vesicle Adsorption and Supported Biomembrane Formation from Vesicles in Solution: Influence of Surface Chemistry, Vesicle Size, Temperature, and Osmotic Pressure. *Langmuir : the ACS journal of surfaces and colloids* **2003,** 19, (5), 1681-1691.
139. Csucs, G.; Ramsden, J. J., Interaction of phospholipid vesicles with smooth metal-oxide surfaces. *Biochimica et Biophysica Acta (BBA) - Biomembranes* **1998,** 1369, (1), 61-70.
140. Gritsch, S.; Nollert, P.; Jähnig, F.; Sackmann, E., Impedance Spectroscopy of Porin and Gramicidin Pores Reconstituted into Supported Lipid Bilayers on Indium-Tin-Oxide Electrodes. *Langmuir* **1998,** 14, (11), 3118-3125.

141. Salamon, Z.; Wang, Y.; Tollin, G.; Macleod, H., Assembly and molecular organization of self-assembled lipid bilayers on solid substrates monitored by surface plasmon resonance spectroscopy. *Biochimica et Biophysica Acta (BBA) - Biomembranes* **1994,** 1195, (2), 267-275.
142. Romer, W.; Steinem, C., Impedance Analysis and Single-Channel Recordings on Nano-Black Lipid Membranes Based on Porous Alumina. *Biophysical journal* **2004,** 86, (2), 955-965.
143. Puu, G.; Gustafson, I., Planar lipid bilayers on solid supports from liposomes - factors of importance for kinetics and stability. *Biochimica et Biophysica Acta (BBA) - Biomembranes* **1997,** 1327, (2), 149-161.
144. Shenoy, D. K.; Barger, W. R.; Singh, A.; Panchal, R. G.; Misakian, M.; Stanford, V. M.; Kasianowicz, J. J., Functional Reconstitution of Protein Ion Channels into Planar Polymerizable Phospholipid Membranes. *Nano Letters* **2005,** 5, (6), 1181-1185.
145. Sackmann, E., Supported Membranes: Scientific and Practical Applications. *Science* **1996,** 271, (5245), 43-48.
146. Elender, G.; Kuhner, M.; Sackmann, E., Functionalisation of Si/SiO2 and glass surfaces with ultrathin dextran films and deposition of lipid bilayers. *Biosensors and Bioelectronics* **1996,** 11, (6-7), 565-577.
147. Gyorvary, E.; Wetzer, B.; Sleytr, U. B.; Sinner, A.; Offenhausser, A.; Knoll, W., Lateral Diffusion of Lipids in Silane-, Dextran-, and S-Layer-Supported Mono- and Bilayers. *Langmuir : the ACS journal of surfaces and colloids* **1999,** 15, (4), 1337-1347.
148. Hillebrandt, H.; Wiegand, G.; Tanaka, M.; Sackmann, E., High Electric Resistance Polymer/Lipid Composite Films on Indium-Tin-Oxide Electrodes. *Langmuir : the ACS journal of surfaces and colloids* **1999,** 15, (24), 8451-8459.
149. Baumgart, T.; Offenhausser, A., Polysaccharide-Supported Planar Bilayer Lipid Model Membranes. *Langmuir* **2003,** 19, 1730-1737.
150. Hermanowska, M. M.; Gorska, A.; Borch, J.; Simonsen, A. C.; Kloesgen, B., Design Concepts For a Biocushion to Comfort Lipid Membranes. *Biophysical journal* **2010,** 98, (3), 606a-607a.
151. Hermanowska, M.; Borch, J.; Simonsen, A. C.; Klosgen, B., Characterization of a New Biomimetic Multilayer System for Biomembrane Interaction Studies. *Biophysical journal* **2009,** 96, (3), 452a.
152. Zhang, L.; Longo, M. L.; Stroeve, P., Mobile Phospholipid Bilayers Supported on a Polyion/Alkylthiol Layer Pair. *Langmuir : the ACS journal of surfaces and colloids* **2000,** 16, (11), 5093-5099.
153. Majewski, J.; Wong, J. Y.; Park, C. K.; Seitz, M.; Israelachvili, J. N.; Smith, G. S., Structural Studies of Polymer-Cushioned Lipid Bilayers. *Biophysical journal* **1998,** 75, (5), 2363-2367.
154. Ma, C.; Srinivasan, M. P.; Waring, A. J.; Lehrer, R. I.; Longo, M. L.; Stroeve, P., Supported lipid bilayers lifted from the substrate by layer-by-layer polyion cushions on self-assembled monolayers. *Colloids and Surfaces B: Biointerfaces* **2003,** 28, (4), 319-329.
155. Spinke, J.; Yang, J.; Wolf, H.; Liley, M.; Ringsdorf, H.; Knoll, W., Polymer-supported bilayer on a solid substrate. *Biophysical journal.* **1992,** 63, (6), 1667-1671.
156. Shen, W. W.; Boxer, S. G.; Knoll, W.; Frank, C. W., Polymer-Supported Lipid Bilayers on Benzophenone-Modified Substrates. *Biomacromolecules* **2001,** 2, (1), 70-79.
157. Hausch, M.; Zentel, R.; Knoll, W., Synthesis and characterization of hydrophilic lipopolymers for the support of lipid bilayers. *Macromolecular Chemistry and Physics* **1999,** 200, (1), 174-179.

158. Seitz, M.; Ter-Ovanesyan, E.; Hausch, M.; Park, C. K.; Zasadzinski, J. A.; Zentel, R.; Israelachvili, J. N., Formation of Tethered Supported Bilayers by Vesicle Fusion onto Lipopolymer Monolayers Promoted by Osmotic Stress. *Langmuir : the ACS journal of surfaces and colloids* **2000,** 16, (14), 6067-6070.
159. Seitz, M.; Wong, J. Y.; Park, C. K.; Alcantar, N. A.; Israelachvili, J., Formation of tethered supported bilayers via membrane-inserting reactive lipids. *Thin Solid Films* **1998,** 327-329, 767-771.
160. Wong, J. Y.; Park, C. K.; Seitz, M.; Israelachvili, J., Polymer-Cushioned Bilayers. II. An Investigation of Interaction Forces and Fusion Using the Surface Forces Apparatus. *Biophysical journal* **1999,** 77, (3), 1458-1468.
161. Wong, J. Y.; Majewski, J.; Seitz, M.; Park, C. K.; Israelachvili, J. N.; Smith, G. S., Polymer-Cushioned Bilayers. I. A Structural Study of Various Preparation Methods Using Neutron Reflectometry. *Biophysical journal* **1999,** 77, (3), 1445-1457.
162. Doshi, D. A.; Dattelbaum, A. M.; Watkins, E. B.; Brinker, C. J.; Swanson, B. I.; Shreve, A. P.; Parikh, A. N.; Majewski, J., Neutron Reflectivity Study of Lipid Membranes Assembled on Ordered Nanocomposite and Nanoporous Silica Thin Films. *Langmuir : the ACS journal of surfaces and colloids* **2005,** 21, (7), 2865-2870.
163. Jani, A. M. M.; Zhou, J.; Nussio, M. R.; Losic, D.; G.Shapter, J.; H.Voelcker, N., Pore spanning lipid bilayers on silanised nanoporous alumina membranes. *Proceedings of SPIE, the International Society for Optical Engineering* **2008,** 7267.
164. Kaufman, Y.; Berman, A.; Freger, V., Supported Lipid Bilayer Membranes for Water Purification by Reverse Osmosis. *Langmuir* **2010,** 26, (10), 7388-7395.
165. Nikolelis, D. P.; Mitrokotsa, M., Stabilized lipid film based biosensor for atenolol. *Biosensors and Bioelectronics* **2002,** 17, (6-7), 565-572.
166. Nikolelis, D. P.; Raftopoulou, G.; Nikoleli, G.-P.; Simantiraki, M., Stabilized Lipid Membrane Based Biosensors with Incorporated Enzyme for Repetitive Uses. *Electroanalysis* **2006,** 18, (24), 2467-2474.
167. Gufler, P. C.; Pum, D.; Sleytr, U. B.; Schuster, B., Highly robust lipid membranes on crystalline S-layer supports investigated by electrochemical impedance spectroscopy. *Biochimica et Biophysica Acta (BBA) - Biomembranes* **2004,** 1661, (2), 154-165.
168. Costa-Balogh, F. O.; Aberg, C.; Sousa, J. J. S.; Sparr, E., Drug Transport in Responding Lipid Membranes Can Be Regulated by an External Osmotic Gradient. *Langmuir : the ACS journal of surfaces and colloids* **2005,** 21, (23), 10307-10310.
169. Ziegler, W.; Gaburjakova, J.; Gaburjakova, M.; Sivak, B.; Rehacek, V.; Tvarozek, V.; Hianik, T., Agar-supported lipid bilayers - basic structures for biosensor design. Electrical and mechanical properties. *Colloids and Surfaces A: Physicochemical and Engineering Aspects* **1998,** 140, 357-367.
170. Tien, H. T.; Ottova, A. L., Supported planar lipid bilayers (s-BLMs) as electrochemical biosensors. *Electrochimica Acta* **1998,** 43, (23), 3587-3610.
171. Costello, R. F.; Peterson, I. P.; Heptinstall, J.; Byrne, N. G.; Miller, L. S., A Robust Gel-Bilayer Channel Biosensor. *Advanced Materials for Optics and Electronics* **1998,** 8, (2), 47-52.
172. Uto, M.; Araki, M.; Taniguchi, T.; Hoshi, S.; Inoue, S., Stability of an agar-supported bilayer-lipid membrane and its application to a chemical sensor. *Analytical Sciences* **1994,** 10, (6), 943-946.

173. Maurer, J. A.; White, V. E.; Dougherty, D. A.; Nadeau, J. L., Reconstitution of ion channels in agarose-supported silicon orifices. *Biosensors and Bioelectronics* **2007,** 22, (11), 2577-2584.
174. Goksu, E. I.; Nellis, B. A.; Lin, W.-C.; Satcher, J. H.; Groves, J. T.; Risbud, S. H.; Longo, M. L., Effect of Support Corrugation on Silica Xerogel-Supported Phase-Separated Lipid Bilayers. *Langmuir* **2009,** 25, (6), 3713-3717.
175. Weng, K. C.; Stalgren, J. J. R.; Duval, D. J.; Risbud, S. H.; Frank, C. W., Fluid Biomembranes Supported on Nanoporous Aerogel/Xerogel Substrates. *Langmuir : the ACS journal of surfaces and colloids* **2004,** 20, (17), 7232-7239.
176. Lodge, T. P., Block copolymers: Past successes and future challenges. *Macromolecular Chemistry and Physics* **2003,** 204, 265-273.
177. Ndoni, S.; Vigild, M. E.; Berg, R. H., Nanoporous Materials with Spherical and Gyroid Cavities Created by Quantitative Etching of Polydimethylsiloxane in Polystyrene-Polydimethylsiloxane Block Copolymers. *Journal of the American Chemical Society.* **2003,** 125, (44), 13366-13367.
178. Hansen, M.; Vigild, M.; Berg, R.; Ndoni, S., Nanoporous Crosslinked Polyisoprene from Polyisoprene—Polydimethylsiloxane Block Copolymer. *Polymer Bulletin* **2004,** 51, (5), 403-409.
179. Sleytr, U. B.; Bayley, H.; Sara, M.; Breitwieser, A.; Kupcu, S.; Mader, C.; Weigert, S.; Unger, F. M.; Messner, P.; Jahn-Schmid, B.; Schuster, B.; Pum, D.; Douglas, K.; Clark, N. A.; Moore, J. T.; Winningham, T. A.; Levy, S.; Frithsen, I.; Pankovc, J.; Beale, P.; Gillis, H. P.; Choutov, D. A.; Martin, K. P., VI. Applications of S-layers. *FEMS Microbiology Reviews* **1997,** 20, (1-2), 151-175.
180. O'Brien, D. F.; Armitage, B.; Benedicto, A.; Bennett, D. E.; Lamparski, H. G.; Lee, Y. S.; Srisiri, W.; Sisson, T. M., Polymerization of Preformed Self-Organized Assemblies. *Accounts of chemical research - publ. monthly by the American Chemical Society* **1998,** 31, (12), 861-868.
181. Heitz, B. A.; Xu, J.; Jones, I. W.; Keogh, J. P.; Comi, T. J.; Hall, H. K.; Aspinwall, C. A.; Saavedra, S. S., Polymerized Planar Suspended Lipid Bilayers for Single Ion Channel Recordings: Comparison of Several Dienoyl Lipids. *Langmuir* **2011,** 27, (5), 1882-1890.
182. Benz, R.; Elbert, R.; Prass, W.; Ringsdorf, H., Polymerization in Black Lipid-Membranes - Influence on Ion-Transport. *European Biophysics Journal with Biophysics Letters* **1986,** 14, (2), 83-92.
183. Heitz, B. A.; Jones, I. W.; Hall, H. K.; Aspinwall, C. A.; Saavedra, S. S., Fractional Polymerization of a Suspended Planar Bilayer Creates a Fluid, Highly Stable Membrane for Ion Channel Recordings. *Journal of the American Chemical Society* **2010,** 132, (20), 7086-7093.
184. Heitz, B. A.; Xu, J.; Hall, H. K.; Aspinwall, C. A.; Saavedra, S. S., Enhanced Long-Term Stability for Single Ion Channel Recordings Using Suspended Poly(lipid) Bilayers. *Journal of the American Chemical Society* **2009,** 131, (19), 6662-6663.
185. Surrey, T.; Schmid, A.; Jahnig, F., Folding and Membrane Insertion of the Trimeric Beta-Barrel Protein OmpF. *Biochemistry : a weekly publication of the American Chemical Society* **1996,** 35, (7), 2283-2288.
186. Jeon, T. J.; Malmstadt, N.; Poulos, J. L.; Schmidt, J. J., Black lipid membranes stabilized through substrate conjugation to a hydrogel. *Biointerphases* **2008,** 3, (2), FA96-FA100.
187. Schuster, B.; Sleytr, U. B.; Diederich, A.; Bahr, G.; Winterhalter, M., Probing the stability of S-layer-supported planar lipid membranes. *European Biophysics Journal: with biophysics letters* **1999,** 28, (7), 583-590.

188. Schuster, B.; Pum, D.; Braha, O.; Bayley, H.; Sleytr, U. B., Self-assembled alpha-hemolysin pores in an S-layer-supported lipid bilayer. *Biochimica et Biophysica Acta (BBA) - Biomembranes* **1998,** 1370, (2), 280-288.
189. Schuster, B.; Pum, D.; Sleytr, U. B., Voltage clamp studies on S-layer-supported tetraether lipid membranes. *Biochimica et Biophysica Acta (BBA) - Biomembranes* **1998,** 1369, (1), 51-60.
190. Schuster, B.; Sleytr, U. B., The effect of hydrostatic pressure on S-layer-supported lipid membranes. *Biochimica et Biophysica Acta (BBA) - Biomembranes* **2002,** 1563, (1-2), 29-34.
191. Sleytr, U. B.; Egelseer, E. M.; Ilk, N.; Pum, D.; Schuster, B., S-Layers as a basic building block in a molecular construction kit. *FEBS Journal* **2007,** 274, (2), 323-334.
192. Ibragimova, S.; Benavente, J.; Berg, R.; Stibius, K.; Larsen, M. S.; Bohr, H.; Hélix-Nielsen, C., Tailoring Properties of Biocompatible PEG-DMA Hydrogels with UV Light In preparation.
193. de Lara, R.; Benavente, J., Electrokinetic and surface chemical characterizations of an irradiated microfiltration polysulfone membrane: Comparison of two irradiation doses. *Journal of Colloid and Interface Science* **2007,** 310, (2), 519-528.
194. Song, L.; Hobaugh, M. R.; Shustak, C.; Cheley, S.; Bayley, H.; Gouaux, J. E., Structure of Staphylococcal a-Hemolysin, a Heptameric Transmembrane Pore. *Science* **1996,** 274, (5294), 1859-1866.
195. Ide, T.; Yanagida, T., An Artificial Lipid Bilayer Formed on an Agarose-Coated Glass for Simultaneous Electrical and Optical Measurement of Single Ion Channels. *Biochemical and Biophysical Research Communications* **1999,** 265, (2), 595-599.
196. Roerdink Lander, M.; Hélix-Nielsen, C.; Geschke, O., In preparation.
197. www.sigmaaldrich.com
198. Vogel, J. Design, fabrication and testing of support structures for biomimetic water filters. PhD thesis, Technical University of Denmark, Kgs Lyngby, 2011.
199. Ibragimova, S.; Rein, C.; Vogel, J.; Perry, M.; Hélix-Nielsen, C., Large arrays of planar biomimetic lipid bilayer membranes supported on hydrogel-polyelectrolyte layers. In preparation.
200. Anzai, J.; Hoshi, T.; Nakamura, N., Construction of Multilayer Thin Films Containing Avidin by a Layer-by-Layer Deposition of Avidin and Poly(anion)s. *Langmuir : the ACS journal of surfaces and colloids* **2000,** 16, (15), 6306-6311.
201. Zhang, L.; Spurlin, T. A.; Gewirth, A. A.; Granick, S., Electrostatic stitching in gel-phase supported phospholipid bilayers. *Journal of Physical Chemistry B* **2006,** 110, (1), 33-35.
202. White, S. H., Formation of "solvent-free" black lipid bilayer membranes from glyceryl monooleate dispersed in squalene. *Biophysical journal.* **1978,** 23, (3), 337-347.
203. Perry, M.; Vissing, T.; Boesen, T. P.; Hansen, J. S.; Emneus, J.; Nielsen, C. H., Automated sampling and data processing derived from biomimetic membranes. *Bioinspiration and Biomimetics* **2009,** 4, (4), 044001.
204. Rein, C.; Ibragimova, S.; Kaufmann, S.; Szewczykowski, P.; Reimhult, E.; Bjørnholm, T.; Helix-Nielsen, C., Supported Lipid Bilayers on engineered nanoporous polymers. In preparation.
205. Kaufmann, S.; Papastavrou, G.; Kumar, K.; Textor, M.; Reimhult, E., A detailed investigation of the formation kinetics and layer structure of poly(ethylene glycol) tether supported lipid bilayers. *Soft Matter* **2009,** 5, (14), 2804-2814.

206. Richter, R. P.; Brisson, A., Characterization of Lipid Bilayers and Protein Assemblies Supported on Rough Surfaces by Atomic Force Microscopy. *Langmuir : the ACS journal of surfaces and colloids* **2003,** 19, (5), 1632-1640.
207. Gonzalez-Perez, A.; Castelletto, V.; Hamley, I. W.; Taboada, P., Biomimetic triblock copolymer membranes: from aqueous solutions to solid supports. *Soft Matter* **2011,** 7, (3), 1129-1138.
208. www.avantilipids.com
209. Ibragimova, S.; Marincel, M.; Kumar, M.; Nguyen, T. H.; Hélix-Nielsen, C.; Zilles, J. L., Supported hybrid lipid-polymer membranes. In preparation.
210. Chang, E. L., Unusual Thermal-Stability of Liposomes Made From Bipolar Tetraether Lipids. *Biochemical and Biophysical Research Communications* **1994,** 202, (2), 673-679.
211. Needham, D.; Zhelev, D., The mechanochemistry of lipid vesicles examined by micropipet manipulation techniques. *Surfactant science series* **1996,** 62, 373-444.
212. Albertorio, F.; Diaz, A. J.; Yang, T.; Chapa, V. A.; Kataoka, S.; Castellana, E. T.; Cremer, P. S., Fluid and Air-Stable Lipopolymer Membranes for Biosensor Applications. *Langmuir : the ACS journal of surfaces and colloids* **2005,** 21, (16), 7476-7482.
213. Grit, M.; Crommelin, J. A., Chemical-Stability of Liposomes - Implications for their Physical Stability. *Chemistry and Physics of Lipids* **1993,** 64, (1-3), 3-18.

Paper I

Research Article

polymers advanced technologies

Received: 7 March 2010, Revised: 2 September 2010, Accepted: 7 September 2010, Published online in Wiley Online Library: 2010

(wileyonlinelibrary.com) DOI: 10.1002/pat.1850

Hydrogels for *in situ* encapsulation of biomimetic membrane arrays

Sania Ibragimova[a,c], Karin Stibius[a,c], Piotr Szewczykowski[b], Mark Perry[c], Henrik Bohr[a] and Claus Hélix-Nielsen[a,c]*

Hydrogels are hydrophilic, porous polymer networks that can absorb up to thousands of times their own weight in water. They have many potential applications, one of which is the encapsulation of freestanding black lipid membranes (BLMs) for novel separation technologies or biosensor applications. We investigated gels for *in situ* encapsulation of multiple BLMs formed across apertures in a hydrophobic ethylene tetrafluoroethylene (ETFE) support. The encapsulation gels consisted of networks of poly(ethylene glycol)-dimethacrylate or poly(ethylene glycol)-diacrylate polymerized using either a chemical initiator or a photoinitiator. The hydrogels were studied with regards to volumetric stability, porosity, and water permeability. All hydrogels had pore sizes around 7 nm with volumetric changes >2% upon crosslinking. Photoinitiated hydrogels had a lower hydraulic water permeability compared to chemically initiated hydrogels; however, for all hydrogels the permeability was several-fold higher than the water permeability of conventional reverse osmosis (RO) membranes. Lifetimes of freestanding BLM arrays in gel precursor solutions were short compared to arrays formed in buffer. However, polymerizing (crosslinking) the gel stabilized the membranes and resulted in BLM arrays that remained intact for days. This is a substantial improvement over lifetimes for freestanding BLM arrays. Optical images of the membranes and single channel activity of incorporated gramicidin ion channels showed that the lipid membranes retained their integrity and functionality after encapsulation with hydrogel. Our results show that hydrogel encapsulation is a potential means to provide stability for biomimetic devices based on functional proteins reconstituted in biomimetic membrane arrays. Copyright © 2010 John Wiley & Sons, Ltd.

Keywords: biomimetic membrane arrays, encapsulation, hydrogel, stabilization, voltage clamp

INTRODUCTION

Transmembrane proteins have many functions in biological systems, and act for example as channels, receptors, or transporters. Recently the notion of biomimetic membranes as technological devices incorporating essential features of biological membranes has attracted considerable interest, for recent reviews see Ref. [1–4]. Working biomimetic membranes require that the protein must be in its native (functional) conformation. This implies that for transmembrane proteins, the protein must be embedded in a matrix compatible with protein structure and function[5–7]. Black lipid membranes (BLMs) formed across single or multi-aperture hydrophobic scaffolds closely resemble the natural environment of membrane spanning proteins. However, freestanding BLMs have notoriously low longevity, which limits many applications, for comprehensive texts on BLMs see Refs.[8,9]. A biomimetic membrane working as a sensor/separation device should be stable and typically be able to withstand osmotic/hydrostatic pressures. This is not compatible with freestanding BLMs.

In order to improve BLM longevity and stability in multi-aperture arrays, we investigated the encapsulation of BLMs in an *in situ* polymerized hydrogel. Hydrogels are hydrophilic polymer networks that can absorb up to thousands of times their dry weight in water[10–12]. Hydrogels have been shown to allow transport of water, electrolytes, and possibly proteins depending on the pore size of the hydrogel network[10,13]. Recently encapsulation of single freestanding biomimetic membranes has been proven to be a successful approach[13–23]. In this work we characterize several hydrogels and show successful hydrogel encapsulation of multiple BLMs formed across an aperture array.

In order for biological membranes to maintain their liquid crystalline state they generally require ambient temperatures between 10 and 40 °C[24]. Although the use of block-copolymers could extend the temperature range for the biomimetic protein matrix *per se*, the proteins themselves will generally denature with increased temperatures[25]. Thus, a required property for a hydrogel for encapsulating biomimetic membranes is that it is liquid and crosslinkable *in situ* at room temperature. Poly(ethylene glycol)-di(meth)acrylate (PEG-D(M)A) based hydro-

* *Correspondence to: C. Hélix-Nielsen, DTU Physics, Fysikvej 309, Building 309, office 138, Technical University of Denmark, DK-2800 Lyngby, Denmark*

a *S. Ibragimova, K. Stibius, H. Bohr, C. Hélix-Nielsen*
DTU Physics, Technical University of Denmark, Fysikvej 309, Building 309, DK-2800 Kgs. Lyngby, Denmark

b *P. Szewczykowski*
DTU Chemical Engineering, Technical University of Denmark, K DK-2800 Kgs. Lyngby, Denmark

c *S. Ibragimova, K. Stibius, M. Perry, C. Hélix-Nielsen*
Aquaporin A/S, Ole Maaløes Vej 3, DK-2200 Copenhagen, Denmark

gels fulfill this requirement. Amongst other requirements is that the crosslinking process should not result in large gel volume changes as this would destabilize the biomimetic membrane. In addition the porosity of the encapsulating gel should be able to provide sufficient stability while preserving good water and solute permeabilities.

We have studied the encapsulation potential of PEG-1000-DMA and PEG-400-DA hydrogels. In particular, we characterized chemically induced and UV-induced polymerized hydrogels with respect to volumetric stability, water permeability, and porosity. We obtained stable hydrogel encapsulated lipid bilayers with lifetimes of several days in an aperture array with 64 individual BLMs as evidenced by monitoring conductance and capacitance using standard voltage-clamp measurements[26,27]. Functionality of the encapsulated BLMs was demonstrated by recording single channel activity of incorporated gramicidin ion channels.

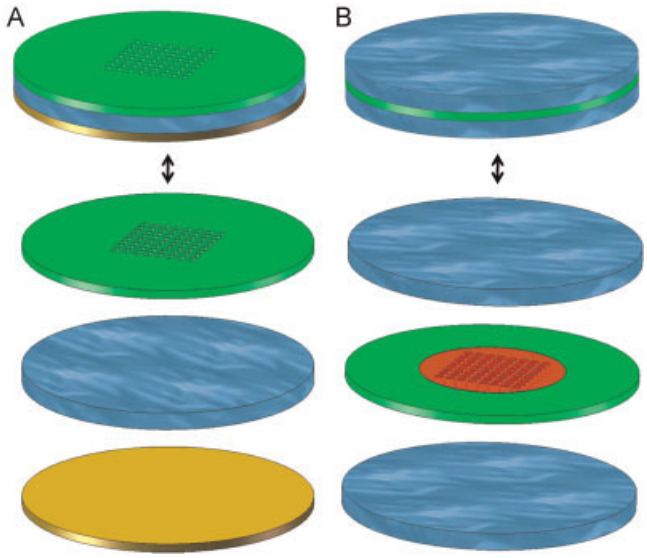

Figure 1. Schematic representations of the hydrogel sandwich and of the hydrogel-encapsulated lipid membrane (closed and exploded views). (a): The sandwich consists of an ETFE partition ø 21 mm with an 8 × 8 aperture (aperture diameter 300 μm) array (green), a crosslinked hydrogel (blue) and a regenerated cellulose membrane (ø 21 mm) on polypropylene support (brown) positioned with the cellulose side toward the gel and the polypropylene side away from the gel. (b): For BLM encapsulation a BLM (semi-transparent red circular area) is formed across the aperture array in the ETFE partition (green disk) and encapsulated by hydrogel on both sides (blue disks). This figure is available in colour online at wileyonlinelibrary.com/journal/pat.

EXPERIMENTAL

Materials

Poly(ethylene glycol)-1000-dimethacrylate (PEG-1000-DMA) and poly(ethylene glycol)-400-diacrylate (PEG-400-DA) were from Polysciences (Warrington, PA, USA). 2-Hydroxy-2-methyl-1-phenyl-propan-1-one (Darocur® 1173) was from Ciba Specialty Chemicals (Basel, Switzerland). KCl, HCl, 1,4-Piperazinediethanesulfonic acid (PIPES), ethylenediamine-tetraacetic acid (EDTA), protease inhibitor cocktail (P2714), sodium hydroxide, *N,N,N′,N′*-tetramethyl-ethylenediamine (TEMED), *n*-decane, ethanol, and ammonium persulfate (APS) were from Sigma Aldrich Denmark (Brøndby, Denmark). Multi-aperture arrays were fabricated from Tefzel ethylene tetrafluoroethylene (ETFE) LZ200 (DuPont, Detroit, USA). Sheets of cellulose membrane on a propylene support (DSS-RC70PP) were from Alfa Laval (Nakskov, Denmark). For the retention experiments 1 kDa beads were from Merck-Schuchardt (Hohenbrunn, Germany) and 3–35 kDa beads from Fluka (Buchs, Switzerland).

production of rubber chamber-sealing O-rings was from DuPont Fluoropolymers (Detroit, USA). Uncoated 35 and 50 mm glass-bottom culture dishes were from MatTek (Ashland, MA, USA). 1,2-diphytanoyl-*sn*-glycero-3-phosphocholine (DPhPC) and 1,2-Diphytanoyl-*sn*-Glycero-3-phosphoethanol-amine-*N*-acrylate (DPhPE-A) were from Avanti Polar Lipids Inc. (Alabaster, AL, USA) and gramicidin was from Sigma Aldrich Denmark (Brøndby, Denmark).

Methods

Preparation of hydrogels

Hydrogels were studied in two experimental configurations (see Fig. 1). For the porosity and water flux characterization, the configuration consisted of a hydrogel sandwiched between a DSS-RC70PP membrane and a partition with an 8 × 8 aperture array fabricated from ETFE as previously described[28] (see Fig. 1a). For the BLM encapsulation experiments BLM arrays were formed across the ETFE partitions and subsequently gel encapsulated (see Fig. 1b). The two configurations can be seen as prototypical for future applications: a sandwich supported membrane for separation applications where hydrostatic pressures are applied (Fig. 1a.), a free-standing encapsulated membrane for sensor applications, where no (or low) pressures are applied.

For all hydrogels, concentrations of PEG and initiator were selected so that the hydrogels crosslinked within 10 min of initiation. Table 1 and Fig. 2 present the hydrogels used in this study.

All hydrogel precursor solutions (HPSs) were prepared in a buffer containing 25 mM PIPES, 2 mM EDTA, 0.2 M KCl and protease inhibitor cocktail in MilliQ water, adjusted to pH 6.5 using HCl.

For photoinitiation, two aqueous HPSs were prepared: a PEG-1000-DMA solution (1000P) containing 65 mM poly(ethylene glycol)-1000-dimethacrylate monomers and 10 mM Darocur1173 photoinitiator and a PEG-400-DA solution (400P) containing

Table 1. The four hydrogel precursor solutions (HPSs) investigated. For details see the Materials and Methods section

Sample	Polymer	Initiator
400P	PEG-400-DA 100 mM	Darocur 5 mM
400C	PEG-400-DA 100 mM	TEMED 15 mM, APS 15 mM
1000P	PEG-1000-DMA 65 mM	Darocur 5 mM
1000C	PEG-1000-DMA 65 mM	TEMED 10 mM, APS 10 mM

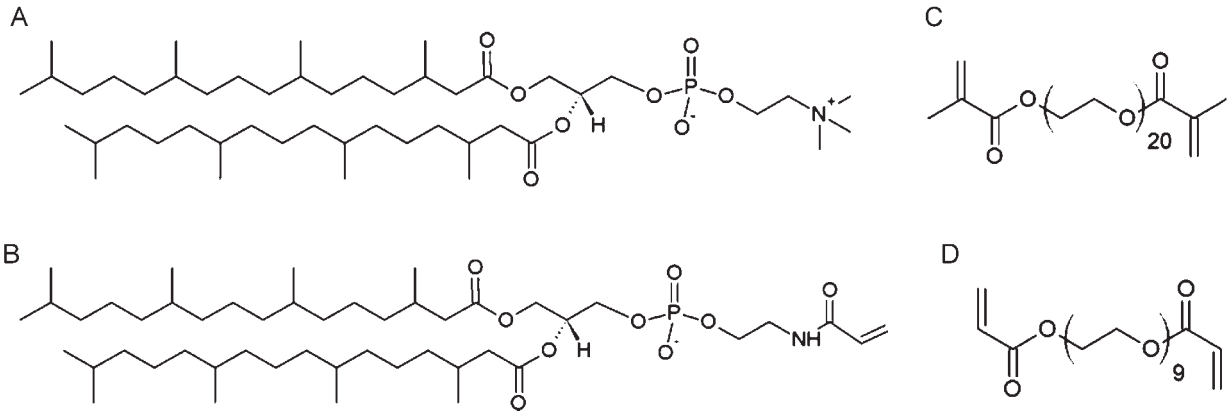

Figure 2. Chemical structures of lipids and polymers used. (a): 1,2-di-(3,7,11,15-tetramethylhexadecanoyl)-sn-glycero-3-phosphocholine (DPhPC). (b): 2-di-(3,7,11,15-tetra-methylhexadecanoyl)-sn-glycero-3-phosphoethanolamine acrylate (DPhPE-A). (c): Poly(ethylene glycol)-1000-dimethacrylate (PEG-1000-DMA). (d): Poly(ethylene glycol)-400-diacrylate (PEG-400-DA).

100 mM poly(ethylene glycol)-400-diacrylate monomers and 10 mM Darocur1173 photoinitiator.

Similarly, for chemical initiation two aqueous HPSs were prepared: a PEG-1000-DMA solution (1000C) with 65 mM PEG-1000-DMA monomers and 10 mM TEMED and a PEG-400-DA solution (400C) containing 100 mM PEG-400-DA monomers and 15 mM TEMED. Ammonium persulfate (same concentration as TEMED in 400 and 1000 C, respectively) was added to initiate polymerization.

In this paper we will refer to the individual HPSs using the nomenclature presented in Table 1. Crosslinking is indicated by the prefix X. Thus, for example, X1000P refers to PEG-1000-DMA crosslinked using UV photo-activation.

Volumetric stability measurements

A glass capillary (diameter 1 mm, length 15 cm) was filled with 50 μl of HPS. Free-radical polymerization of 1000P and 400P was initiated by 5 min irradiation of the HPS by an EA-140 UV lamp with $I = 800\ \mu W\,cm^{-2}$ at 15 cm, $\lambda = 365$ nm (Spectroline, Westbury, NY, USA) at a lamp distance of 1 cm. Gelation of 1000C and 400C was initiated when APS was added to and vortexed with the HPS prior injection into the capillary. The relative change in volume, ΔV, was defined as

$$\Delta V = \frac{V_2 - V_1}{V_1} 100\% = \frac{L_2 - L_1}{L_1} 100\% \quad (1)$$

where V_1 and L_1 are the initial volume and length and V_2 and L_2 are the final volume and length of the hydrogel cylinder in the capillary. L_1 and L_2 were measured as the distances between the bottoms of the two menisci using graph paper. ΔV was determined for the crosslinking reaction at room temperature (ΔV_X) and for cooling of the crosslinked sample from room temperature to 4 °C ($\Delta V_{X,Cool}$) for each sample.

Preparation of a hydrogel sandwiched between ETFE and DSS-RC70PP membrane supports for retention and water permeability measurements

The sandwich assembly consists of hydrogel sandwiched between a perforated ETFE structure and a sheet of DSS-RC70PP membrane (see Fig. 1a).

Microstructuring of the ETFE support structure was performed as described in Ref. [28]. Briefly, a carbon dioxide laser was used to fabricate 21 mm diameter partitions of ETFE LZ200 film (50.8 μm thick) with a centered 8×8 rectangular aperture array. The apertures had a center-to-center distance of 400 μm and a diameter of 300 ± 5 μm. A disk with a diameter of 21 mm was cut out of a sheet of a DSS-RC70PP membrane and sonicated 10 min in 60/40 ethanol/water followed by 10 min sonication in water. The prewetted DSS-RC70PP membrane was placed with the cellulose side positioned upwards facing the hydrogel solution.

For the photoinitated hydrogel sandwiches, 1 ml of HPS was distributed evenly on the DSS-RC70PP membrane. An ETFE partition (as described above) was placed on top of the liquid HPS. Then the sandwich was UV irradiated using the EA-140 UV lamp described above at a distance of 1 cm for 10 min. Chemically initiated hydrogel sandwiches were prepared in a similar manner. After 10 min the crosslinked sandwiches were packed in water-soaked cotton wool and stored at 4 °C.

An empty sandwich (no hydrogel) made up of an ETFE partition with an 8×8 aperture array on top of a sheet of DSS-RC70PP (cellulose side toward ETFE) served as control.

Retention measurements

A feed solution containing a mixture of 1, 3, 5, 8, 12, and 35 kDa poly(ethylene glycol) (PEG) beads each at a concentration of 0.5 mg/ml in MilliQ water was passed through the hydrogel sandwich using a homemade water flux measurement setup.

Size exclusion chromatography was performed using a 717PLUS Autosampler configured with a 600E controller and a 410 Refractive Index Detector from Waters Corporation (Waters, Milford, MA, USA). Measurements were done using Waters Ultrahydrogel 250 6 μm $7.8 \times 300\ mm^2$ GPC column with MilliQ water as eluent at a flow rate of $0.6\ ml\ min^{-1}$ and a sample injection volume of 40 μl. Three consecutive permeates for each hydrogel sandwich sample were collected and results reported using the third permeate chromatogram as it was identical to the second permeate chromatogram indicating that a steady-state was reached.

Water permeability measurements

The hydrogel sandwich was placed in a homemade flow unit cell. The time t needed to collect a given volume V of permeate

(approximately 1 ml) was measured at 1, 1.5, and 2 bars of the feed pressure *P*. The water flux J_w was calculated as $J_w = \frac{V}{tV_w}$, where V_w is the partial molar volume of water (1.8×10^{-5} $m^3 \cdot mol^{-1}$). The hydraulic permeability L_p [$m \cdot s^{-1} \cdot Pa^{-1}$] and the diffusional permeability P_w [m/s] of the membrane were calculated from Equation (2), where R is the gas constant (8.3145 $m^3 \cdot Pa \cdot K^{-1} \cdot mol^{-1}$) and T is the temperature.

$$L_p = \frac{J_w V_w}{\Delta P}, \quad P_w = \frac{J_w RT}{\Delta P} = \frac{L_p RT}{V_w} \tag{2}$$

Formation of hydrogel-encapsulated BLMs across multi-aperture ETFE partitions

2 ml DPhPC or 1 ml DPhPE-A in chloroform (10 mg ml^{-1}) was placed under nitrogen flow to evaporate the solvent and the dry lipid films were rehydrated in 400 µl and 193 µl *n*-decane respectively to a final concentration of 59 mM. The lipid solutions were prepared 1 day prior to use and stored at –20 °C.

Briefly, the experimental chamber for bilayer formation consisted of an open top compartment and an open bottom compartment (35 and 50 mm culture dishes, respectively). The glass cover slip of the 35 mm glass-bottom dish was replaced with an ETFE partition with an 8×8 aperture array by first removing the cover slip by adding 0.5 ml n-heptane to the dishes for 10 min, and then gluing the ETFE LZ200 partition array on the dish using silicone-based glue (Dow Corning, Midland, MI, USA). A Viton ring was placed between the two Petri dishes to create two independently accessible compartments and a reusable aluminium holder was used to clamp the upper dish/viton ring/lower dish sandwich together.

The bottom and top compartments were filled with 4.5 ml of a HPS. The experimental chamber was placed in a Faraday cage and Ag/AgCl electrodes were placed in each compartment. 2 µl of the lipid solution was deposited over the apertures using a Pasteur pipette to form BLMs, simultaneously monitoring the current between the electrodes. To facilitate bilayer thinning, an air bubble was created at the tip of the Pasteur pipette and swept gently across the entire ETFE partition array.

When all apertures were filled with lipid membranes, an electrical seal was obtained and the capacitance (C) and conductance (G) of the formed membrane array could be measured by applying triangular (10 mV_{pp}) and rectangular (10 mV_{pp}) voltage clamp waveforms, respectively. Membrane capacitance values ($C = I(dU/dt)^{-1}$ was determined by measuring the peak-to-peak amplitude of the square-shaped response signal, while the membrane conductance ($G = I/U$) was determined from the post-transient steady-state amplitudes. Thinning of the array membranes was evidenced electrically as increase in C and optically with a light microscope with the appearance of Plateau-Gibbs borders. As the measurements recorded *C* and *G* from the entire array, rupture of even a single membrane in the array was evident as a complete loss of the electrical seal ($G \approx 0\,\Omega$). For details on chamber assembly and multi-array BLM monitoring and characterization see Ref. [26,27,29].

After BLM formation, encapsulation in X1000P was performed by UV irradiation of the 1000P solution with a 100 W EXFO Omnicure1000 UV-lamp (EXFO Photonic Solutions Inc, Canada). Irradiation was performed at 2% of the lamp intensity at a lamp distance of 3 cm from the ETFE partition, and with a total UV irradiation time of 15 min divided into intervals of 5 min UV irradiation followed by 5 min intervals without UV irradiation. The experimental chamber was covered in order to minimize evaporation.

Incorporation of the channel forming peptide gramicidin into lipid membrane arrays was carried out by drying 120 nM gramicidin in ethanol under a nitrogen flow and re-dissolving to a final concentration of 3 nM in the bilayer forming solution. The gramicidin-containing multiple BLMs were encapsulated in X1000P as described above with buffer adjusted to 1 M KCl as electrolyte. For single channel recordings, a 60 mV DC potential was applied across the membranes and current traces were acquired at 1 kHz using a patch-clamp amplifier (A-M Systems, Sequim, WA, USA) and filtered through a low pass Bessel filter (Frequency Devices, IL, USA) with a 10 Hz cutoff.

RESULTS AND DISCUSSION

We first examined material properties of the selected hydrogels relevant for the use of hydrogels as an encapsulation material for biomimetic membranes. Then we proceeded by demonstrating that crosslinked hydrogels can be used for *in situ* encapsulation of biomimetic membranes formed across multi-aperture arrays.

Hydrogel material properties

Volumetric stability

Amongst the requirements for an encapsulating hydrogel is that it should not undergo large volume changes upon crosslinking as the expanding gel would exert a pressure on the lipid membrane and rupture it. We observed that the HPSs containing PEG-400-DA or PEG-1000-DMA only shrank slightly upon crosslinking ($\Delta V_X < 1.1\%$) (see Table 2). Bringing the crosslinked gels from room temperature to 4 °C resulted in further shrinkage ($\Delta V_X < 2.0\%$), which exceeded the shrinkage due to crosslinking *per se*, but was still very small. The low degree of shrinkage upon gelation and temperature change is an attractive property as it makes it feasible to encapsulate biomimetic membranes and store them at 4 °C, thus minimizing evaporation and degradation.

Polymer mesh size

The hydrogel pore sizes were characterized by passing an aqueous feed solution containing a mixture of PEG beads of various sizes at 1 bar through each assembled hydrogel sandwich (see Fig. 1a).

The permeate analysis is shown in Fig. 3. Figure 3a shows the permeate profiles for the feed, for the hydrogel sandwiches

Table 2. Volumetric stability of HPSs upon crosslinking. Shrinkage of each HPS upon crosslinking is expressed in percent of the volume of the HPS and upon cooling in percent of the volume of the gel. All values are given as mean ± sd ($n = 3$)

Hydrogel	ΔV_X (%)	$\Delta V_{X,Cool}$ (%)
X1000P	–0.5±0.4	–1.0±0.4
X1000C	–0.6±0.2	–1.3±0.4
X400P	–0.8±0.4	–0.5±0.4
X400C	–0.4±0.1	–1.4±0.6

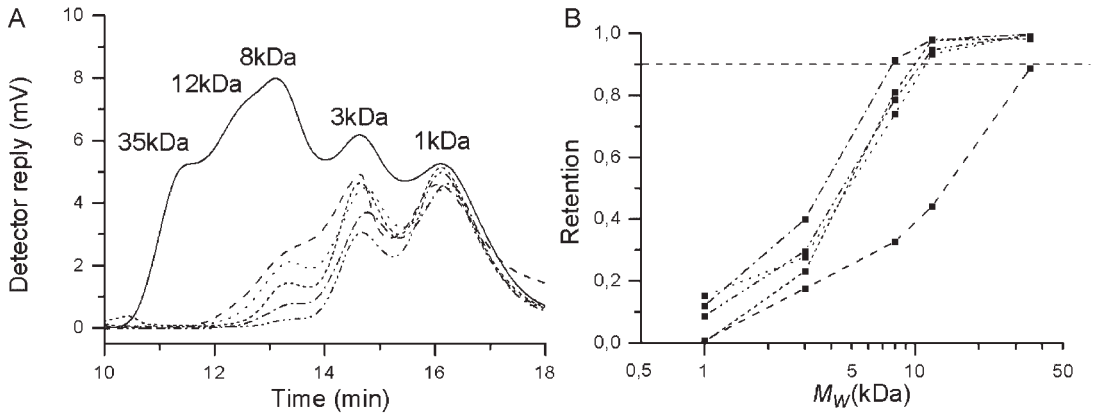

Figure 3. Hydrogel retention measurements. (a): Size-exclusion chromatograms of the feed (black line), the permeates through DSS-RC70PP(- - -), X1000C (· · ·), X1000P (— · — · —), X400P (· · — · ·), and X400C (·····) hydrogel sandwiches. The bead size corresponding to each peak is indicated. (b): Retention curves for the data in (a) showing the retention for each PEG molecular weight. The cut-off level is defined as a 90% rejection level and indicated by the dashed line.

analyzed, and for the PEG bead solution when permeated through DSS-RC70PP alone. Larger beads are able to pass through the DSS-RC70PP membrane than through the hydrogel sandwich, which indicates that the bead retention R observed in the hydrogel sandwiches is caused by the hydrogels. Figure 3b shows R for the hydrogel sandwiches as a function of molecular weight:

$$R = \frac{c_f - c_p}{c_f} \quad (3)$$

where c_f is the detected peak height of the feed and c_p is the detected peak height of the permeate for each PEG bead molecular weight. The cut-off size, defined as the bead molecular weight for which 90% of the beads are retained by the sandwich[30], was around 10 kDa for all gels and about three times lower than for the DSS-RC70PP membrane (>30 kDa). A 10 kDa bead size corresponds to a bead hydrodynamic diameter of about 7 nm[31]. This is similar to the mesh-size of PEG-1000-DMA reported previously[13]. X1000P had a marginally smaller cut-off diameter than the other gels. Thus both crosslinked PEG-400-DA and PEG-1000-DMA have nanoscale mesh structures suitable for biomimetic membrane support.

Water permeability

In order to ascertain whether the nanoscale mesh hydrogels would impede solute and solvent flux across the membrane, we performed water flux measurements on the hydrogel sandwiches and the results are summarized in Table 3. Fluxes were compared to the flux through DSS-RC70PP membrane alone and flux through an 'empty' sandwich consisting of a perforated ETFE disk on top of a disk of DSS-RC70PP membrane. The DSS-RC70PP membrane had a mean L_p value of 1.65×10^{-10} m·s^{-1} ·Pa^{-1}, not significantly different from the mean value of 1.52×10^{-10} m·s^{-1}·Pa^{-1} measured when the perforated ETFE partition was put on top of the cellulose. The presence of crosslinked hydrogel reduced L_p for all hydrogels investigated (see Table 3). The reduction was larger for photoinitiated gels than for chemically initiated gels with no correlation between hydrogel PEG chain length/mesh size and flux reduction. The photoinitiated gels contain the Darocur 1173 initiator which is hydrophobic (c.f. CIBA Darocur 1173 datasheet), and the reduction in water permeability may be due to photoinitiated gels having residual amounts of initiator left in contrast to the chemically initiated gels tested. The highest gel L_p was found for X400C (1.06×10^{-10} m·s^{-1}·Pa^{-1}), i.e. reduced to about 60% of the L_p of the empty sandwich whereas the lowest $L_p = 3.4 \times 10^{-11}$ m·s^{-1}·Pa^{-1} was found for X400P. A typical reverse osmosis (RO) membrane flux is about 12 L·m^2·h^{-1} operated at 600 kPa (brackish water feed)[32] corresponding to $L_p = 5.6 \times 10^{-12}$ m·s^{-1}·Pa^{-1}. Thus all hydrogels tested have water permeabilities at least five-fold higher than the permeability for a typical RO membrane. The hydrogels do therefore not constitute the limiting factor in biomimetic separation devices, allowing the overall device permeability (and selectivity) properties to be determined by the biomimetic membrane *per se*.

Table 3. Water permeability data. For each sample flux was measured at 1, 1.5, and 2 bars and the water permeability L_p was obtained from a linear fit to the flux-pressure relationships with $r > 0.99$. The effective sample area was 3.46 cm^2. All values given as mean ± sd ($n = 3$)

Sample	L_p (10^{-12} m·s^{-1}·Pa^{-1})	P_w (cm·s^{-1})
Cellulose	165±18	2.28±0.25
Cellulose + ETFE	152±24	2.09±0.33
X1000P	39±7	0.53±0.10
X1000C	55±19	0.76±0.27
X400P	34±14	0.46±0.19
X400C	106±41	1.46±0.56
RO*	5.6	0.08

* Based on 12L m^{-2} h^{-1} at 600 kPa, see Ref.[32].

Hydrogels as encapsulation materials

Having established that the PEG-DMA- and PEG-DA-based hydrogels have mesh size, water flux, and volumetric stability parameters compatible with their use as encapsulation material we now investigated *in situ* encapsulation of biomimetic lipid

membranes. We characterized lipid membrane lifetimes in hydrogel precursor solution and lifetimes and membrane characteristics of hydrogel-encapsulated lipid membranes. We selected photoinitiated hydrogels, as the initiator can be added directly to the HPS yielding a homogeneous distribution of initiator. Also UV irradiation yielded precise control of the time point at which the polymerization reaction began.

Effects of HPS on BLM formation and stability

We tested both *n*-decane containing DPhPC and DPhPE-A lipid bilayers. DPhPC is a commonly used lipid for BLMs[1]. DPhPE-A contains an acrylate group which has the potential to covalently link to the acrylate group of PEG-1000-DMA or PEG-400-DA upon crosslinking.

Free-standing DPhPC and DPhPE-A BLMs in buffer had lifetimes up to 20 hr for DPhPC and up to 19 hr for DPhPE-A (see Table 5). Adding polymer to the buffer resulted in BLMs with lifetimes up to 18 hr for DPhPC and up to 14 hr for DPhPE-A (see Table 4). When both photoinitiator and polymer were present in the HPS, stability was reduced significantly with BLM lifetimes up to 139 min.

In order to identify whether the reduced BLM stability was due to specific interactions between photoinitiator and BLM, we investigated DPhPE-A membrane formation in the presence of photoinitiator alone in buffer where we obtained lifetimes ranging from 9 to 139 min. The minimum DPhPE-A membrane lifetime was substantially larger than the minimum lifetimes (seconds) observed for solutions containing PEG-based polymers with or without initiator. From this we conclude that the initiator *per se* does not compromise BLM *formation,* but it affects BLM *lifetime*. Thus the pre-encapsulation step, where both polymer and initiator are present, generally tends to destabilize the BLMs.

Stability of encapsulated BLMs

A sufficient minimum membrane lifetime is more critical than a maximum membrane lifetime as the membranes need to survive long enough in the HPS to become encapsulated. We selected the 1000P HPS for encapsulating BLMs, as we observed a higher minimum lifetime (albeit still < 1 min) for membranes in 1000P than in the 400P HPS.

We then encapsulated DPhPE-A and DPhPC with 1000P using UV-initiation started as soon as the membrane array was formed. The presence of X1000P seemed to "freeze" the membrane array protecting it from rupture. Once membranes were encapsulated, they all survived more than 1 day. Although several DPhPC membrane arrays ruptured during crosslinking we were able to have a DPhPC membrane array surviving in X1000P for more than a day (see Table 5), which is 12 times longer than the maximum lifetime we obtained for DPhPC membrane arrays in 1000P.

The DPhPE-A membranes generally performed better than DPhPC membranes, with lifetimes ranging from 47 hr to 3.6 days in X1000P (compared to 1 min in 1000P). Encapsulated membrane arrays were stored at room temperature with no visible degradation. The hydrogel seemed to stabilize these membranes considerably, which suggested that the gel was covalently linking to the membranes via the headgroup acrylate moiety. Alternatively, the observed stabilizing effect could be due to DPhPE-A lipids stabilized by crosslinking the lipid headgroups with each other and not due to the hydrogel. We therefore analyzed DPhPE-A BLM stability in Darocur1173 solution alone exposed to the same UV dose as the membranes in hydrogel (XP solution), and obtained lifetimes ranging from 30 min to 34.8 hr. This is below the minimum lifetime obtained for DPhPE-A in X1000P, and indicates that the increased longevity of the DPhPE-A membranes is caused by the presence of encapsulating hydrogel.

In order to assess whether the hydrogel encapsulation affected BLM properties, we measured conductance *G* and capacitance *C* as described previously[27]. Membrane conductance ranged from 115 to 220 nS and membrane capacitance ranged from 1560 to 3950 pF with no significant differences between hydrogel-encapsulated membranes and freestanding membranes (see Fig. 4). This shows that encapsulation of the membranes does not change their characteristics. The capacitance values correspond to an overall specific membrane capacitance of 0.035–0.088 $\mu F\,cm^{-2}$ (assuming that the total membrane area was equal to the area of the aperture array, 0.045 cm^2), which is

Table 4. Lifetimes of DPhPC and DPhPE-A lipid membranes in hydrogel precursor solution components. DPhPC and DPhPE-A bilayers were formed in HPS across an ETFE partition with an 8×8 rectangular aperture (300 μm diameter) array. The minimum and maximum observed lifetimes of membranes with $C > 2000$ pF are given. For each HPS composition tested, the success rate (s) (success = survival of the membrane for at least 5 min) for these membranes is indicated as the number of successful membranes out of the total number of membranes formed

HPS	Lipid	t_{min} (min)	t_{max}(min)	$S_{(t>5\ min)}$
1000	DPhPC	0.05	189	6/32
1000	DPhPE-A	1	835	14/16
1000P	DPhPC	0.08	139	2/7
1000P	DPhPE-A	0.03	1	0/9
400	DPhPC	0.03	1135	3/7
400	DPhPE-A	0.03	28	4/25
400P	DPhPC	0.02	9	1/4
400P	DPhPE-A	0.02	32	1/6
P	DPhPE-A	9	139	3/3

Table 5. Lifetimes of DPhPC and DPhPE-A lipid membranes in buffer or encapsulated in X1000P hydrogel. The minimum and maximum observed lifetimes of membranes are given. The success rate (s) (success = survival of the membrane for at least 12 hr) for these membranes is indicated as the number of successful membranes out of the total number of membranes formed

Sample	UV time (min)	Lipid	t_{min} (hr)	t_{max} (hr)	$S_{(t>12\ hr)}$
Buffer	None	DPhPC	0.02	20.8	2/6
Buffer	None	DPhPE-A	0.6	19.8	2/5
XP	15	DPhPE-A	0.6	37.8	2/5
X1000P	15	DPhPC	0.8	34.8	1/2
X1000P	None	DPhPE-A	47.3	219.1	3/3

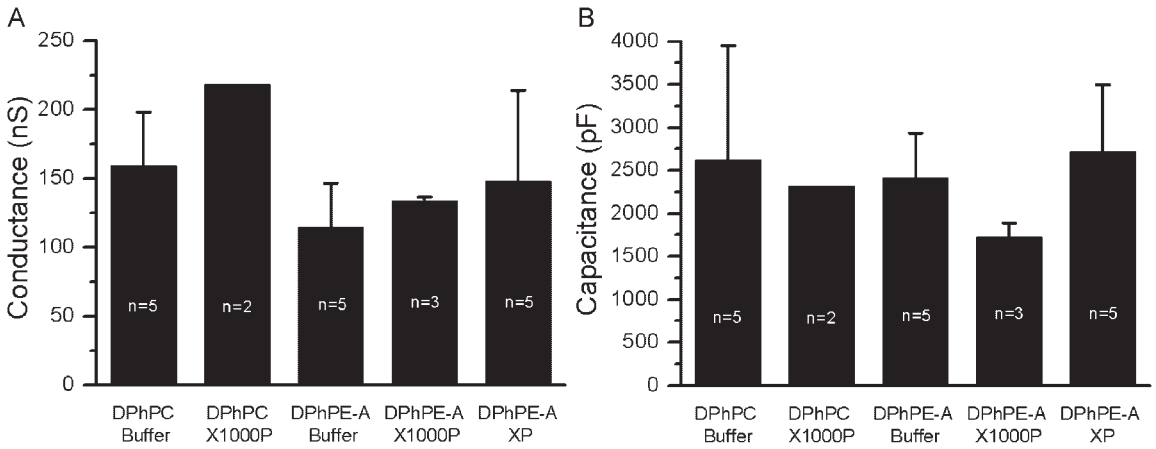

Figure 4. Freestanding X1000P-encapsulated BLM electrical properties. (a): conductance G (b): capacitance C. Mean $\pm$ sd values of each membrane were determined using the methods described in Ref. [26] after 50 min for membranes with lifetime >60 min or the last 10 min for membranes with lifetime < 60 min.

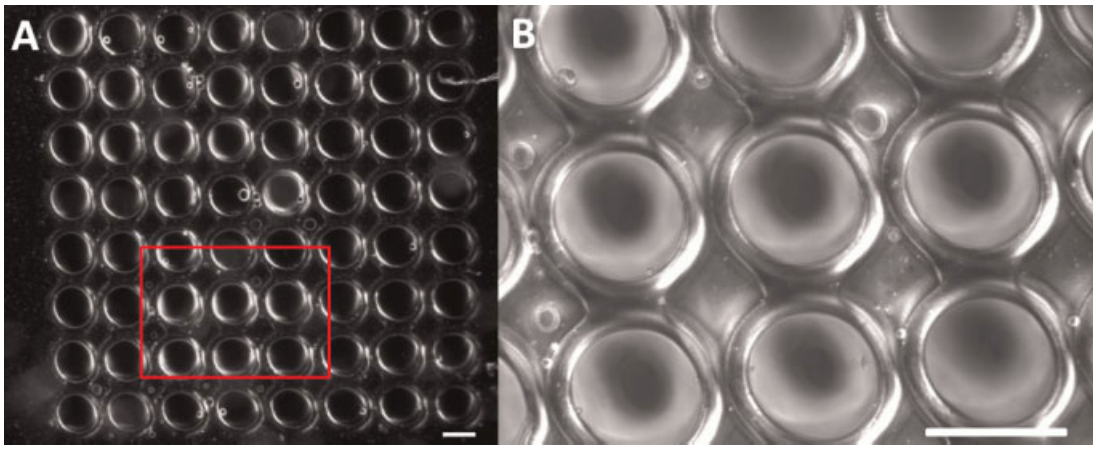

Figure 5. Optical microscope images of a hydrogel-encapsulated lipid membrane obtained as described in Ref. [26]. (a): The entire 8×8 array. (b): magnified image of the apertures in the red square in (a), showing lipid membranes with clearly recognizable Plateau-Gibbs borders (light annular regions). Scale bar 300 μm. This figure is available in colour online at wileyonlinelibrary.com

much lower than the specific capacitance for fully thinned solvent-containing membranes (0.4–0.6 μF cm^{-2}) reported in the literature[33]. The low specific overall capacitance value measured does not preclude the existence of bilayer patches, but if they exist they only constitute 9–22% of the total aperture area and the rest of the aperture array area has solvent-containing lipid patches. This is consistent with the bright field image of the 8×8 arrays where the Plateau-Gibbs borders[34] with large annuli are clearly visible (see Fig. 5). Of course, an optimized thinning of the BLMs would increase the effective bilayer area. On the other hand this would also tend to make membranes even more unstable before crosslinking. Thus we are faced with a compromise between larger bilayer areas and reasonable BLM formation success rates and lifetimes.

Functionality of encapsulated BLMs

In order to verify that we have areas where the lipid bilayer thickness is compatible with the hydrophobic spanning segments of transmembrane proteins, we incorporated the channel-forming peptide gramicidin A into the BLMs followed by X1000P encapsulation (see Fig. 6).

Figure 6. Single channel gramicidin current trace from an X1000P-encapsulated 5 day old DPhPE-A membrane in buffer adjusted to 1 M KCl. A 60 mV DC potential was applied across the membrane and the signal was filtered at 10 Hz.

Current trace recordings showed single channel events with current amplitudes around 2 pA, corresponding to a single channel conductance of 33 pS, consistent with previous results for gramicidin in 1 M KCl[35]. The current trace recordings confirmed functional reconstitution of gramicidin ion channels, which strongly suggested that functional lipid bilayer areas are present in the X1000P-encapsulated and stabilized membranes.

CONCLUSION

Hydrogels show promise as materials for encapsulating biomimetic membranes. They have volumetric stability and their nano-scale cut-off sizes and water flux properties make them promising in biomimetic devices where they can support the biomimetic membranes and yet allow vectorial flux of matter to (and through) the biomimetic membrane. We have demonstrated that multi-aperture arrays of membranes can be successfully encapsulated and that it is possible to create a robust biomimetic membrane in which proteins can be reconstituted. However, the main challenge still remains: how to improve the stability of the membranes in the HPS before crosslinking and to ensure that protein function is not compromised by maneuvers used to crosslink the hydrogels.

Acknowledgements

We thank Kamila Pszon for preparing Fig. 1. This work was supported through MEMBAQ, a Specific Targeted Research Project (STREP), by the European Commission under the Sixth Framework Programme (NMP4-CT-2006-033234), by the Danish National Advanced Technology Foundation (023-2007-1) and by a grant to DTU Physics from the Danish National Research Foundation.

REFERENCES

[1] C. H. Nielsen, *Anal. Bioanal. Chem.* **2009**, *395*, 697–718.
[2] E. Sackmann, M. Tanaka, *Trends Biotechnol.* **2000**, *18*, 58–64.
[3] E. Reimhult, K. Kumar, *Trends Biotechnol.* **2008**, *26*, 82–89.
[4] J. Jagur-Grodzinski, *Polym. Adv. Technol.* **2009**, *21*, 27–47.
[5] C. H. Nielsen, Lipid-protein interactions in biomembranes. in *Handbook of Molecular Biophysics* (Eds. H. G. Bohr), Wiley, Berlin, **2009**, 329–358.
[6] F. N. R. Petersen, I. Laursen, H. Bohr, C. H. Nielsen, *Biochem. Biophys. Res. Commun.* **2009**, *387*, 760–765.
[7] F. N. R. Petersen, C. H. Nielsen, *Spectroscopy* **2009**, *24*, 26–35.
[8] H. Ti Tien, *Bilayer lipid membranes (BML) Theory and practice*. Marcel Dekker Inc, New York **1974**.
[9] H. T Tien,, A. Ottova-Leitmannova, (Eds.) *Planar Lipid Bilayers (BLMs) and Their Applications*. Elsevier, Amsterdam, **2003**.
[10] A. S. Hoffman, *Adv. Drug Delivery Rev.* **2002**, *54*, 3–12.
[11] N. A. Peppas, Y. Huang, M. Torres-Lugo, J. H. Ward, J. Zhang, *Annu. Rev. Biomed. Eng.* **2000**, *2*, 9–29.
[12] N. A. Peppas, P. Bures, W. Leobandung, H. Ichikawa, *Eur. J. Pharm. Biopharm.* **2000**, *50*, 27–46.
[13] T. J. Jeon, N. Malmstadt, J. J. Schmidt, *J. Am. Chem. Soc.* **2006**, *128*, 42–43.
[14] N. Malmstadt, T-J. Jeon, J. J. Schmidt, *Adv. Mater.* **2008**, *20*, 84–89.
[15] J. W. Shim, L. Q. Gu., *Anal. Chem.* **2007**, *79*, 2207–2213.
[16] X. F. Kang, S. Cheley, A. C. Rice-Ficht, H. Bayley, *J. Am. Chem. Soc.* **2007**, *129*, 4701–4705.
[17] R. F. Costello, I. R. Peterson, J. Heptinstall, N. G. Byrne, L. S. Miller, *Adv. Mater. Opt. Electron.* **1998**, *8*, 47–52.
[18] R. F. Costello, I. R. Peterson, J. Heptinstall, D. J. Walton, *Biosens. Bioelectron.* **1999**, *14*, 265–271.
[19] J. A. Beddow, I. R. Peterson, J. Heptinstall, D. J. Walton, *Anal. Chem.* **2004**, *76*, 2261–2265.
[20] H. T. Tien, A. L. Ottova, *Electrochim. Acta* **1998**, *43*, 3587–3610.
[21] W. Ziegler, J. Gaburjakova, M. Gaburjakova, B. Sivak, V. Rehacek, V. Tvarozek, T. Hianik, *Colloids Surf., A* **1998**, *140*, 357–367.
[22] T. Baumgart, A. Offenhausser, *Langmuir* **2003**, *19*, 1730–1737.
[23] M. Uto, M. Araki, T. Taniguchi, S. Hoshi, S. Inoue, *Anal. Sci.* **1994**, *10*, 943–946.
[24] J. R. Hazel, *Physiol. Regul. Membr. Fluidity* **1988**, 149–188.
[25] Ed., T. E Creighton, *Proteins, Structures and Molecular Properties*, 2nd Ed., W.H. Freeman & Co., New York, **1993**.
[26] J. S. Hansen, M. Perry, J. Vogel, J. Groth, T. Vissing, M. Larsen, O. Geschke, J. Emneus, H. Bohr, C. H. Nielsen, *Anal. Bioanal. Chem.* **2009**, *395*, 719–727.
[27] M. Perry, T. Vissing, T. P. Boesen, J. S. Hansen, J. Emneus, C. H. Nielsen, *Bioinspir. Biomim.* **2009**, *4*, 44001.
[28] J. Vogel, M. E. Perry, J. S. Hansen, P-Y. Bollinger, C. H. Nielsen, O. Geschke, *J. Micromech. Microeng.* **2009**, *19*, 025026.
[29] J. S. Hansen, M. E. Perry, J. Vogel, T. Vissing, O. Geschke, J. Emneus, C. H. Nielsen, *J. Micromech. Microeng.* **2009**, *19*, 025014.
[30] M. Mulder, *Basic Principles of Membrane Technology*. Kluwer Academic Publishers, Dordrecht, **1996**.
[31] P. Szewczykowski, Nano-porous materials from diblock copolymers and their membrane application. PhD Thesis. In Department of Chemical and Biochemical Engineering. Technical University of Denmark, Lyngby. **2009**.
[32] L. F. Greenlee, D. F. Lawler, B. D. Freeman, B. Marrot, P. Moulin, *Water Res.* **2009**, *43*, 2317–2348.
[33] R. Benz, O. Fröhlich, P. Läuger, M. Montal, *Biochim. Biophys. Acta* **1975**, *394*, 323–334.
[34] S. H. White, *Biophys. J.* **1970**, *10*, 1127–1148.
[35] O. S. Andersen, *Biophys. J.* **1983**, *41*, 119–133.

Paper II

TAILORING PROPERTIES OF BIOCOMPATIBLE PEG-DMA HYDROGELS WITH UV LIGHT

Sania Ibragimova [a, b], Juana Benavente [c], Rolf W. Berg [d], Karin Stibius [a, b], Marianne S. Larsen[b], Henrik Bohr [a] and Claus Hélix-Nielsen [a, b, *]

[a] DTU Physics, Technical University of Denmark, DK-2800 Kgs. Lyngby, Denmark

[b] Aquaporin A/S, Diplomvej 377, DK-2800 Kgs.Lyngby, Denmark

[c] Grupo de Caracterización Electrocinética en Membranas e Interfases. Departamento de Física Aplicada I. Facultad de Ciencias. Universidad de Málaga. E-29071 Málaga, Spain

[d] DTU Chemistry, Technical University of Denmark, DK-2800 Kgs. Lyngby, Denmark

Email addresses:

Sania Ibragimova sania.ibragimov@gmail.com

Juana Benavente j_benavente@uma.es

Rolf W. Berg rwb@kemi.dtu.dk

Karin Stibius karin_stibius@hotmail.com

Marianne S. Larsen msl@aquaporin.dk

Henrik Bohr hbohr@fysik.dtu.dk

Claus Hélix-Nielsen claus.nielsen@fysik.dtu.dk

Keywords:

Hydrogel, UV-induced polymerization, FTIR, Raman spectroscopy, swelling, impedance spectroscopy

Address correspondence to:

Claus Hélix-Nielsen
DTU Physics
Fysikvej 309, Building 309, office 138
Technical University of Denmark
DK-2800 Kgs Lyngby
Phone +45 60 68 10 81
Fax +45 45 93 16 69
Email: claus.nielsen@fysik.dtu.dk

Abstract

Hydrogels are highly absorbent (can contain over 90% water) hydrophilic polymer networks. Hydrogels are favored as scaffolds for tissue engineering where they act as supports for cells and biomimetic membranes. Photoactivated poly(ethylene glycol)-dimethacrylate (PEG-DMA) hydrogels are formed from PEG-DMA monomers suspended in aqueous solution and gelated by radical polymerization in the presence of a photoinitiator. The polymerization reaction starts when the solution is exposed to UV light. Each PEG-DMA monomer has two methacrylate groups which can react with other methacrylate groups to make covalent bonds. Thus, each PEG-DMA monomer can covalently link to up to four other PEG-DMA monomers and the resulting polymer forms a covalently crosslinked branched network. We show that the properties of a PEG-DMA hydrogel formed by photoinitiated polymerization can be tailored by varying the photocrosslinking time. We were able to vary the water content of the gels between 50-90 wt% and the specific electrical resistance of the gel between 0.8-3.5 Ωm. With Fourier Transform Infrared Spectroscopy and Raman Spectroscopy we identified spectral features of the hydrogel, which may be applicable as a diagnostic tool to study changes in the gel due to variation in parameters such as time, pH, temperature, aging or exposure to chemicals or biological material, which can be useful for tissue engineering applications.

1. Introduction

Hydrogels are highly absorbent (can contain over 90% water) hydrophilic polymer networks [1-3]. Hydrogels are favored as scaffolds for tissue engineering where they act as supports for cells [4-9] and biomimetic membranes [10-25]. Poly(ethylene oxide) (PEO) synthetic hydrogels are the most commonly used synthetic hydrogel polymers for tissue engineering. Poly(ethylene glycol) (PEG)-based hydrogels are structurally similar to PEO and can be crosslinked by modifying each end with acrylates or methacrylates [7]. These materials are suitable for tissue engineering for several reasons. Firstly, their chemistry and properties can be controlled by varying for example molecular weight, chemical composition, the amount and type of initiator used and the degree of crosslinking, which modifies their mass transport properties, physical properties and biological properties. Secondly, poly(ethylene glycol)-diacrylate (PEG-DA) hydrogels have been shown to be compatible in vivo with porcine islet cells [8] and poly(ethylene glycol)-dimethacrylate (PEG-DMA) hydrogels to be compatible with chondrocytes in vitro [9]. Lastly, these hydrogels have been shown to allow transport of water, electrolytes, nutrients and proteins depending on the pore size of the hydrogel network [1, 10, 20, 26], which is vital for cell viability when encapsulated in these gels.

Photoactivated PEG-DMA hydrogels are formed from PEG-DMA monomers suspended in aqueous solution and gelate by radical polymerization in the presence of a photoinitiator. The polymerization reaction starts when the solution is exposed to UV light. Each PEG-DMA monomer has two methacrylate groups which can react with up to two other methacrylate groups to make covalent bonds. Thus, each PEG-DMA monomer can covalently link to up to four other

PEG-DMA monomers and the resulting polymer forms a covalently crosslinked branched network (fig. 1).

In previous work [10, 26] we characterized chemically activated and photoactivated PEG-DMA and PEG-DA hydrogels with respect to volumetric stability, water permeability, ionic permeability and porosity and showed successful hydrogel encapsulation and stabilization with photoactivated PEG-DMA-based hydrogels of multiple black lipid membranes formed across an aperture array. We showed that the gels had a mesh pore size of 7 nm and allowed transport of water, electrolytes and macromolecules of up to 10 kDa [10], which is large enough to allow transport of oxygen and nutrients such as glucose to cells [7].

FIGURE 1 ABOUT HERE

In this work we address how PEG-DMA hydrogel properties can be tailored by varying the photocrosslinking time and thereby the degree of crosslinking. We show that we can change the water-absorption/soaking capability and the ionic conductivity of the gel. Using Fourier Transform Infrared spectroscopy (FTIR) and Raman spectroscopy (RS) we obtain the spectral fingerprint profile of the gel and find that there is a waveshift in the C=O peak due to crosslinking and that the intensity of the C=C peak decreases also due to crosslinking. Furthermore, we show how the fingerprint is altered with specific spectral peaks receding and others appearing with increased UV dose. The spectral fingerprint of the gel may be applicable as a diagnostic tool to detect changes in the gel in response to variation in parameters, such as temperature, pH, aging and exposure to chemicals.

2. Materials and Methods

2.1. Materials

Poly(ethylene glycol)-1000-dimethacrylate (PEG-1000-DMA) was from Polysciences (Warrington, PA, USA). 2-Hydroxy-2-methyl-1-phenyl-propan-1-one (Darocur®1173) was from Ciba Specialty Chemicals (Basel, Switzerland). Phosphate buffered saline was from Sigma Aldrich Denmark (Brøndby, Denmark).

2.2. Preparation of hydrogel

The hydrogel was prepared as in [10, 26]. Briefly, the hydrogel precursor solution (HPS) consisted of 65 mM PEG-1000-DMA and 10 mM Darocur®1173 (a photoinitiator) in phosphate buffered saline. We will refer to this solution as 1000P. Free-radical polymerisation of 1000P was initiated by 4, 6, 8, 10 or 15 min of photocrosslinking of the HPS by UV light from an EA-140 UV lamp with wavelength λ=365 nm (Spectroline, Westbury, NY, USA) at a lamp distance of 1 cm. The lamp intensity at a distance of 15 cm was 800 $\mu W.cm^{-2}$. We will refer to the crosslinked gel as X1000P.

2.3. Swelling

Equilibrium swelling experiments were used to determine the structural characteristics of the PEG-DMA gels. Hydrogel samples were prepared and excess water was poured off. The gel samples were allowed to equilibrate overnight in order to get rid of water which was not part of the swollen gel, but could not be poured off. Thereafter, the gels were weighed to determine the swollen gel weight, W_s. After these measurements they were dried in a dessicator overnight to remove all water and weighed to determine the dry gel weight W_d. The percentage of water

content was calculated as in [27] using *% water content* = $(W_s\text{-}W_d)/W_s \cdot 100\%$. The gels were rehydrated in water, allowed to dry overnight to remove excess water, and weighed again to determine the new swollen gel weight. The percentage of water content was calculated.

2.4. Fourier Transform Infrared Spectroscopy (FTIR)

Fourier transform infrared (FTIR) spectroscopy was performed on a Thermo Nicolet Nexus 870 with a Ge 45 deg Smart Ark attenuated total reflectance (ATR) crystal from Thermo Scientific, MA, USA. The FTIR spectra were recorded using OMNIC software from Thermo Nicolet Corporation with an average of 32 scans in the range 650-4000 cm^{-1} and at a resolution of 4 cm^{-1}. Samples were dried in a vacuum dessicator prior to analysis in order to reduce the contribution from water in the recorded spectrum. The recorded spectra were normalized to obtain the same intensity for the spectral peak corresponding to the C=O functional group. The relative number of C=C bonds in the gels was obtained by comparing the area under the spectral peak corresponding to the C=C functional group, which was used as a measure of the degree of crosslinking.

2.5. Raman Spectroscopy

Raman spectra were obtained as in [28] by use of a DILOR-XY 800 mm focal length multichannel spectrometer with horizontal Nd:YVO_4 laser excitation (532.8 nm, ~300 mW, vertically polarized). Rayleigh-scattered light was filtered off with a double pre-monochromator (slit width 500 µm). The Raman light was collected after 90 degrees of scattering, dispersed by use of an 1800 lines/mm grating, and focused onto a charge-coupled device (CCD) detector,

cooled to 140 K by liquid nitrogen. The spectral resolution was approximately 4 cm^{-1}. Hydrogel samples were prepared as described in section 2.2 and were not dried prior to measurements.

2.6. Impedance spectroscopy (IS)

The test cell for impedance spectroscopy measurements consisted of a teflon support with two Pt electrodes between which a cylindrical crown rubber support (approximately 2.2 mm height and 1.5 cm diameter) filled with gel sample (dried in a dessicator for 24 hours, then rehydrated in MilliQ water for 24 hours) was placed and clamped [29]. The electrodes were connected to a Frequency Response Analyzer (Solartron 1260, England) and measurements were recorded for 100 data points in the frequency range of 1 Hz - 10 MHz, at a maximum voltage of 0.01 V.

3. Results and discussion

3.1. Water content of the gel

Due to their high water content, hydrogels are useful for applications such as tissue engineering, silicone lenses and drug delivery, for a review see [7]. By modifying the water content of the gel, the gel-cell interaction can be affected, for example it has been shown to influence extracellular matrix production [30]. In silicone lenses, hydrogels increase the comfort and breathability of the lens due to their high water content. The water content of the gel influences the mechanical integrity and strength of the gel as well as the diffusion of nutrients and metabolites through the gel to a cell/tissue [7]. Clearly, the high water absorbance of hydrogels is one of their most important material properties and therefore, it is crucial to be able to tailor the water content of the gels to suit the application that they are intended for.

FIGURE 2 AROUND HERE

We found that the swollen PEG-DMA hydrogels contained ~90 wt% water immediately after photocrosslinking (fig. 2). This initial water content in the swollen gels did not vary significantly with the photocrosslinking time. However, after the gels were dried and rehydrated overnight, the water uptake ability of the gels increased with an increase in the photocrosslinking time and the final water content ranged from 50 to 90 wt%. After 15 min of photocrosslinking, the water content of the gel was restored to the original water content of the swollen gel. Interestingly, Andreopoulos et al [31] report the swelling of a prepared wet PEG-based gel and find that the degree of swelling decreases with increased photocrosslinking time. Here, we report the swelling of a completely dried gel.

We interpret our results based on the notion that the wet gel contains what we term "bound water" and "free water". The "bound water" is water which interacts strongly with the gel meshwork and the "free water" is water which fills the pores (we have shown in [10] that the gel network is porous, with pores of circa 7 nm), but does not interact strongly with the gel network. The hydrogel precursor solution is a colloidal suspension of PEG-DMA monomers in water, and as the gel starts crosslinking, the water is trapped by the crosslinked polymer meshwork, making the gel bloated with "free water". Drying the gel effectively removes the free water. Thus the reswollen gel contains only bound water, as it may be energetically unfavorable to force the water back into the pores. The degree of reswelling was found to depend on the photocrosslinking time. The chemical structure of the gel (see fig. 1) reveals that the geometrical alignment of monomers in the gel can change with the degree of crosslinking. When the gel is not crosslinked, the PEG-DMA monomers contain conjugated double bonds, which give the ends

of the molecule a planar structure. As the gel is crosslinked, some C=C double bonds are converted to single bonds so both carbons have sp^3 orbitals and a three-dimensional structure. The gel network becomes more crosslinked with increased photocrosslinking time and should be more stable as well as form a 3D meshwork and thus be able to contain more bound water.

It is thus possible to tailor the water content of PEG-DMA hydrogels by selecting a suitable photocrosslinking time, thereby varying the water content of the PEG-DMA hydrogel from 50 wt% to 90 wt%.

3.2. Crosslinking revealed by Fourier Transform Infrared spectroscopy (FTIR)

We found that the hydrogels showed a clear trend with a higher water uptake for gels which had been polymerized at longer photocrosslinking times. In order to check whether this trend corresponded to an increase in crosslinking with increased photocrosslinking time, we studied samples with FTIR. With FTIR we could compare spectral peaks at 1680-1780 cm^{-1}[32] (assigned to C=O bond vibrations and indicated by the label "a" in fig.1) and 1620-1680 cm^{-1} [32] (due to C=C bonds and indicated by the label "b" in fig. 1). These bands originate from the methacrylate groups, which form covalent bonds through an addition reaction during the polymerization. In the addition reaction, the alkene functionality is converted to an alkane functionality. Therefore, the number of C=C bonds can be used as a measure of the degree of crosslinking of the polymer meshwork.

The FTIR spectra showed that the C=O peak is shifted when comparing crosslinked PEG-DMA hydrogels with the PEG-DMA monomer (fig. 3). The PEG-DMA wax has a C=O peak at 1716 cm^{-1}, and with the addition of phosphate buffered saline, the C=O peak is still at 1716 cm^{-1}. The

hydrogel photocrosslinked for 15 min had a C=O peak at 1728 cm^{-1}. Hence, the photocrosslinking must change the chemical environment in the vicinity of the C=O bond. The PEG-DMA monomer contains C=O bonds conjugated with the adjacent C=C bonds. In the crosslinked gel the C=C bond is converted by addition polymerization to a C-C bond and the C=O bonds are no longer conjugated. This conversion is observed as a peak shift of the C=O peak in the FTIR spectra, which is in agreement with observations in the literature [33]. The spectral C=O peak of the PEG-DMA monomer before photocrosslinking is at 1716 cm^{-1}, and does not have an additional peak or a shoulder at 1728 cm^{-1}, showing that no polymerization has occurred. After 15 min of photocrosslinking, the C=O peak is cleanly off-shifted to 1728 cm^{-1} without any residual peak remaining at 1716 cm^{-1}, indicating that virtually all the PEG-DMA monomer is used up in the reaction and effectively no C=O bonds conjugated with C=C bonds remain.

FIGURE 3 AROUND HERE

Furthermore, we investigated the effect of varied photocrosslinking times on the position of the C=O peak and C=C peak intensity (area under the C=C peak) (fig. 4). We found that for photocrosslinking times exceeding 6 min the C=O peak is off-shifted to 1728 cm^{-1}, and that the turning point is after 4 min photocrosslinking, when some samples have a C=O peak at 1728 cm^{-1} and others at 1718 cm^{-1}. This shows that the polymerization reaction once started occurs very rapidly because no intermediate peak shifts were found. Either there was no crosslinking and the C=O peak was at 1716-1718 cm^{-1} (resolution in FTIR was 4 cm^{-1}) or the crosslinking reaction was complete and the C=O peak was at 1728-1730 cm^{-1}. Photocrosslinking times of 1 min and 2

min were not sufficient to cause any crosslinking of the gel (results not shown). At a photocrosslinking time of 4 min, the crosslinking reaction starts as shown by the shift in the C=O peak with FTIR.

Examining the C=C peak, we found that at t=4 min, less than 40% of the original C=C bonds remain and at photocrosslinking times exceeding 8 min, 80% of the original C=C bonds are used up in the crosslinking reaction and the standard deviation of the number of C=C bonds for each photocrosslinking time is small. After 8 min of photocrosslinking, the PEG-DMA gel seems to be fully crosslinked. For photocrosslinking times of 8 and 15 min there is a variation in the water uptake, but no observed difference in the degree of crosslinking.

FIGURE 4 AROUND HERE

3.3. Detecting crosslinking reaction production by Raman Spectroscopy (RS)

FTIR provided us with a good indication of how many C=C bonds are used up in the gelation reaction, but this technique is limited as water has spectral peaks at the same wavenumbers as the C=O and C=C peak, which means that FTIR cannot be used to directly study the wet gels. Thus RS is a useful complementary technique, because of its low sensitivity to bulk water, and can be used on the wet gel.

We found by RS that the spectral signature of the wet hydrogel changes with the photocrosslinking time and have indicated the peaks in which changes occur in figure 5. Raman peaks at 1410 cm^{-1}, 1640 cm^{-1} (interpreted as stretching of C=C bonds) and 1705 cm^{-1} decrease

in intensity as the photocrosslinking time increases and disappear entirely at photocrosslinking time of 10 min. At a photocrosslinking time of 15 min, new Raman peaks appear at 618 cm^{-1}, 700 cm^{-1}, 1003 cm^{-1}, 1035 cm^{-1}, 1174 cm^{-1}, 1600 $cm^{-}1$ and 1676 cm^{-1}. The appearance of Raman peaks at 15 min is likely to be due to reaction end products from the Darocur1173 initiator used in the photocrosslinking reaction. This initiator is split by UV light into a benzoyl radical and an alkyl radical and one of the possible reaction end products is benzoic acid [34]. Benzoic acid Raman peaks that match closely to those observed at 15 min crosslinking are at 618 cm^{-1}, 708 cm^{-1}, 1035 cm^{-1} and 1165 cm^{-1} [35] and the Raman peaks at 1003 cm^{-1} and 1600 cm^{-1} are attributed to C=C aromatic ring stretching from other biproducts of the benzoyl radical. The reaction end products from the benzoyl radical are yellow and those from the alkyl radical generally evaporate during the polymerization process. Although no yellowing of gels was observed, the appearance of additional Raman peaks after 15 min crosslinking indicates that it may be optimal to stop after 10 min of photocrosslinking to avoid contamination of the gel with reaction end products.

FIGURE 5 AROUND HERE

3.4. Hydrogel specific electrical resistance

A physical parameter of great interest in determining sample changes is the specific electrical resistance, which can be determined from impedance spectroscopy (IS) measurements using equivalent circuits as models [36, 37]. We collected the impedance plots for the hydrogel at different photocrosslinking times, and clear differences could be observed as shown in figure 6a. The fitting of the impedance data by using a non-linear program [38] allows determination of the

electrical resistance of the different gel samples (R_G), which can be converted to specific electrical resistance, ρ, using $\rho = R_G \cdot A/l$, where A=177 mm^2 is the surface area of the gel sample and l=2.2 mm is the thickness of the gel. Specific electrical resistance values obtained for gel samples are shown in figure 6b. The electrical resistance of the gels ranged from 0.7 Ωm for 4 min photocrosslinking to 3.5 Ωm for 15 min photocrosslinking. An increase in the specific electrical resistance as a result of an increase in the photocrosslinking time was obtained, which is an indication of an increase in the crosslinking density of the gel network.

FIGURE 6 AROUND HERE

4. Conclusion

We show that the properties of a PEG-DMA hydrogel formed by photoinitiated polymerization can be tailored by varying the photocrosslinking time. We were able to vary the water content of the gels between 50-90 wt% and the specific electrical resistance of the gel between 0.7-3.5 Ωm. With FTIR and RS we identified spectral features of the hydrogel, which could be used as a diagnostic tool to study changes in the gel due to various parameters such as time, pH, temperature, aging or exposure to chemicals or biological materials, which would be useful when studying gels for tissue engineering applications.

5. Acknowledgements

This work was supported through MEMBAQ, a Specific Targeted Research Project (STREP), by the European Commission under the Sixth Framework Programme (NMP4-CT-2006-033234), by the Danish National Advanced Technology Foundation (023-2007-1) and by a grant to DTU

Physics from the Danish National Research Foundation. CHN was also supported by the Environment & Water Industry Programme Office of Singapore (EWI) through project #MEWR 651/06/169.

References

1. Hoffman AS. Hydrogels for biomedical applications. Adv Drug Deliv Rev 2002:54(1):3-12.
2. Peppas NA, Huang Y, Torres-Lugo M, Ward JH, Zhang J. Physicochemical foundations and structural design of hydrogels in medicine and biology. Annu Rev Biomed Eng 2000:2:9-29.
3. Peppas NA, Bures P, Leobandung W, Ichikawa H. Hydrogels in pharmaceutical formulations. Eur J Pharm Biopharm 2000:50(1):27-46.
4. Tanaka S, Ogura A, Kaneko T, Murata Y, Akashi M. Adhesion behavior of peritoneal cells on the surface of self-assembled triblock copolymer hydrogels. Biomacromolecules 2004:5(6):2447-2455.
5. Tanaka M, Tutus M, Kaufmann S, Rossetti FF, Schneck E, Weiss IM. Native supported membranes on planar polymer supports and micro-particle supports. J Struct Biol 2009:168(1):137-142.
6. Tanaka M, Sackmann E. Supported membranes as biofunctional interfaces and smart biosensor platforms. Physica Status Solidi a-Applications and Materials Science 2006:203(14):3452-3462.
7. Drury JL, Mooney DJ. Hydrogels for tissue engineering: scaffold design variables and applications. Biomaterials 2003:24(24):4337-4351.
8. Cruise GM, Hegre OD, Lamberti FV, Hager SR, Hill R, Scharp DS, Hubbell JA. In vitro and in vivo performance of porcine islets encapsulated in interfacially photopolymerized poly(ethylene glycol) diacrylate membranes. Cell Transplant 1999:8(3):293-306.
9. Elisseeff J, McIntosh W, Anseth K, Riley S, Ragan P, Langer R. Photoencapsulation of chondrocytes in poly(ethylene oxide)-based semi-interpenetrating networks. J Biomed Mater Res 2000:51(2):164-171.
10. Ibragimova S, Stibius K, Szewczykowski P, Perry M, Bohr H, Hélix-Nielsen C. Hydrogels for in situ Encapsulation of Biomimetic Membrane Arrays. Polymers for Advanced Technologies:doi 10.1002/pat.1850 (in press).
11. Malmstadt N, Jeon LJ, Schmidt JJ. Long-Lived Planar Lipid Bilayer Membranes Anchored to an in situ Polymerized Hydrogel. Advanced Materials 2008:20(1):84-89.
12. Shim JW, Gu LQ. Stochastic sensing on a modular chip containing a single-ion channel. Anal Chem 2007:79(6):2207-2213.
13. Kang XF, Cheley S, Rice-Ficht AC, Bayley H. A storable encapsulated bilayer chip containing a single protein nanopore. J Am Chem Soc 2007:129(15):4701-4705.
14. Costello RF, Peterson IR, Heptinstall J, Walton DJ. Improved Gel-Protected Bilayers. Biosens Bioelectron 1999:14:265-271.
15. Beddow JA, Peterson IR, Heptinstall J, Walton DJ. Reconstitution of Nicotinic Acetylcholine Receptors into Gel-Protected Lipid Membranes. Anal Chem 2004:76(8):2261-2265.
16. Tien HT, Ottova AL. Supported planar lipid bilayers (s-BLMs) as electrochemical biosensors. Electrochim Acta 1998:43(23):3587-3610.
17. Ziegler W, Gaburjakova J, Gaburjakova M, Sivak B, Rehacek V, Tvarozek V, Hianik T. Agar-supported lipid bilayers - basic structures for biosensor design. Electrical and mechanical properties. Colloids Surf A 1998:140:357-367.

18. Baumgart T, Offenhausser A. Polysaccharide-Supported Planar Bilayer Lipid Model Membranes. Langmuir 2003:19:1730-1737.
19. Uto M, Araki M, Taniguchi T, Hoshi S, Inoue S. Stability of an Agar-Supported Bilayer Lipid Membrane and Its Application to a Chemical Sensor. Anal Sci 1994:10:943-946.
20. Jeon TJ, Malmstadt N, Schmidt JJ. Hydrogel-encapsulated lipid membranes. J Am Chem Soc 2006:128(1):42-43.
21. Heron AJ, Thompson JR, Mason AE, Wallace MI. Direct detection of membrane channels from gels using water-in-oil droplet bilayers. J Am Chem Soc 2007:129(51):16042-16047.
22. Thompson JR, Heron AJ, Santoso Y, Wallace MI. Enhanced stability and fluidity in droplet on hydrogel bilayers for measuring membrane protein diffusion. Nano Lett 2007:7(12):3875-3878.
23. Lander MR, Ibragimova S, Rein C, Vogel J, Stibius K, Geschke O, Perry M, Hélix-Nielsen C. Biomimetic membrane arrays on cast hydrogel supports. Langmuir:submitted.
24. Costello RF, Peterson IP, Heptinstall J, Byrne NG, Miller LS. A Robust Gel-Bilayer Channel Biosensor. Advanced Materials for Optics and Electronics 1998:8(2):47-52.
25. Nielsen CH. Biomimetic membranes for sensor and separation applications. Anal Bioanal Chem 2009:395(3):697-718.
26. Peláez L, Romero V, Escalera S, Scileira V, Ibragimova S, Stibius K, Benavente J, Nielsen CH. Electrochemical Characterisation of Hydrogels for Biomimetic Applications. Polymers for Advanced Technologies:submitted.
27. Myung D, Waters D, Wiseman M, Duhamel PE, Noolandi J, Ta CN, Frank CW. Progress in the development of interpenetrating polymer network hydrogels. Polym Adv Technol 2008:19(6):647-657.
28. Jensen L, Mortensen PM, Trane R, Harris P, Berg RW. Reaction kinetics of acetone peroxide formation and structure investigations using Raman spectroscopy and X-ray diffraction. Appl Spectrosc 2009:63(1):92-97.
29. Benavente J, Vázquez MI, Hierrezuelo J, Rico R, López-Romero JM, López-Ramirez MR. Modification of a Regenerated Cellulose Membrane with Lipid Nanoparticles and Layers. Nanoparticle Preparation, Morphological and Physicochemical Characterization of Nanoparticles and Modified Membranes. Journal of Membrane Science 2010:355(1-2):45-52.
30. Bryant SJ, Anseth KS. Hydrogel Properties Influence ECM Production by Chondrocytes Photoencapsulated in Poly(ethylene glycol) Hydrogels. J Biomed Mater Res 2002:59(1):63-72.
31. Andreopoulos FM, Beckman EJ, Russell AJ. Light-induced tailoring of PEG-hydrogel properties. Biomaterials 1998:19(15):1343-1352.
32. Ladd M. Introduction to Physical Chemistry. Cambridge: Cambridge University Press, 1998.
33. Suh KY, Seong J, Khademhosseini A, Laibinis PE, Langer R. A simple soft lithographic route to fabrication of poly(ethylene glycol) microstructures for protein and cell patterning. Biomaterials 2004:25(3):557-563.
34. Green WA. Photoproducts and the Yellowing of Coatings. CRC Press, 2010. p. 139-148.
35. Krishnakumar V, Mathammal R. Density functional and experimental studies on the FT-IR and FT-Raman spectra and structure of benzoic acid and 3,5-dichloro salicylic acid. Journal of Raman Spectroscopy 2009:40(3):264-271.
36. Asaka K. Dielectric-Properties of Cellulose-Acetate Reverse-Osmosis Membranes in Aqueous Salt-Solutions. Journal of Membrane Science 1990:50(1):71-84.
37. Benavente J, in “Surface Electrical Phenomena in Membranes and Microchannels” (A. Szymczyk, Ed.). Transworld Research Network, Kerala, 2008.
38. Boukamp BA. A Package for Impedance Admittance Data-Analysis. Solid State Ionics 1986:18-9:136-140.

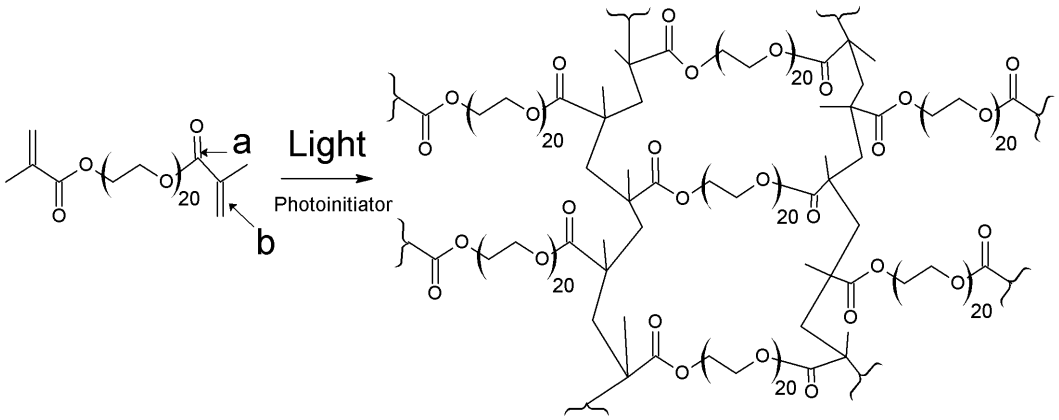

Fig. 1. Chemical structure of PEG-1000-DMA and of a crosslinked PEG-1000-DMA meshwork found in the gel. Gelation occurs through radical polymerization in which the methacrylate groups participate in an addition reaction to form a branched polymeric network. The crosslinked gel, X1000P, was made from a hydrogel precursor solution containing 65 mM PEG-1000-DMA with 10 mM Darocur photoinitiator in aqueous buffer. The C=O (a) and C=C (b) bonds to which FTIR spectral peaks are assigned are indicated.

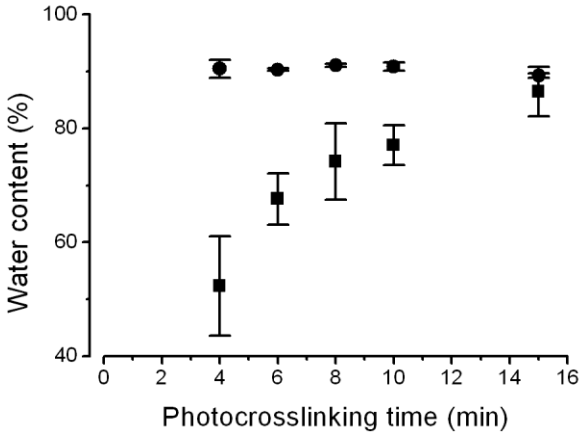

Fig. 2. Variation in water content of X1000P hydrogel with photocrosslinking time. Gel samples were crosslinked with photocrosslinking times of 4, 6, 8, 10 and 15 min (n=3 per photocrosslinking time). The "wet gel" (circles) samples were weighed, dried in a dessicator and weighed again to determine the water content of the "wet gel". The dry gels were reswollen and weighed to determine the water absorption as a function of photocrosslinking time (squares).

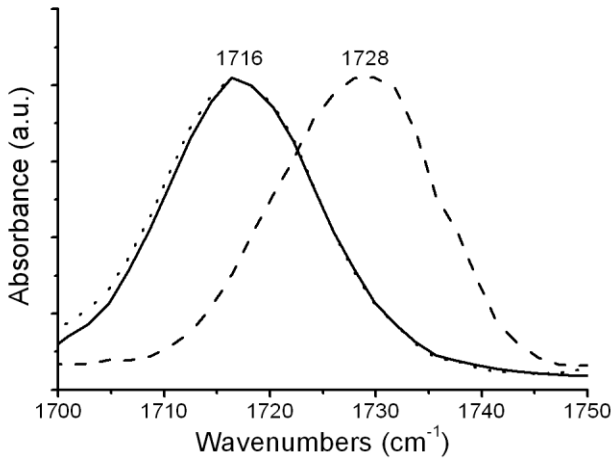

Fig. 3. Peak shift of the C=O peak due to crosslinking obtained by FTIR. FTIR C=O peaks of PEG-1000-DMA wax (solid), 65mM PEG-1000-DMA in PBS (dotted) and 65 mM PEG-1000-DMA and 10 mM Darocur in PBS crosslinked with ultraviolet light (X1000P) for 15 min (dashed) are shown. Photocrosslinking the gel thus results in a peak shift of circa 12 cm^{-1}. Samples were dried in a vacuum dessicator prior to analysis in order to reduce the contribution from water in the recorded spectrum.

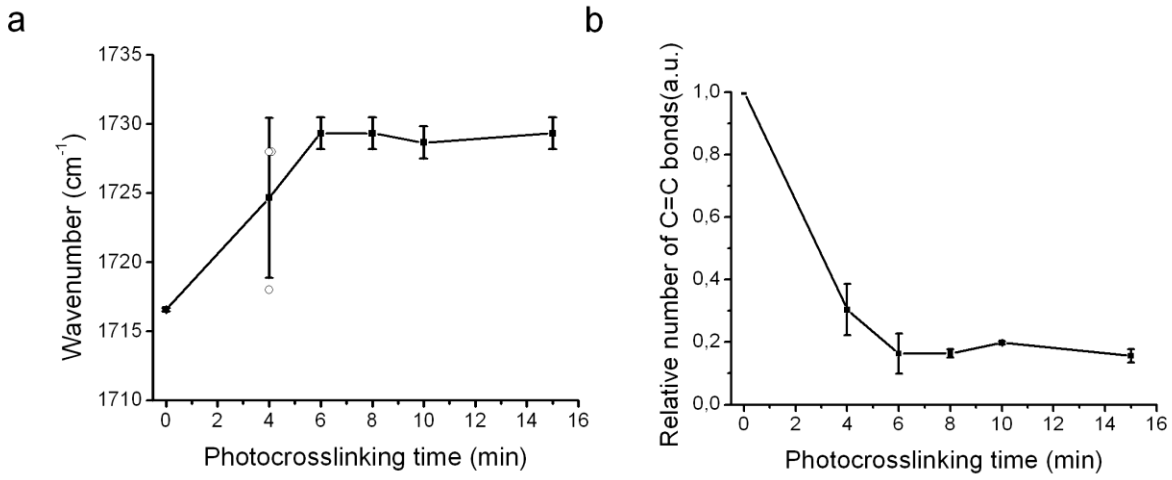

Fig. 4. Effect of photocrosslinking time on FTIR spectra of X1000P hydrogel. (a) The wavenumber of the C=O peak for gels with different photocrosslinking times (n=3). (b) The relative number of C=C bonds in the hydrogel as a function of photocrosslinking time (n=3).

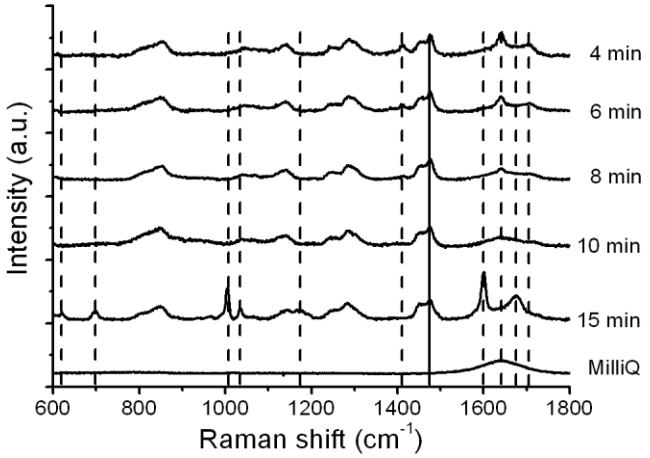

Fig. 5. Spectral fingerprints of X1000P hydrogel as a function of photocrosslinking time obtained by Raman spectroscopy. Raman spectra were normalized to make the peak at 1470 cm^{-1} (attributed to H-C-H bending, indicated with a solid line) have equal intensity and then the spectra were offset for clarity. Dashed lines indicate Raman peaks of the gel that change with increased photocrosslinking time.

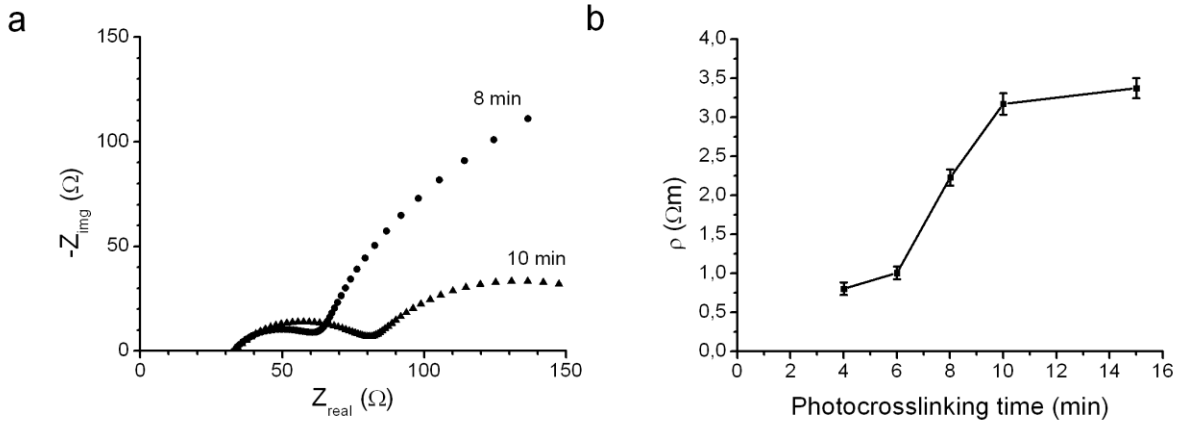

Fig. 6. Gel impedance (a) and specific electrical resistance, ρ, (b) of X1000P hydrogel as a function of the photocrosslinking time.

Paper III

Langmuir

ARTICLE

pubs.acs.org/Langmuir

Biomimetic Membrane Arrays on Cast Hydrogel Supports

Monique Roerdink Lander,[†,⊥] Sania Ibragimova,[‡,§,⊥] Christian Rein,[§,∥,⊥] Jörg Vogel,[†,§] Karin Stibius,[‡,§] Oliver Geschke,[†,§] Mark Perry,[§] and Claus Hélix-Nielsen*[,‡,§]

[†]DTU-Nanotech and [‡]DTU-Physics, Technical University of Denmark, DK-2800 Kgs. Lyngby, Denmark

[§]Aquaporin A/S, Ole Maaløes Vej 3, DK-2200 Copenhagen N, Denmark

[∥]Nano-Science Center and Department of Chemistry, University of Copenhagen, Universitetsparken 5, DK-2100 Copenhagen Ø, Denmark

ABSTRACT: Lipid bilayers are intrinsically fragile and require mechanical support in technical applications based on biomimetic membranes. Tethering the lipid bilayer membranes to solid substrates, either directly through covalent or ionic substrate−lipid links or indirectly on substrate-supported cushions, provides mechanical support but at the cost of small molecule transport through the membrane−support sandwich. To stabilize biomimetic membranes while allowing transport through a membrane−support sandwich, we have investigated the feasibility of using an ethylene tetrafluoroethylene (ETFE)/hydrogel sandwich as the support. The sandwich is realized as a perforated surface-treated ETFE film onto which a hydrogel composite support structure is cast. We report a simple method to prepare arrays of lipid bilayer membranes with low intrinsic electrical conductance on the highly permeable, self-supporting ETFE/hydrogel sandwiches. We demonstrate how the ETFE/hydrogel sandwich support promotes rapid self-thinning of lipid bilayers suitable for hosting membrane-spanning proteins.

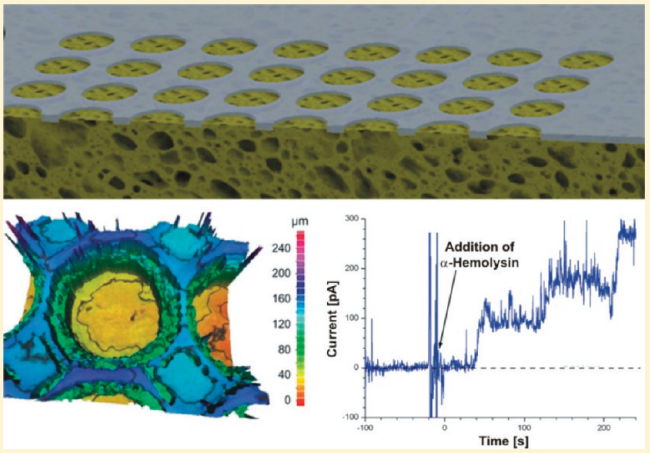

INTRODUCTION

Biomimetic membranes based on lipid bilayers are increasingly being recognized as a platform not only for the study of reconstituted membrane-associated proteins but also as building blocks in devices for sensor and separation applications.[1,2] Lipid bilayer membranes are extremely fragile and require mechanical support,[3,4] and deposition of planar lipid bilayers onto supports allows for the biofunctionalization of surfaces, providing a natural environment for the immobilization of highly specialized membrane-associated proteins.[5] Support surfaces with nanoscale smoothness based on gold, silicon, or cleaved mica have been investigated intensively with several membrane−protein systems.[6] Such systems are well-suited for biomimetic sensors where the sensor readout is based on, e.g., detecting electrochemical impedance changes induced by ligand binding to membrane-stabilized proteins of the supported membrane−protein complex via gold electrodes or detection based on optical (fluorescence) signals.

Membrane-spanning proteins often have hydrophilic moieties that may hinder optimal support of bilayers with reconstituted proteins on solid surfaces. This has led to the development of "cushions" in the form of polymeric structures that effectively separate the bilayers from the solid surface using, for example, polyacrylamide and agarose as the cushion material.[7−9] In these approaches the bilayers were formed across a single aperture (100−500 μm diameter), and the cushion supported the membrane in the aperture area. Later developments include the formation of membranes where the bilayer is cushioned by poly(ethylene glycol) (PEG)-conjugated lipids that effectively separate the bilayer from a solid surface.[10,11] A different approach consists of using supports with submicrometer porosity where the bilayers are formed directly on top of, for example, nanoporous alumina substrates.[12,13] Bilayer formation has also been demonstrated using ordered arrays of submicrometer-sized pores formed in silicon substrates with well-defined pore diameters ranging from 250 to 1000 nm.[14,15] In this case, the membranes span the pores without additional support. Supports using hydrogels have also been demonstrated.[16,17]

Applications relying on mass transport across planar biomimetic membranes mediated by transmembrane proteins require that the supported membrane is stable against external forces, such as osmotic and hydrostatic forces, and concomitantly sufficiently porous to allow for vectorial transport of solutes and solvents. Tethering the lipid bilayer membranes to solid substrates, either directly through covalent or ionic substrate−lipid conjugates or indirectly by substrate-supported cushions, provides mechanical support but is not optimal for large-scale

Received: December 22, 2010
Revised: March 24, 2011

mass transport across the membrane. Large-scale transport across biomimetic membranes also requires that the entire system is readily upscalable. Approaches using nanoporous alumina require arduous preparation,[13] and the use of nanopore silicon arrays is limited by material cost and wafer size. These are issues that need to be addressed to harness the unique opportunities that lipid bilayer membranes offer in technological applications where large-scale transport is desired.

Previously, we reported the fast fabrication of dense arrays of 300 μm diameter circular apertures in 50 μm thick partitions made of ethylene tetrafluoroethylene (ETFE) for biomimetic membranes using a CO_2 laser ablation method that is cost-effective and that can be easily scaled up to square centimeters.[18] We also reported successful formation of planar, free-standing black lipid membranes (BLMs) in these hydrophobic multi-aperture partitions.[19,20] In this study we aimed at stabilizing lipid membranes further against pressure-induced disruptions in a construction that tolerates large flux through the supported BLMs using a relatively simple upscalable porous support structure. Specifically, we formulated a composite hydrogel that demonstrates high water permeability. The hydrogel support is formed by in situ polymerization of an aqueous solution of 2-hydroxyethyl methacrylate (HEMA) and poly(ethylene glycol) dimethacrylate (PEG-DMA) in the presence of silicon dioxide particles. The composite hydrogel was cast using a mold such that the polymerized hydrogel would form a supportive layer across apertures formed in an ETFE array as shown in Figure 1A–C. The rationale behind this design was to optimize the lipid–partition interactions at the aperture rim while providing maximal support for the membranes across the aperture arrays. To ensure good contact between the hydrophilic composite hydrogel and the hydrophobic multiaperture ETFE partition, we modified the ETFE surface using a plasma surface treatment on the partition side facing the hydrogel. We demonstrate how the composite support is capable of promoting rapid self-thinning of BLMs and that the supported BLMs are suitable for hosting membrane-spanning proteins.

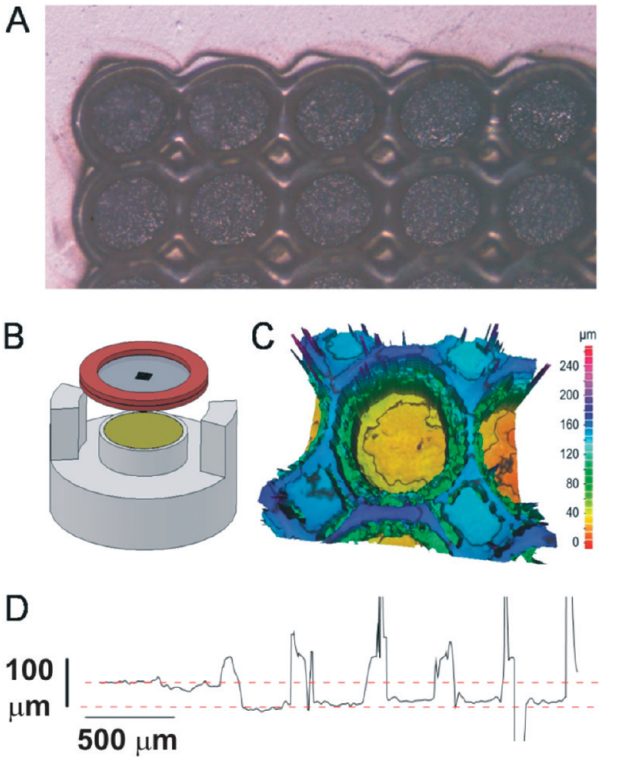

Figure 1. (A) Top view of a section of the ETFE/hydrogel sandwich. The composite hydrogel is attached to the back of the ETFE without penetrating the apertures. (B) Schematic of the ETFE scaffold with PMMA rings (red) and the Teflon mold used for casting of the hydrogel support. The hydrogel-forming solution (green) is contained in a reservoir with a depth of 500 μm. (C) Optical scanning image of a single aperture with the composite hydrogel. The green toroidal structure inside the aperture represents the sloping wall of the aperture. The spikes are measurement artifacts due to missing data points. (D) Profile scan across five apertures. The red dashed lines indicate the surfaces of the ETFE sheet.

EXPERIMENTAL SECTION

Materials. PEG-DMA (M_w(PEG block) = 1000 g/mol) was purchased from Polysciences, Inc. (Warrington, PA). *N,N,N′,N′*-Tetramethylethylenediamine (TEMED), α-hemolysin (*Staphylococcus aureus*), 10× phosphate-buffered saline (PBS), pH 7.4, HEMA, 1,4-butanediol diacrylate (BDDA), silicon dioxide particles (0.5–10 μm diameters), ammonium persulfate (APS), *n*-decane, and ethanol were purchased from Sigma-Aldrich Denmark (Brøndby, Denmark). Tefzel ETFE LZ200 for fabrication of multiaperture arrays and Viton A fluoroelastomer used for the production of rubber chamber-sealing O-rings were supplied by DuPont Fluoropolymers (Detroit, MI). 1,2-Diphytanoyl-*sn*-glycero-3-phosphocholine (DPhPC), 1,2-dioleoyl-3-(trimethylammonium)-propane (DOTAP), 1,2-distearoyl-*sn*-glycero-3-phosphoethanolamine-*N*-[biotinyl(poly(ethylene glycol))-2000] (ammonium salt) (DSPE-PEG2000-biotin), and 1-oleoyl-2-[6-[(7-nitro-2,1,3-benzoxadiazol-4-yl)-amino]hexanoyl]-*sn*-glycero-3-phosphocholine (NBD-PC) were purchased from Avanti Polar Lipids, Inc. (Alabaster, AL). All materials were used as received.

Fabrication of the ETFE/Hydrogel Sandwich. In the first production step the ETFE partition was plasma-treated on one side of the ETFE with HEMA in a custom-built 50 Hz two-phase plasma chamber[21] using 1 sccm of Ar as the activation/carrier gas with 10 Pa of total pressure and 10 W of plasma power (20 mA, 500 V). The partition and monomer solution were left overnight to cure. Casting was performed with a solution consisting of 23 mg of PEG-DMA, 560 μL of HEMA, 8 μL of TEMED, 5 μL of BDDA, 140 mg of SiO_2, and 1000 μL of Milli-Q water vortexed to create a milky suspension. To 400 μL of this solution was added 15.3 μL of an initiator solution (170 mg of APS in 1000 μL of Milli-Q water). The mixture was vortexed for 10 s and immediately transferred to a reservoir (2 cm diameter, 0.5 mm height) in a Teflon mold (see Figure 1B). A surface-functionalized ETFE partition with 8 × 8 apertures (300 μm diameter, 400 μm center-to-center spacing),[18] glued between two custom-made poly(methyl methacrylate) (PMMA) rings, was fitted on top of the mold, resulting in direct contact between the monomer solution and the functionalized side of the ETFE partition. This setup allowed for the monomer solution to cover but not fill up the apertures. After 10–20 min the hydrogel-coated partitions could be removed from the mold and were stored in Milli-Q water. The hydrogel surface topography was characterized by focus-variation optical scanning of the surface (InfiniteFocus, Alicona Instruments, GmbH, Graz, Austria), shown in Figure 1C,D. Before membrane formation, excess water was removed from the hydrogel-coated partitions by blotting with tissue.

BLM Formation. The membrane formation chamber used was a modified version of the horizontal chamber design described by Hansen et al.[19] The chamber was assembled by placing the hydrogel-coated partition with the ETFE side up in the *cis* chamber between two O-rings. An open lid sealed the assembly. Both the *cis* chamber and the channel

dx.doi.org/10.1021/la1050699 |*Langmuir* XXXX, XXX, 000–000

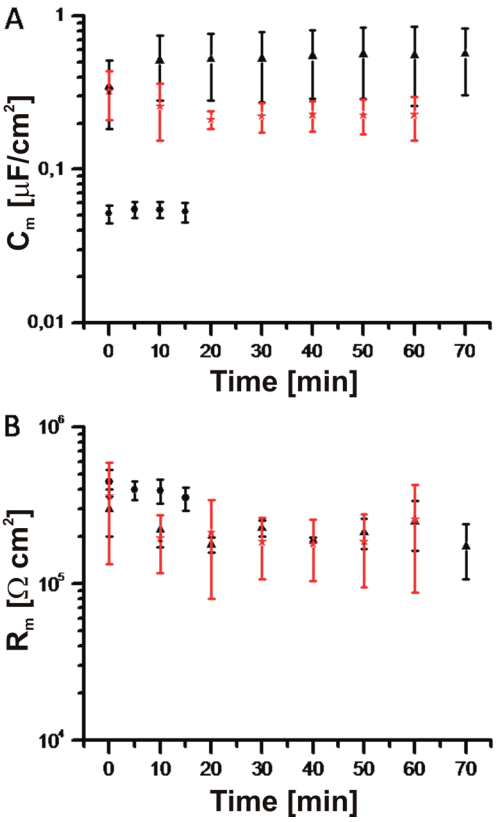

Figure 2. (A) Comparison of mean ± SD specific capacitance values C_m of unsupported free-standing (black circles, n = 9) and hydrogel-supported (triangles and asterisks, n = 8) membrane arrays consisting of 8 × 8 individual membranes versus time. Two trends were observed for the hydrogel-supported membranes: (1) development of the specific capacitance to a mean value of 0.3 μF/cm^2 (red asterisks, n = 4); (2) development of the specific capacitance to a mean value of 0.6 μF/cm^2 (black triangles, n = 4). (B) Specific resistance for the membranes shown in (A).

between the *cis* and *trans* chambers were filled with 1 mL of 1× PBS (filtered through a 0.2 μm filter). The apertures were pretreated by depositing 4 μL of lipid solution and incubating for 1 h. The lipid solution used in membrane preparation for electrical measurements contained 294 μL of DPhPC (72 mol %), 61 μL of DOTAP (18 mol %), and 145 μL of DSPE-PEG2000-biotin (10 mol %). Lipid solutions in chloroform (10 mg/mL) were dried under nitrogen gas. The dried lipid film was subsequently redissolved in 200 μL of decane (25 mg/mL). The lipid solution used in membrane preparation for fluorescence measurements contained 292 μL of DPhPC (71 mol %), 61 μL of DOTAP (18 mol %), 146 μL of DSPE-PEG2000-biotin (10 mol %), and 39 μL of NBD-PC (1 mol %). Lipid solutions in chloroform (10 mg/mL) were dried and redissolved in decane as described above. Lipid solutions were deposited on top of the apertures in 2 μL aliquots up to 10 μL. One mL of 1× PBS (filtered through a 0.2 μm filter) was added to the *cis* chamber, which was subsequently sealed. Membrane formation was monitored by electrical capacitance and conductance measurements using standard electrophysiological methods as previously described.[22] Briefly, the membranes were voltage clamped using AgCl electrodes in each chamber compartment, and transmembrane currents were recorded using a patch-clamp amplifier. The membrane resistance R_m and capacitance C_m were measured by applying rectangular and triangular waveforms, respectively (V_{pp}= 10 mV). The response signal was low pass filtered at <100 Hz and logged via analog to digital conversion for off-line analysis. Measured total R_m and C_m values for the hydrogel-supported membrane were converted into specific values by normalizing with the combined aperture array area, neglecting the vanishingly small Plateau—Gibbs regions (see Figure 3B,C). The empty ETFE/hydrogel sandwich had negligible resistance and capacitance.

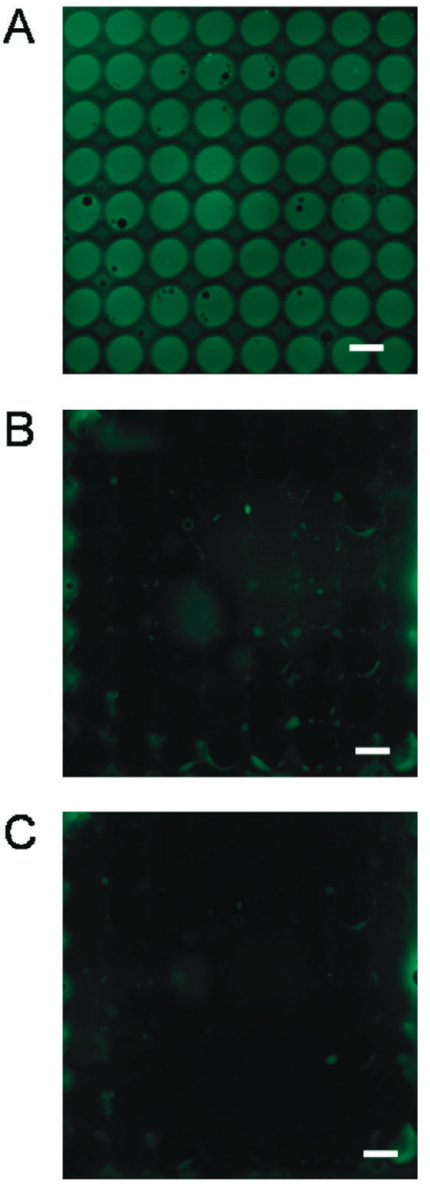

Figure 3. (A) Fluorescent images of established nonsupported free-standing membranes immediately after formation. (B) Same for hydrogel-supported membrane arrays directly after formation. (C) Same as in (B) but 20 min after formation. Scale bars are 300 μm.

Fluorescence Microscopy. Fluorescent imaging was performed on a Zeiss Axiovert 200 M epifluorescence microscope (Carl Zeiss, Jena, Germany) equipped with a monochrome Deltapix DP450 charge-coupled device camera (Deltapix, Maalov, Denmark). Images were acquired using Deltapix DpxView Pro acquisition software (Deltapix) and air-corrected Plan-Neofluar 2.5×/0.075 numerical aperture (NA) and 10×/0.25 NA objectives.

Ion Channel Insertion. α-Hemolysin was added to the *cis* chamber 10 min after a membrane array was established, resulting in a final concentration of 1 μg/mL in 10× PBS (filtered through a 0.2 μm filter). A potential of 60 mV was applied across the membrane, and current traces were filtered at 20 Hz.

dx.doi.org/10.1021/la1050699 |*Langmuir* XXXX, XXX, 000–000

RESULTS AND DISCUSSION

The presence of silica particles in the polymer hydrogel greatly enhances both the mechanical stability of the gel and the flux of water through the hydrogel.[23] The permeability increased with the amount of silica present in the hydrogel composite. We measured permeabilities up to 24 g m^{-2} min^{-1} at 1 bar for a 1 mm thick slab of composite hydrogel, which contained 44 wt % silica. For comparison, commercial nanofiltration membranes have permeabilities of 1−4 g m^{-2} min^{-1} at applied pressures of 7−30 bar for 0.1 μm pore size films.

The hydrogel was cast using a Teflon mold to form a hydrogel support in each aperture over the entire array (Figure 1B) as described in the Experimental Section. The surface topography of the hydrogel areas in the ETFE/hydrogel sandwich was characterized by focus-variation optical scanning and revealed the desired backing of the ETFE partition apertures with the composite hydrogel (Figure 1C). We evaluated the arithmetical mean roughness R_a of the hydrogel surface inside each aperture from

$$R_a = \frac{1}{l}\int_0^l |f(x)|\, dx \quad (1)$$

which corresponds to averaging over a section of standard length l sampled from mean value curves (described by $f(x)$) on the optical scan roughness chart. From this the average R_a value of an ETFE/hydrogel surface fabricated using the mold method was determined to be 1.036 ± 0.178 μm (mean ± SD, n = 5 scans). By comparison, R_a is 0.583 ± 0.088 μm (mean ± SD, n = 5 scans) for a glass−hydrogel interface prepared on a glass slide. The difference reflects the increased roughness of the mold-cast, air-cured interface of the hydrogel. The surface roughness corresponds to an increment of the interfacial area of the sampled surface area relative to an ideally flat surface. The increment, or surface area ratio S_{dr}, of the hydrogel surface relative to the area of the projected $x-y$ surface, can be determined from

$$S_{dr} = \frac{\left(\sum_{k=0}^{M-2}\sum_{l=0}^{N-2} A_{kl}\right) - (M-1)(N-1)\,\delta x\,\delta y}{(M-1)(N-1)\,\delta x\,\delta y} \times 100 \quad (2)$$

where M and N represent the numbers of pixels in the x and y directions, respectively, and

$$A_{kl} = \frac{1}{4}\left(\sqrt{\delta y^2 + (z(x_k, y_l) - z(x_k, y_{l+1}))^2} + \sqrt{\delta y^2 + (z(x_{k+1}, y_l) - z(x_{k+1}, y_{l+1}))^2}\right) \times \left(\sqrt{\delta x^2 + (z(x_k, y_l) - z(x_{k+1}, y_l))^2} + \sqrt{\delta x^2 + (z(x_k, y_{l+1}) - z(x_{k+1}, y_{l+1}))^2}\right) \quad (3)$$

The surface area ratio is 11% for the ETFE/hydrogel support. Figure 1A shows the ETFE/hydrogel support. A pore size distribution analysis of the composite hydrogel, based on environmental scanning electron microscopy image analysis, showed a bimodal distribution with some pore diameters of <500 nm and the majority of the pore diameters between 2 and 5 μm. The smaller pores (with radii less than the surface roughness) reflect some degree of interfacial skin layer formation.[23] However, water flux and electrical properties of the composite hydrogel were not affected by this.[24] The composite hydrogel support covered the apertures with marginal penetration into the apertures (see Figure 1D).

Using the ETFE/hydrogel sandwich support, we established lipid membranes across 8 × 8 aperture arrays. ETFE partition arrays without hydrogel served as the reference. Membranes were formed by manually applying a lipid−decane solution to the apertures.[19] The membrane-forming solution contained DOTAP and PEG-conjugated lipid. The rationale behind including the cationic DOTAP comes from the observation that DOTAP is able to electrostatically "stitch" gel-state bilayers together to form defect-free membranes of several square micrometers; therefore, DOTAP can be seen as a bilayer-stabilizing agent.[25,26] PEG-conjugated lipids were included to provide a soft cushion for the bilayers resting on top of the hydrogel surface.[5] The array electric specific capacitance, C_m, and specific resistance, R_m, for the free-standing and the hydrogel-supported membranes are shown in Figure 2. F2

When using apertures without a cast hydrogel support, the membranes appeared thick and did not thin automatically, as evidenced by a stable, low membrane array specific capacitance not exceeding 0.06 μF/cm^2 (Figure 2A). In contrast, C_m values of 0.35 μF/cm^2 were observed for membranes formed on ETFE/hydrogel directly after membrane formation, indicating thin, decane-containing lipid bilayer membranes. Two trends in the specific capacitance values were observed for the hydrogel-supported membranes after membrane formation: (1) the specific capacitance stabilized at C_m = 0.30 μF/cm^2, which is comparable to the 0.3−0.4 μF/cm^2 reported for decane-containing free-standing bilayers;[27] (2) the membranes spontaneously thinned further, and average specific capacitance values of 0.6 μF/cm^2 were observed, occasionally exceeding 0.9 μF/cm^2 (Figure 2A). Theoretical estimates for the specific capacitance of solvent-free lipid bilayers range from 0.75 to 0.81 μF/cm^2, while 0.78 μF/cm^2 was found experimentally for "solvent-free" membranes formed from squalene.[28] Our measurements suggest that the membranes formed in ETFE/hydrogel sandwiches, if not solvent-free, then at least contain only a small solvent fraction. The "solventless" membranes thus formed should be favorable for protein incorporation. On the basis of these results, we conclude that the hydrogel support significantly facilitates the formation of thin BLMs in the aperture arrays without the need for the manual thinning (painting) that is typically necessary to form thin membranes. Alternatively, the increase in specific capacitance observed for the supported BLMs (Figure 2A) could be attributed to an increase in the effective bilayer area due to hydrogel surface corrugation or due to a surface-induced expulsion of hydrocarbon solvent. Since the increment of the interfacial area is ≤11%, we conclude that the increase in capacitance is mainly due to an induced thinning of the lipid film. The average specific membrane resistance R_m was above 10^5 Ω cm^2 for all membranes (Figure 2B), indicating that the thinned membranes formed in the ETFE/hydrogel arrays cover all apertures in the array, as rupture of even a single aperture membrane would lead to a several-orders-of-magnitude increase in membrane conductance.[20,22] Furthermore, both the C_m and R_m values are comparable with reported results obtained for PEG-cushioned bilayers.[10]

Figure 2 monitors the lifetime of the membranes until the first out of 64 membrane apertures ruptures, leading to an immediate increase in total conductance. After 15 min, membrane rupture occurred in the free-standing, non-thinned membranes. By

dx.doi.org/10.1021/la1050699 |Langmuir XXXX, XXX, 000–000

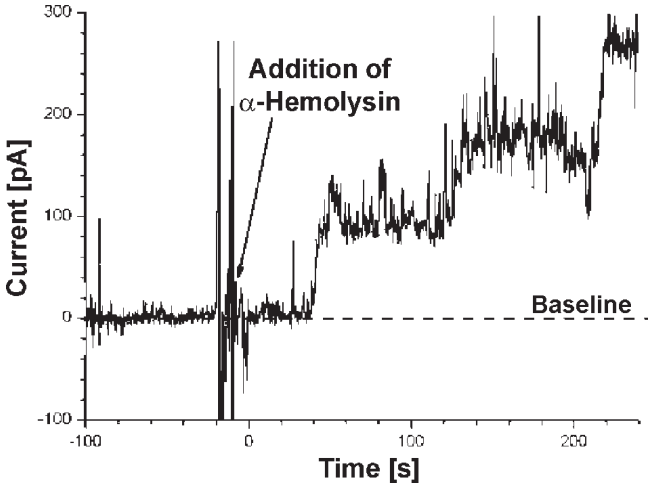

Figure 4. Current trace of a hydrogel-supported BLM indicating the formation of α-HL pores (mean step size 57 pA).

comparison, the first membrane ruptured after 60 min in the hydrogel-supported membrane arrays. Thus, addition of the composite hydrogel support significantly increased the time until first rupture. Although some membranes lasted for many hours with C_m values >0.9 μF/cm^2, we believe that observing the time of first rupture as a better way to quantify membrane array lifetimes instead of reporting the "best mode" (i.e., the longest living membranes in each case), which may only correspond to a small number of successful experiments.

To obtain further insight into the membrane thinning, we used fluorescence microscopy to image formed membranes (Figure 3). Free-standing lipid films are thick, as indicated by the apertures being evenly filled with fluorescently labeled lipids (Figure 3A), and did not thin spontaneously until the time of first aperture rupture. When using the ETFE/hydrogel sandwich array structure, the lipid bilayer membranes formed immediately upon applying the lipid solution and thinned spontaneously with negligible Plateau−Gibbs tori (Figure 3B,C). The negligible Plateau−Gibbs tori and the apparent reduction in the diamond-shaped lipid area between apertures (compare part A with parts B and C of Figure 3) indicate that excess decane solvent from the lipid solution has been "squeezed out" during the membrane self-assembly and thinning process. The bright, nebulous region in Figure 3B is the residual bilayer-forming solution (primarily decane). In the horizontal chamber used, this solution floats to the water/air interface and thus appears as a diffuse area since the microscope focus plane is kept at the level of the upper surface of the ETFE/hydrogel sandwich. Over time this excess solution accumulates along the inner rim of the chamber outside the microscope field (compare part B with part C of Figure 3). To confirm the existence of thin lipid membranes located in the aperture array and demonstrate the functionality of the hydrogel-supported BLMs, α-hemolysin (α-HL) was added to the *cis* chamber of an existing hydrogel-supported BLM while the current trace of the BLMs was measured. The results are shown in Figure 4. The measurement was performed with a transmembrane potential of 60 mV in 10× PBS to obtain a sufficient signal-to-noise ratio for voltage-clamp recording of the 8 × 8 BLM array. In less than 1 min, α-HL heptamer channel formation in the membrane was observed as indicated by a stepwise increase in the current with a mean single channel current amplitude of 57 pA, which compared well to previously reported values obtained at equivalent ionic strength.[29]

In conclusion, we designed a highly water permeable composite hydrogel support consisting of polyHEMA, PEG, and silica particles to create a support for lipid membranes formed across an array of apertures in an ETFE partition. The hydrogel support significantly facilitates the formation of thin BLMs in the aperture arrays without the need for the manual thinning (painting) that is typically necessary to form thin membranes. The solventless hydrogel-supported membranes form rapidly over arrays of apertures and thin spontaneously with an increase rather than a decrease in membrane array lifetime, as compared to thicker, solvent-containing, free-standing membranes. Successful incorporation of α-hemolysin demonstrated that the BLMs are fully functional in close proximity to the polymeric material. With this approach, rapid fabrication of large arrays of BLMs that allow large flux transport across the supported membranes should be feasible.

AUTHOR INFORMATION

Corresponding Author

*Phone: +45 60 68 10 81. Fax: +45 45 93 16 69. E-mail: claus.helix.nielsen@fysik.dtu.dk.

Author Contributions

⊥Shared first coauthorship.

ACKNOWLEDGMENT

We thank H. Nørgaard Hansen and S. Gasparin at DTU-Mechanical Engineering for placing the Alicona InfiniteFocus at our disposal and for their help in its operation. This work was supported through MEMBAQ, a Specific Targeted Research Project (STREP), by the European Commission under the Sixth Framework Programme (Grant NMP4-CT-2006-033234), by the Danish National Advanced Technology Foundation (Grant 023-2007-1), and by a grant to DTU-Physics from the Danish National Research Foundation. C.H.N. was also supported by the Environment & Water Industry Development Council of Singapore (EWI) through Project MEWR 651/06/169.

REFERENCES

(1) Martin, D. *Nanobiotechnology of Biomimetic Membranes*; Springer Verlag: New York, 2007.
(2) Nielsen, C. H. *Anal. Bioanal. Chem.* **2009**, *395*, 697–718.
(3) Tien, H. T.; Ottova, A. L. *J. Membr. Sci.* **2001**, *189*, 83–117.
(4) Ottova, A.; Ti Tien, H. *Bioelectrochemistry* **2002**, *56*, 171–173.
(5) Sackmann, E. *Science* **1996**, *271*, 43–48.
(6) Tamm, L. K.; McConnell, H. M. *Biophys. J.* **1985**, *47*, 105–113.
(7) Kuhner, M.; Tampe, R.; Sackmann, E. *Biophys. J.* **1994**, *67*, 217–226.
(8) Ide, T.; Yanagida, T. *Biochem. Biophys. Res. Commun.* **1999**, *265*, 595–599.
(9) Costello, R. F.; Peterson, I. R.; Heptinstall, J.; Walton, D. J. *Biosens. Bioelectron.* **1999**, *14*, 265–271.
(10) Lin, J.; Szymanski, J.; Searson, P. C.; Hristova, K. *Langmuir* **2010**, *26*, 3544–3548.
(11) Wagner, M. L.; Tamm, L. K. *Biophys. J.* **2000**, *79*, 1400–1414.
(12) Drexler, J.; Steinem, C. *J. Phys. Chem. B* **2003**, *107*, 11245–11254.
(13) Schmitt, E. K.; Vrouenraets, M.; Steinem, C. *Biophys. J.* **2003**, *91*, 2163–2171.

(14) Simon, A.; Girard-Egrot, A.; Sauter, F.; Pudda, C.; D'Hahan, N. P.; Blum, L.; Chatelain, F.; Fuchs, A. *J. Colloid Interface Sci.* **2007**, *308*, 337–343.
(15) Mey, I.; Stephan, M.; Schmitt, E. K.; Muller, M. M.; Ben Amar, M.; Steinem, C.; Janshoff, A. *J. Am. Chem. Soc.* **2009**, *131*, 7031–7039.
(16) Jeon, T.-J.; Malmstadt, N.; Schmidt, J. J. *J. Am. Chem. Soc.* **2005**, *128*, 42–43.
(17) Ibragimova, S.; Stibius, K.; Szewczykowski, P.; Perry, M.; Bohr, H.; Hélix-Nielsen, C. *Polym. Adv. Technol.* DOI: 10.1002/pat.1850 (in press).
(18) Vogel, J.; Perry, M.; Hansen, J. S.; Bolinger, P.-Y.; Nielsen, C. H.; Geschke, O. *J. Micromech. Microeng.* **2009**, *19*, 025026.
(19) Hansen, J. S.; Perry, M.; Vogel, J.; Groth, J. S.; Vissing, T.; Larsen, M. S.; Geschke, O.; Emneus, J.; Bohr, H.; Nielsen, C. H. *Anal. Bioanal. Chem.* **2009**, *395*, 719–727.
(20) Hansen, J. S.; Perry, M.; Vogel, J.; Vissing, T.; Hansen, C. R.; Geschke, O.; Emneus, J.; Nielsen, C. H. *J. Micromech. Microeng.* **2009**, 025014.
(21) Winther-Jensen, B.; Norrman, K.; Kingshott, P.; West, K. *Plasma Processes Polym.* **2005**, *2*, 319–327.
(22) Perry, M.; Vissing, T.; Boesen, T. P.; Hansen, J. S.; Emneus, J.; Nielsen, C. H. *Bioinspir. Biomimetics* **2009**, *4*, 044001.
(23) Pinneau, I.; Koros, W. J. *J. Polym. Sci., Part B: Polym. Phys.* **1993**, *31*, 419–427.
(24) Roerdink Lander, M., Nielsen, C. H., Geschke, O. Manuscript in preparation.
(25) Zhang, L. F.; Spurlin, T. A.; Gewirth, A. A.; Granick, S. *J. Phys. Chem. B* **2006**, *110*, 33–35.
(26) Gurtovenko, A. A.; Parta, M.; Karttunen, M.; Vattulainen, I. *Biophys. J.* **2004**, *86*, 3461–3472.
(27) Benz, R.; Frölich, O.; Läuger, P.; Montal, M. *Biochim. Biophys. Acta* **1975**, *394*, 323–334.
(28) White, S. H. *Biophys. J.* **1978**, *23*, 337–347.
(29) Hemmler, R.; Bose, G.; Wagner, R.; Peters, R. *Biophys. J.* **2005**, *88*, 4000–4007.

Paper IV

Supported hybrid lipid-polymer membranes

Sania Ibragimova[1,3], Michelle Marincel[2], Manish Kumar[2], Thanh H. Nguyen[2],

Claus Hélix-Nielsen[1,3], Julie L. Zilles[2,]*

[1]DTU Physics, Technical University of Denmark, Fysikvej 309, Building 309, DK-2800 Kgs. Lyngby, Denmark

[2]Department of Civil and Environmental Engineering, University of Illinois at Urbana-Champaign, 205 North Mathews Avenue, Urbana, Illinois 61801

[3]Aquaporin A/S, Ole Maaløes Vej 3, DK-2200 Copenhagen N, Denmark

Received date:

Running Title: Supported hybrid lipid-polymer membranes

* To whom correspondence should be addressed. Mailing address: 3230C Newmark Civil Engineering Laboratory, MC250, 205 North Mathews Avenue, Urbana, IL 61801. Tel. +1-217-244-2925. Fax. +1-217-333-6968. E-mail. jzilles@illinois.edu

Abstract

Biomimetic membranes constructed of self-assembling triblock copolymers with a hydrophilic-hydrophobic-hydrophilic pattern show promise as model systems of biological membranes and for biosensor applications. Polymer membranes are typically more stable than lipid membranes and they can be easily modified to control membrane properties. For many biosensor applications a solid-supported polymeric membrane allowing insertion of functional transmembrane proteins is required. Previously it has been shown that functional transmembrane proteins can be incorporated in PMOXA-PDMS-PMOXA polymer vesicles, but these vesicles do not form a planar monolayer on a support. Here we tested how the rupture propensity of hybrid triblock copolymer- lipid vesicles could be tuned to create either vesicular or planar membranes on solid supports. Specifically we combined $PMOXA_{15}$-$PDMS_{110}$-$PMOXA_{15}$ triblock copolymer and zwitterionic or positively charged lipids at several ratios and demonstrated that planar supported membranes or immobilized vesicles could be formed on mica and quartz and that the type of membrane structure formed depends on the lipid/polymer ratio.

Keywords:

Biomimetic membranes, vesicles, bilayers, block copolymer, lipid, deposition, stability, permeability

Introduction

Lipid bilayers and biomimetic copolymer membranes are available for use both as model systems, for example to investigate membrane protein insertion[1] and activity[2, 3], and for applications, including screening platforms for drug discovery[4], biosensors[5, 6], and immunoassays[7]. While lipids have the advantage of being better understood and of being similar to the native environment for membrane proteins, copolymer membranes also have some advantages, particularly in the area of stability. For example, polyethyleneoxide-polyethylethylene (PEO-PEE) vesicles are 5-50 times tougher than lipid membranes[8] and exhibit greater thermal and temporal stability[9]. Another promising biomimetic membrane consists of a triblock hydrophilic-hydrophobic-hydrophilic copolymer (poly-(2-methyloxazoline)-polydimethylsiloxane-poly-(2-methyloxazoline) or PMOXA-PDMS-PMOXA). Functional incorporation of a variety of transmembrane proteins in PMOXA-PDMS-PMOXA triblock copolymers has been demonstrated[2, 3, 10-19]. There are also many possibilities for engineering block copolymer membranes to achieve the desired combination of properties, by adjusting parameters such as the block length, molecular weight, chemical composition, hydrophilic/hydrophobic balance and molecular architecture[20].

For many biosensor applications and analytical techniques it is desirable to produce planar, solid-supported membranes. Techniques for developing such membranes are more advanced for lipids. Planar lipid membranes can be made in the apertures of hydrophobic scaffolds either by painting solvent-containing black lipid membranes across the aperture[21], by folding solvent-free lipid monolayers across the aperture so that they are either free-standing[22] or by supporting them on a solid surface via a soft polymeric cushion[23-26]. Planar supported lipid membranes on a solid support can be made by Langmuir-Blodgett (vertical) or Langmuir-Schäfer (horizontal) transfer

from a water-air interface[27] or through vesicle collapse[28]. For vesicle collapse, the solid supports must be hydrophilic, and common support materials include silica[29-31] and freshly cleaved mica[32, 33]. Similar to the scaffolding method, vesicles can be collapsed either onto bare substrate or with a cushioning layer[34-37]. Common cushions include poly(ethylene glycol)[38] and polyelectrolytes[26, 39-42]. Various strategies are used for incorporation of membrane proteins into lipid membranes. Peptides can be directly inserted into free-standing lipid membranes from solution, some proteins can be added from solution with the aid of a suitable detergent, whereas other more bulky proteins can only be added by inserting them into proteoliposomes which are subsequently fused with the planar lipid membrane[1]. It is difficult to incorporate transmembrane proteins into the lipid bilayer with the Langmuir-Blodgett and Langmuir-Schäfer technique[43], because prior to transfer portions of the proteins within the monolayer are exposed to air and can become irreversibly denatured. Protein insertion into solid-supported lipid membranes is most commonly carried out by inserting the protein into proteoliposomes and collapsing them on the solid surface. A problem that arises is that the distance between the lipid membrane and the support is less than 2 nm[44] and the inserted protein which typically extends up to tens of nm from the membrane[44] hits the surface and becomes denatured. The distance from the membrane to the support can be increased by adding a spacer layer, such as a cushioning polymer layer.

Solid-supported, planar copolymer membranes have been made by vesicle deposition[45], by synthesis on a gold surface and subsequent detachment[46], and by Langmuir-Blodgett transfer[20]. We focus in the current work on vesicle deposition because it presents the fewest obstacles for incorporation of membrane proteins. However, the high rupture strength of these triblock copolymer vesicles presents some difficulty for this method. Previous work used a charged copolymer to facilitate adsorption[45]. In this work, we investigated the possibility of using mixed lipid-copolymer vesicles to facilitate formation of a planar membrane. The occurrence of mixed

vesicles has been documented[47, 48], but to our knowledge the deposition and rupture properties of such vesicles have not been reported before.

We synthesized vesicles with different ratios of $PMOXA_{15}$-$PDMS_{110}$-$PMOXA_{15}$ copolymer to zwitterionic or positively charged lipids and investigated the deposition and rupture of these vesicles on quartz and mica. We characterized the mixed polymer/lipid vesicles by transmission electron microscopy (TEM), dynamic light scattering (DLS) and osmotic shock stopped-flow measurements, and investigated their deposition behavior with quartz crystal microbalance with dissipation (QCM-D) and atomic force microscopy (AFM). These mixed lipid-polymer vesicles show promise for formation of robust membranes and can be designed either for tethering of vesicles or formation of planar, solid-supported membranes.

Materials and methods

Materials. $PMOXA_{15}$-$PDMS_{110}$-$PMOXA_{15}$ was a kind gift from Dr. Wolfgang Meier at the University of Basel, Switzerland. 1-palmitoyl-2-oleoyl-*sn*-glycero-3-phosphocholine (POPC, 25 mg/ml in chloroform) and 1,2-dioleoyl-3-trimethylammonium-propane (DOTAP, 10 mg/ml in chloroform) were purchased from Avanti Polar Lipids (Alabaster, USA). Dodecyl maltoside detergent sol grade was purchased from Anatrace (Santa Clara, USA). Sodium azide and chloroform were purchased from Sigma (St Louis, USA).

Vesicle preparation. Mixed lipid-polymer vesicles were prepared by dissolving $PMOXA_{15}$-$PDMS_{110}$-$PMOXA_{15}$ ABA polymer in chloroform (2 ml) and adding POPC or DOTAP in the specified molar ratios (0, 33, 67, 89, 100% lipid) and using a film rehydration technique[19]. A thin lipid-polymer film was formed by evaporating the solvent in a round-bottomed flask using a rotary vacuum evaporator (vacuum <110 mbar) at room temperature. Trace chloroform was removed under a high vacuum (<2.5 mbar) for 1- 2 hours before the dried lipid polymer film was rehydrated with 2.8 mM PBS (8 $g.L^{-1}$ NaCl, 0.2 $g.L^{-1}$ KCl, 0.144 $g.L^{-1}$ Na_2HPO_4, 2.4 $g.L^{-1}$ KH_2PO_4, pH 7.2) containing 0.04% dodecyl maltoside and 0.13% sodium azide to a final lipid-polymer concentration of 6 mg/ml. The films were sonicated to ensure that the polymer lifted off from the bottom of the flask. The films were rehydrated at 4° C under continuous rotational stirring for 24 hours. The resulting multilamellar vesicles were extruded using a pneumatic thermobarrel extruder (Northern Lipids, Burnaby, Canada) through 0.6 μm and 0.2 μm track-etched Isopore™ membranes (Millipore, Billerica, MA, USA) 5 and 11 times respectively. The vesicles were purified by size-exclusion with a Superdex 200 pressurized column (GE

Healthcare, Piscataway, NJ, USA) using an Äkta prime plus instrument (GE Healthcare, Piscataway, NJ, USA). The fraction corresponding to the vesicles was collected after 10 minutes.

Vesicle characterization. The hydrodynamic diameter and zeta potential of the vesicle preparations were determined using dynamic light scattering and electrophoretic light scattering, respectively, on a 4W Zetasizer Nano-ZS90 (Malvern Instruments, Malvern, UK) with a He-Ne standard laser, wavelength 632.8 nm and 90° scattering angle. Three 10-measurement series were taken for each preparation and averaged. The refractive index for the vesicles was set as 1.48[49]. Zeta potential measurements were carried out at 25°C with an equilibration time of 2 minutes and signal processing used M3-PALS (second generation Phase Analysis Light Scattering) to measure the particle electrophoretic mobility. Zeta potential was calculated using a built-in monomodal analysis model assuming the Smoluchowski approximation and a dispersant viscosity of 0.8872 cP.

In preparation for transmission electron microscopy, thin film holey carbon grids (Ted Pella, Redding, CA, USA) were glow-discharged with a Denton DPG-1 glow-discharge system (Denton Vacuum Inc., Moorestown, NJ, USA) at a glow current of 200 mA for 2 minutes to make them hydrophilic. Vesicle samples were allowed to adsorb on the grid surface for 2 minutes, stained with 1% uranyl acetate (SPI, West Chester, PA, USA) for 30 seconds, and air-dried. Vesicles were viewed with a 2100 Cryo transmission electron microscope (JEOL, Tokyo, Japan) at 200 kV.

Vesicle permeability determination. Vesicle permeability to water was determined using an SX.18MV-R stopped-flow spectrometer (Applied Photophysics, Surrey, UK) with light scattering[19, 50]. The vesicles were subjected to a hyperosmotic shock by mixing them with an

equal volume of 1 M NaCl PBS pH 7.2. The change in vesicle size with water efflux was monitored by light scattering at 600 nm. Six or more light scattering curves per sample were averaged and fitted using an exponential rise equation in Origin (version 8.1) to obtain the exponential rise rate constant, *k*. Water permeability was calculated using

$$P_f = k / \left\lfloor S / V_0 \cdot V_w \cdot \Delta_{osm} \right\rfloor \quad (1.1)$$

where S/V_o is the initial vesicle surface area to volume ratio, V_w the molar volume of water (18 cm^3/mol), and Δ_{osm} is the difference in osmolarity (1 osmol/L) driving the shrinkage of the vesicles. The hydrodynamic radius of the vesicles was derived from dynamic light scattering data.

Quartz crystal microbalance with dissipation monitoring. We used a QCM-D300 system and polished AT-cut, 5 MHz quartz crystals (Q-Sense AB, Gothenburg, Sweden) to measure deposition kinetics of vesicles on a bare silica surface, using the software Q-Soft for data collection. The application of the QCM-D technique for determining deposition kinetics is described in Rodahl et al[51]. Briefly, the QCM-D technique monitors the change in frequency of vibration due to deposition of wet mass on the quartz crystal sensor. As wet mass deposits onto the quartz sensor, the frequency of vibration decreases. During ideal conditions, there is a linear relationship between the change in frequency Δf and the mass coverage (in ng/cm^2) Δm. The mass coverage can be calculated with the Sauerbrey equation:

$$\Delta m = \frac{c}{n} \Delta f \quad (1.2)$$

where *c* (=17.7 ng cm^{-2} Hz^{-1} at *f*=5 MHz) is the mass-sensitivity constant and *n* (=1, 3, ...) is the overtone number. Combined frequency and energy dissipation measurements give

information about both the adsorbed amount (Δf) and the viscoelastic properties (ΔD) of the adsorbed film.

The fractional bilayer coverage was calculated as previously described by Graneli et al[29] based on two assumptions: (i) The water-exposed domains on a planar SPB do not contribute significantly to D. (ii) There exists a linear relationship between the dissipation change at saturation and liposome size, as previously demonstrated for pure PC liposomes in the size regime between 25 and 200 nm. The fractional bilayer coverage, α, and fractional coverage of intact liposomes, 1 - α, are estimated using

$$\alpha = 1 - \Delta D_{fin} / \Delta D_{sat}$$
$$\Delta D_{sat} = x\Theta \qquad (1.3)$$

where ΔD_{sat} is the dissipation value expected when α=0, i.e., for the whole surface covered by intact liposomes, ΔD_{fin} is the actual measured change in D at saturation, Θ is the liposome diameter (Table 1) in nanometers, and x=0.15 is the proportionality constant between the change in D for nonruptured liposomes on TiO_2[31] and the liposome diameter (change in D/nm of liposome diameter).

The thickness of the adsorbed film was obtained using a built-in Voigt model in the software Q-tools. In this model the adsorbed film is represented by a homogeneous thickness, viscosity, and complex shear modulus. All data shown was measured at the third harmonic, n= 3, i.e., at 15 MHz. For clarity, the frequency response is divided by 3 in all graphs (this makes the data directly comparable to data measured at n = 1, for ideal conditions).

Before each experiment, the silica sensors were soaked in 2% Hellmanex II (Hellma GmbH & Co. KG, Müllheim, Germany) cleaning solution for 30 min, rinsed thoroughly with DI water, dried with ultra high-purity N_2, and treated in an ozone/UV chamber (BioForce Nanosciences

Inc., Ames, IA) for 30 min. To ensure that the silica surface was maintained, we discarded the sensor after seven uses. All test solutions were fed into the chamber using a syringe and adsorption was measured in stagnant conditions. For each experiment, the silica sensor frequency and dissipation in air and in double distilled water were measured as a quality control of the sensor. A baseline was obtained in PBS buffer pH adjusted to 7.2, with the frequency signals stabilized at an approximately 2 Hz change in frequency over 10 min. 1 ml of vesicles were injected and allowed to deposit on the silica sensor until the frequency signal stabilized at an approximately 2 Hz change in frequency over 10 min. More vesicles were injected until no further increase in frequency was observed. PBS buffer was thereafter added to remove any unadsorbed vesicles. Then 1 ml of 5 mM $CaCl_2$ was injected and the signal was monitored for 10 minutes. Then the system was allowed to equilibrate with PBS buffer again. Each experiment was repeated at least two times.

Atomic force microscopy. Visualization of the deposited mixed vesicles on the hydrophilic surface of mica (SPI Supplies Division of Structure Probe, Inc., West Chester, PA) was determined with an MFP-3D atomic force microscope (Asylum Research, Santa Barbara, CA, USA) in tapping mode in air with a Si cantilever with aluminum reflex coating (Tap300Al, Budget Sensors, Sofia, Bulgaria) at room temperature. The length of the cantilever was 125 μm, the resonant frequency 300 kHz, and the force constant 40 N/m. 20 μl of vesicle solution was incubated on a freshly cleaved mica surface for 2 minutes, rinsed with 1 ml DI water, blotted with a kimwipe at the edge of the mica, and allowed to dry for 10 minutes. Vesicle adsorption time was reduced to 2 minutes to obtain bilayer patches rather than a flat continuous bilayer formation.

Results and discussion

Large scale flat polymer membranes with incorporated proteins are desirable for some applications. So far these have not been made, because the methods for making the polymer membranes flat preclude incorporation of functional, correctly folded transmembrane proteins. Recently, functional incorporation of a variety of transmembrane proteins in PMOXA-PDMS-PMOXA triblock copolymer vesicles has been demonstrated ([2, 3, 10-19]). However these block copolymer vesicles have a high rupture strength and do not readily form a planar monolayer on a support surface by vesicle rupture[8]. Mixing triblock copolymers with lipids may improve vesicle rupture, a strategy which is promising in terms of transmembrane protein functionality. Some studies have shown that it is possible to make mixed lipid/block copolymer vesicles[47, 48]. In this work, we combine triblock PMOXA-PDMS-PMOXA copolymers and lipids and demonstrate that we can form mixed vesicles and characterize their size, charge and permeability properties. Then we address whether addition of lipids improved vesicle deposition and rupture properties and allowed us to form planar membranes or tethered vesicular membranes on two hydrophilic supports – quartz and mica. We show how the type and concentration of lipid added to the triblock copolymer can be used to tailor whether the planar membrane configuration, the tethered vesicular configuration or a tethered vesicular configuration that can be triggered to form a planar membrane is achieved.

Vesicle systems investigated

Unilamellar vesicle populations were prepared from poly-(2-methyloxazoline)$_{15}$-poly-(dimethylsiloxane)$_{110}$-poly-(2-methyloxazoline)$_{15}$ (**ABA**) polymer, 1-palmitoyl-2-oleoyl-*sn*-glycero-3-phosphocholine (**POPC**) lipids, 1,2-dioleoyl-3-trimethylammonium-propane

(**DOTAP**) lipids as well as from mixtures of POPC:ABA and DOTAP:ABA. A POPC lipid has a zwitterionic headgroup, whereas a DOTAP lipid has a positively charged headgroup. POPC and DOTAP lipids were selected to compare the effect of using a charged or a zwitterionic lipid in the mixed vesicles. Vesicles with the following compositions were prepared: POPC, 89 mol% POPC: 11 mol% ABA, 67 mol% POPC:33 mol% ABA, 33 mol% POPC:67 mol% ABA, DOTAP, 89 mol% DOTAP:11 mol% ABA, 67 mol% DOTAP:33 mol% ABA, 33 mol% DOTAP:67 mol% ABA and ABA.

Characterization of vesicles and proof of lipid-polymer mixing

To take advantage of the properties of both lipids and polymers, the two materials need to be present in the same membrane. All vesicles were characterized by transmission electron microscopy (TEM), dynamic light scattering (DLS), electrophoretic light scattering (ELS) and osmotic shock stopped-flow measurements to address lipid-polymer mixing.

Visual examination of vesicles. In TEM, POPC (fig. 1a) liposomes adsorbed to the hydrophilic grid and did not resist dehydration in TEM, leading to collapsed structures in vacuum. DOTAP (fig. 1b) liposomes were difficult to find on the hydrophilic grid. ABA vesicles (fig. 1c) formed spherical particles which did not shrivel. All ABA/POPC mixtures resulted in the formation of spheres similar to those obtained for ABA alone and did not give rise to two distinct populations of vesicles (fig. 1d). ABA/DOTAP mixtures also formed a single population of spherical vesicles (fig. 1f), with the exception of 89 mol%DOTAP:11 mol% ABA (fig. 1e), which resulted in fused structures.

Vesicle size and charge. DLS measurements showed that POPC, DOTAP and ABA vesicles had an average hydrodynamic diameter of 159 nm, 160 nm and 198 nm respectively (table 1)

and that the ABA/lipid mixtures ranged from 105 nm to 217 nm. Table 1 shows that each ABA/lipid mixture gives rise to a monomodal vesicle population.

ELS measurements showed that vesicles composed of DOTAP, a positively charged lipid, had a zeta potential of +36 mV and vesicles made up of POPC, a zwitterionic lipid, had a zeta potential of ca 0 mV. Addition of ABA to DOTAP lipid resulted in a drastic reduction of zeta potential.

Three lines of evidence suggest that mixed lipid-polymer vesicles were formed in the current work. First, DLS showed that we have a uniformly sized vesicle population and second TEM was consistent with this showing that the vesicle population was visually uniform. Thirdly, even more compelling evidence of mixing for DOTAP-containing mixed vesicles was that the zetapotential of DOTAP was screened in the presence of ABA, which means that the ABA and DOTAP molecules must reside within the same vesicle. Thus TEM, DLS and ELS results are consistent in that hybrid vesicles are formed when using a mixture of ABA and lipids. These results are also consistent with a study in Wolfgang Meier's group[48], which showed that it is possible to make mixed PMOXA-PDMS-PMOXA/egg-PC/egg-PE vesicles and that the mixing is homogeneous on a molecular scale. We have not addressed whether PMOXA-PDMS-PMOXA/POPC and PMOXA-PDMS-PMOXA/DOTAP mix homogeneously or whether they separate to make patches (fig. 2). Another question that remains is whether ABA spans the membrane fully or only inserts partially (fig. 2) and how the ABA insertion is affected by the polymer to lipid ratio.

Vesicle permeability and strength. Since the ABA block copolymer has a larger hydrophobic thickness than a lipid membrane, we wanted to see how the presence of a hydrophobically thicker ABA affected the water permeability of the vesicular membrane and whether the mixed

vesicles could withstand osmotic pressure better than lipid vesicles. This also provides insight into how the ABA inserts into the membrane. We investigated the vesicles' water permeability, P_f, with stopped flow measurements and found that mixed vesicles are more impermeable to water than pure lipid vesicles (fig. 3 and table 4). DOTAP vesicles had a P_f of 13.2 μm/s, which compares well to P_f(E.Coli total lipid extract)=15 μm/s at 6.5°C reported by Agre[50]. Zwitterionic POPC vesicles had a higher P_f of 22.6 μm/s at 10°C. This value deviates greatly from what is reported for POPC in the literature (P_f=72±18 μm/s[52]), but could be because this value is obtained by another method (fluorescence quenching). A polymer content of 11 mol% ABA in the mixed vesicles reduced the water permeability threefold compared to pure POPC vesicles and by a third compared to pure DOTAP vesicles. A molar content of polymer exceeding 33% makes vesicles very water impermeable, such that a normalized light scattering could not be fit to an exponential function and it was not possible to obtain a P_f value. Water permeability of ABA vesicles measured with a more sensitive apparatus has been reported to be 0.8 μm/s[19], significantly lower than the water permeability of pure lipid membranes. The decrease in water permeability with an increased ABA content suggests that the vesicular membrane becomes thicker, which may be due to a progressive change from partial ABA insertion into the membrane to ABA fully spanning the membrane. Increasing polymer content provides the mixed vesicles with an impassive barrier, an attractive property for vesicles used as drug delivery vehicles.

The strength of the ABA-containing vesicles is also demonstrated in TEM and stopped flow experiments. The TEM images show that lipid vesicles shrivel in vacuum, whereas ABA vesicles are more robust and maintain their spherical shape. Mixed lipid/polymer vesicles, similarly to ABA vesicles, do not rupture in vacuum (except 89 mol% DOTAP:11 mol% ABA), which shows that they gain stability from the addition of ABA polymer.

In stopped flow measurements the vesicles were exposed to a hypertonic solution, which created a nominal osmotic pressure of 23 bars across the vesicle membrane. This osmotic pressure makes internal vesicle water efflux through the vesicle membrane by osmosis and results in shrinkage of the vesicles. Pure lipid vesicles experienced a detectable change in size, and had a measurable water permeability. 89 mol% lipid:11 mol% ABA vesicles had a lower water permeability than pure lipid vesicles, which means that they were less sensitive to the osmotic pressure. At ABA content of 33 mol% or more, we could not see a change in vesicle size at 23 bars osmotic pressure, which means that the vesicles could better withstand this pressure. Increasing polymer content provides the mixed vesicles with an ability to withstand higher osmotic pressure.

Vesicle deposition and rupture on quartz and mica

Having proved that lipids and polymers can be mixed in the same vesicles, we investigated whether their deposition and rupture properties on a solid hydrophilic support were changed and could be tailored by varying the mixing ratio.

The deposition kinetics of lipid, polymer and mixed lipid/polymer vesicles on a quartz support were studied with QCM-D, where a decrease in resonance frequency corresponds to an increase in bound mass and an increase in dissipation indicates an increase in the softness of the bound film. QCM-D shows both the adsorption kinetics of vesicles on a quartz substrate and can be used to lean about the layer formed when the adsorption reaches equilibrium.

Adsorption kinetics of vesicles on quartz. Pure lipid vesicles differed significantly in adsorption kinetics on quartz depending on the choice of lipid. Adsorption of pure POPC vesicles onto silica (fig. 4b Δ) is a two-phase process. In the first phase the frequency decreases

monotonically and the dissipation increases monotonically until they reach an extreme at Δf=-56 Hz and ΔD=5.9·10^{-6}, and in the second phase the frequency increases again and the dissipation decreases until they reach equilibrium at Δf=-36 Hz and ΔD=1.8·10^{-6}. This behavior is similar to a response previously reported for adsorption of egg-PC vesicles on silica by Keller and Kasemo[53], and is interpreted as follows: in the initial phase vesicles adsorb onto the surface up to a critical surface coverage and in the second phase the vesicles rupture and form a continuous supported lipid bilayer.

Adsorption of pure DOTAP vesicles onto silica (fig. 4c Δ) is a one-phase process. Upon adsorption, the frequency decreases to an equilibrium of Δf=-30 Hz and the dissipation increases up to ΔD=3.6·10^{-6}. This adsorption behavior was interpreted by Richter et al[28] as immediate onset of bilayer formation at low vesicular surface coverage.

ABA vesicles adsorbed on quartz in a one-phase process (fig. 4a), with an equilibrium of Δf=-42 Hz and ΔD=11.8·10^{-6}. Although the equilibrium Δf for ABA is similar to that for pure lipid vesicles indicating that a similar bound mass is obtained, the ΔD for ABA vesicles is much larger, indicating that it forms a softer layer. That the layer is soft is indicative of that the layer contains a lot of water, typical of vesicles.

POPC:ABA mixed vesicles (fig. 4b) adsorbed on quartz in a one-phase process with -300 Hz<Δf<-138 Hz and 24·10^{-6}<ΔD<49·10^{-6}. The Δf is tenfold higher for mixed POPC:ABA vesicles than for pure POPC or pure ABA vesicles, which corresponds to a tenfold higher mass coverage. The high ΔD values are indicative of an adsorbed vesicular layer.

89 mol% DOTAP:11 mol% ABA (fig. 4c □) had a similar adsorption behavior to DOTAP vesicles, reaching a low Δf=-70 Hz and ΔD=5.7·10^{-6}. 67 mol% DOTAP:33 mol% ABA (fig. 4c ◊) and 33 mol% DOTAP:67 mol% ABA (fig. 4c ○) had a similar adsorption behavior to

POPC:ABA vesicles with a high $|\Delta f|$ and a high ΔD, reaching Δf=-115 Hz and Δf=-120 Hz respectively.

Biomimetic membrane formed on quartz (scenario I-III). When vesicle adsorption reached equilibrium and steady frequency and dissipation values were reached, we calculated the mass coverage, the fractional bilayer coverage, the degree to which the vesicles were deformed and the thickness of the adsorbed layer as described in methods (table 2). Since the mass coverage values, $m_{bilayer}$, expected for a fully ruptured membrane are similar (table 2), the large observed differences in mass coverage are attributed to a difference in water content inside the vesicles. While the mass coverage quantifies the amount of water in the adsorbed layer, the fractional bilayer coverage, α, tells what percentage of vesicles rupture on the quartz surface. The ratio $\Delta D_{fin}/\Delta f_{fin}$ can be used as a measure of vesicle deformation. A high ratio corresponds to a low degree of deformation (spherical vesicles) and a low ratio to a high degree of deformation (much flatted vesicles or bilayer). The film thickness was obtained from the QCM-D data using a Voigt model.

We found that we could obtain three scenarios depending on the type and amount of lipid added (see fig. 6). In scenario I, vesicles adsorbed to the quartz substrate and ruptured to form a planar biomimetic membrane. In scenario II vesicles adsorbed until the quartz surface was saturated, but did not rupture even upon addition of the fusogen calcium and finally in scenario III, vesicles adsorbed until the quartz surface was saturated with vesicles and could be made to rupture by adding calcium.

Scenario I

In scenario I, vesicles adsorbed to the quartz substrate and ruptured to form a planar supported biomimetic membrane. Vesicle compositions that were found to follow this scenario were pure lipid vesicles (POPC and DOTAP) and mixed DOTAP:ABA vesicles consisting of predominantly DOTAP (89 mol% DOTAP:11 mol% ABA and 67 mol% DOTAP:33 mol% ABA). The evidence that indicates that these vesicles follow scenario I is based on the mass coverage of the membrane, the fractional bilayer coverage, the degree of vesicle deformation as well as the thickness of the membrane.

POPC vesicles adsorbed on quartz up to a mass coverage of 982 ng/cm^2 and in the second phase experienced a loss of mass coverage down to 637 ng/cm^2. The decrease in mass coverage is attributed to rupture of the POPC vesicles at a critical coverage and release of the intervesicular water. The mass coverage did not decrease to the mass coverage expected for a bilayer, 388 ng/cm^2, which means that not all POPC vesicles ruptured and released their intervesicular water. The deformation ratios for POPC vesicles were higher than what is expected for POPC bilayers[28], which is consistent that complete bilayer coverage was not obtained. The mean thickness of the adsorbed POPC film was 9 nm, which is higher than expected[54], and is due to the presence of a few nonruptured POPC vesicles. The fractional bilayer coverage was calculated to quantify what area percentage of the quartz sensor was covered with lipid bilayer, and this was found to be 93%, which means that only 7% of the sensor area is occupied by POPC vesicles. QCM-D showed that POPC vesicles adsorbed and ruptured on quartz to make supported lipid bilayers, which is consistent with previous studies[53].

DOTAP vesicles adsorbed on quartz with a low mass coverage and no change in mass coverage was observed. This is interpreted as immediate onset of DOTAP vesicle rupture upon adsorption to the quartz surface together with release of intervesicular water. The deformation

ratios for DOTAP vesicles are higher than what is expected for DOTAP bilayers[28], which is consistent that complete bilayer coverage was not obtained. DOTAP vesicles directly adsorb on quartz as films with a thickness of 7 nm. The fractional bilayer coverage values showed that 86% of the sensor area is occupied by DOTAP lipid bilayer and 14% by DOTAP vesicles. QCM-D showed that DOTAP vesicles adsorbed and ruptured on quartz to make supported lipid bilayers, which is consistent with previous studies[28].

89 mol% DOTAP:11 mol% ABA vesicles had a higher mass coverage than pure DOTAP vesicles, and no decrease in mass coverage was observed, which is interpreted as immediate onset of vesicle rupture upon adsorption to the quartz surface. The adsorbed film had a mean thickness of 14 nm, which is attributed in part to the presence of a small percentage of vesicles and in part to an increase in thickness due to the presence of ABA polymer in the membrane. The fractional bilayer coverage values showed that 79% of the sensor area is occupied by DOTAP lipid bilayer: ABA monolayer/bilayer and 21% by vesicles.

67 mol% DOTAP:33 mol% ABA vesicles had a high mass coverage, which means that they had a high water content. The film thickness was 66 nm, which indicates that vesicles are flattened on the surface, which is consistent with the deformation ratio. The fractional bilayer coverage value shows that a small portion, 17%, of the sensor area is covered by DOTAP lipid bilayer: ABA monolayer/bilayer and 83% by flattened vesicles.

Scenario II

In scenario II vesicles adsorbed until the quartz surface was saturated, but did not rupture even upon addition of the fusogen calcium. Vesicle compositions that were found to follow this

scenario were pure polymer vesicles and mixed lipid:ABA vesicles consisting of predominantly ABA (33 mol% DOTAP:67 mol% ABA and 33 mol% POPC:67 mol% ABA).

Pure polymer vesicles adsorbed as a soft (high $\Delta D_{fin}/\Delta f_{fin}$) layer with a low mass coverage (734 ng/cm^2) on quartz. The ABA film had a thickness of 81 nm, which together with the deformation ratio indicates that ABA vesicles adsorb and are flattened on the surface (DLS indicated that the vesicles have a hydrodynamic diameter of 198 nm). Interestingly, these are more flattened than vesicles containing 67 mol% ABA. We attribute the low mass coverage to steric repulsion of the polymer chains, which cause the polymer vesicles to pack less efficiently than the lipid-containing vesicles. Addition of calcium had no effect on the adsorbed ABA vesicles.

33 mol% POPC:67 mol% ABA vesicles had a high mass coverage (5310 ng/cm^2) indicating a large water content in the adsorbed layer. The deformation ratio for this composition is highest of all the POPC-containing vesicles, which means that these vesicles are the least flattened on the surface, which is consistent with the film thickness (t_{min} =104 nm). The fractional bilayer coverage value indicates that the adsorbed film consists entirely of unruptured vesicles. Addition of calcium had no effect.

33 mol% DOTAP:67 mol% ABA had a high mass coverage (2115 ng/cm^2), which means that they had a high water content. The deformation ratio for these vesicles was highest of those for the DOTAP-containing vesicles, i.e. these vesicles were least flattened on quartz. This is consistent with the film thickness (101 nm). The fractional bilayer coverage value indicates that the adsorbed film consists entirely of unruptured vesicles. Addition of calcium had no effect, which is in agreement with a finding by Richter et al[28] that calcium only enhances the tendency of supported lipid bilayer formation for negatively charged and zwitterionic vesicles.

Scenario III

In scenario III, vesicles adsorbed until the quartz surface was saturated with vesicles and could be made to rupture by adding calcium. Calcium is a fusogen that promotes fusion of lipid membranes[28]. Vesicle compositions that were found to follow this scenario were mixed POPC:ABA vesicles consisting of predominantly POPC (89 mol% POPC:11 mol% ABA and 67 mol% POPC:33 mol% ABA).

We found that 89 mol% POPC:11 mol% ABA vesicles had a high mass coverage (2437 ng/cm^2) and adsorbed as flattened vesicles (t_{max}=33 nm) on quartz. Addition of calcium to the adsorbed vesicles reduced the thickness to 16 nm and the mass coverage to 979 ng/cm^2, which shows together with the fractional bilayer coverage, that the vesicles ruptured to provide an area coverage of 66% POPC lipid bilayer: ABA monolayer/bilayer and 34% flattened vesicles.

We found that 67 mol% POPC:33 mol% ABA had a high mass coverage (3334 ng/cm^2) and adsorbed as flattened vesicles (t_{max}= 49 nm). Addition of calcium to the adsorbed vesicles reduced the thickness slightly to 47 nm and the mass coverage to 3074 ng/cm^2, which shows together with the fractional bilayer coverage, that the vesicles ruptured to provide an area coverage of 38% POPC lipid bilayer: ABA monolayer/bilayer and 62% flattened vesicles.

We show that for mixed POPC:ABA vesicles with a low ABA content (<33 mol%), the ABA polymer confers stability to the mixed POPC/ABA vesicles, while making it possible to form a supported bilayer by adding calcium to the adsorbed vesicle layer. The user gains the advantage of having strong unruptured vesicles, which can be induced to rupture and form a supported planar membrane when desired.

Effect of the polymer:lipid ratio on mixed vesicle deposition and rupture on quartz. The progressive change in adsorption properties as the molar ratio of lipid in the vesicles is

decreased, is indicative of both that mixing of lipid and polymer is taking place and that different ratios of lipid to polymer can be obtained in the vesicles. Mixed lipid/ABA vesicles reached a considerably higher mass coverage than pure ABA vesicles, which indicates that adding as little as 33 mol% lipid helps vesicles to adsorb onto the silica surface. Increasing the lipid content of the mixed vesicles decreases the mass coverage, decreases the film thickness and increases the fractional bilayer coverage. This indicates that increasing the lipid content leads to progressively increased flattening of the mixed vesicles on the silica surface until the vesicles reach a transition from scenario II rupture behavior to scenario I where they spontaneously rupture (for DOTAP-containing vesicles) or scenario III where they can be induced to rupture by adding calcium (for POPC-containing vesicles). This also means that a decrease in polymer content has the same effect, and proves that the polymer makes the vesicles more stable from rupture.

Biomimetic membrane formed on mica. Although QCM-D provides a thickness value for the film, it is an averaged value and does not provide information about how the layer thickness is spatially distributed. Such information was obtained by atomic force microscopy. For AFM we switched to using a mica substrate, which was selected over silica due to its flatness. Both mica and silica are hydrophilic, but supported bilayer formation on the two surfaces has been reported to differ[33]. We use mica to assess the effect of lipid concentration in the mixed vesicles which followed scenario I or III (i.e. which ruptured on quartz) on vesicle rupture/stability and to visually study the effect of calcium on POPC-containing vesicles.

We found that ABA vesicles adsorb as vesicles on mica (fig. 5a), just as on silica. POPC vesicles ruptured on mica to make bilayer patches (fig. 5b) with a mean thickness of 3.2 nm (table 3). On mica 89 mol% POPC:11 mol% ABA vesicles rupture (fig. 5d) to make bilayer patches with a mean thickness of 5 nm (table 3). 67 mol% POPC:33 mol% ABA vesicles do not

rupture on mica (fig. 5e), vesicles are observed with a mean thickness of 26.6 nm and a broad thickness distribution (table 3). Addition of calcium to 67 mol% POPC:33 mol% ABA results in formation of structures with a mean thickness of 19.4 nm (fig. 5h, table 3). Adding calcium to 89 mol% POPC:11 mol% ABA might result in formation of a continuous bilayer, since we can only see small irregular structures which we believe are small contaminants and because addition of calcium caused rupture of 67 mol%POPC:33 mol% ABA, which contains more polymer and is expected to be tougher.

DOTAP (fig. 5c) and 89 mol% DOTAP:11 mol% ABA (fig. 5f) either make a perfect continuous bilayer on the surface (where the observed structures are junk), or very small collapsed structures. A control image of only PBS, without any vesicles (fig. 5i) shows small structures, which are broadly scattered in height and are therefore assumed to be junk. This is reminiscent of what the DOTAP-containing vesicle images looked like. Therefore, we are inclined to believe that the images show a continuous bilayer with small contaminating particles on top.

The mixed vesicles have similar rupture behavior on mica as they did on silica. Calcium was shown to induce vesicle rupture of POPC-containing vesicles as on silica. An increased lipid content in the mixed vesicles resulted in a decrease in the thickness of the ruptured layer.

Mechanism of deposition

We show that the ABA content of the mixed vesicles determines whether they will deposit on the quartz substrate by scenario I or II. The transition from rupture to stability occurs at 11-33 mol% ABA for DOTAP:ABA vesicles and at <11 mol% ABA for POPC:ABA vesicles. Although it seems surprising that such a low molar percentage of ABA can cause such a

significant difference in vesicle stability, it actually seems reasonable when one considers the lipid to polymer area ratio. If one ABA polymer molecule has a surface area of 4 nm^2[2,55] and one lipid has a head group area of 0.6 nm^2, then 11 mol% polymer corresponds to 62% of the surface area. 33 mol% corresponds to 87% of the vesicle surface area. At such a high relative surface area, it seems intuitive that the polymer properties take over the behavior of the vesicle.

The ABA polymer clearly confers stability to the vesicles, although the exact mechanism is not known. We propose several possible mechanisms of action. Firstly, ABA chains may physically shield the POPC lipids due to the large headgroup size of the PMOXA, preventing vesicles from coming close together by steric repulsion, which would decrease the strength of vesicle-vesicle interactions. Secondly, in mixed DOTAP/ABA vesicles, ABA screens DOTAP charge. This would reduce the electrostatic attraction of DOTAP to the quartz and mica surfaces, reducing vesicle-surface interactions and thereby vesicle stability. Thirdly, ABA increases the hydrophobic thickness of the membrane. The ABA has a hydrophobic thickness of 10 nm[48], whereas a lipid membrane has a hydrophobic thickness of 3 nm[54]. The increased membrane thickness should also increase vesicle stability. Also the ABA polymer consists of one piece which may span the entire membrane, whereas two lipids make up a bilayer and they are not covalently joined. This should make the membrane more rigid and provide it with stability from mechanical stress as has been shown for bolalipids, lipids which span the entire membrane[56, 57]. Lastly, the ABA polymer has the intrinsic polymer ability to be stretched, whereas lipid membranes cannot be stretched beyond 5% of their original area without rupture under osmotic or other stresses[58].

The polymer stabilizes vesicles by diminishing vesicle-vesicle and vesicle-support interactions. The choice of solid support influences the strength of vesicle-support interactions and thereby the vesicle rupture and stability behavior. We used two hydrophilic supports: mica and quartz.

Freshly cleaved mica has a high density of negative surface charges, whereas silicon oxide is only weakly anionic[45]. We observed that 89 mol% POPC:11 mol% ABA vesicles ruptured readily on mica, but not on quartz, which indicates that mica has stronger interactions with the vesicles than quartz does. Calcium induced vesicle rupture on both quartz and mica. By comparing the thicknesses obtained on quartz by QCM-D and on mica by AFM, we found that POPC and POPC/ABA mixed vesicles were more flattened on mica than on quartz. This result is consistent with our hypothesis that mica has stronger interactions than quartz with the vesicles. Interestingly, ABA vesicles were actually more flattened on quartz than on mica, which suggests that the stronger mica-vesicle interactions of mixed vesicles are due to the presence of lipid in the vesicles.

Another parameter which can change vesicular deposition behavior is the choice of lipid. We have compared zwitterionic POPC lipids to positively charged DOTAP lipids. Both types of lipids were able to make mixed vesicles with ABA and both experienced stabilization by ABA. However, TEM and QCM-D results showed that ABA stabilizes POPC-containing vesicles better than it stabilizes DOTAP-containing vesicles. The mechanism of rupture for DOTAP-containing and POPC-containing vesicles on quartz was also found to be different: POPC-containing vesicles adsorbed up to a critical coverage on quartz and then ruptured to form planar layers, whereas DOTAP-containing vesicles ruptured immediately upon reaching the surface. This indicates that DOTAP has stronger interactions with the negatively charged surfaces (quartz and mica) studied. This seems reasonable as DOTAP has a positively charged headgroup and will experience stronger electrostatic attraction to the negatively charged surfaces. By using a low concentration of vesicles containing a positively charged lipid we can form separate bilayer patches and by selecting vesicles with zwitterionic lipids we can obtain defect-free continuous

planar membranes. Another difference between using DOTAP or POPC was that calcium had no effect on DOTAP-containing vesicles, but helped to rupture POPC-containing vesicles. The results obtained for mixed lipid/ABA vesicles are consistent with results reported by Richter et al[28, 33] for pure DOTAP or POPC vesicles.

We have shown that it is possible to make mixed lipid/polymer vesicles and show preparation of solid-supported mixed membranes. These systems should be well suited for incorporation of functional transmembrane proteins as lipids have the fluidity of biological membranes and the triblock copolymers provide a spacer that prevents the protein from being squashed down on the surface and denatured. The versatility of polymer chemistry allows modification to block length, molecular weight, chemical composition, hydrophilic/hydrophobic balance and molecular architecture[20]. Changing these parameters allows control of membrane morphology, molecular packing, membrane stability, fluidity, thickness and permeability. Such solid-supported mixed membranes are accessible for surface-sensitive techniques and could find large interest as model systems for biological membranes, as supports for the development of more stable biosensors.

Conclusions

Mixing ABA polymer and lipids gave rise to hybrid vesicles composed of both polymer and lipid. These vesicles gained stability properties from the polymer and adhesion properties from the lipid. These vesicles could tether well to negatively charged quartz and mica surfaces. We can control whether adsorbed vesicles or supported bilayer structures are formed on the support by varying the lipid content of the vesicles. These stable hybrid structures with good adhesion to hydrophilic surfaces could be attractive as drug delivery vehicles. Solid-supported mixed membranes could find large interest as model systems for biological membranes, as supports for the development of more stable biosensors.

Acknowledgements

We thank Christian Rein (University of Copenhagen), Prof. Erik Reimhult (University of Natural Resources and Life Sciences, Vienna), Wacek Swiech (Frederick Seitz Materials Research Laboratory Central Facilities, University of Illinois) and Scott McLaren (Frederick Seitz Materials Research Laboratory Central Facilities, University of Illinois) for valuable discussions. AFM and TEM experiments were carried out in the Frederick Seitz Materials Research Laboratory Central Facilities, University of Illinois. Glow-discharging of copper grids for TEM was carried out at the Microscopy Suite in the Beckman Institute, University of Illinois. This work was supported through MEMBAQ, a Specific Targeted Research Project (STREP), by the European Commission under the Sixth Framework Programme (NMP4-CT-2006-033234), by the Danish National Advanced Technology Foundation (023-2007-1) and by a grant to DTU Physics from the Danish National Research Foundation. CHN was also supported by the

Environment & Water Industry Programme Office of Singapore (EWI) through project #MEWR 651/06/169.

Supporting information

Lipid polymer ratio (mol %)			Ca^{2+}	Δf_{min}	ΔD_{max}	Δf_{fin}	ΔD_{fin}
POPC	DOTAP	ABA	mM	Hz	10^{-6}	Hz	10^{-6}
100	0	0	0	56±9	5.9±1.2	36±8	1.8±1.2
89	0	11	5	138±20	24.4±2.1	55±9	9.7±2.7
67	0	33	5	188±3	25.4±4	174±16	20.3±2.0
33	0	67	5	300±5	48.6±1.7	300±5	48.6±1.7
0	100	0	5	30±4	3.6±1.1	30±4	3.6±1.1
0	89	11	5	70±7	5.7±0.7	70±7	5.7±0.7
0	67	33	5	115±19	16.4±3.5	115±19	16.4±3.5
0	11	80	5	120±15	22.4±12.0	120±15	22.4±12.0
0	0	100	5	42±1	13.7±3.2	42±1	11.8±5.9

References

1. Nielsen, C. H., Biomimetic membranes for sensor and separation applications. *Anal Bioanal Chem* 2009, 395, (3), 697-718.

2. Meier, W.; Nardin, C.; Winterhalter, M., Reconstitution of channel proteins in (polymerized) ABA triblock copolymer membranes. *Angewandte Chemie-International Edition* 2000, 39, (24), 4599-4602.

3. Nardin, C.; Widmer, J.; Winterhalter, M.; Meier, W., Amphiphilic block copolymer nanocontainers as bioreactors. *European Physical Journal E* 2001, 4, (4), 403-410.

4. Kelety, B.; Diekert, K.; Tobien, J.; Watzke, N.; Dorner, W.; Obrdlik, P.; Fendler, K., Transporter assays using solid supported membranes: A novel screening platform for drug discovery. *Assay and Drug Development Technologies* 2006, 4, (5), 575-582.

5. Eray, M.; Dogan, N. S.; Reiken, S. R.; Sutisna, H.; Vanwie, B. J.; Koch, A. R.; Moffett, D. F.; Silber, M.; Davis, W. C., A Highly Stable and Selective Biosensor using Modified Nicotinic Acetylcholine-Receptor (NACHR). *Biosystems* 1995, 35, (2-3), 183-188.

6. Nikolelis, D. P.; Siontorou, C. G., Bilayer-Lipid Membranes for Flow-Injection Monitoring of Acetylcholine, Urea, and Penicillin. *Analytical Chemistry* 1995, 67, (5), 936-944.

7. Moran-Mirabal, J. M.; Edel, J. B.; Meyer, G. D.; Throckmorton, D.; Singh, A. K.; Craighead, H. G., Micrometer-sized supported lipid bilayer arrays for bacterial toxin binding studies through total internal reflection fluorescence microscopy. *Biophysical Journal* 2005, 89, (1), 296-305.

8. Discher, B. M.; Won, Y. Y.; Ege, D. S.; Lee, J. C. M.; Bates, F. S.; Discher, D. E.; Hammer, D. A., Polymersomes: Tough vesicles made from diblock copolymers. *Science* 1999, 284, (5417), 1143-1146.

9. Lee, J. C. M.; Bermudez, H.; Discher, B. M.; Sheehan, M. A.; Won, Y. Y.; Bates, F. S.; Discher, D. E., Preparation, stability, and in vitro performance of vesicles made with diblock copolymers. *Biotechnology and Bioengineering* 2001, 73, (2), 135-145.

10. Choi, H. J.; Germain, J.; Montemagno, C. D., Effects of different reconstitution procedures on membrane protein activities in proteopolymersomes. *Nanotechnology* 2006, 17, (8), 1825-1830.

11. Graff, A.; Fraysse-Ailhas, C.; Palivan, C. G.; Grzelakowski, M.; Friedrich, T.; Vebert, C.; Gescheidt, G.; Meier, W., Amphiphilic Copolymer Membranes Promote NADH:Ubiquinone Oxidoreductase Activity: Towards an Electron-Transfer Nanodevice. *Macromolecular Chemistry and Physics* 2010, 211, (2), 229-238.

12. Graff, A.; Sauer, M.; Van Gelder, P.; Meier, W., Virus-assisted loading of polymer nanocontainer. *Proceedings of the National Academy of Sciences of the United States of America* 2002, 99, (8), 5064-5068.

13. Grzelakowski, M.; Onaca, O.; Rigler, P.; Kumar, M.; Meier, W., Immobilized Protein-Polymer Nanoreactors. *Small* 2009, 5, (22), 2545-2548.

14. Ho, D.; Chu, B.; Lee, H.; Montemagno, C. D., Protein-driven energy transduction across polymeric biomembranes. *Nanotechnology* 2004, 15, (8), 1084-1094.

15. Nardin, C.; Thoeni, S.; Widmer, J.; Winterhalter, M.; Meier, W., Nanoreactors based on (polymerized) ABA-triblock copolymer vesicles. *Chemical Communications* 2000, (15), 1433-1434.

16. Onaca, O.; Sarkar, P.; Roccatano, D.; Friedrich, T.; Hauer, B.; Grzelakowski, M.; Guven, A.; Fioroni, M.; Schwaneberg, U., Functionalized nanocompartments (synthosomes) with a reduction-triggered release system. *Angewandte Chemie-International Edition* 2008, 47, (37), 7029-7031.

17. Sauer, M.; Haefele, T.; Graff, A.; Nardin, C.; Meier, W., Ion-carrier controlled precipitation of calcium phosphate in giant ABA triblock copolymer vesicles. *Chemical Communications* 2001, (23), 2452-2453.

18. Wong, D.; Jeon, T. J.; Schmidt, J., Single molecule measurements of channel proteins incorporated into biomimetic polymer membranes. *Nanotechnology* 2006, 17, (15), 3710-3717.

19. Kumar, M.; Grzelakowski, M.; Zilles, J.; Clark, M.; Meier, W., Highly permeable polymeric membranes based on the incorporation of the functional water channel protein Aquaporin Z. *Proc Natl Acad Sci U S A* 2007, 104, (52), 20719-20724.

20. Belegrinou, S.; Dorn, J.; Kreiter, M.; Kita-Tokarczyk, K.; Sinner, E. K.; Meier, W., Biomimetic supported membranes from amphiphilic block copolymers. *Soft Matter* 2010, 6, (1), 179-186.

21. Mueller, P.; Rudin, D. O.; Ti Tien, H.; Wescott, W. C., Reconstitution of Cell Membrane Structure in vitro and its Transformation into an Excitable System. *Nature* 1962, 194, (4832), 979-980.

22. Montal, M.; Mueller, P., Formation of Bimolecular Membranes from Lipid Monolayers and a Study of their Electrical Properties. *Proceedings of the National Academy of Sciences of the United States of America* 1972, 69, (12), 3561-3566.

23. Ibragimova, S.; Stibius, K.; Szewczykowski, P.; Perry, M.; Bohr, H.; Hélix-Nielsen, C., Hydrogels for in situ Encapsulation of Biomimetic Membrane Arrays. *Polymers for Advanced Technologies*, doi 10.1002/pat.1850 (in press).

24. Jeon, T. J.; Malmstadt, N.; Poulos, J. L.; Schmidt, J. J., Black lipid membranes stabilized through substrate conjugation to a hydrogel. *Biointerphases* 2008, 3, (2), FA96.

25. Jeon, T. J.; Malmstadt, N.; Schmidt, J. J., Hydrogel-encapsulated lipid membranes. *J Am Chem Soc* 2006, 128, (1), 42-3.

26. Lander, M. R.; Ibragimova, S.; Rein, C.; Vogel, J.; Stibius, K.; Geschke, O.; Perry, M.; Hélix-Nielsen, C., Biomimetic membrane arrays on cast hydrogel supports. *Langmuir*, in press.

27. Cruz, A.; Perez-Gil, J., Langmuir films to determine lateral surface pressure on lipid segregation. *Methods Mol Biol* 2007, 400, 439-57.

28. Richter, R.; Mukhopadhyay, A.; Brisson, A., Pathways of lipid vesicle deposition on solid surfaces: a combined QCM-D and AFM study. *Biophys J* 2003, 85, (5), 3035-3047.

29. Graneli, A.; Rydstrom, J.; Kasemo, B.; Hook, F., Formation of supported lipid bilayer membranes on SiO2 from proteoliposomes containing transmembrane proteins. *Langmuir* 2003, 19, (3), 842-850.

30. Reimhult, E.; Hook, F.; Kasemo, B., Temperature dependence of formation of a supported phospholipid bilayer from vesicles on SiO2. *Phys Rev E Stat Nonlin Soft Matter Phys* 2002, 66, (5 Pt 1), 051905.

31. Reimhult, E.; Hook, F.; Kasemo, B., Vesicle adsorption on SiO2 and TiO2: Dependence on vesicle size. *Journal of Chemical Physics* 2002, 117, (16), 7401-7404.

32. Richter, R. P.; Brisson, A., QCM-D on mica for parallel QCM-D-AFM studies. *Langmuir* 2004, 20, (11), 4609-13.

33. Richter, R. P.; Brisson, A. R., Following the formation of supported lipid bilayers on mica: a study combining AFM, QCM-D, and ellipsometry. *Biophys J* 2005, 88, (5), 3422-3433.

34. Tanaka, M.; Sackmann, E., Polymer-supported membranes as models of the cell surface. *Nature* 2005, 437, (7059), 656-63.

35. Naumann, C. A.; Prucker, O.; Lehmann, T.; Ruhe, J.; Knoll, W.; Frank, C. W., The polymer-supported phospholipid bilayer: tethering as a new approach to substrate-membrane stabilization. *Biomacromolecules* 2002, 3, (1), 27-35.

36. Purrucker, O.; Fortig, A.; Jordan, R.; Tanaka, M., Supported membranes with well-defined polymer tethers--incorporation of cell receptors. *Chemphyschem* 2004, 5, (3), 327-35.

37. Wagner, M. L.; Tamm, L. K., Tethered polymer-supported planar lipid bilayers for reconstitution of integral membrane proteins: silane-polyethyleneglycol-lipid as a cushion and covalent linker. *Biophys J* 2000, 79, (3), 1400-14.

38. Munro, J. C.; Frank, C. W., In situ formation and characterization of poly(ethylene glycol)-supported lipid bilayers on gold surfaces. *Langmuir* 2004, 20, (24), 10567-75.

39. Delajon, C.; Gutberlet, T.; Steitz, R.; Mohwald, H.; Krastev, R., Formation of polyelectrolyte multilayer architectures with embedded DMPC studied in situ by neutron reflectometry. *Langmuir* 2005, 21, (18), 8509-14.

40. Kohler, G.; Moya, S. E.; Leporatti, S.; Bitterlich, C.; Donath, E., Stability and fusion of lipid layers on polyelectrolyte multilayer supports studied by colloidal force spectroscopy. *Eur Biophys J* 2007, 36, (4-5), 337-47.

41. Kugler, R.; Knoll, W., Polyelectrolyte-supported lipid membranes. *Bioelectrochemistry* 2002, 56, (1-2), 175-8.

42. Reich, C.; Neff, P. A.; Bausch, A. R.; Radler, J. O.; Nickel, B., Supported membranes on polyelectrolyte layers studied by X-ray reflectometry. *Physica Status Solidi a-Applications and Materials Science* 2006, 203, (14), 3463-3467.

43. Castellana, E. T.; Cremer, P. S., Solid supported lipid bilayers: From biophysical studies to sensor design. *Surface Science Reports* 2006, 61, (10), 429-444.

44. Tanaka, M.; Sackmann, E., Supported membranes as biofunctional interfaces and smart biosensor platforms. *Physica Status Solidi a-Applications and Materials Science* 2006, 203, (14), 3452-3462.

45. Rakhmatullina, E.; Meier, W., Solid-supported block copolymer membranes through interfacial adsorption of charged block copolymer vesicles. *Langmuir* 2008, 24, (12), 6254-6261.

46. Rakhmatullina, E.; Mantion, A.; Burgi, T.; Malinova, V.; Meier, W., Solid-Supported Amphiphilic Triblock Copolymer Membranes Grafted from Gold Surface. *Journal of Polymer Science Part a-Polymer Chemistry* 2009, 47, (1), 1-13.

47. Wang, J. Y.; Chin, J. M.; Marks, J. D.; Lee, K. Y. C., Effects of PEO-PPO-PEO Triblock Copolymers on Phospholipid Membrane Integrity under Osmotic Stress. *Langmuir* 26, (15), 12953-12961.

48. Ruysschaert, T.; Sonnen, A. F.; Haefele, T.; Meier, W.; Winterhalter, M.; Fournier, D., Hybrid nanocapsules: interactions of ABA block copolymers with liposomes. *J Am Chem Soc* 2005, 127, (17), 6242-6247.

49. Jin, Y. L.; Chen, J. Y.; Xu, L.; Wang, P. N., Refractive index measurement for biomaterial samples by total internal reflection. *Physics in Medicine and Biology* 2006, 51, (20), N371.

50. Borgnia, M. J.; Kozono, D.; Calamita, G.; Maloney, P. C.; Agre, P., Functional Reconstitution and Characterization of AqpZ, the E. coli Water Channel Protein. *J Mol Biol* 1999, 291, (5), 1169-1179.

51. Rodahl, M.; Hook, F.; Fredriksson, C.; Keller, C. A.; Krozer, A.; Brzezinski, P.; Voinova, M.; Kasemo, B., Simultaneous frequency and dissipation factor QCM measurements of biomolecular adsorption and cell adhesion. *Faraday Discuss* 1997, (107), 229-246.

52. Lande, M. B.; Donovan, J. M.; Zeidel, M. L., The Relationship between Membrane Fluidity and Permeabilities to Water, Solutes, Ammonia, and Protons. *Journal of general physiology* 1995, 106, 67-84.

53. Keller, C. A.; Kasemo, B., Surface specific kinetics of lipid vesicle adsorption measured with a quartz crystal microbalance. *Biophys J* 1998, 75, (3), 1397-1402.

54. Lewis, B. A.; Engelman, D. M., Lipid Bilayer Thickness Varies Linearly with Acyl Chain-Length in Fluid Phosphatidylcholine Vesicles. *Journal of Molecular Biology* 1983, 166, (2), 211-217.

55. Kita-Tokarczyk, K.; Itel, F.; Grzelakowski, M.; Egli, S.; Rossbach, P.; Meier, W., Monolayer interactions between lipids and amphiphilic block copolymers. *Langmuir* 2009, 25, (17), 9847-9856.

56. Chang, E. L., Unusual Thermal-Stability of Liposomes Made From Bipolar Tetraether Lipids. *Biochemical and Biophysical Research Communications* 1994, 202, (2), 673-679.

57. Dannenmuller, O.; Arakawa, K.; Eguchi, T.; Kakinuma, K.; Blanc, S.; Albrecht, A. M.; Schmutz, M.; Nakatani, Y.; Ourisson, G., Membrane properties of archaeal macrocyclic diether phospholipids. *Chemistry-a European Journal* 2000, 6, (4), 645-654.

58. Needham, D.; Zhelev, D., The mechanochemistry of lipid vesicles examined by micropipet manipulation techniques. *Surfactant science series* 1996, 62, 373-444.

Figures

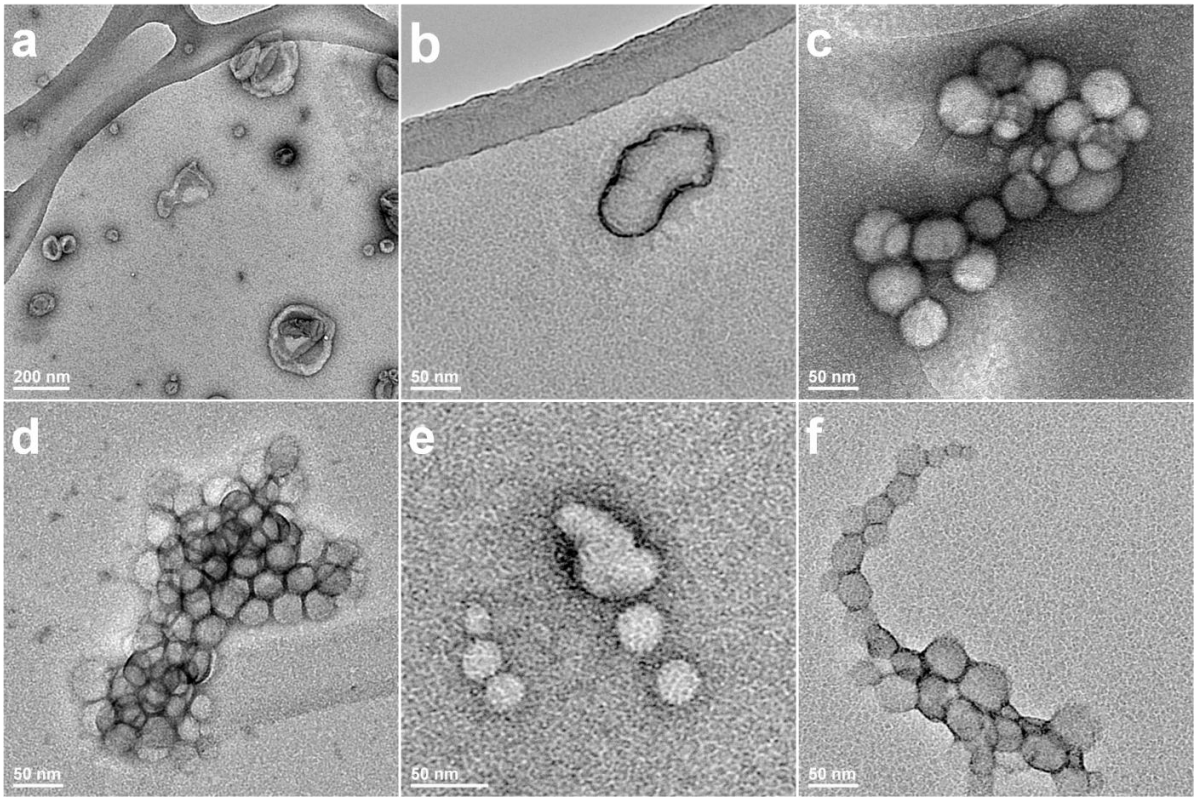

Figure 1. TEM of lipid vesicles, polymer vesicles and mixed lipid/ABA vesicles. a) POPC, b) DOTAP, c) ABA, d) 89 mol% POPC:11 mol% ABA, e) 89 mol% DOTAP:11mol% ABA and f) 67 mol% DOTAP:33 mol% ABA.

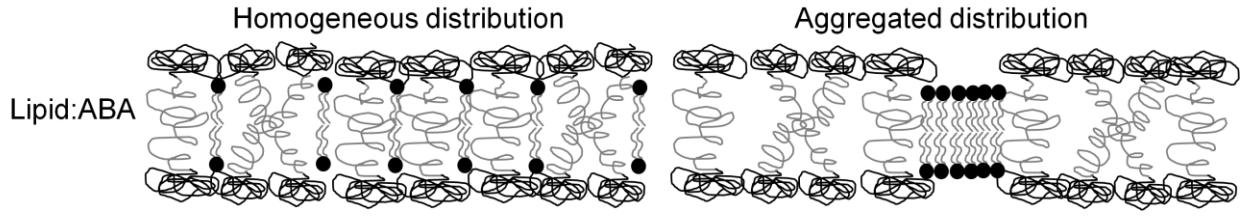

Figure 2. Hypothetic structures of hybrid membranes composed of ABA triblock copolymers and POPC or DOTAP lipids. Lipids might either disperse evenly into the ABA membrane in a homogenous distribution or segregate into domains leading to an aggregated distribution. ABA triblock copolymers might fully span the lipid bilayer or partially insert the PDMS unit into the acyl chain portion of the lipid bilayer and form a "U"-shape.

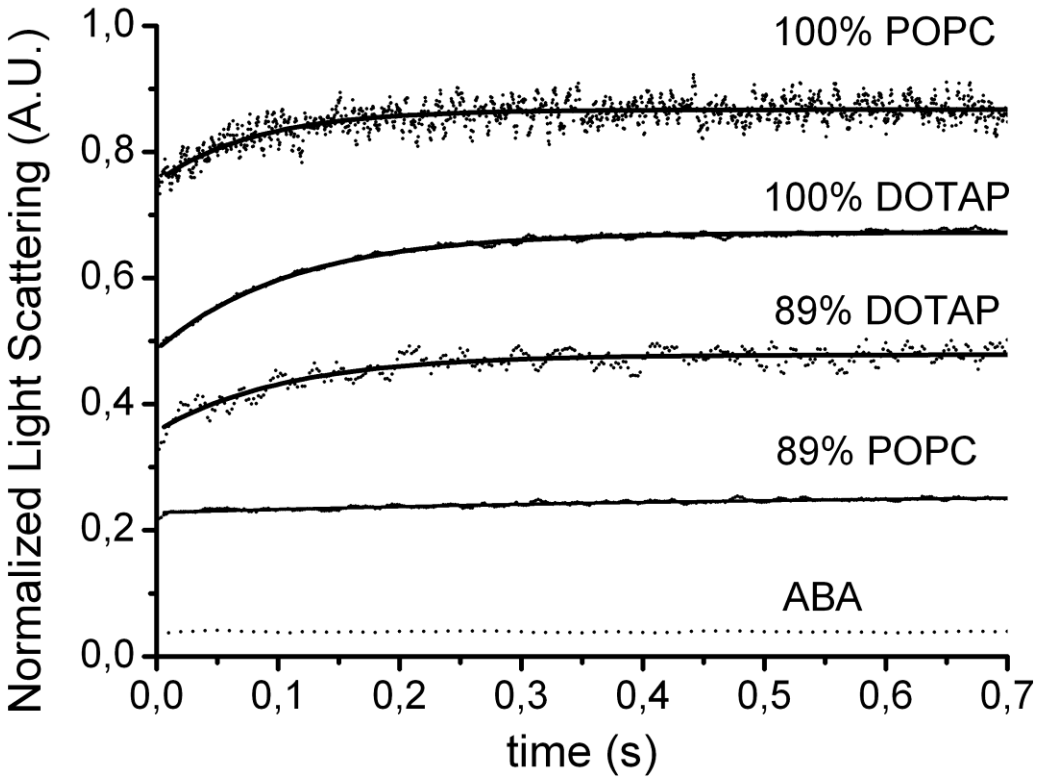

Figure 3. Water permeability of promising bi/monolayer formation systems determined by stopped-flow light-scattering experiments.

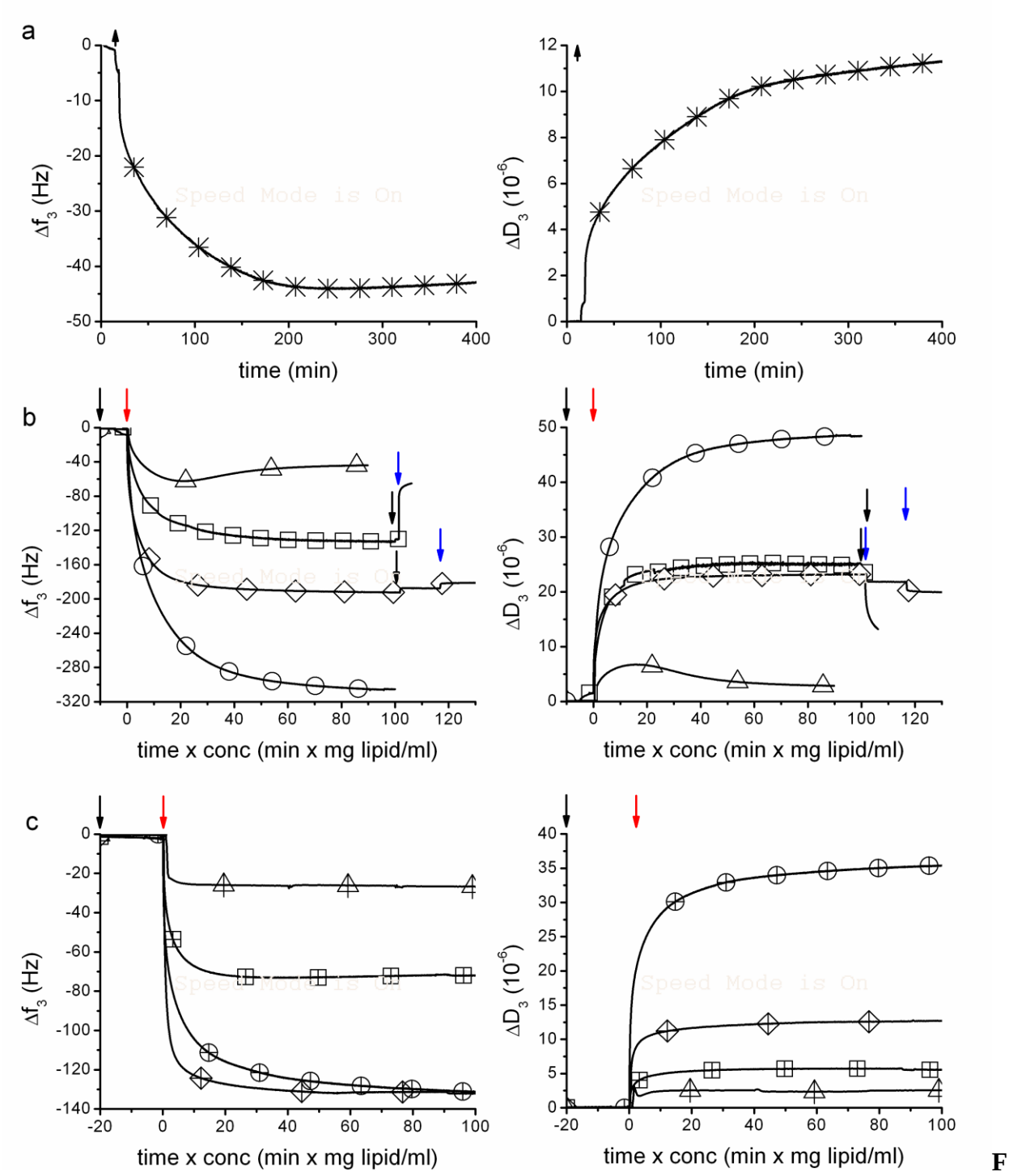

Figure 4. QCM-D responses for the deposition of different polymer/lipid mixtures on SiO_2. Changes in frequency (solid lines) and dissipation (dotted lines) at 15 MHz. a) ABA vesicles, b) POPC vesicles (100 mol% POPC (Δ), 89 mol% POPC:11 mol% ABA (□), 67 mol% POPC 33 mol% ABA (◊, 33 mol% POPC: 67 mol% ABA (○)) and c) DOTAP vesicles (100 mol% DOTAP (Δ), 89 mol% DOTAP:11 mol% ABA (□), 67 mol% DOTAP:33 mol% ABA (◊), 33 mol% DOTAP: 67 mol% ABA (○)). Arrows show addition of PBS (black), 1ml of vesicles (red) and 5mM $CaCl_2$ (blue).

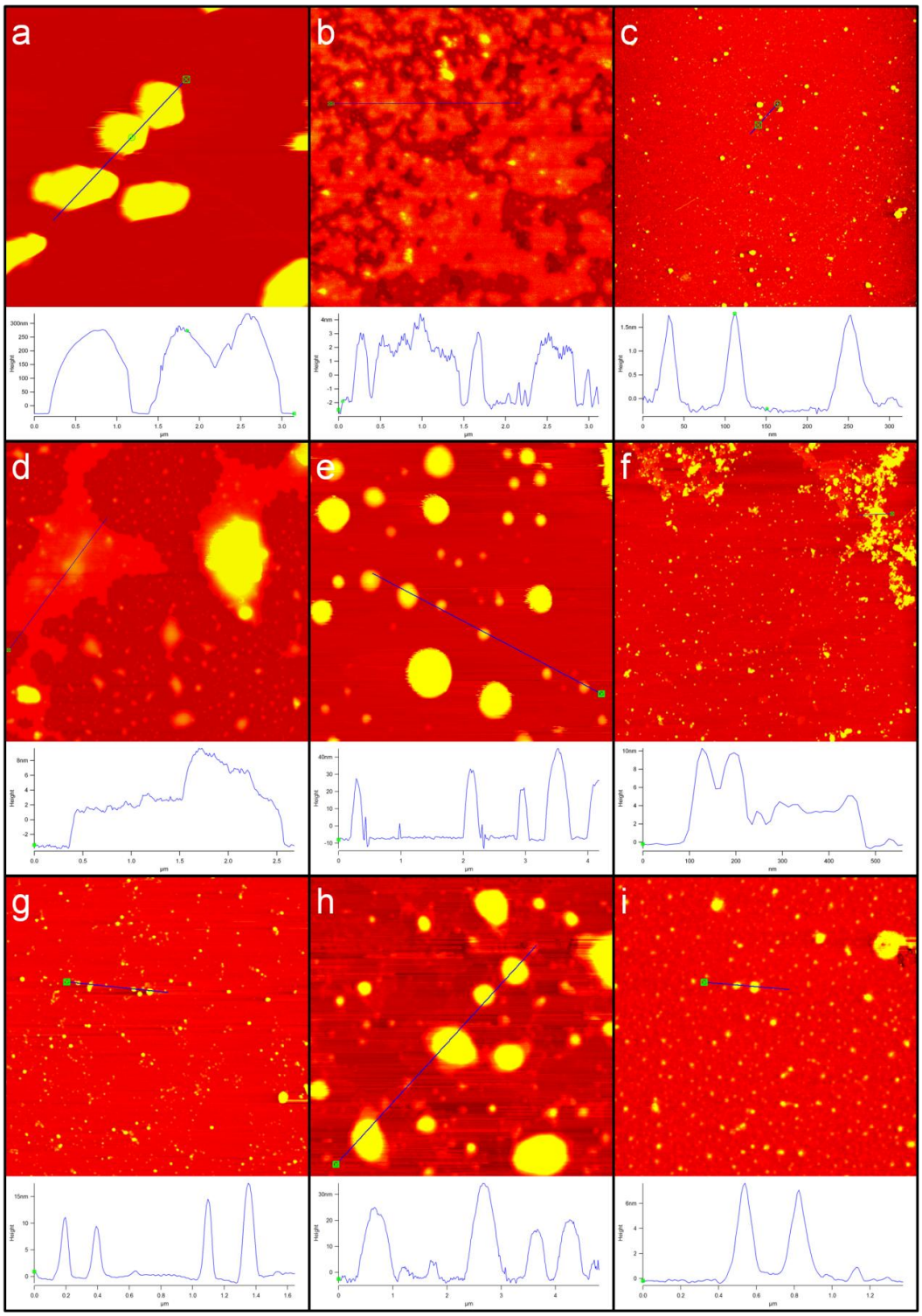

Figure 5. AFM images. a)ABA, b) POPC, c) DOTAP, d) 89 mol% POPC:11 mol% ABA, e) 67 mol% POPC:33 mol% ABA, f) 89 mol% DOTAP:11 mol% ABA, g) 89 mol% POPC:11 mol% ABA with 5 mM CaCl2, h) 67 mol% POPC:33 mol% ABA with 5 mM $CaCl_2$, i) PBS. Each block is 5 µm x 5 µm. A height profile is shown for each figure.

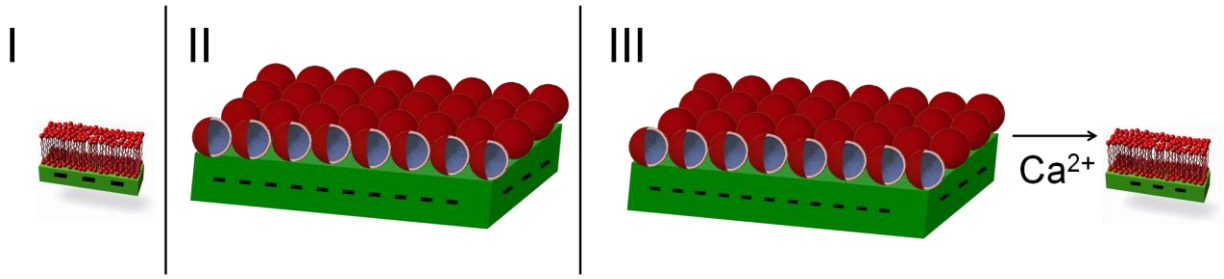

Figure 6. The type of supported membrane formed can be decided by varying the type and concentration of lipid in the membrane. (I) Planar membrane, (II) vesicular membrane and (III) vesicular membrane which can be triggered to form a planar membrane by addition of calcium.

Tables

Table 1. Hydrodynamic diameter and zeta potential of lipid vesicles, polymer vesicles and mixed lipid/ABA vesicles obtained by DLS and ELS.

Lipid polymer ratio (mol%)			D_h (nm)	PDI	ζ(mV)
POPC	DOTAP	ABA			
100	-	-	159±2	0.13	0.2±0.3
89	-	11	194±3	0.17	-5.7±0.8
67	-	33	217±3	0.19	-2.0±0.3
33	-	67	189±5	0.12	-2.6±0.4
-	100	-	160±3	0.085	35.6±0.4
-	89	11	109±0	0.24	2.5±0.1
-	67	33	105±1	0.21	-1.7±0.9
-	33	67	175±1	0.15	0.8±0.1
-	-	100	198±5	0.12	-4.9±0.8

Table 2. Deposition of lipid vesicles, polymer vesicles and hybrid vesicles on quartz by QCM-D. m_{max}-maximum mass coverage observed, m_{min}-minimum mass coverage observed, $m_{bilayer}$-expected mass coverage if the surface is completely covered by a lipid bilayer/copolymer monolayer, t_{max}-maximum adsorbed layer thickness observed, t_{min}-minimum adsorbed layer thickness observed, α- fractional bilayer coverage, ΔD_{fin}-change in dissipation from buffer baseline at the start of the experiment to the buffer baseline at the end of the experiment, Δf_{fin}-change in frequency from buffer baseline at the start of the experiment to the buffer baseline at the end of the experiment.

Lipid polymer ratio (mol %)			Ca^{2+}	m_{max}	m_{min}	$m_{bilayer}$	α	t_{max}	t_{min}	$\Delta D_{fin}/\Delta f_{fin}$
POPC	DOTAP	ABA	mM	ng/cm^2	ng/cm^2	ng/cm^2	%	nm	nm	
100	0	0	0	982±163	637±150	388	93±6	12±2	9±1	0.05±0.02
89	0	11	5	2437±356	979±159	422	66±8	33±5	16±3	0.17±0.03
67	0	33	5	3334±57	3074±287	436	38±6	49±12	47±13	0.12±0.00
33	0	67	0	5310±92	5310±92	442	0	104±2	104±2	0.17±0.00
0	100	0	0	531±71	531±71	332	86±4	7±2	7±2	0.15±0.02
0	89	11	0	1239±124	1239±124	398	79±3	14±1	14±1	0.09±0.02
0	67	33	0	2041±335	2041±335	427	17±15	66±15	66±15	0.15±0.04
0	33	67	0	2115±263	2115±263	439	-6±40	101±28	101±28	0.23±0.06
0	0	100	0	734±13	734±13	444	-	81±21	81±21	0.33±0.08

Table 3. Comparison of film thickness obtained by QCM-D on silica and film thickness obtained by AFM on mica.

Vesicle composition	t_{QCM} (nm)	t_{AFM} (nm)
POPC	9±1	3.2±1.4
89 mol% POPC:11 mol% ABA	33±5	5.0±1.4
89 mol% POPC:11 mol% ABA + $CaCl_2$	16±3	-0.1±0.1
67 mol% POPC:33 mol% ABA	49±12	26.6±48.4
67 mol% POPC:33 mol% ABA + $CaCl_2$	47±13	19.4±7.0
DOTAP	7±2	10±4.0
89 mol% DOTAP:11 mol% ABA	14±1	1.0±0.6
ABA	81±21	199.3±39.5
PBS	0	-0.2±0.2

Table 4. Water permeability of mixed lipid/polymer vesicles.

Lipid polymer ratio (mol%)			P_f (μm/s)
POPC	DOTAP	ABA	
100	-	-	22.6±1.3
89	-	11	7.5±0.6
-	100	-	13.2±0.1
-	89	11	9.5±0.5
-	-	100	0.8 [19]

Appendix I

ELECTROCHEMICAL CHARACTERISATION OF HYDROGELS FOR BIOMIMETIC APPLICATIONS

L. Peláez [1], V. Romero [1], S. Escalera [1], S. Ibragimova [2,3], K. Stibius [2,3],

J . Benavente [1], and C.H. Nielsen[2,3]

[1] Grupo de Caracterización Electrocinética en Membranas e Interfases. Departamento de Física Aplicada I. Facultad de Ciencias. Universidad de Málaga. E-29071 Málaga, Spain

[2]DTU Physics, Technical University of Denmark, Fysikvej 309, Building 309, DK2800 Kgs. Lyngby, Denmark

[3]Aquaporin A/S / Diplomvej 377, DK2800 Kgs. Lyngby, Denmark

Running Title:
Electrochemical properties of hydrogels

Keywords:
Biomimetic membrane encapsulation,

Address correspondence to:

Claus Hélix Nielsen
DTU Physics
Fysikvej 309, Building 309, office 138
Technical University of Denmark
DK-2800 Lyngby
Phone +45 60 68 10 81
Fax +45 45 93 16 69
EMB: claus.helix.nielsen@fysik.dtu.dk

Abstract

Hydrogels are increasingly being recognized as having potential in bio-compatible applications. In the previous paper we investigated the feasibility of poly(ethylene glycol)-dimethacrylate (PEG-1000-DMA) and poly(ethylene glycol)-diacrylate (PEG-400-DA) polymerized using either a chemical initiator (C) or a photoinitiator (P) to encapsulate and stabilize biomimetic membranes for novel separation technologies or biosensor applications. In this paper we have investigated the electrochemical properties of the hydrogels used for membrane encapsulation. Specifically we studied the crosslinked hydrogels using electrochemical impedance spectroscopy (EIS) and we demonstrated that chemically crosslinked hydrogels had lower values for the effective electrical resistance and higher values for the electrical capacitance compared to hydrogels with photoinitiated crosslinking. Transport numbers were obtained using electromotive force measurements and demonstrated that at low salt concentrations both PEG-400-DA-C and PEG-400-DA-P hydrogels presented an electropositive character while PEG-1000-DMA-P was approximately neutral and PEG-1000-DMA-C showed electronegative character. Sodium transport numbers approached the bulk NaCl electrolyte value at high salt concentrations for all hydrogels indicating screening of fixed charges in the hydrogels. The average salt diffusional permeability $<P_s>$ and water permeability $<P_w>$ were found to correlate with EIS results. PEG-1000-DMA-C and PEG-400-DA-C both had higher $<P_s>$ and $<P_w>$ values than PEG-1000-DMA-P and PEG-400-DA-P hydrogels. In conclusion our results show that hydrogel electrochemical properties can be controlled by the choice of polymer and type of crosslinking used, and that their water and salt permeability properties are congruent with the use of hydrogels for biomimetic membrane encapsulation.

INTRODUCTION

Since the pioneering work of Wichterle and Lim where the first hydrogels were synthesized for applications in ophthalmology [1, 2] there has been a strong development in synthesis and design of hydrogels for a variety of applications, for recent reviews see [3-5]. Due to their high water content they have excellent biocompatibility and have thus found use as biomaterials (e.g. contact lenses and implants) and drug delivery systems [6]. Recently they have also attracted interest in the design of microfluidic biosensors [7, 8] and biomimetic membranes [9-11]. In the previous paper we examined the feasibility of using poly(ethylene glycol)-di(meth)acrylate (PEG-D(M)A) based hydrogels for encapsulating biomimetic membrane arrays [11]. In the present paper we examine hydrogel electrochemical properties as well as water and salt diffusive permeabilities and demonstrate how these properties depends on the choice of polymer and type of crosslinking.

Electric impedance spectroscopy (EIS) represents a noninvasive method to assess electro-chemical properties of composite layered structures as EIS allows for the separation of contributions from the individual layers [12]. Thus the electrical capacitance (C) and resistance (R) can be characterized under working conditions i.e. in contact with saline solutions. Previously EIS has been used to characterize conductivity and transport properties in aliphatic/aromatic membranes [13]; in membranes with different degrees of sulfonation [14]; in membranes with added lignosulfonate [15], in irradiated membranes [16]; and in active and porous sublayes of composite membranes [17]. Thus EIS is well suited to analyse electrochemical properties of porous hydrogel structures sandwiched between supporting encapsulation layers.

Here we specifically investigate how the differences in hydraulic water flux between hydrogels crosslinked chemically or via photoinitiation reported in the previous paper as well as water and salt diffusional permeabilities reported here relate to the electrochemical properties of the hydrogels as revealed by EIS. Our results illustrate how transport properties of hydrogels suitable for biomimetic applications can be controlled by the choice of polymer and type of crosslinking used.

MATERIALS AND METHODS

Preparation of hydrogel sandwich samples

Four different hydrogels samples were prepared as described in the previous paper. Briefly the gels consist of poly(ethylene glycol) PEG with diacrylate (DA) or dimethacrylate (DMA) moieties. The gels were crosslinked using photoinitiation (P) or chemical initiation (C) [11]. Table 1 presents the four samples investigated. The composite structures consist of a hydrogel sandwiched between a flat regenerated cellulose membrane with a polypropylene layer and a Tefzel ethylene tetrafluoroethylene film (ETFE) LZ200 with a thickness of 50.8 μm perforated with a rectangular array of 8 x 8 apertures with aperture radii of 150 μm and a center to center distance of 400 μm [18-20].

Table 1 around here

Each crosslinked hydrogel sample contains the corresponding hydrogel between the RC70PP support (gel in contact with the regenerated cellulose side) and the ETFE partitioning as is schematically represented in Fig. 1, and they will hereafter be identified as X400P, X400C, X1000P and X1000C, respectively.

Measurement setup

Electrochemical measurements were carried out with NaCl solutions at various concentrations at room temperature (23 ± 2) ºC. In order to avoid the loss of hydrogel, the concentration gradients

needed to cause flow of ions and solute across the systems were established in the way indicated in Fig. 1.

Figure 1around here

The dead-end test cell used for electrochemical characterization is similar to that described in [21]. Briefly, the samples were clamped between two glass half-cells by using silicone rubber rings. Two magnetic stirrers were placed at the bottom of the half-cells to minimize the concentration polarization at the membrane surfaces, and the measurements were performed at a stirring rate of (500 ± 30) rpm.

Electrochemical impedance spectroscopy

Electrochemical impedance spectroscopy (EIS) was performed with an Impedance Analyzer (Solartron 1260, Durham, UK) controlled by a computer and connected to the solution in both half-cells by Pt electrodes. 100 different frequencies in the range 1 Hz-10^7 Hz at a maximum voltage of 0.01 V were measured. The experimental data was corrected for the influence of connecting cables and other parasite capacitances. The NaCl solutions at the cis and trans sides of the samples had the same concentration and the measurements were carried out with five different solutions ranging between 10^{-3} M and 10^{-2} M. In order to determine solution impedance, measurements at the same concentrations were also performed with the electrolyte alone.

Electromotive force measurements

The electromotive force (ΔE) between solutions of different concentration separated by the membrane was measured by connecting two Ag/AgCl electrodes to a digital voltmeter (Yokohama 7552, 1GΩ input resistance). Measurements were carried out by keeping the concentration of the solution at one cell side constant, c_c = 0.01 M NaCl, and gradually changing the concentration of the solution at the other side, c_v. ΔE measurements were always carried out with the highest concentration in contact with the ETFE partitioning (cis side).

Salt diffusional permeability measurements

For salt diffusion measurements each sample was initially separating a feed concentrated solution (c_f) from a diluted receiving solution (initially distilled water, $c_r(t=0)=0$), without any pressure difference. Changes in the conductivity of feed and receiving solutions (σ_f and σ_r, respectively) were recorded versus time by means of conductivity cells connected to digital conductivity meters (Crison GLP 31, Crison Instruments, Barcelona, Spain). Measurements were carried out at five different NaCl feed concentrations ranging between 0.005 M and 0.1 M.

Water diffusional permeability measurements

Water diffusion measurements were performed following a similar procedure, but using triated water (TOH) from Perkin Elmer España, S.A., Madrid. A water solution containing 120 µl TOH in 15 ml distilled water was used as feed, and the time variation of the tritium activity in the receiving chamber was determined at different time intervals by taking out 50 µl volumes which were analyzed in a Beckman LS6500 scintillation counter (Beckman Coulter, Brea, CA, USA). These measurements were performed at the Radioisotope Laboratory (Central Research Services, Málaga University, Spain) observing radiation safety protocols.

RESULTS AND DISCUSSION

Electrical impedance spectroscopy

Electrical impedance spectroscopy (EIS) is commonly used for electrical characterization of layered systems since it allows a separate determination of the electrical parameters (resistance and capacitance) of individual layers with different electrical/structural characteristics [12, 22]. Impedance is defined as $Z = V(t)/I(t)$ where $V(t)$ and $I(t)$ are voltage and current as functions of time t. Z is generally an imaginary number related to the transport of charge (electrical resistance, R) and charge adsorption (capacitance, C), and is represented by $Z = Z_{re} + jZ_{im}$ where Z_{re} and Z_{im} are the real and imaginary parts of the impedance.

The studied systems can be described as a layered complex:

electrode//cis solution//sample//trans solution //electrode

We analyzed the impedance plots using equivalent RC circuits as models for each layer. This allows for the determination of the electrical resistance and capacitance associated with each layer of the heterogeneous system. Thus for each layer we have:

$$Z_{re} = \frac{R}{1+(\omega RC)^2} \qquad Z_{im} = \frac{-\omega R^2 C}{1+(\omega RC)^2} \tag{1}$$

where ω represents the angular frequency ($\omega = 2\pi f$).

Figure 2around here

Fig. 2 shows Nyquist (-Z_{im} *vs* Z_{re}) and Bode (Z_{im} vs f) plots for the solution/ETFE/RC70PP sandwich in contact with 0.002 M NaCl solution and for the electrolyte solution alone (without any sample in the measuring cell). For the electrolyte solution alone, a unique relaxation process (a semi-circle) was obtained and the equivalent circuit is a parallel RC-circuit corresponding to a electrolyte solution resistance R_e and a electrolyte solution capacitance C_e, while for the solution/ETFE/RC70PP system two different relaxation processes can be observed. These results allow the assignation of the semi-circle at highest frequencies (f_{max} = 2.66 MHz) to the electrolyte placed between the electrodes and the membrane surface, while the other semicircle (frequency ranging between 1 kHz and 1 Mhz with f_{max} = 560 kHz) corresponds to the ETFE/RC70PP sandwich and the total equivalent circuit is: (R_eC_e)-(R_mC_m), that is, two *RC*-circuits in series, one (R_mC_m) representing the ETFE/RC70PP sandwich and the other (R_eC_e) representing the electrolyte solutions between the sandwich and the Pt electrodes.

We then introduced the crosslinked hydrogels between the ETFE and the RC70PP membrane and studied the effects on the impedance and this is shown in Fig. 3. For X400P and X1000P, the Nyquist and Bode plots showed two RC contributions corresponding to those previously obtained for the ETFE/RC70PP sandwich without hydrogel. For X1000C the two *RC* contributions can also be identified in the Bode plot whereas for X400C there is no clear separation between the two contributions: the Bode plot shows a wide peak for the total system.

Figure 3 around here

The observed differences in the impedance plots could be due to differences in porosity or effective electrical charge in hydrogels where crosslinking was chemically initiated compared to hydrogels where the crosslinking was photoinitiated. In the accompanying paper we observed that while X400C and X1000C had markedly higher water fluxes than X400P and X1000P hydrogels, retention measurements did not reveal major differences in porosity. In order to clarify this we analyzed the equivalent circuit parameters and this is shown in Fig. 4.

Figure 4 around here

We used a non-linear program to determine the equivalent circuit electrical parameters (R_m and C_m) from the Nyquist and Bode plots as a function of NaCl concentration [23]. For all hydrogels R_m decreases and reaches a plateau with increasing salt concentration due to the hydrogels' uptake of electrolyte (see Fig. 4a). X400P and X1000P have R_m plateau values higher than R_e for the electrolyte alone. R_m plateau values for X400C is comparable to R_e whereas X1000C has R_m plateau values lower than for electrolyte alone. For all gels C_m values were higher than for electrolyte alone. For X400C,

X1000C and X1000P C_m increases with a linear trend as a function of salt concentration (see Fig. 4b). For X400P C_m showed a weaker dependence on salt concentration with a modest increase at higher concentrations.

We then extrapolated the results to $c_{NaCl} \rightarrow 0$ in order to determine electrical resistance and capacitance values (R_o^{Gel} and C_o^{Gel}) for the hydrogel *per se*. These were obtained by rearranging the expressions for series configuration of electrical resistances and capacitances, where 'Sample' refers to the complete system and 'Control' refers to measurements with the 'emtpy' ETFE/regenerated cellulose membrane sandwich:

$$R_0^{Gel} = R_0^{Sample} - R_0^{Control}$$
$$C_0^{Gel} = \frac{C_0^{Control} C_0^{Sample}}{C_0^{Control} - C_0^{Sample}} \quad (2)$$

The ranked R and C values were: $R_o^{X400C} << R_o^{X1000C} < R_o^{X400P} < R_o^{X1000P}$ and $C_o^{X400P} < C_o^{X1000P} << C_o^{X1000C} < C_o^{X400C}$. Assuming a similar area A and thickness d for all hydrogel samples we have the ranked conductivity values ($\sigma = R_0 A/d$) as $\sigma^{X1000P} > \sigma^{X400P} > \sigma^{X1000C} >> \sigma^{X400C}$ and the ranked relative dielectric constants ($\varepsilon = C_0 d/\varepsilon_0 A$) as $\varepsilon^{X400P} < \varepsilon^{X1000P} << \varepsilon^{X1000C} < \varepsilon^{X400C}$. This shows that the effective charge in the hydrogel depends on the polymer and crosslinking method used. Taken together with the results in our previous paper this indicates that hydrogel effective charge affects transport though the hydrogel.

Electromotive force measurements

In order to further investigate this we analyzed ion transport number, t_i, which represents the fraction of the total electric current across a permeable system carried by ion species i [24]. For a porous

medium where the Donnan exclusion of co-ions can be neglected, the electrical potential across the medium arises purely as a diffusion potential, $\Delta\Phi_{dif}$, due to the different ion mobilities:

$$\Delta\Phi_{dif} = \frac{RT}{F}(1-2t_+)\ln\left(\frac{a_2}{a_1}\right) \quad (3)$$

where R and F are the gas and Faraday constants, T is the thermodynamic temperature of the system and a_i is the mean activity of the electrolyte solution at each membrane interface [25]. Thus $t_i = I_i/I_T$, where I_i is the current carried by ion i and I_T the total current. Thus $\Sigma_i t_i = 1$. t_i can be determined by measuring the electromotive force ΔE across a permeable system separating two solutions of the same electrolyte, but with different activities (a_1 and a_2). However, as reversible electrodes are used, the electrode potential is part of ΔE ($\Delta E = \Delta E_{elc} + \Delta\Phi_{dif}$). ΔE_{elc} is given by the Nernstian value $\Delta E_{elc} = (RT/F) \ln (a_2/a_1)$. Thus

$$t_+ = \Delta E / \Delta E_{max} \quad (4)$$

where $\Delta E_{max} = (2RT/F) \ln (a_2/a_1)$.

We determine the Na^+ transport number t_{Na^+} across the studied gel-samples from the electromotive force measured for the two different external conditions by using Eq. (4) and its variation with the NaCl average activity, $\langle a_{NaCl} \rangle$. This is shown in Fig. 5 for the four hydrogel samples together with the Na^+ transport number in solution $t_{Na+}^{o} = 0.385$ [24] indicated by the dashed line.

Figure 5around here

These results show the electropositive character of X400P and X400C ($t_{Na+} < t_{Na+}^{o}$). X400C has a higher positive effective charge than X400P at low salt concentrations, but both gels show a reduction of the net charge at higher salt concentrations as a result of fixed charge screening. For X1000P, t_{Na^+} is practically constant (0.375±0.004, mean±sd) for the whole concentration range. X1000C and the ETFE/RC70PP control sample present an electronegative character at the lowest salt concentrations. Taken together these results complement the EIS results. At low salt concentrations X400C and X1000C have more effective charges (lower electrical resistance) as compared to X400P and X1000P. At salt concentrations above 0.05 M the electrical charges are effectively screened and the gels are unable to modify ion flux and the transport numbers approach the solution value. This is in contrast to the active layer of reverse osmosis (RO) membranes under similar conditions where t_{Na^+} values between 0.65 and 0.8 have been reported [13, 26]. Thus the gels do not seem to present a limiting step in terms of ionic permeability.

Salt and water diffusional permeabilities

In order to quantify hydrogel permeability we determined the salt and water diffusional permeabilities. Fick's first law relates the diffusive flux, J_s to the diffusional salt permeability, P_s, and a concentration gradient $\Delta c = c_f - c_r$, where c_f and c_r are the feed and receiving concentrations respectively, across a permeable system under steady-state condition:

$$J_s = \frac{1}{A}\frac{dn}{dt} = P_s\left(c_f - c_r\right) = P_s\Delta c \qquad (5)$$

where dn represents the molar mass crossing the permeable area A during the time dt. As $dc=dn/dV$ where dV represents the volume change during dt associated with the transport of dn, Eq. (5) can be expressed as:

$$\frac{dc_r}{c_f - c_r} = \frac{A}{V_r} P_s dt \tag{6}$$

where V_r is the volume of the receiving solution.

Mass conservation then leads to the following expression [27, 28]:

$$\ln\left(1 - \frac{2c_r(t)}{c^0}\right) = \frac{-2AP_s}{V_r} t \tag{7}$$

where $c_r(t)$ is the concentration as a function of time t in the receiving solution and c^o is the initial concentration in the feed solution. Thus from the linear relation between $\ln\left(1 - 2c_r(t)/c^0\right)$ and t, P_s can be determined for each electrolyte concentration and sample and the results are collected in Fig. 6.

Figure 6around here

Fig. 6 shows P_s values due to diffusive transport in the four samples. Each point was obtained from linear regression (r > 0.99) of the time-dependent concentration changes, where the changes were measured as changes in electrolyte conductivity. Permeability values for the different hydrogels are congruent with the tendency obtained from EIS results; the lower permeability of X400P and X1000P is concordant with their higher electrical resistance, while X400C and X1000C show the opposite behaviour, that is, higher permeabilities and lower electrical resistances. Although P_s for X400C and X1000C shows stronger concentration dependence than P_s for X400P and X1000P we calculated sample average permeabilities, $\langle P_s \rangle$, for the whole range of NaCl concentrations and this is indicated in Table 2. Thus $\langle P_s^{X1000P} \rangle < \langle P_s^{X400P} \rangle < \langle P_s^{X400C} \rangle \approx \langle P_s^{X1000C} \rangle$. $\langle P_s \rangle$ for X1000C and X400C were around $1 \cdot 10^{-7}$ m/s

which is only 3-7 fold less than what has been reported for microfiltration polysulfone (MFPS) membranes with a nominal pore size of 0.2 μm [16] – much larger than the nm size pores for the gels investigated here [11]. This reflects the high water content of the gels. On the other hand X1000P and X400P had $<P_s>$ values less than $3 \cdot 10^{-8}$ m/s – more than tenfold lower than for MFPS membranes reflecting the hydrophobic nature of the photoinitiator used [11].

Table 2 around here

In order to determine if the electrical interactions between the solute (NaCl) and the hydrogel also affected the diffusive water transport, we determined the water diffusive permeability P_w from tritiated water measurements by following a procedure similar to that indicated for NaCl diffusion where the concentration changes were measured as changes in tritium activity. The results are listed in Table 2 and the ranked P_w sequence is: $<P_w^{X1000P}> < <P_w^{X400P}> < <P_w^{X400C}> < <P_w^{X1000C}>$, which agrees well with the diffusional salt permeability results.

CONCLUSION

Complex structures for support/encapsulation of proteins or specific substances consisting of partitioning/gel/support have been electrochemically characterized by different *in situ* and/or "working conditions" measurements such as electrochemical impedance spectroscopy, concentration potential and salt and water diffusional permeability, which gives qualitative and quantitative information on electrical and structural characteristics of the gels. Photoinitiated hydrogels had a lower salt and water diffusional permeability compared to chemically initiated hydrogels The results show that hydrogels provide a nanoporous support material with sufficient salt and water permeability to be suitable for encapsulation of biomimetic membranes.

ACKNOWLEDGEMENTS

This work was supported through MEMBAQ, a Specific Targeted Research Project (STREP), by the European Commission under the Sixth Framework Programme (NMP4-CT-2006-033234), by the Danish National Advanced Technology Foundation (023-2007-1) and by a grant to QuP from the Danish National Research Foundation.

REFERENCES

[1] O. Wichterle, D. Lim, *Nature* **1960**, *185*, 117-118.
[2] M. Dreifus, O. Wichterle, D. Lim, *Cesk Oftalmol* **1960**, *16*, 154-159.
[3] J. Kopocek, J. Yang, *Polymer International* **2007**, *56*, 1078-1098.
[4] S. R. Van Tomme, G. Storm, W. E. Hennink, *Int J Pharm* **2008**, *355*, 1-18.
[5] N. A. Peppas, Y. Huang, M. Torres-Lugo, J. H. Ward, J. Zhang, *Annu Rev Biomed Eng* **2000**, *2*, 9-29.
[6] N. A. Peppas, P. Bures, W. Leobandung, H. Ichikawa, *Eur J Pharm Biopharm* **2000**, *50*, 27-46.
[7] S. Löfås, B. J. Johnsson, *Chem. Soc. Chem. Commun.* **1990**, 1526-1528.
[8] G. Justin, S. Finley, A. R. Abdur Rahman, A. Guiseppi-Elie, *Biomed Microdevices* **2009**, *11*, 103-115.
[9] T. J. Jeon, N. Malmstadt, J. J. Schmidt, *J Am Chem Soc* **2006**, *128*, 42-43.
[10] C. H. Nielsen, *Anal Bioanal Chem* **2009**, *395*, 697-718.
[11] S. Ibragimova, K. B. Stibius, P. Szewczykowski, M. Perry, H. Bohr, C. H. Nielsen, *Polym. Adv. Technol.* **2009**, (submitted).
[12] J. R. Macdonald, *Impedance spectroscopy*, Wiley, **1987**.
[13] J. Benavente, J. M. Garcia, J. G. d. l. Campa, J. d. Abajo, *J.Mem.Sci.* **1996**, *114*, 51-57.
[14] J. Benavente, A. Canas, M. J. Ariza, A. E. Lozano, J. d. Abajo, *Solid State Ionics* **2001**, *145*, 53-60.
[15] C. Torras, X. Zhang, R. Garcia-Valls, J. Benavente, *J.Mem.Sci.* **2007**, *297*, 130-140.
[16] R. d. Lara, J. Benavente, *J. Coll.Int.Sci.* **2007**, *310*, 519-528.
[17] J. Benavente, G. Jonsson, *Desalination* **2006**, *200*, 364-366.
[18] J. Vogel, M. E. Perry, J. S. Hansen, P.-Y. Bollinger, C. H. Nielsen, O. Geschke, *J. Micromech. Microeng.* **2009**, *19*, 025026.
[19] J. S. Hansen, M. E. Perry, J. Vogel, T. Vissing, O. Geschke, J. Emneus, C. H. Nielsen, *J. Micromech. Microeng.* **2009**, *19*, 025014.
[20] J. S. Hansen, M. Perry, J. Vogel, J. Groth, T. Vissing, M. Larsen, O. Geschke, J. Emneus, H. Bohr, C. H. Nielsen, *Anal Bioanal Chem* **2009**, *395*, 719-727.
[21] J. Benavente, A. Munoz, A. Heredia, *Solid State Ionics* **1997**, *97*, 89-95.
[22] R. P. Buck, *Electroanalytical chemistry of membranes*, CRC Press, **1976**.
[23] B. A. Boukamp, *Solid State Ionics* **1986**, *18-19*, 136-140.
[24] M. Ladd, *Introduction to physical chemistry*, Cambridge University Press, Cambridge, **1998**.
[25] N. Laksimarayanahia, *Transport phenomena in membranes*, Academic Press, New York, **1969**.
[26] G. Jonsson, J. Benavente, *J.Mem.Sci.* **1992**, *69*, 29-42.
[27] G. M. Zentner, J. R. Cardinal, J. Feijen, S. Z. Song, *J Pharm Sci* **1979**, *68*, 970-975.
[28] D. L. Gilbert, T. Okano, T. Miyata, S. Wan Kim, *Int J Pharm* **1988**, *47*, 79-88.

FIGURE LEGENDS

Figure 1. Cross-sectional representation of the hydrogel sandwich sample. Hydrogels (grey) are sandwiched between the perforated ETFE partition (black) and the DSS-RC70PP membrane (white). The *cis* side is the feed side with NaCl concentration c_f and the *trans* side is the receiving side with NaCl concentration c_r. For all experiments concentration gradients were directed *cis* → *trans*.

Figure 2. Impedance diagrams of the DSS-RC70PP/ETFE support in contact with NaCl solution (c=0.002 M) (□) and NaCl solution alone (×). **(a):** Nyquist plot, **(b):** Bode plot.

Figure 3. Impedance diagrams of the DSS-RC70PP/hydrogel/ETFE support in contact with NaCl solution (c=0.002 M). Hydrogels: X400P (▼), X1000P (▲), X400C (○) and X1000C (▷). **(a):** Nyquist plot, **(b):** Bode plot.

Figure 4. Electrical resistance R **(a)** and capacitance C **(b)** as function of NaCl concentration (c_{NaCl}) for the four DSS-RC70PP/hydrogel/ETFE samples. Hydrogels: X400P (▼), X1000P (▲), X400C (○), X1000C (▷), and NaCl solution alone (×).

Figure 5. Sodium transport number for the four DSS-RC70PP/hydrogel/ETFE samples as a function of average NaCl activity $\langle a_{NaCl} \rangle$. Hydrogels: X400P (▼), X1000P (▲), X400C (○), X1000C (▷), and DSS-RC70PP/ETFE sandwich alone (×). The dotted horizontal line indicates the Na^+ transport number in solution $t_{Na+}^{o} = 0.385$.

Figure 6. Diffusional salt permeability P_s as a function of NaCl concentration (c_{NaCl}) for the four DSS-RC70PP/hydrogel/ETFE samples. Hydrogels: X400P (▼), X1000P (▲), X400C (○), X1000C (▷).

TABLES

Sample	Polymer	Initiator
X400P	PEG-400-DA 100 mM	Darocur 5 mM
X400C		TEMED 15 mM APS 15 mM
X1000P	PEG-1000-DMA 65 mM	Darocur 5 mM
X1000C		TEMED 10 mM APS 10 mM

Table 1. The four hydrogels investigated. For details see the previous paper [11].

Sample	**X400P**	**X400C**	**X1000P**	**X1000C**
$\langle P_s \rangle$ m/s	$(3.3 \pm 1.3)\times10^{-8}$	$(9.5 \pm 1.0)10^{-8}$	$(1.6 \pm 0.4)10^{-8}$	$(9.6 \pm 2.0)10^{-8}$
P_w^s m/s	3.0×10^{-8}	5.3×10^{-8}	1.2×10^{-8}	9.8×10^{-8}

Table 2: Average NaCl diffusional permeability, $\langle P_s \rangle$, and water permeability, P_w, across the four hydrogel samples.

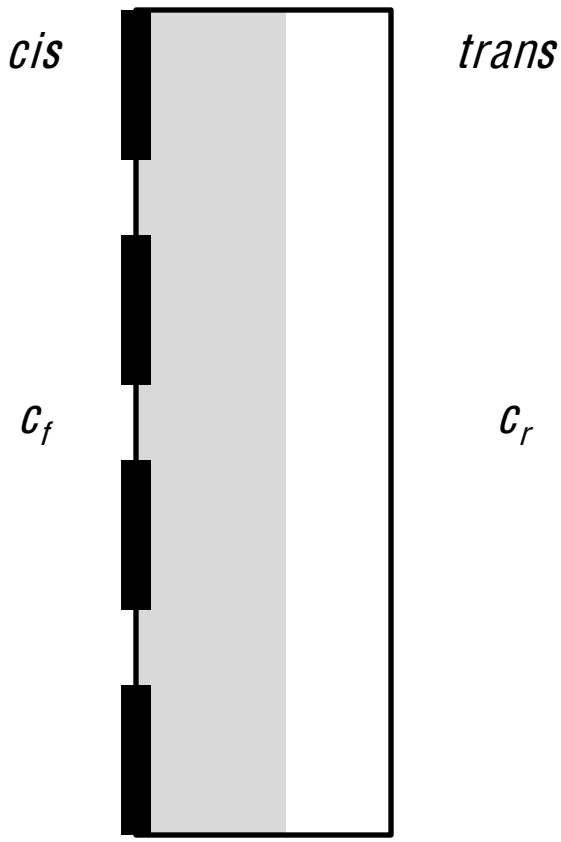

Pelaez et al. Figure 1

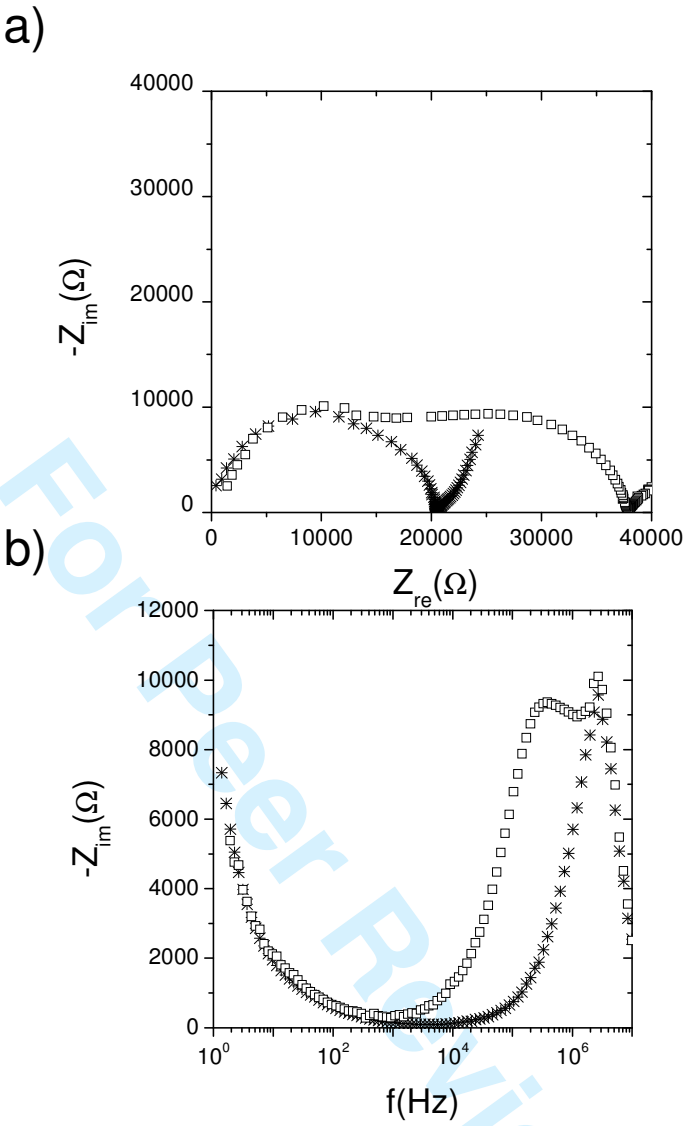

Pelaez et al. Figure 2

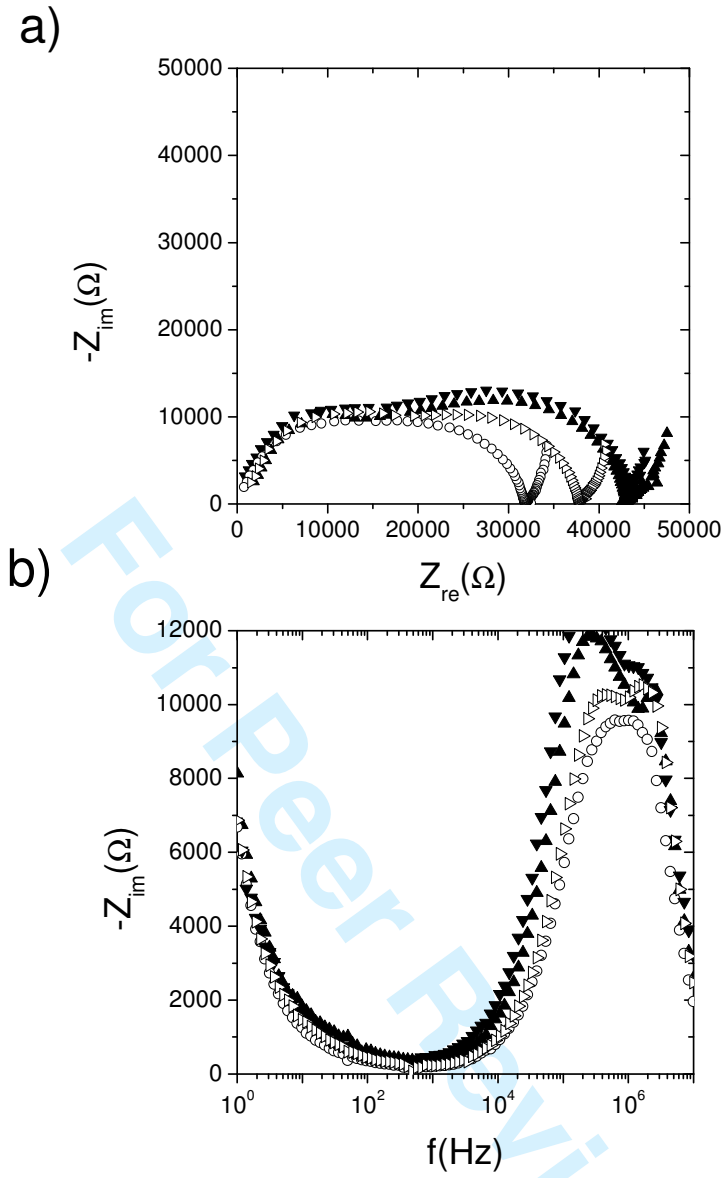

Pelaez et al. Figure 3

a)

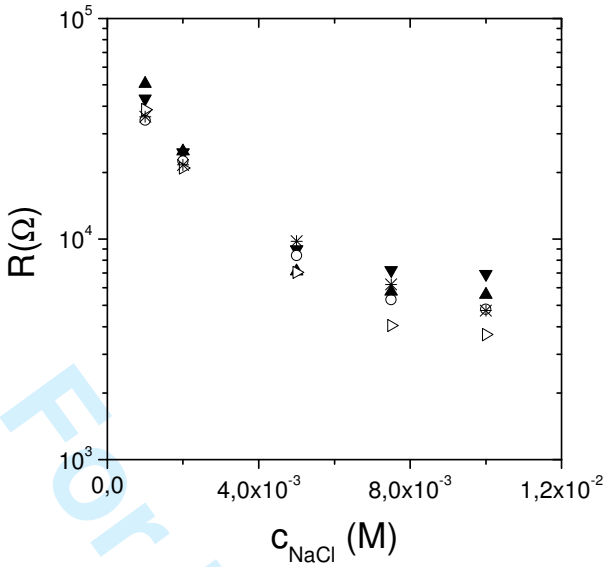

b)

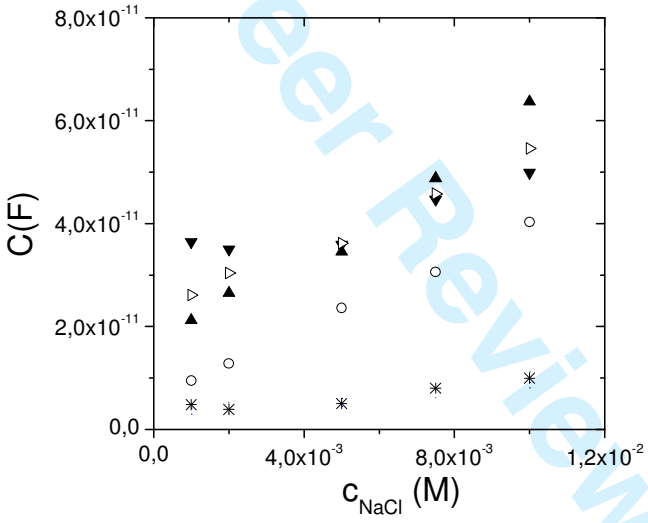

Pelaez et al. Figure 4

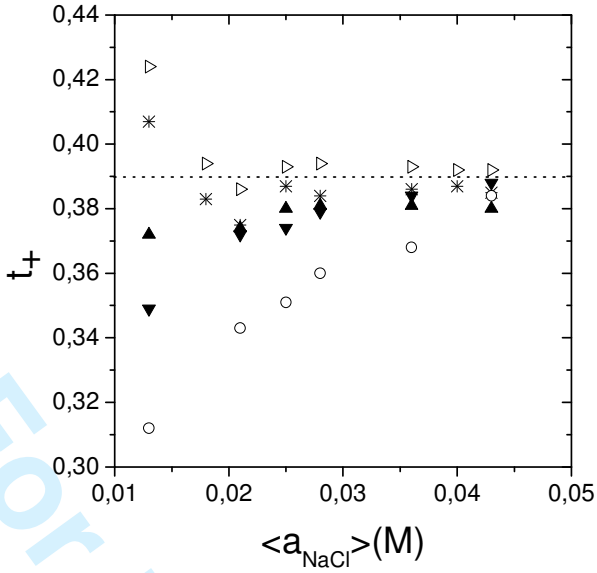

Pelaez et al. Figure 5

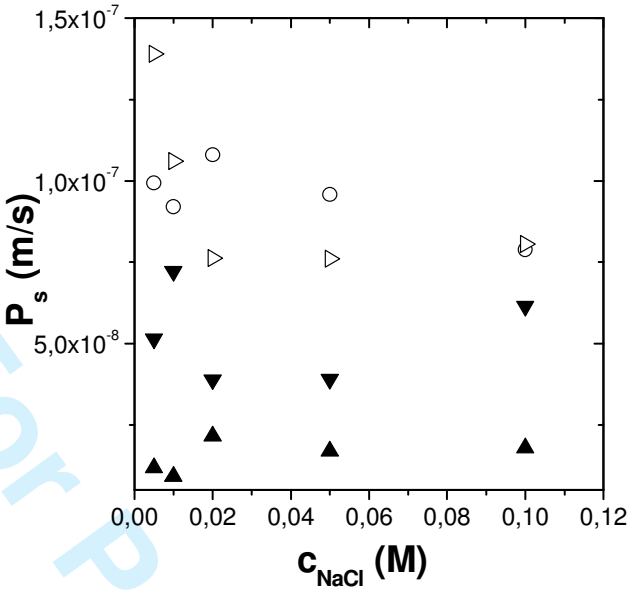

Pelaez et al. Figure 6

Appendix II

OPEN ACCESS Freely available online

PLoS one

Structure and Stability of the Spinach Aquaporin SoPIP2;1 in Detergent Micelles and Lipid Membranes

Inés Plasencia[1]*, Sabeen Survery[2], Sania Ibragimova[3,5], Jesper S. Hansen[4,5], Per Kjellbom[2], Claus Helix-Nielsen[3,5], Urban Johanson[2], Ole G. Mouritsen[1]

1 Department of Physics and Chemistry, MEMPHYS-Center for Biomembrane Physics, University of Southern Denmark, Odense, Denmark, **2** Department of Biochemistry and Structural Biology, Center for Molecular Protein Science, Lund University, Lund, Sweden, **3** DTU Physics, Technical University of Denmark, Lyngby, Denmark, **4** DTU Nanotech, Technical University of Denmark, Lyngby, Denmark, **5** Aquaporin A/S, Copenhagen, Denmark

Abstract

Background: SoPIP2;1 constitutes one of the major integral proteins in spinach leaf plasma membranes and belongs to the aquaporin family. SoPIP2;1 is a highly permeable and selective water channel that has been successfully overexpressed and purified with high yields. In order to optimize reconstitution of the purified protein into biomimetic systems, we have here for the first time characterized the structural stability of SoPIP2;1.

Methodology/Principal Finding: We have characterized the protein structural stability after purification and after reconstitution into detergent micelles and proteoliposomes using circular dichroism and fluorescence spectroscopy techniques. The structure of SoPIP2;1 was analyzed either with the protein solubilized with octyl-β-D-glucopyranoside (OG) or reconstituted into lipid membranes formed by *E. coli* lipids, diphytanoylphosphatidylcholine (DPhPC), or reconstituted into lipid membranes formed from mixtures of 1-palmitoyl-2-oleoyl-phosphatidylcholine (POPE), 1-palmitoyl-2oleoyl-phosphatidylethanolamine (POPE), 1-palmitoyl-2-oleoyl-phosphatidylserine (POPS), and ergosterol. Generally, SoPIP2;1 secondary structure was found to be predominantly α-helical in accordance with crystallographic data. The protein has a high thermal structural stability in detergent solutions, with an irreversible thermal unfolding occurring at a melting temperature of 58°C. Incorporation of the protein into lipid membranes increases the structural stability as evidenced by an increased melting temperature of up to 70°C.

Conclusion/Significance: The results of this study provide insights into SoPIP2;1 stability in various host membranes and suggest suitable choices of detergent and lipid composition for reconstitution of SoPIP2;1 into biomimetic membranes for biotechnological applications.

Citation: Plasencia I, Survery S, Ibragimova S, Hansen JS, Kjellbom P, et al. (2011) Structure and Stability of the Spinach Aquaporin SoPIP2;1 in Detergent Micelles and Lipid Membranes. PLoS ONE 6(2): e14674. doi:10.1371/journal.pone.0014674

Editor: Maria Moran, Hospital 12 Octubre Madrid, Spain

Received July 2, 2010; **Accepted** December 23, 2010; **Published** February 14, 2011

Funding: This study has been undertaken in the MEMBAQ project (Incorporation of Aquaporins in Membranes for Industrial Applications) supported by the Sixth European Research Framework Programme under contract [NMP4-CT-2006-033234] and the Danish National Advanced Technology Foundation (Industrial biomimetic water membranes) under contract [023-2007-1]. MEMPHYS-Center for Biomembrane Physics is supported by the Danish National Research Foundation. Financial support was also provided by Formas and the Swedish Research Council (VR). The funding agencies had no role in study design, data collection and analysis, decision to publish or preparation of the manuscript.

Competing Interests: The authors have declared that no competing interests exist.

* E-mail: miplsen@memphys.sdu.dk

Introduction

MIPs (major intrinsic proteins) are found in eubacteria, archae, fungi, plants and animals [1]. According to substrate specificity, MIPs are mainly classified into AQPs (aquaporins - or water channels) if they are only permeable to water, or GLPs (aquaglyceroporins - or glycerol-uptake facilitators) if they also facilitate passive diffusion of small solutes such as glycerol or urea [2,3]. In addition, a structural role in the formation of cell junctions has been described for some MIPs [4].

Most members of the aquaporin super family have molecular masses, ranging from 25 to 31 kDa. The three-dimensional structures of several MIPs have been determined [5–7], and the quaternary structures of the proteins reveal that they all form homotetramers where each monomer acts as a functional unit [2]. Based on sequence similarity, the functional unit of all members in this family are predicted to have six hydrophobic, membrane-spanning α-helices connected by five loops of variable length that delimit a polar channel with two wide vestibules and a narrow pore [8,9]. Two of the connecting loops, namely B and E, interact with each other from opposite sides through two highly conserved NPA (Asn-Pro-Ala) motifs forming a seventh transmembrane region that contributes to the pore region [10]. Highly conserved residues that stabilize the structure are found in the helices, e.g. the transmembrane helix-helix packing motif GXXXG [11], as well as conserved polar and charged buried residues that have been proposed to form hydrogen bonds and ion pairs [12].

Plants encode a very large and diverse MIP family. They have been classified into at least five subfamilies in higher plants: plasma membranes intrinsic proteins (PIPs), tonoplast intrinsic proteins (TIPs), the small basic intrinsic proteins (SIPs), NOD26-like intrinsic proteins (NIPs), and the recently discovered X intrinsic

protein (XIPs) [13,14]. PIPs form the most highly conserved subfamily in plants and are further divided into two groups named PIP1 and PIP2 [15]. In addition to several single amino acid residue substitutions, PIP2s are characterized by a short N-terminal and a longer C-terminal relative to PIP1s [16]. Moreover, differences are found in the water transport activity in oocytes where PIP2s are more active than PIP1s [16]. It has been suggested that PIP2s are specific for water, whereas PIP1s have been reported to facilitate the transport of solutes such as glycerol, boric acid, urea, and carbon dioxide in addition to water [17–19].

The spinach (*Spinacia oleracea*) genome contains at least three PIP1 and four PIP2 genes [20]. Recently, a new nomenclature which reflects the phylogenetic classification of plants MIP genes and proteins has been adopted [14]. In accordance with this nomenclature, the spinach PIPs PM28A, PM28B and PM28C have been renamed SoPIP2;1, SoPIP1;1 and SoPIP1;2, respectively. SoPIP2;1 can be overexpressed and purified with high yields [21] and its structure has been solved with Angstrom resolution [5,22]. However, the structural stability parameters of SoPIP2;1 have not been examined neither when solubilized by detergents nor after the protein reconstitution into membranes subsequent to the heterologous expression.

Due to the fact that the transport characteristics of SoPIP2;1 is well described (e.g. from protein reconstitution into oocytes and *E. coli* membranes [23]) it is a good candidate for being used in technological applications, and the high selectivity and water permeability of SoPIP2;1 makes it particularly interesting for a biomimetic water filtration technology. AQP mediated water transport is a prominent example of how Nature itself has developed an effective mechanism for purifying water, and many technologies based on biomimetic membrane transport is now attracting considerable interest (for a review see [24]). However, successful reconstitution and stabilization of functional proteins in biomimetic membranes depends on suitable choices of both detergent and host lipid membrane components.

Detergents are commonly used to solubilize membrane proteins, and many membrane proteins have been solubilized with various detergents without the loss of biological activity [25]. Sugar-based detergents and poly(oxyethylen)-based detergents are at presently the most commonly used. In the particular case of SoPIP2;1 different detergents like octyl-β-D-thioglucopyranide (OTG) and octyl-β-D-glucopyranoside (OG) have been used. We encountered problems with protein stability using OTG, presumably related to the low solubility of OTG at low temperatures, leading to aggregation of the protein under these conditions. Consequently we performed our work using OG micelles where no stability problems occurred with any of the preparations used in this work.

One of the major challenges in designing biomimetic systems based on integral membrane proteins is the reconstitution of the proteins into the membrane. A common strategy involves the incorporation of detergent solubilized proteins into vesicles followed by detergent extraction. The detergent-free vesicles are then fused with a receiving membrane. Typical lipid species for fusogenic vesicles are palmitoyl-oleoyl-phosphatidylethanolamine (POPE) -phosphatidylcholine (POPC) and -phosphatidylserine (POPS) lipids supplied with sterols e.g. ergosterol [26]. Other common lipids for biomimetic membranes are *E. coli* lipid extracts and diphytanoylphosphatidylcholine (DPhPC). In this study we examine SoPIP2;1 stability in four different membrane systems: *E. coli* lipids, DPhPC, POPE: POPC: POPS:ergosterol and POPE: POPC mixtures.

In this paper we present results from an extended secondary and ternary structural characterization of the protein in detergent micelles and in lipid membranes using spectroscopic techniques. Specifically we study the thermal secondary structure stability of SoPIP2;1 when reconstituted in detergent micelles or in lipid membranes using a detailed analysis by Circular Dichroism spectroscopy. In addition we performed Emission Fluorescent spectroscopy analysis of the six tryptophan (Trp) amino acids present in the primary sequence of SoPIP2;1 in order to obtain information about the thermal ternary structure stability of the protein.

Results

First we characterize the folding patterns for SoPIP2;1 in detergent and lipid. Then we characterized the thermal stability of SoPIP2;1 secondary and tertiary structure.

SoPIP2;1 α-helical content in different systems

The far-UV CD spectra of SoPIP2;1 dissolved in PBS with 1% OG display the characteristics of a predominantly α-helical protein with negative bands around 209 nm and 222 nm (Figure 1, full line). The deconvolution analysis reported a α-helix content of 63% (Table 1). This value matches perfectly with the one obtained after the analysis of the PDB file 1Z98 from the X-ray diffraction data of this protein [22]. Although light scattering tend to flatten out the CD spectra obtained from protein in lipid vesicles making a direct comparison to micelles difficult, the characteristic α-helical structure for aquaporins is rather well preserved when the SoPIP2;1 is reconstituted in lipid complex membranes of *E. coli* lipids (Figure 1 and Table 1). This is consistent with previous results demonstrating protein activity (water flux) regardless if SoPIP2;1 is purified in OTG [21] or OG (unpublished results, J.S. Hansen). Other aquaporins have also been successfully reconstituted in *E. coli* lipid membranes [27,28].

We then tested whether SoPIP2;1 could be reconstituted in DPhPC membranes as DPhPC is generally recognized as forming stable black lipid membranes [29–31], making this lipid, in principle, suitable for being used in the design of water-filtration systems. However our CD analysis of the SoPIP2;1-DPhPC mixture suggested that this lipid does not preserve the structure of this protein. Although spectra could be obtained (see Figure 1) reproducibility was low for SoPIP2;1-DPhPC mixtures. White precipitate particles were commonly observed during the reconstitution process which may be directly related to the apparition of denatured protein aggregates. The aggregation of the protein in DPhPC could be related to the difficulties encountered in forming liposomes even when extrusion methods were used. Also dynamic light scattering analysis of the DPhPC suspension reported very broad structural features. Specimens with diameters ranging from 51 to 2669 nm (range of the diameters taken from the calculated

Table 1. Summary of the SoPIP2;1 secondary structure results.

	%			
	α-Helix	**β-sheet**	**Turns**	**Random**
OG micelles	63	20	3	15
***E. coli* lipid**	61	17	7	16
POPE:POPC:POPS:Ergosterol	48	25	6	18
POPE:POPC	43	27	9	21
DPhPC	42	30	7	21

doi:10.1371/journal.pone.0014674.t001

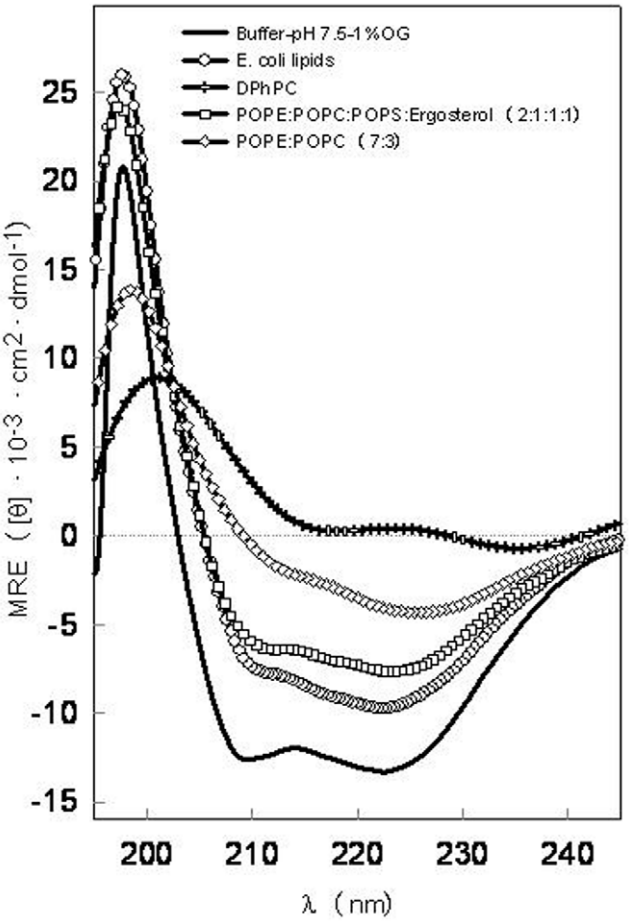

Figure 1. Far-UV CD spectra of SoPIP2;1. The measurements were obtained at 20°C in phosphate buffer, pH 7.5, NaCl 150 mM containing 1% OG and in different lipid membranes.
doi:10.1371/journal.pone.0014674.g001

Gaussian distribution of the sizes between 10% and 90% of the total distribution) were found in the same sample. The polydispersity index was 0.308, confirming a high liposome structural heterogeneity. These results suggest that this lipid does not provide a good membrane environment for a successful and stable SoPIP2;1 membrane incorporation. Hence, we exclude DPhPC bilayers as a host lipid membrane for SoPIP2;1.

We then examined POPE:POPC:POPS:Ergosterol (2:1:1:1 molar ratio) as this mixture has been shown to be as a good fusogenic lipid mixture [32] applicable for the further incorporation of aquaporins into industrial membrane water-filtration systems. The CD spectrum from SoPIP2;1/POPE:POPC:POPS:Ergosterol mixture does not look very different from the one obtained when the protein is reconstituted into *E. coli* lipid membranes (Figure 1). However, the α-helical content reported after the deconvolution analysis is lower (Table 1) and associated with an increase in the β-sheet content and the other analyzed structures. The spectra obtained with another suitable fusogenic lipid mixture, POPE:POPC (7:3 molar ratio), showed even less helical-like spectra although the deconvolution results report values similar to those obtained with the more complex fusogenic mixture (Figure 1 and Table 1).

Taken together we conclude that the best lipid system identified for the reconstitution of SoPIP2;1 is *E. coli* lipid membranes, followed by POPE:POPC:POPS:Ergosterol and POPE:POPC. In contrast DPhPC was found not to be suitable for the SoPIP2;1 membrane reconstitution.

Thermal stability of SoPIP2;1 secondary structure

One method to characterize the unfolding process of a protein is to study the effect of temperature changes on its structure. This provides important information about the conformational stability of protein. The thermal stability of SoPIP2;1 was found to differ between detergent micelles and the different lipid species studied here, as evidenced by CD spectroscopy (Figure 2). The changes in the secondary structure spectra associated with temperature increase was found to be larger for the protein reconstituted into detergent micelles (Figure 2, A) compared to *E. coli* lipids (Figure 2, B), the POPE:POPC:POPS:Ergosterol mixture (Figure 2, C) and the POPE:POPC mixture (Figure 2, D).

A summary of the results can be found in Figure 3 for the thermal stability of the secondary structure where the Mean residue ellipticity (MRE) at 222 nm were plotted as a function of the temperature for all systems studied. The different MRE values at 20°C (initial state) demonstrate that the protein is structured or interacting in different ways with the different detergents or lipids used. Therefore it can be assumed that the protein acquires different structural initial states as quantified by the deconvolution analyses in the different environments tested (Table 1). The SoPIP2;1 structure is more sensitive to the temperature changes when it is reconstituted into detergent micelles than when it is reconstituted into lipid membrane systems. Although the unfolding transition is not reversible, the transition midpoint can be used to quantify the thermal stability of the protein [33].

The variation of MRE 222 nm with increasing temperature shows that the protein in detergent micelles solution has a melting temperature around 58°C. The decreasing temperature ramp measurement failed to report the same initial state (data not shown), indicating an irreversible unfolding of the protein under these conditions. A white precipitate in the sample after incubation at the melting temperature was observed probably caused by the presence of unfolded protein aggregates that precipitated at the bottom of the sample cuvette. Thus the structural stability of the protein can be maintained up to 50°C. The melting temperature value around 58°C was also confirmed by SDS-PAGE (Figure 4). Presence of monomers and dimer bands can be observed at temperatures below 58°C but these bands disappear at higher temperatures and aggregated protein was retained in the well. Bands corresponding to complexes larger than the tetrameric protein are visible between 55 and 60°C.

Protein reconstitution in complex membranes lipid mixtures (*E. coli* or POPE:POPC:POPS:Ergosterol) increases the stability of SoPIP2;1 against temperature changes in the system. The spectra of the protein reconstituted in these membranes exhibited a different behavior in response to the temperature increase compared to the protein reconstituted in detergent-micelles (Figure 2). In this case of reconstitution in membrane lipid mixtures, only minor changes were observed in the spectra and appeared first above 70°C. This is clearly evident in the MRE 222 nm value representation (Figure 3).

Thermal stability of SoPIP2;1 tertiary structure

SoPIP2;1 contains six tryptophan (Trp) residues in the primary sequence. These residues can be used as intrinsic fluorophores for analyzing the protein ternary structure (see the cartoon in Figure 5A) as the Trp fluorescence emission spectrum is sensitive to both the polarity and the dynamics of the environment surrounding the aromatic side chain. Therefore, the variation in the Trp fluorescence emission spectra reports changes in tertiary

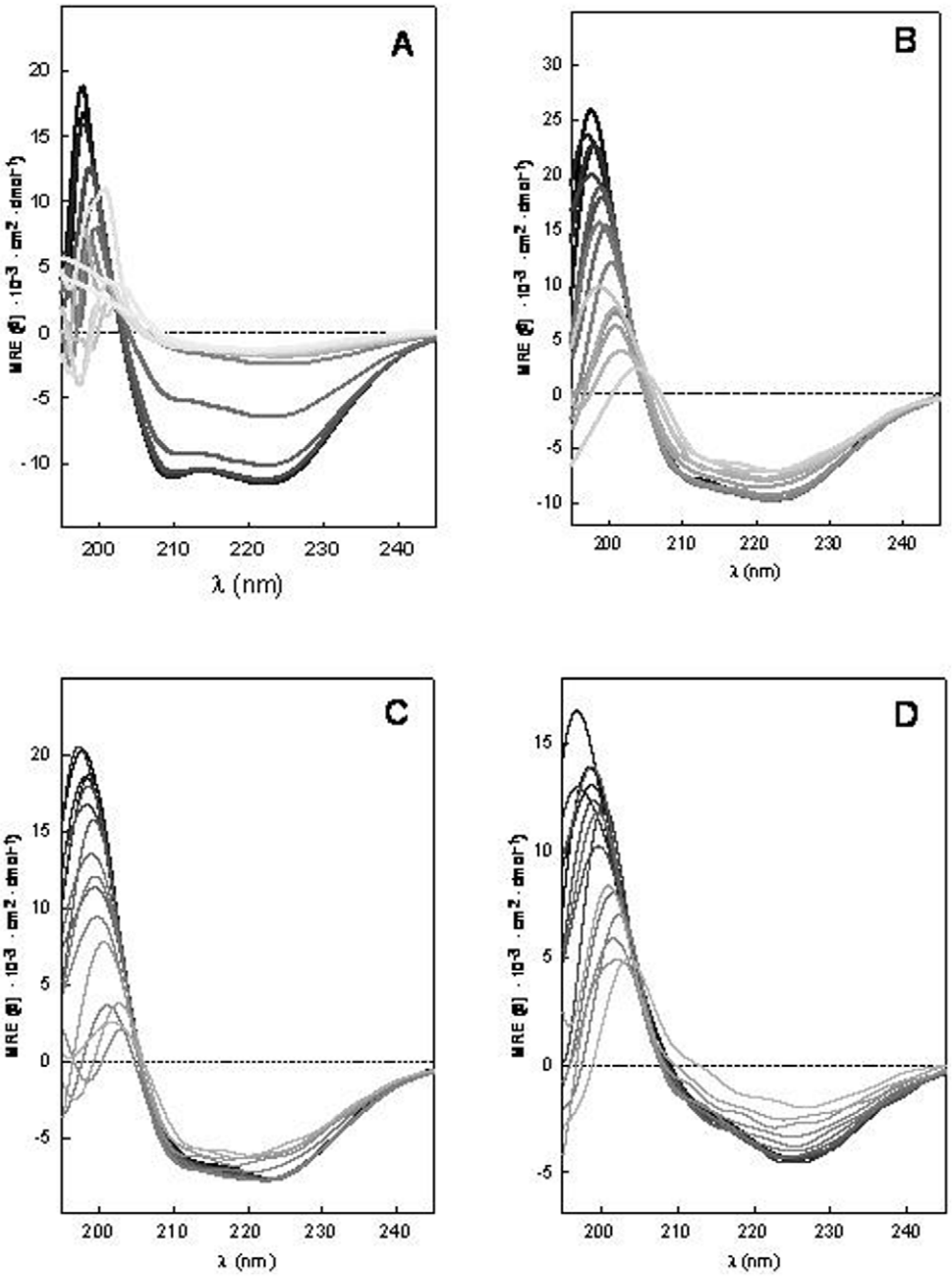

Figure 2. Thermal unfolding of the secondary structure of SoPIP2;1. Protein was reconstituted in A) OG micelles, B) *E. coli* lipid membranes, C) POPE:POPC:POPS:Ergosterol membranes and D) POPE:POPC membranes. Temperatures are represented by the grayscale colors from black, 20°C to very light gray, 95°C.
doi:10.1371/journal.pone.0014674.g002

structure of the protein. Thus the Trp is generally blue-shifted from 350 nm in environments of low polarity such as the hydrophobic interior of a protein or in a lipid membrane environment and Trp fluorescence in proteins has been classified into five classes by Reshetnyak et al. [34]. According to this classification, the dominant fluorescence around 329 nm corresponds to a class of Trp side chains that are in a relatively non-polar environment and H-bonded in an 2:1 exciplex that fluoresces at 331 nm [34]. Inspection of the three-dimensional structure of SoPIP2;1 indicated that the Trps of this protein are positioned close to the surface of the protein (see cartoon i in Figure 5A) [22]. SoPIP2;1 reconstituted into detergent-micelles exhibited a maximum fluorescence at 330 nm indicating that the region of the protein where the Trps are located is positioned at the edge of the detergent micelles thereby facilitating the contacts between Trps and water molecules (see cartoon ii in Figure 5A and experimental results in Figure 5B). The easier accessibility of the water to the Trp environment is due to the loosely packed hydrophobic tails of the detergents interacting with the protein in detergent-micelles. A shift to lower wavelength values was always observed when the protein was reconstituted into lipid membranes (representative spectra showed with the *E. coli* membranes in Figure 5B). It demonstrates that the lipid membrane environment offers a more extensive hydrophobic surface for interaction with

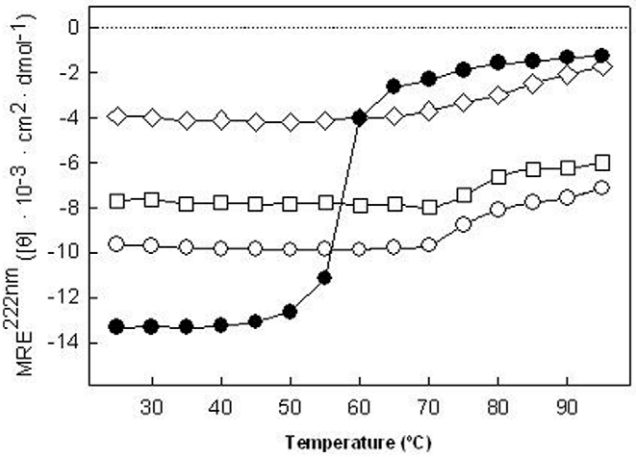

Figure 3. MRE at 222 nm as a function of temperature. SoPIP2;1 in OG micelles (●), *E. coli* lipid membranes (□), POPE:POPC:POPS:Ergosterol (o) and POPE:POPC (◇).
doi:10.1371/journal.pone.0014674.g003

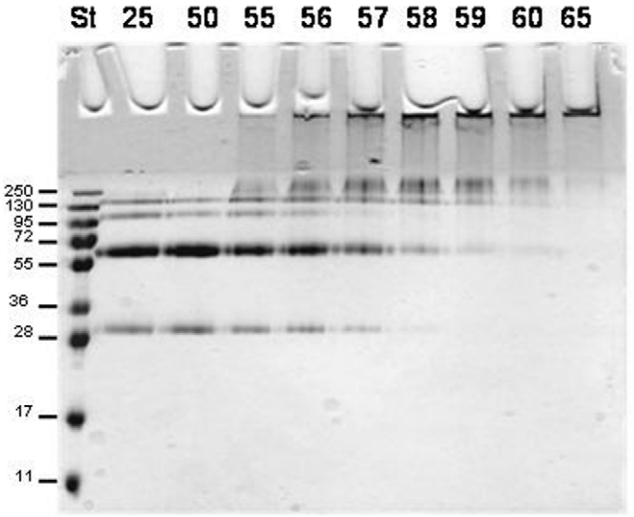

Figure 4. Thermal denaturation of SoPIP2;1. It can be visualized by SDS-PAGE since large aggregates are formed that cannot enter the gel. After incubation at room temperature the normal bands corresponding to monomeric, dimeric, trimeric and tetrameric SoPIP2;1 are evident. No aggregates were found at 50°C whereas at the melting point, 58°C, as determined by CD, part of the protein was aggregated. At 65°C the aggregation was complete. The samples were incubated at the indicated temperatures (25–65°C) for 10 minutes before sample loading buffer was added followed by 10 minutes incubation at room temperature. St, standard with indicated Mw in kDa in the left side of the gel.
doi:10.1371/journal.pone.0014674.g004

the transmembrane protein (cartoon iii in figure 5A). It is also consistent with the higher temperature stability exhibited by the protein in the membrane systems. Thermal stability of the protein was also monitored by following the Trp fluorescence vs. increasing temperature. The Trp fluorescence was quenched at higher temperatures while the wavelength at which maximum emission took place was not affected significantly (Figure 5B and 6).

For transmembrane proteins two components are generally contributing to a higher water access to the Trp location. One is the fluidity of the micelles or membranes and the other is the progressive unfolding of the protein. In case of detergent micelles, the effect of possible micelle fluidity is not very high. The protein reconstituted into micelle solution exhibited a very similar profile to the protein unfolding analyzed by CD. In this situation the principal transition occur around 58°C (Figure 6). When the protein is reconstituted in lipid membranes the profile is more complex with more than one transition indicating the contribution of both components to the final state (Figure 6). The first transition may reflect a change in the lipids that allows water to access the Trp environment without any structural change in the protein. In any case the steeper slope, likely to be related to the protein unfolding, occurs around 70°C correlating well with the data obtained by CD spectroscopy.

Discussion

The structural stability of the protein is important as a precedent for good functionality after reconstitution. Here we used CD spectroscopy as an effective and fast tool for testing the structural properties of SoPIP2;1 and its stability in different environments. CD spectroscopy has already been used with many other proteins and it has been used for determining the melting temperature of proteins [33,35,36].

A high-resolution X-ray structure (PDB data 1Z98) has been published for untagged SoPIP2;1 [22], but the structural stability properties of SoPIP2;1 have never before been studied after overexpression and reconstitution into different membrane or membrane-like environments. A helical content of 60% was reported in the 1Z98 SoPIP2;1 crystallographic structure. However, the helical content determination is not complete as 1Z98 does not report the first 23 and the last 7 residues of the protein. Our CD measurements of His-tagged SoPIP2;1 in OG micelles, the same detergent also used to solubilize the protein for crystalization, showed a 63% helical content, a value that matches well with the high resolution structure of SoPIP2;1 demonstrating that CD spectroscopy is a very useful tool for testing the secondary structure stability of the protein reconstituted in different systems.

Regarding the tetrameric quaternary structure of SoPIP2;1, two mechanisms could explain the results shown in Figure 3: unfolding or dissociation of the tetrameric protein complex. The moderate change in MRE as function of temperature observed when the protein is reconstituted in phospholipid membranes could be related to protein unfolding in a small protein population. Considering that the CD results are giving an average value of the folding pattern this would imply that most of the protein is correctly folded. However, it is also possible that the change in MRE is due to dissociation of the aquaporin tetrameric complexes. In that case also monomers and dimers may occur in the membrane at higher temperatures giving rise to the changes in MRE as observed.

The information obtained by CD was also validated with Trp fluorescence emission. These measurements provided information about the protein tertiary structure and incorporation into the membrane. Our results revealed that POPE:POPC:POPS:Ergosterol, POPE:POPC and *E. coli* lipids all are appropriate lipid systems for reconstitution of SoPIP2;1 as they supported structural and thermal stability of the protein. The results from the latter system is consistent with the work by Karlsson et al. [21] using stop-flow measurements demonstrating water transport functionality for SoPIP2;1 in *E. coli* lipids. In contrast DPhPC does not provide a suitable host lipid membrane for SoPIP2;1.

It have been suggested that aquaporins exhibit greater stability [37–42] compared to the structurally closely related glycerol facilitators (aquaglyceroporins) [28,43–45]. Galka and collabora-

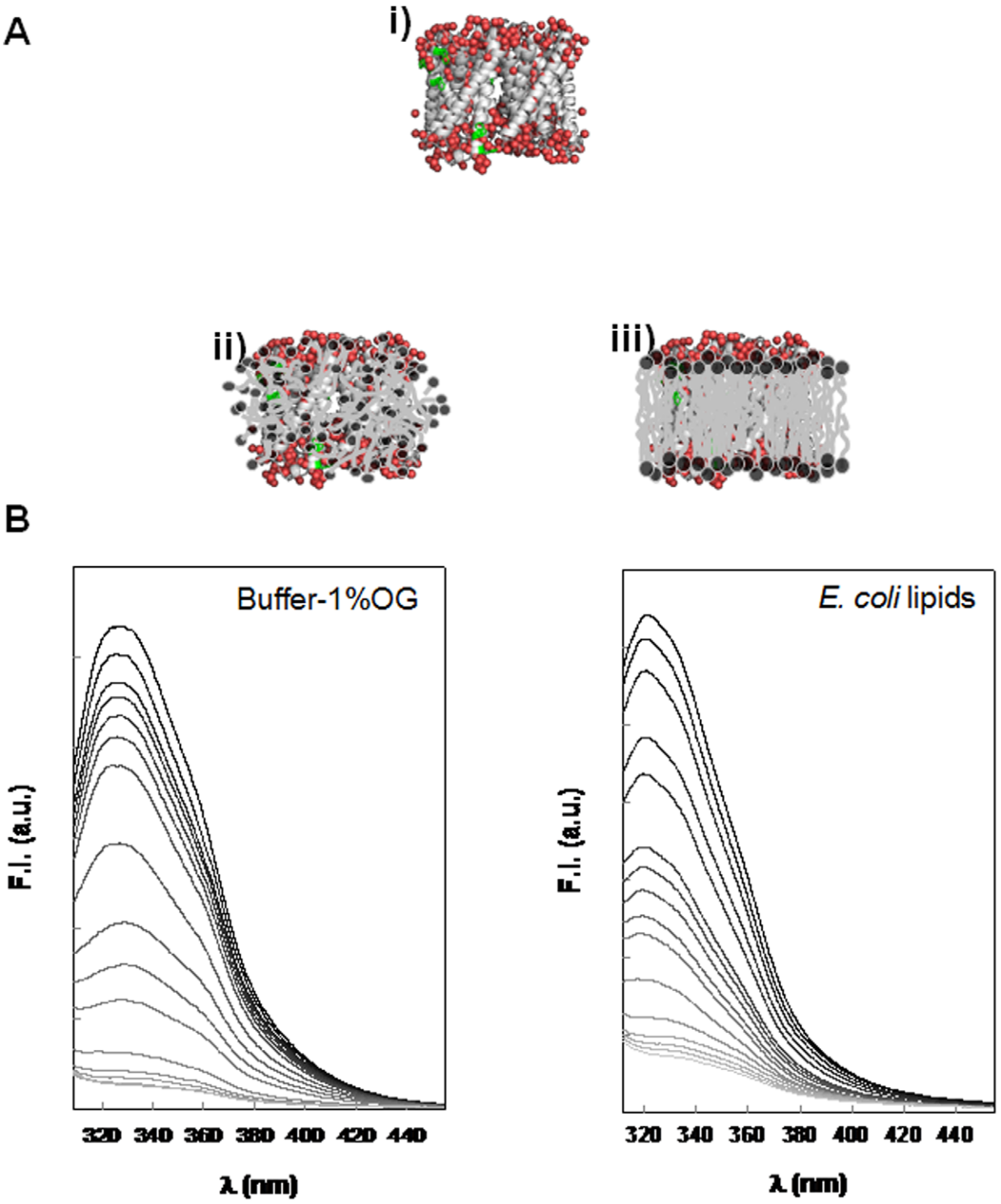

Figure 5. Fluorescence spectroscopy analysis of the protein ternary structure behavior. A) Cartoons illustrating the Trp residues (green) position in the protein ternary structure SoPIP2;1. The structure derives from the PDB file 1Z98 [22] using VMD software is shown in i [50], an illustration of the protein position in detergent micelles in ii and in lipid bilayers in iii. B) Thermal unfolding of SoPIP2;1 monitored by tryptophan fluorescence. To the left, the protein is reconstituted into OG micelles and to the right the protein is reconstituted into *E. coli* lipid membranes. Temperatures are represented by the grayscale colors from black, 20°C to very light gray, 95°C.
doi:10.1371/journal.pone.0014674.g005

tors [36] showed using SDS-PAGE electrophoresis that *E. coli* GlpF aquaglyceroporin has an unfolding temperature of the tetramer around 60°C in detergent solutions of dodecyl β-D-maltoside (DDM). The same temperature was obtained for the tertiary structure monitored by Trp fluorescence [36]. When these authors studied the secondary thermal stability by far-UV CD

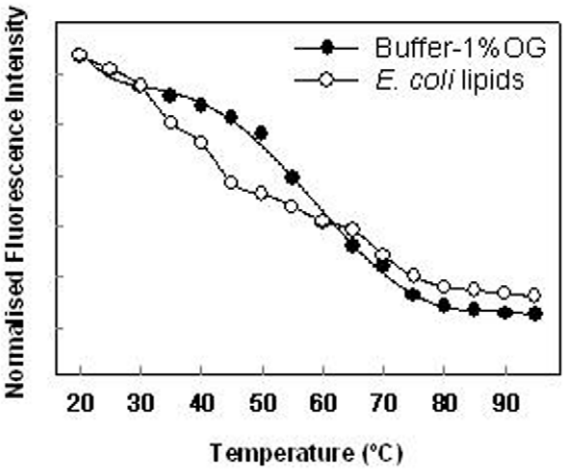

Figure 6. Fluorescence intensity at the maximum of the emission spectra as a function of temperature. The protein reconstituted in detergent micelles show one principal transitions in comparison with the protein reconstituted in lipid membranes where at least three different transitions can be observed. Fluorescence intensity values are normalized to the higher intensity value observed with the protein in micelles suspension at 20°C.
doi:10.1371/journal.pone.0014674.g006

spectroscopy they observed a two-state unfolding transition occurring around 70°C for GlpF in DDM. When GlpF was reconstituted into lysomyristoylphophatidylcholine (LMPC) micelles, the tetramer unfolded around 80°C and the thermal stability of the secondary structure was reported to have a transition temperature of 87°C. Compared with our results obtained for SoPIP2;1, GlpF in LMPC micelles apparently has a higher stability than SoPIP2;1 in OG micelles and phospholipid bilayers. On the other hand SoPIP2;1 reconstituted into the bilayer-forming phospholipid mixtures tested here shows a similar melting temperature as GlpF in DMM. Unfortunately a direct comparison is not possible as we do not have the same GlpF/lipid systems to compare with.

In conclusion we have shown that SoPIP2;1 can exist as a stable folded protein in OG detergent micelles solutions and that the protein can be transferred from detergent micelles solutions and reconstituted into selected phospholipid membranes preserving its structural characteristics. It is likely that more suitable reconstitution systems exist for SoPIP2;1 than those studied in the present work. In order to efficiently test a range of systems, new methods are called for. Presently we are working on developing a new microscopic method that will allow us to test at the same time the incorporation and distribution of the protein in different membrane systems and evaluate the yield of the incorporation and characterize the protein functionality.

Materials and Methods

E. coli lipids total extract, 1,2-Diphytanoyl-sn-Glycero-3-Phosphocholine (DPhPC), 1-palmitoyl-2-oleoyl-*sn*-glycero-3-phosphoethanolamine (POPE), 1-palmitoyl-2-oleoyl-*sn*-glycero-3-phosphocholine (POPC) and 1-palmitoyl-2-oleoyl-*sn*-glycero-3-phospho-L-serine (sodium salt) (POPS) were purchased from Avanti Polar Lipids, Inc. (Alabaster, AL). Octyl-β-D-glucopyranoside (OG) was purchased from Anatrace (Maumee, OH) and Sigma-Aldrich (Brondby, Denmark). Ergosterol and all the other chemicals were obtained from Sigma-Aldrich (Brondby, Denmark).

Heterologous protein overexpression

Functional SoPIP2;1 was overproduced in the methylotrophic yeast *Pichia pastoris* as His-tagged protein with a myc epitope [21]. The fusion protein has 303 amino acid and a molecular weight (Mw) of 32512 Da. The strain was grown in a 3 L fermentor typically resulting in 230 g wet cells/L culture after 24 h of methanol induction. Urea/NaOH washed membranes were prepared as described previously [21] and SoPIP2;1 was solubilised in 5% OG. Solubilized His-tagged material was purified using Ni-affinity chromatography as previously published [21]. The eluted protein was concentrated using a VivaSpin 20 concentrator (cutoff MW 10 kDa, VivaScience) and the buffer was then changed to 10 mM phosphate buffer, pH 7.5, NaCl 150 mM (PBS) supplemented with 10% glycerol and 1% OG using a PD-10 column resulting in a final concentration of 10–15 mg/ml as determined by Bearden [46].

Electrophoresis

Pure protein (5 μg) in 20 μL of phosphate buffer (10 mM potassium phosphate, 150 mM NaCl, 1% OG and 10% glycerol pH 7.5) was incubated for 10 minutes at different temperatures (25°C–65°C). After incubation, sample loading buffer (125 mM Tris-HCl pH 6.8, 20% glycerol, 4% SDS, 10% (v/v) β-mercaptoethanol 0.1% bromophenol blue) was added to the protein and further incubated for 10 minutes at room temperature. SDS- PAGE (12%) of the sample was performed as described by Laemmli [47]. Protein was visualized by staining the gel with Coomassie brilliant blue R250.

Dynamic Light Scattering (DLS)

Multilamellar 4 mg/ml DPhPC vesicles were formed by evaporation of the chloroform solvent by nitrogen gas and drying 30 minutes in the dessicator, followed by resolvation of the lipid film in sterile filtered 0.2 M KCl in double distilled water. The vesicle solution was extruded 11 times through a 100 nm polycarbonate filter. DLS size distribution analyses of 0.1 mg/ml DPhPC vesicles in 0.2 M KCl at 25°C were performed with a Malvern Zetasizer NanoZS instrument courtesy of LiPlasome Pharma A/S. Standard cuvettes (67.740 from Hounisen, Denmark) were used. 3 measurements of 13 runs each were taken and averaged. The analysis was carried out with the software program DTS 5.10, using an in-built general purpose analysis model.

Liposome and Protoliposome reconstitution

Purified SoPIP2;1 was reconstituted into vesicles by mixing with *E. coli* lipids total extract or DPhPC or POPE:POPC:POPS:Ergosterol (2:1:1:1 mol ratio) (complex fusogenic mixture) or POPE:POPC (7:3 mol ratio) (binary fusogenic mixture) solubilized in 1% OG at a lipid-to-protein molar ratio (LPR) of 200 in phosphate buffer 10 mM, NaCl 150 mM, pH 7.5 at a final 0.1 mg/mL concentration of protein. The mixture was dialyzed in Slide-A-Lyzer® Dialysis Cassettes from Thermo Scientific, Pierce Biotechnology, (Rockford, IL) with a molecular cut-off of 10,000 Mw at room temperature for 4 days with two buffer changes per day. Control vesicles were made in the same manner without protein.

Circular Dichroism (CD) and Fluorescence

CD spectra were acquired with a Jasco 815 spectrometer (Jasco UK, Essex, UK). The sample temperature was controlled by a built-in Peltier device. The protein or lipid-protein solutions were placed in a quartz cuvette with a 0.1 cm path length and the spectra were collected at 20 nm/min between 250–190 nm with a

response time of 0.25 s and a data pitch of 0.1 nm. Baselines were collected in the same manner and spectra were baseline corrected. CD spectra for samples without protein, i.e. buffer or buffer with detergent and lipid did not exhibit ellipticity. Mean residue ellipticity (MRE) ($[\theta]\times10^{-3}$ deg cm^2 dmol^{-1}) as calculated using the equation $[\theta]_M = M\theta/10\cdot l\cdot c\cdot n$, where M is 32512 g/mol, θ is the measured ellipticity in millidegrees, l is the cell path length, c is the protein concentration in grams per liter, and n = 303 residues. Deconvolution of the CD spectra into pure component spectra was performed using the algorithm CDSSTR [48] accessed through Dichroweb [49]. α-helical changes were followed observing the variation in MRE at 222 nm for the temperature stability measurements between 20°C and 95°C.

Fluorescence spectra were collected in an ISS Chronos fluorometer (ISS Champaign, IL) using a 280 nm diode as excitation source.

Acknowledgments

Adine Karlsson is gratefully acknowledged for technical assistance in providing purified SoPIP2;1. We are grateful for the helpful comments provided by anonymous referees.

Author Contributions

Conceived and designed the experiments: IP. Performed the experiments: IP SS SI. Analyzed the data: IP. Contributed reagents/materials/analysis tools: PK UJ OGM. Wrote the paper: IP JSH CHN UJ OGM.

References

1. Engel A, Stahlberg H (2002) Aquaglyceroporins: channel proteins with a conserved core, multiple functions, and variable surfaces. Int Rev Cytol 215: 75–104.
2. Engel A, Fujiyoshi Y, Agre P (2000) The importance of aquaporin water channel protein structures. Embo J 19: 800–806.
3. Park JH, Saier MH, Jr. (1996) Phylogenetic characterization of the MIP family of transmembrane channel proteins. J Membr Biol 153: 171–180.
4. Engel A, Fujiyoshi Y, Gonen T, Walz T (2008) Junction-forming aquaporins. Curr Opin Struct Biol 18: 229–235.
5. Kukulski W, Schenk AD, Johanson U, Braun T, de Groot BL, et al. (2005) The 5A structure of heterologously expressed plant aquaporin SoPIP2;1. J Mol Biol 350: 611–616.
6. Murata K, Mitsuoka K, Hirai T, Walz T, Agre P, et al. (2000) Structural determinants of water permeation through aquaporin-1. Nature 407: 599–605.
7. Savage DF, Egea PF, Robles-Colmenares Y, O'Connell JD, 3rd, Stroud RM (2003) Architecture and selectivity in aquaporins: 2.5 a X-ray structure of aquaporin Z. PLoS Biol 1: E72.
8. Gorin MB, Yancey SB, Cline J, Revel JP, Horwitz J (1984) The major intrinsic protein (MIP) of the bovine lens fiber membrane: characterization and structure based on cDNA cloning. Cell 39: 49–59.
9. Preston GM, Jung JS, Guggino WB, Agre P (1994) Membrane topology of aquaporin CHIP. Analysis of functional epitope-scanning mutants by vectorial proteolysis. J Biol Chem 269: 1668–1673.
10. Zardoya R (2005) Phylogeny and evolution of the major intrinsic protein family. Biol Cell 97: 397–414.
11. Russ WP, Engelman DM (2000) The GxxxG motif: a framework for transmembrane helix-helix association. J Mol Biol 296: 911–919.
12. Heymann JB, Engel A (2000) Structural clues in the sequences of the aquaporins. J Mol Biol 295: 1039–1053.
13. Danielson JA, Johanson U (2008) Unexpected complexity of the aquaporin gene family in the moss Physcomitrella patens. BMC Plant Biol 8: 45.
14. Johanson U, Karlsson M, Johansson I, Gustavsson S, Sjovall S, et al. (2001) The complete set of genes encoding major intrinsic proteins in Arabidopsis provides a framework for a new nomenclature for major intrinsic proteins in plants. Plant Physiol 126: 1358–1369.
15. Kammerloher W, Fischer U, Piechottka GP, Schaffner AR (1994) Water channels in the plant plasma membrane cloned by immunoselection from a mammalian expression system. Plant J 6: 187–199.
16. Chaumont F, Barrieu F, Jung R, Chrispeels MJ (2000) Plasma membrane intrinsic proteins from maize cluster in two sequence subgroups with differential aquaporin activity. Plant Physiol 122: 1025–1034.
17. Biela A, Grote K, Otto B, Hoth S, Hedrich R, et al. (1999) The Nicotiana tabacum plasma membrane aquaporin NtAQP1 is mercury-insensitive and permeable for glycerol. Plant J 18: 565–570.
18. Dordas C, Chrispeels MJ, Brown PH (2000) Permeability and channel-mediated transport of boric acid across membrane vesicles isolated from squash roots. Plant Physiol 124: 1349–1362.
19. Gaspar M, Bousser A, Sissoëff I, Roche O, Hoarau j, et al. (2003) cloning and characterization of ZmPIP1-5b, and aquaporin transporting water and urea. Plant Sci 165: 21–31.
20. Fraysse LC, Wells B, McCann MC, Kjellbom P (2005) Specific plasma membrane aquaporins of the PIP1 subfamily are expressed in sieve elements and guard cells. Biol Cell 97: 519–534.
21. Karlsson M, Fotiadis D, Sjovall S, Johansson I, Hedfalk K, et al. (2003) Reconstitution of water channel function of an aquaporin overexpressed and purified from Pichia pastoris. FEBS Lett 537: 68–72.
22. Tornroth-Horsefield S, Wang Y, Hedfalk K, Johanson U, Karlsson M, et al. (2006) Structural mechanism of plant aquaporin gating. Nature 439: 688–694.
23. Johansson I, Karlsson M, Shukla VK, Chrispeels MJ, Larsson C, et al. (1998) Water transport activity of the plasma membrane aquaporin PM28A is regulated by phosphorylation. Plant Cell 10: 451–459.
24. Nielsen CH (2009) Biomimetic membranes for sensor and separation applications. Anal Bioanal Chem.
25. Seddon AM, Curnow P, Booth PJ (2004) Membrane proteins, lipids and detergents: not just a soap opera. Biochim Biophys Acta 1666: 105–117.
26. Rand RP, Parsegian VA (1986) Mimicry and mechanism in phospholipid models of membrane fusion. Annu Rev Physiol 48: 201–212.
27. Borgnia MJ, Kozono D, Calamita G, Maloney PC, Agre P (1999) Functional reconstitution and characterization of AqpZ, the E. coli water channel protein. J Mol Biol 291: 1169–1179.
28. Manley DM, McComb ME, Perreault H, Donald LJ, Duckworth HW, et al. (2000) Secondary structure and oligomerization of the E. coli glycerol facilitator. Biochemistry 39: 12303–12311.
29. Baba T, Toshima Y, Minamikawa H, Hato M, Suzuki K, et al. (1999) Formation and characterization of planar lipid bilayer membranes from synthetic phytanyl-chained glycolipids. Biochim Biophys Acta 1421: 91–102.
30. Janko K, Benz R (1977) Properties of lipid bilayer membranes made from lipids containing phytanic acid. Biochim Biophys Acta 470: 8–16.
31. Lindsey H, Petersen NO, Chan SI (1979) Physicochemical characterization of 1,2-diphytanoyl-sn-glycero-3-phosphocholine in model membrane systems. Biochim Biophys Acta 555: 147–167.
32. Woodbury DJ (1999) Nystatin/ergosterol method for reconstituting ion channels into planar lipid bilayers. Methods Enzymol 294: 319–339.
33. Minetti CA, Remeta DP (2006) Energetics of membrane protein folding and stability. Arch Biochem Biophys 453: 32–53.
34. Reshetnyak YK, Burstein EA (2001) Decomposition of protein tryptophan fluorescence spectra into log-normal components. II. The statistical proof of discreteness of tryptophan classes in proteins. Biophys J 81: 1710–1734.
35. Sehgal P, Mogensen JE, Otzen DE (2005) Using micellar mole fractions to assess membrane protein stability in mixed micelles. Biochim Biophys Acta 1716: 59–68.
36. Galka JJ, Baturin SJ, Manley DM, Kehler AJ, O'Neil JD (2008) Stability of the glycerol facilitator in detergent solutions. Biochemistry 47: 3513–3524.
37. Aerts T, Xia JZ, Slegers H, de Block J, Clauwaert J (1990) Hydrodynamic characterization of the major intrinsic protein from the bovine lens fiber membranes. Extraction in n-octyl-beta-D-glucopyranoside and evidence for a tetrameric structure. J Biol Chem 265: 8675–8680.
38. Beuron F, Le Caherec F, Guillam MT, Cavalier A, Garret A, et al. (1995) Structural analysis of a MIP family protein from the digestive tract of Cicadella viridis. J Biol Chem 270: 17414–17422.
39. Konig N, Zampighi GA, Butler PJ (1997) Characterisation of the major intrinsic protein (MIP) from bovine lens fibre membranes by electron microscopy and hydrodynamics. J Mol Biol 265: 590–602.
40. Ringler P, Borgnia MJ, Stahlberg H, Maloney PC, Agre P, et al. (1999) Structure of the water channel AqpZ from Escherichia coli revealed by electron crystallography. J Mol Biol 291: 1181–1190.
41. Smith BL, Agre P (1991) Erythrocyte Mr 28,000 transmembrane protein exists as a multisubunit oligomer similar to channel proteins. J Biol Chem 266: 6407–6415.
42. Verbavatz JM, Brown D, Sabolic I, Valenti G, Ausiello DA, et al. (1993) Tetrameric assembly of CHIP28 water channels in liposomes and cell membranes: a freeze-fracture study. J Cell Biol 123: 605–618.
43. Bron P, Lagree V, Froger A, Rolland JP, Hubert JF, et al. (1999) Oligomerization state of MIP proteins expressed in Xenopus oocytes as revealed by freeze-fracture electron-microscopy analysis. J Struct Biol 128: 287–296.
44. Duchesne L, Deschamps S, Pellerin I, Lagree V, Froger A, et al. (2001) Oligomerization of water and solute channels of the major intrinsic protein (MIP) family. Kidney Int 60: 422–426.
45. Stahlberg H, Braun T, de Groot B, Philippsen A, Borgnia MJ, et al. (2000) The 6.9-A structure of GlpF: a basis for homology modeling of the glycerol channel from Escherichia coli. J Struct Biol 132: 133–141.
46. Bearden JC, Jr. (1978) Quantitation of submicrogram quantities of protein by an improved protein-dye binding assay. Biochim Biophys Acta 533: 525–529.
47. Laemmli UK (1970) Cleavage of structural proteins during the assembly of the head of bacteriophage T4. Nature 227: 680–685.

48. Compton LA, Johnson WC, Jr. (1986) Analysis of protein circular dichroism spectra for secondary structure using a simple matrix multiplication. Anal Biochem 155: 155–167.
49. Whitmore L, Wallace BA (2004) DICHROWEB, an online server for protein secondary structure analyses from circular dichroism spectroscopic data. Nucleic Acids Res 32: W668–673.
50. Humphrey W, Dalke A, Schulten K (1996) VMD: visual molecular dynamics. J Mol Graph 14: 33—3827—38.

Appendix III

Working Title: Supported Lipid Bilayers on engineered nanoporous polymers

Christian Rein[1], Sania Ibragimova[1], Stefan Kaufmann, Piotr Szewczykowski, Erik Reimhult, Thomas Bjørnholm, Claus Helix Nielsen
1 Shared first authors

Abstract

Supported lipid bilayers (SLB) bla bla..
PEGylated lipid vesicles in both mushroom and brush regime were deposited on nanoporous polybutadiene. The hydrophobic/hydrophilic characteristic of the porous surface were compared to reference silica surfaces. Rupture of the PEGylated vesicles created stable SLBs on the porous surface and especially with PEG chains in brush regime the bilayer was found to be requiring a higher yield force verified by indentation experiments using atomic force microscopy.

YP = Yielding Point (Force level for rupturing a membrane)
AFM = Atomic Force Microscopy
QCM-D = Quartz Crystal Microbalance with Dissipation Monitoring

Introduction

Stable lipid membranes suitable for protein incorporation require a substrate which can provide mechanical support without having a disruptive interaction on the supported lipid bilayer (SLB). Having the SLB directly on a silicon wafer or other atomically flat metallic surfaces have repeatedly (Tanaka 2006) been shown to denature the proteins and limit the horizontal mobility of lipid bilayers which are necessary to proper mimic the proteins natural environment. Also for the study of transmembrane proteins and membranes systems in general it is often necessary to have access to both the top (cis) volume and the bottom (trans) volume of the SLB. Porous polybutadiene allows monitoring of transmembrane transport (C. H. Nielsen 2009)

By combining the QCM-D and AFM for study of DOPC-vesicle deposition on silica both high time and special resolution of SLB formation have been elucidated (Richter 2003). In that study a high electrostatical dependency of the SLB formation was found.

Previous work (Kaufmann 2009) with PEGylated lipid vesicles deposited on quartz crystals that formed an SLB and silicon wafers showed significant improvement in both horizontal mobility indicating a better biomimical system for protein insertion. The work focused on low PEG concentrations where the PEG chains would be in a so-called "mushroom" regime due to problems with deposition of vesicles containing higher concentrations.

We here present our study of both vesicle depositions containing high concentrations of PEG in so-called "brush" regime" and of the stability-enhancing of such PEGylated SLBs on engineered nanoporous polymers. Through the use of QCM-D and force spectrometry of the deposited vesicle we show that it is possible to create such SLBs on both silica and nanoporous polymers and that UV-treated polybutadiene improves stability.

Materials and Methods

Vesicle preparation.
Lipid vesicles were prepared by mixing appropriate amounts of 1,2-dioleoyl-*sn*-glycero-3-phosphocholine (DOPC), 1,2-dioleoyl-*sn*-glycero-3-phosphoethanolamine-N-[methoxy(polyethylene glycol)-750] (DOPE-PEG750) and 1,2-dioleoyl-*sn*-glycero-3-phosphoethanolamine-N-[methoxy(polyethylene glycol)-2000] (DOPE-PEG2000) lipid stock solutions in chloroform (10 mg/ml) to prepare lipid solutions with the following compositions: 1) DOPC:DOPE-PEG750 (90 mol: 10 mol), 2) DOPC:DOPE-PEG2000 (95 mol: 5 mol) and 3) DOPC:DOPE-PEG2000 (98 mol: 2 mol). A thin lipid film was formed by evaporating the solvent using nitrogen gas at room temperature. Residual solvent was removed by overnight storage in vacuum (<0.3 mbar). The dried lipid film was rehydrated with PBS pH 7.2 for a final lipid concentration of 8 mg/ml. The formed multilamellar vesicles were extruded using a hand-held extruder (name? from xx) through 0.2 μm track-etched membranes (Isopore, Millipore) 21 times.

Dynamic light scattering (DLS).
DLS size distribution analyses of vesicle solutions at 25ºC were performed with a Malvern Zetasizer NanoZS instrument courtesy of Liplasome A/S. Three 10-measurement series were taken for each system and averaged. The analysis was carried out with the software DTS 5.10, using an in-built general purpose analysis model. The detection angle was 173 and the refractive index for the vesicles was taken to be 1,59.

QCM-D.

We used a QCM-D-E4 system (Q-Sense AB, Gothenburg, Sweden) to measure deposition kinetics of lipid vesicles on a silica surface, using the software Q-Soft for data collection. Polished AT-cut, 5 MHz quartz crystal sensors were supplied by Q-Sense. The application of the QCM-D technique for determining deposition kinetics is described in Rodahl et al[3]. Briefly, the QCM-D technique monitors the change in frequency of vibration due to deposition of wet mass on the quartz crystal sensor. As wet mass deposits onto the quartz sensor, the frequency of vibration decreases. During ideal conditions, there is a linear relationship between the change in frequency Δf and the adsorbed mass Δm:

$$\Delta m = \frac{c}{n}\Delta f \qquad (0.1)$$

where c (=17.7 ng cm^{-2} Hz^{-1} at f=5 MHz) is the mass-sensitivity constant and n (=1, 3, ...) is the overtone number. Combined frequency and energy dissipation measurements give information about both the adsorbed amount (Δf) and the viscoelastic properties (ΔD) of the adsorbed film.

The fractional bilayer coverage was calculated as previously described by Graneli et al[29] based on two assumptions: (i) The water-exposed domains on a planar SPB do not contribute significantly to D. (ii) There exists a linear relationship between the dissipation change at saturation and liposome size, as previously demonstrated for pure PC liposomes in the size regime between 25 and 200 nm. The fractional bilayer coverage, α, and fractional coverage of intact liposomes, 1 - α, are estimated using

$$\alpha = 1 - \Delta D_{fin} / \Delta D_{sat}$$
$$\Delta D_{sat} = x\Theta \qquad (0.2)$$

where ΔD_{sat} is the dissipation value expected when α=0, i.e., for the whole surface covered by intact liposomes, ΔD_{fin} is the actual measured change in D at saturation, Θ is the liposome diameter (Table 1) in nanometers, and x=0.15 is the proportionality constant between the change in D for nonruptured liposomes on TiO_2[31] and the liposome diameter (change in D/nm of liposome diameter).

The thickness of the adsorbed film was obtained using a built-in Voigt model in the software Q-tools. In this model the adsorbed film is represented by a homogeneous thickness, viscosity, and complex shear modulus.

All data shown was measured at the fifth harmonic, n= 5, i.e., at 25 MHz. For clarity, the frequency response is divided by 5 in all graphs (this makes the data directly comparable to data measured at n = 1, for ideal conditions).

Before each experiment, the silica sensors were soaked in 2% Hellmanex II (Hellma GmbH & Co. KG, Müllheim, Germany) cleaning solution for 30 min, rinsed thoroughly with DI water, dried with ultra high-purity N_2, and treated in an ozone/UV chamber (BioForce Nanosciences, Inc., Ames, IA) for 30 min.

Cleaned sensors were mounted in a temperature-controlled (25 °C) chamber of the QCM-D system, with one side of the sensor exposed to the solution. All test solutions were fed into the chamber using a syringe and adsorption was measured in stagnant conditions. A baseline was obtained in PBS buffer pH adjusted to 7.2, with the frequency signals stabilized at an approximately 2 Hz change in frequency over 10 min. 1 ml of vesicles were injected and allowed to deposit on the silica sensor until the frequency signal stabilized at an approximately 2 Hz change in frequency over 10 min. More vesicles were injected until no further increase in frequency was observed. The system was equilibrated again with PBS buffer. Each experiment was repeated at least four times.

Atomic Force Microscopy (AFM).

An MFP-3D atomic force microscope (Asylum Research, Santa Barbara, CA, US) was used for both topographic imaging and for force curves. Force curves were collected by using a force volume (FV) scanning routine where maps consisting of force-distance (deflection of probe vs. the Z-distance) data were arranged in 2D grids.

For the indentation experiments a silicon nitride probes (ORC8-PS, Olympus Denmark, Ballerup, Denmark) with spring constants ($k_{factory}$ = 0.1 N/m) of 80.16-115.87 pN/nm was used (found by thermal calibration). For the indentations, the scan rates varied from 0.1 Hz to 0.2 Hz, and the probed Z-distance were 0.5 µm to 1 µm (i.e. the retraction distance after reaching target force value). Target force (the force at which the probe begins to retract again) was 4 nN to 10 nN. Same scanning parameters were used for indentation experiments using biolever probes (12.03 pN/nm, thermal calibration) on silicon substrates. For probing on the corrugated polished polybutadiene (PB) surface, force-volume data were obtained with the more hydrophilic ORC8 which had a better aspect-ratio than a biolever.

For the adhesion measurements, biolever probes (Olympus Denmark, Ballerup, Denmark) with a spring constant of 6.13-9.01 pN/nm was used (found by thermal calibration). The biolever, which have a gold coating on the tip, were stored for 2 weeks in a 0.1 M hexadecanethiol in ethanol solution and rinsed in both ethanol and milli-Q grade water before use. 1 hours equilibration time was used with biolever probes in order to avoid pre-stress interfering with measurements.

Topographic imaging of the substrates in air was made in tapping mode.

For vesicles deposition either 30 ul or 100 ul 8 mg/ml vesicle solution was used containing 2 or 5 mol% PEG2000, respectively. Incubation time was between 10 min (for 5 mol%) to 1 hour (for 2 mol%) before gentle rinsing excess vesicles with PBS. The larger volume and incubation time for 2 mol% PEG2000 were necessary to have proper coverage for statistical analysis.

All AFM work with vesicles and deposited vesicles were done with PBS solution as imaging buffer.

Analysis: Igor Pro 6.03A (Wavemetrics, Lake Oswego, OR, US) was used together with custom made software that automated the calculation of adhesion energy.

The adhesion energy was calculated as the area delimited by the retraction force curve and a virtual line going from the point where the retraction force curve crossed the baseline to the point where the probe looses contact with the surface and jumps away from the surface (the Snap-Back Point).

Only data points which show lipid bilayer rupture events were used for analysis (see figure 3) and the bilayer coverage measured with AFM was calculated as the number of events over total number of pixels (table 4). Analysis of membrane breakage (yielding) was done manually.

Distance between two grafting sites (s), radius of gyration (Rg) and the total SLB thickness of the 5 mol% PEGylated SLBs on silica were obtained by fitting the force curves to equation 1 which were derived by Dolan and Edwards (Dolan 1974 – no access) and modified by Li and Pincet (Li 2007). Total thickness was measured as the average separation from hard-wall contact to the onset of compression of the PEG chains. The onset of the compression was defined as the separation where the exponential fit to the data exceeds 3 mN/m (just above the baseline noise) as used in previous studies (Kaufmann 2009).

Equation 1: $F(D)/R = 144 \cdot \pi \cdot k_B \cdot T \cdot s^{-2} \cdot e^{(-3^{1/2} \cdot D \cdot 1/2 \cdot R_g^{-1})}$

Results and discussion

Investigation of the support surface by AFM

The polybutadiene (PB) samples used in this study was often covered with a so-called "skinlayer" (see figure 1a) that reduced the porosity of the surface. Removal of this layer by gentle grinding exposed the gyroid morphology (see figure 1b) similar to that what have previously been observed for same polymer in SEM. And this made the substrate porous, allowing bulk transport across the membrane. Treating the surface with UV-light changed the surface chemistry without changes to the surface topology (see figure 1c). As reference a silicon wafer surface (figure 1d) was used for hydrophobic/hydrophilic comparison and for inspecting the prior to vesicles deposition. Also, the silica surface were used as a substrate for deposition of vesicles containing 5 mol% PEG2000. Both surface roughness (see figure 1) and hydrophobicity (table 1) of the silicon wafer were similar to the UV-treated PB glass side surface on which 2 mol% PEG200 vesicles were deposited, and except for porosity they can therefore be regarded as similar surfaces in this study.

For decreasing the number of artefacts in the force-measurements a less corrugated PB surface (glass side) were also UV-treated and used for vesicle deposition (figures 1e & 1f). From the topographic image the glass side surface were found to be porous like the polished air side, but without the same clear gyroidal morphology or skinlayer as the unpolished air side.

***Figure 1**: AFM topographic images obtained by scanning in tapping mode.a) PB air side, b) PB air side polished, c) PB air side polished and UV-treated, d) Silicon, e) PB glass side, f) PB glass side UV-treated*

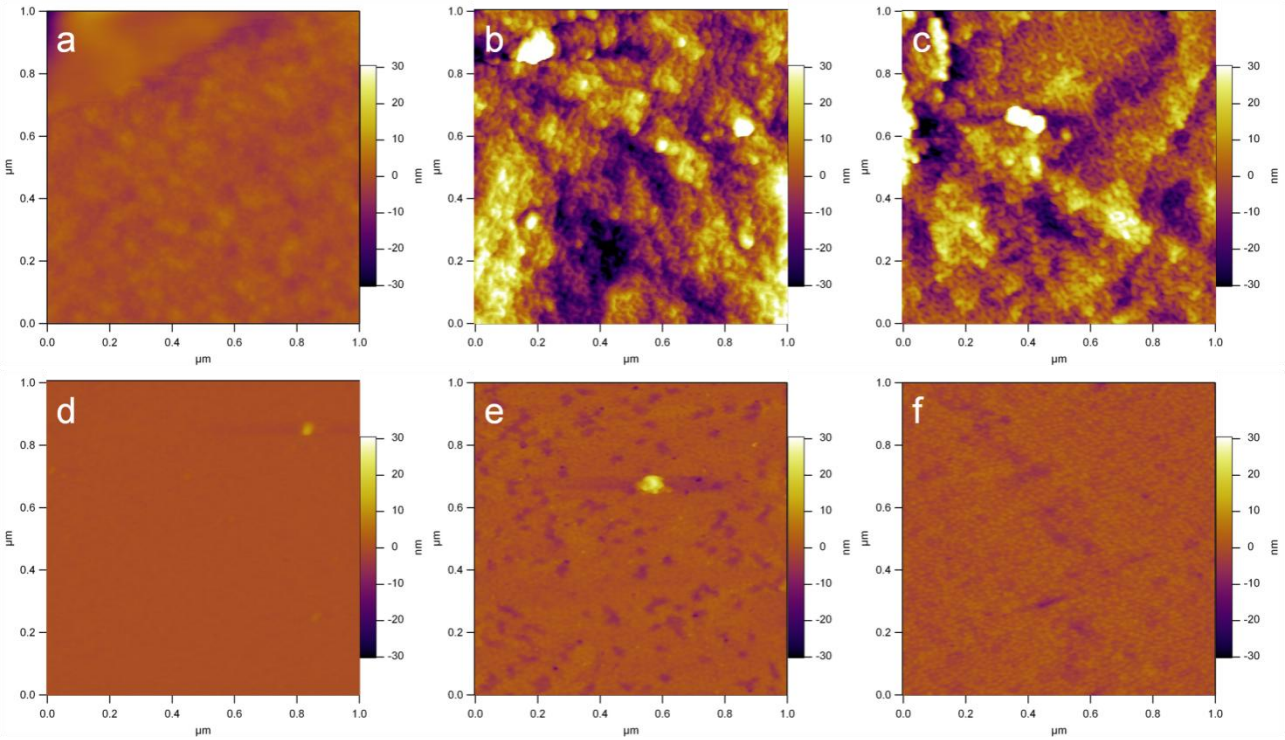

The effect of UV-treatments was measured by probing the adhesion of an AFM tip coated with a monolayer of hexadecanethiols under water. The adhesion energy between the coated tip and the surface would give a value of the "hydrophobicity" of the surface (see table 1). A low adhesion energy would indicate a more hydrophilic support surface compared to one with a high adhesion. As reference a silicon wafer surface with a natural oxide layer was used. The low adhesion energy for the reference verified the "hydrophobicity" of the tip. The data is for comparative uses. The UV-treatments reduced the adhesion energy to just 9.7% and 6.4% of the original level of the polished air side and glass side, respectively. The "hydrophobicity" of the UV-treated glass side was similar to the reference silicon surface, while for the UV-treated polished air side it was 10 times higher.

***Table 1:** Adhesion strength of the PB and silicon surfaces obtained from force curves measurements using a biolever coated with a monolayer of hexadecanethiols. n indicates number of force-curves used for the statistics. Note that for the native PB air surface the skin layer interfere with the probing causing problems with adhesion calculations.*

Surface		**n**	**Adhesion energy (aJ)**
PB air side	As is	400	N/A
	Polished	400	770±1100
	UV –treated	400	49±190
PB glass side	As is	100	38± 27
	UV-treated	2500	3.7± 17
Si	As is	100	4.7± 10

Characterization of vesicles

The compositions of the vesicles used for deposition on the surfaces were chosen such that the fractions of PEG2000 represented two different conformation-regimes. Vesicles containing only 2 mol% PEG2000 would have the PEG-chains in the more folded "mushroom-regime", while vesicles containing 5 mol% PEG2000 would have the chains in a more elongated "brush-regime" (Kaufmann). The vesicles of both types were similar in size to that of plain DOPC vesicles (see table 2) and the deposition shouldn't be affected by this parameter.

Table 2: *Vesicle diameter obtained by DLS. All vesicle solutions are extruded 21 times through a 200 nm polycarbonate filter. Averaged over 3 experiements.*

Vesicle composition (mol%)		d_H (nm)	PDI
DOPC	DOPE-PEG2000		
100		136±x	0.076
95	5	133±1	0.125
98	2	142±2	0.095

Deposition of vesicles on silica and polybutadiene

QCM experiments (see figure 2) on the two types of PEG-containing vesicles were carried out in order to verify the vesicles ability to dock and fuse. Figure 2 shows that the vesicle deposition kinetics increases with concentration, but the thermodynamic equilibrium for them all is similar. For the concentrations used in this study, a 5 min waiting time can be assumed to be sufficient for the system to reach equilibrium. Similar kinetics were also observed for vesicles containing 5 mol% PEG2000, but had a more pronounced crystal dependency with 2 out of 6 experiments showing no vesicle rupture.

Figure 2: *Vesicle deposition kinetics on silica obtained by QCM-D. Kinetics of DOPC:DOPE-PEG2000 (98 mol: 2mol) vesicles with concentrations of 0.1 mg/ml (black/grey), 0.5 mg/ml (red/mauve) and 5 mg/ml (blue/royal blue).*

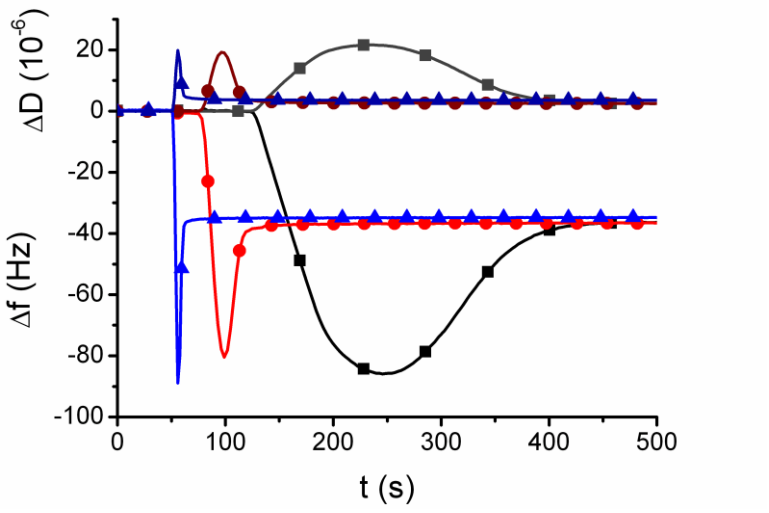

QCM data (see table 3) shows a 0.9 nm decrease in thickness when going from 5% to 2% PEG2000 content in the lipid bilayers. This difference couldn't be observed by AFM where the thickness of both 2% and 5% PEG-lipid bilayers were similar at yielding point (see figure 3). The increased thickness of 5% PEG-lipid bilayers might therefore be contributed mostly by the conformation of the top PEG-layer which is not being probed at yielding point.

Table 3: *Adsorbed vesicle layer characteristics (mass coverage, thickness and bilayer area) obtained with QCM-D.*

Vesicle composition	Δf (Hz)	ΔD (10^{-6})	Γ (ng.cm^{-2})	t (nm)	Bilayer area (%)
DOPC:DOPE-PEG2000(98:2)	-35.60±2.39	1.06±0.06	630±42	7.7±0.3	94.4±0.3
DOPC:DOPE-PEG2000(95:5)	-42.48±2.49	0.72±0.29	752±44	8.6±0.3	96.4±1.5

Coverage

UV-treated polybutadiene surfaces had a hydrophilicity and roughness similar to that of the silica surface used in QCM and the coverage on this support was therefore expected to be close to that measured with QCM. Measuring the number of detected membrane ruptures with AFM (table 4) revealed less coverage compared to data from QCM (table 3) for both 2 mol% and 5 mol% PEGylated lipids. While this might be due to the use of an extra rinsing step and the fact that AFM don't measure the systems ensamble properties (i.e. mass coverage). Also the fact that about 1/3 of the QCM experiments with 5 mol% PEG2000, the vesicles didn´t rupture could explain the lower coverage since the lipids in the intact vesicles would not contribute to the coverage. Previous work by Richter et. al. (Richter 2003) shows that electrostatic interactions greatly influence SLB formation and that a critical vesicle coverage of the neutrally charged DOPC vesicles is needed for bilayer formation. Also, different lipid coverages measured by AFM and QCM were found, which might be due to slight differences in chemical properties of the supports.

The measured coverage by AFM of 5 mol% PEGylated lipids on silicon was found to vary on the same sample (table 4) and the coverage on the polymer surface was found to lie within this range, indicating a correlation between the coverage of hydrophilicity and deposition.

Table 4: *SLB coverage on both Pb surface and on the reference silica surface measured by AFM. Two separate areas on the silica were investigated, giving two different values.*

Surface	Coverage (%)
2 mol% Pb (n=1)	28
5 mol% Pb (n=1)	46
5 mol% Si (n=2)	36-80

Membrane thickness & Breakthrough force

One noticeable difference between the AFM data and QCM-D data is the large difference in measured bilayer thickness, which allows us to identify the thickness of various parts of the PEG-bilayer-PEG system.

Applying high force (> 1 nN) on the silicon-supported system distort the bilayer significantly and at YP the AFM probe only detects thickness (and rupture) of the hydrophobic core of the bilayer, which for 5 mol% PEG2000 was found to be 3.5 nm (thickness of bare lipid bilayer without PEG). Scanning in tapping mode with the same probe produced reproducible topographic images and can be assumed to be non-disruptive for the bilayer system. Histogram analysis of a topographic image obtained in tapping mode showed a peak-to-peak height difference of 4.65 nm, slightly higher than 3.8 nm which is expected for a bilayer of DOPC without PEG2000-cushion beneath (Lewis 1983). This indicates a compressed 5 mol% PEG2000-cushion beneath the lipid

bilayer when resting on a silicon-substrate and it is possible that PEG-chains are in a mushroom- rather than a brush-conformation. The tapping mode topography does not give us any information about the top PEG2000 layer.

Fitting the repulsive force of the PEG chains using a Derjaguins approximation (Derjaguin 1934) allowed us to derive both the distance between grafting sites, radius of gyration and the total thickness of the 5 mol% PEGylated SLB as presented in table 5.

Table 5: *Properties of 5 mol% PEGylated SLB on silica derived from Dolan and Edwards fit. Variations in the theoretical values are based on the variations in the average area per lipid molecule from 50 Å^2 to 70 Å^2 and the size of one PEG monomer from 3.5 Å to 3.9 Å.*

5 mol% on Si	**Experimental**		**Theory**
[nm]	Mean	Std	
s	1.25848	0.22958	3.16 – 3.74
Rg	3.8508	0.5262	0.96 - 1.07
Total Thickness	19.61667	2.04784	3.25-4.35 (for PEG chain in brush regime)

The Flory radius (Rf) for PEG2000 is calculated to be around 3.46 nm – 3.85 nm. The experimental data clearly indicates s < Rf, which is shows that the PEG chains are in the brush regime.

The total thickness is significantly higher that found with QCM and what have been previously reported with AFM for just 2 mol% PEGylated lipid bilayers (11.4+-1.1, Kaufmann 2009). This shows both a significant increase in SLB thickness when PEG chains change conformation to brush regime, but also between the QCM and AFM methods. Comparing the thickness from our QCM data for 2 mol% (7.7±0.3 nm) with that previously observed for 2 mol% with AFM it shows a 48 % increase in measured thickness.

While this thickness indicates a discrepancy between the QCM-D and the AFM methods it allows us to use these data for comparison of vesicles deposition the PB surfaces.

Figure 3: *Overview of breakthrough force (yielding point, YP), Thickness at YP and total thickness.*

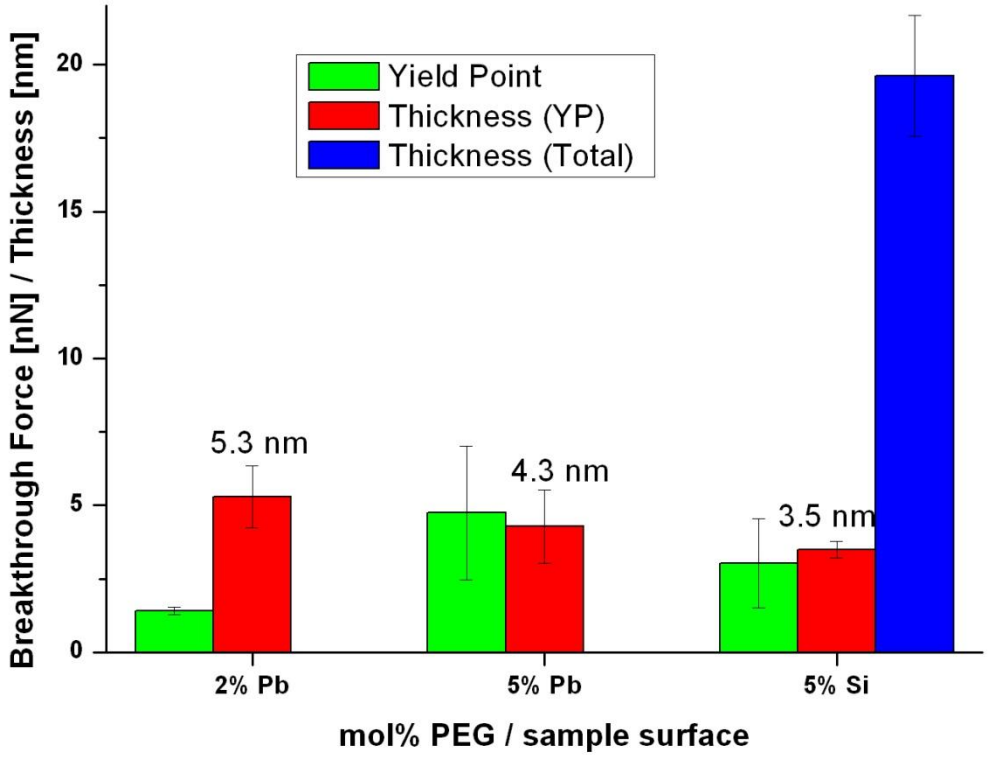

For 5 mol% PEG2000 both breakthrough force (4.75 nN) and thickness (4.3 nm) was improved on the PB-sample compared to silica. The surface might stabilize the brush-regime for the bottom PEG layer better than silicon and thereby improved both thickness and overall membrane stability.

2 mol% PEG2000 on a more smooth PB-substrate gave a thickness (5.3 nm) slightly higher than 5 mol% PEG2000 on the polymer, but with much lower breakthrough force (1.4 nN). The slight increase in thickness for the 2 mol% PEG2000 SLB on the polymer compared to the 5 mol% might be explained by a difference in horizontal mobility of the two different conformations (see figure 4 C & D). Then compressing the SLB the PEG chains could migrate away from the stress, which give a lower jump-in once the membrane ruptures. The mushroom-regime PEG chains might not be as mobile and/or responsive to mechanical and therefore stays trapped beneath the stressed SLB area.

Figure 4: *Illustration of vesicle deposition (A-B) and effect of indentation on a brush-regime PEGylated SLB (C-D). When pressing down on the system the mobility of the PEG chains in the lower leaflet migrates away from the site.*

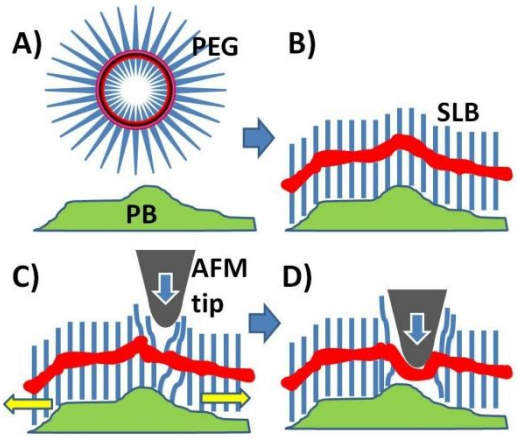

Force-curves of 2 mol% PEG lipid bilayers on silicon obtained with biolever probes gave a similar low YP (2.1 nN) which were below that observed for 5 mol% on same support (3 nN). This could indicate a reduced mechanical stability of membranes supported by PEG-cushions in the mushroom-regime as previous studies have shown (Kaufmann 2009) where increased mol% of PEG-PE lipids acted as a barrier to rupture. The stabilising effect using porous PB as substrate is also indicated by these results.

QCM data shows a 0.9 nm decrease in thickness when going from 5% to 2% PEG2000 content in the lipid bilayers. This difference couldn't be observed by AFM where the thickness of both 2% and 5% PEG-lipid bilayers were similar at yielding point. The increased thickness of 5% PEG-lipid bilayers might therefore be contributed mostly by the conformation of the top PEG-layer.

These data all points towards a stressed system when supported on silica where the SLB is less resistant to rupture.

Conclusion

We have here shown that depositing PEGylated lipid vesicles on hydrophilic porous substrates is not only possible but it also enhances the membrane stability towards mechanical stress. The efficiency of the deposition method was shown with QCM-D where the systems rapid kinetics quickly established a complete coverage of a ~ 8 nm lipid layer. The system was found through AFM indentation experiments to be extremely compressible before rupture which gives the system a method for dissipating mechanical stress. A possible response of the PEG chain in brush regime to the mechanical stress is migration of the chains away from the affected area before membrane rupture.

The best stabilization was observed when the PEG-chains were in a brush-configuration on the porous polymer surface. A discrepancy between thickness values found with AFM and QCM illustrates the challenge to compare such parameters between ensemble and non-ensemble methods. The enhanced stability of the 5 mol% PEGylated SLB were also found to be a challenge since some of the vesicles were found to not rupture.

While this work has shown the advantages of both PEGylated lipids in brush-regime and porous polymer support it is clear that many aspects of this complex system still needs to be illuminated.